UNIVERSITY OF SOUTHAMPTON

Hydrological Effects and Avoidance of Thermal Runaway

Nadiah Salwi Hudi-Jahit

Doctor of Philosophy

FACULTY OF ENGINEERING, SCIENCE AND MATHEMATICS
SCHOOL OF ELECTRONICS AND COMPUTER SCIENCE

July 2005

UNIVERSITY OF SOUTHAMPTON

ABSTRACT

FACULTY OF ENGINEERING, SCIENCE AND MATHEMATICS
SCHOOL OF ELECTRONICS AND COMPUTER SCIENCE

Doctor of Philosophy

HYDROLOGICAL EFFECTS AND AVOIDANCE OF THERMAL RUNAWAY

By Nadiah Salwi Hudi-Jahit

Existing underground cable ratings are very conservative and therefore underestimate the full system capacity especially during high times of high power consumption during summer months. There is a need for improved and more accurate rating calculations. An objective of this project has been to investigate the heat and moisture migration initiated by the heating of the medium surrounding buried cables, which when subjected to prolonged heating under extreme conditions can lead to 'thermal runaway'. Identification of conditions under which 'thermal runaway' occurs will allow the improvement in estimation of the external parameters (such as soil thermal resistivity and capacitance) used in the existing cable ratings.

A controlled experiment pertaining to heat and moisture transfer has been conducted in order to verify the model developed by Philips and de Vries using the finite element analysis method. Experiments involved the use of soil of various low moisture contents and the results are compared to the model which used variable soil properties. Thermal conductivity and soil suction are two essential soil properties that have been determined experimentally. Whereas, other hydrological soil properties are obtained theoretically using established methods. Soil properties that are used in the model are made variable to temperature and volumetric moisture content. Investigation has revealed that a strong correlation exists between moisture and temperature due to heat transfer.

The verified Philip-de Vries model has been used to simulate the effects of drying-out. This involves looking at the changes of moisture content of the surrounding medium, the dry/wet interface and the effects of different heat losses and initial volumetric moisture contents have on the heated backfill.

ACKNOWLEDGEMENT

I am indebted to all of the following people, without whom, this thesis would not have been possible.

The work described in this thesis was performed under the direction of Dr. Paul Lewin. Special acknowledgement and gratitude to Dr. Paul Lewin, without whose professional and friendly guidance and assistance this thesis might never have become a reality.

I wish to thank The National Grid Transco Plc for the support that made it possible to write this thesis, particularly by providing funding for the experimental equipments and software packages.

A special recognition and acknowledgement for their contributions to this work are extended to Mr. Neil Palmer, late Mr. Roland Caldecutt, Mr. Richard Durrant and fellow colleagues in the High Voltage Group.

Last but not least, a special thank you to my husband, Mr F Mansor for his everlasting patience and support.

CONTENTS

LIST OF FIGURES AND TABLES

CHAPTER 4

CHAPTER 5

CHAPTER 6

LIST OF SYMBOLS

a	a constant	-
a_b	absorption coefficient (FEMLAB related)	-
a_v	volumetric air content in percentage	-
a_{tl}	fitting parameter related to breaking point of the curve	-
a_f	soil parameter, primarily a function of air entry value of soil	-
A	a constant between 1.08 and 2.00	-
b	parameter used to vary estimation in (3.7)	-
c	concentration of vapour flux	kgm^{-3}
c_b	diffusion coefficient (FEMLAB related)	-
c_{qs}	specific heat of quartz in soil	$Jkg^{-1}\,°C^{-1}$
C	volumetric heat capacity of soil/backfill	$kJm^{3}°C^{-1}$
C_a	volumetric heat capacity of air	$kJm^{3}°C^{-1}$
C_o	volumetric heat capacity of organic matter	$kJm^{3}°C^{-1}$
C_{qs}	volumetric heat capacity of quartz soil	$kJm^{3}°C^{-1}$
C_s	volumetric heat capacity of soil solids	$kJm^{3}°C^{-1}$
C_u	coefficient of uniformity	-
C_w	volumetric heat capacity of water	$kJm^{3}°C^{-1}$
d_a	mass coefficient, time dependant matrix (FEMLAB related)	-
D	diffusion coefficient of vapour flux	$m^{-2}s^{-1}$
D_{atm}	molecular diffusivity of water vpour in air	$m^{-2}s^{-1}$
D_T	thermal diffusivity	$m^{-2}s^{-1}\,°C^{-1}$
D_{TL}	thermal liquid diffusivity	$m^{-2}s^{-1}\,°C^{-1}$
D_{TV}	thermal vapour diffusivity	$m^{-2}s^{-1}\,°C^{-1}$
$D_{\theta L}$	isothermal liquid diffusivity	$m^{-2}s^{-1}$
$D_{\theta V}$	isothermal vapour diffusivity	$m^{-2}s^{-1}$
D_θ	moisture diffusivity	$m^{-2}s^{-1}$
D_{10}	ratio of weight of soil particles being 10% finer	-
D_{20}	grain diameter with 20% coverage on the grain	mm
D_{60}	ratio of weight of soil particles being 60% finer	-
e	voids ratio	-
$\mathbf{f}$	a given function	-
f	coefficient form: source term (FEMLAB related)	-
F	general form: source term (FEMLAB	-

	related)	
F_i	general form: source term in *i*th equation (FEMLAB related)	-
g	gravity acceleration	ms^{-2}
g_b	boundary source term (FEMLAB related)	-
G	general form: boundary source term (FEMLAB related)	-
G_i	general form: boundary source term in *i*th equation (FEMLAB related)	-
G_a	air shape factor	-
G_s	specific gravity	-
h	relative humidity expressed in percentage	-
h_b^T	transposed scalar coefficient for Lagrange multiplier (FEMLAB related)	-
h_b	scalar coefficient for Lagrange multiplier (FEMLAB related)	-
h_c	convective heat transfer coefficient of vertical surfaces	$Wm^{-2}\,°C^{-1}$
h_{cl}	convective heat transfer coefficient of horizontal surfaces	$Wm^{-2}\,°C^{-1}$
h_d	depth of cable axis from ground surface	m
h_r	suction at which residual moisture content occurs	kPa
i	unit vector in positive z direction	-
I	input current	A
j	rate of diffusive vapour flux	$kgm^{-2}s^{-1}$
k	thermal conductivity	$Wm^{-1}°C^{-1}$
k_{unsat}	unsaturated hydraulic conductivity	ms^{-1}
k_{sat}	saturated hydraulic conductivity	ms^{-1}
$k_{v\theta}$	isothermal vapour permeability	ms^{-1}
k_{vT}	thermal vapour permeability	$ms^{-1}°C^{-1}$
Ke	Kersten number	-
$Ke_{0.125}$	Kersten number at $Ke_{0.125}$	-
Ke(T)	Kersten number as a function of temperature	-
K_c	proportionality constant	ms^{-1}
l	distance	m
L	volumetric latent heat of vapourisation	Jm^{-3}
L_{cable}	length of simulated cable	m
L_{diff}	differential operator	-
m_f	soil parameter, primarily a function of residual	-
m_{tl}	fitting parameter related to curvature of the curve	-
M_{dry}	weight of dry soil sample	kg

M_s	mass of soil solids	kg
M_w	mass of soil water	kg
M_{wet}	weight of wet soil sample	kg
n	outward unit normal vector on $\partial\Omega$ (FEMLAB related)	-
n_f	soil parameter, primarily a function of the rate of moisture extraction from the soil once air entry value is exceeded	-
n_{t1}	fitting parameter related to maximum slope of the curve	-
p	partial pressure of water vapour	kPa
P	air pressure	kPa
P_{or}	porosity of soil	-
q	heat flux	Wm^{-2}
q_b	boundary absorption coefficient (FEMLAB related)	-
q_c	quartz content percentage over solid content	-
q_L	liquid flux density	$kgm^{-2}s^{-1}$
q_v	vapour flux density	$kgm^{-2}s^{-1}$
q_{loss}	cable heat loss per meter length	Wm^{-1}
q_m	moisture flux density	$kgm^{-2}s^{-1}$
Q	heating rate	$Wm^{-1}s^{-1}$
r	coefficient form: boundary term (FEMLAB related)	-
R	general form: boundary term (FEMLAB related)	-
R_i	general form: boundary term in *i*th equation (FEMLAB related)	-
R	gas constant	$Jkg^{-1}K^{-1}$
S	saturation degree, expressed in percentage	-
t	time	s
T	absolute temperature in Kelvin	K
T	temperature	°C
T_{amb}	ambient temperature	°C
T_s	surface temperature	°C
T_1....T_7	Labelled thermocouples	-
u	vector of dependant field variable (FEMLAB related)	-
u_i	vector of dependant field variable in *i*th equation (FEMLAB related)	-
u_o	initial value of u (FEMLAB related)	-
u	unknown function	-
$\tilde{u}$	dependant field variable when linearised	-
$\underline{U}$	equivalent liquid velocity	ms^{-1}

$\underline{V}$	vapour velocity	ms^{-1}
V	input voltage	V
V_a	a unit volume of air in an unsaturated soil	-
V_s	a unit volume of soil solids in an unsaturated soil	-
V_T	total of a unit volume of an unsaturated soil	-
V_v	a unit volume of voids in an unsaturated soil	-
V_w	a unit volume of water in an unsaturated soil	-
α	conservative flux convection coefficient (FEMLAB related)	-
β	non scalar convection coefficient (FEMLAB related)	-
β_s	temperature derivative of saturated water vapour density	-
ϕ_1	hydraulic potential greater than ϕ_2	m
ϕ_2	hydraulic potential greater than ϕ_1	m
Φ_a	volume fraction of air	-
Φ_o	volume fraction of organic matter	-
Φ_s	volume fraction of soil solids	-
Γ	flux vector (FEMLAB related)	-
Γ_i	flux vector in *i*th equation (FEMLAB related)	-
γ_b	conservative source flux term (FEMLAB related)	-
γ	defined as $\frac{1}{\sigma}\frac{\partial\sigma}{\partial T}$ in (3.13)	$\frac{1}{°C}$
η	dynamic viscosity of water	Nsm^{-1}
η_{ref}	dynamic viscosity of water at reference temperature	Nsm^{-1}
η_T	dynamic viscosity of water at temperature T	Nsm^{-1}
Λ	equivalent vapour flow area	-
λ	soil thermal conductivity	$Wm^{-1}°C^{-1}$
λ_i	thermal conductivity of individual material in soil	$Wm^{-1}°C^{-1}$
λ_o	thermal conductivity of pore medium in soil	$Wm^{-1}°C^{-1}$
λ_a	thermal conductivity of air in soil	$Wm^{-1}°C^{-1}$
λ_w	thermal conductivity of water in soil	$Wm^{-1}°C^{-1}$
λ_v	thermal conductivity of vapour in soil	$Wm^{-1}°C^{-1}$
λ_{dry}	thermal conductivity of soil at dry state	$Wm^{-1}°C^{-1}$
λ_{sat}	thermal conductivity of soil at saturated state	$Wm^{-1}°C^{-1}$
λ_s	thermal conductivity of soil solid	$Wm^{-1}°C^{-1}$
λ_{quartz}	thermal conductivity of quartz	$Wm^{-1}°C^{-1}$
λ_{min}	thermal conductivity of soil minerals	$Wm^{-1}°C^{-1}$

μ	Lagrange multiplier (FEMLAB related)	-
μ_i	Lagrange multiplier in *i*th equation (FEMLAB related)	-
ν	moisture flux	ms^{-1}
θ	volumetric moisture content	m^3m^{-3}
θ_g	gravimetric moisture content	$kgkg^{-1}$
θ_s	saturated gravimetric moisture content	m^3m^{-3}
θ_{sat}	volumetric moisture content at which saturation occurs	m^3m^{-3}
$\theta_{critcal}$	volumetric moisture content at which critical point occurs	m^3m^{-3}
θ_{wilt}	volumetric moisture content at which wilting point occurs	m^3m^{-3}
$\theta_{0.125}$	θ at 0.125 , expressed in percentage	-
ρ_w	density of liquid water	kgm^{-3}
ρ_v	vapour density	kgm^{-3}
ρ_{ref}	liquid water density at reference temperature	kgm^{-3}
ρ_o	saturated water vapour density	kgm^{-3}
ρ_d	soil dry density	kgm^{-3}
ρ_b	soil bulk density	kgm^{-3}
ρ_s	density of soil solid particles	kgm^{-3}
ρ_{sat}	density of saturated soil	kgm^{-3}
σ	water surface tension	Jm^{-3}
σ_{ref}	water surface tension at reference temperature	Jm^{-3}
σ_T	water surface tension at temperature T	Jm^{-3}
υ	mass flow factor	-
ψ	soil suction	kPa
$\psi(\theta)_{ref}$	suction at reference temperature	kPa
Ω	union of all subdomains of interest (FEMLAB related)	-
$\partial\Omega$	domain boundary (FEMLAB related)	-
∇	vector differential operator (FEMLAB related)	-
∇c	gradient of concentration of vapour flux	-
∇T	temperature gradient	
$(\nabla T)_a$	average temperature gradient in air filled pores	-

CHAPTER 1

1.0 INTRODUCTION

Underground cable systems are an alternative means to overhead lines for transmission and distribution. Although comparatively costly to install, cable systems have become increasingly favourable due to advantages of protection against lightning and as well as eliminating the possibility of imposing hazards to aircrafts. Due to the expensive cost of installing underground cable circuits, it has always been in the interest of the power provider to optimise cable capacities for the full range of expected operating conditions. The existing method is to determine the maximum operating current so that the maximum operating temperature is never exceeded. This is called cable rating.

The cable rating practiced by The National Grid Transco plc involves a mathematical formula that includes known parameters of the system such as burial depth, separation, conductor size, material size and the thickness of the cable insulation. These can be accurately determined. There are two other parameters essential to the cable rating that cannot be accurately determined. These are the soil thermal resistivity and soil ambient temperature. These are impossible to determine because the soil along the cable length and around the cable may not have the same physical, thermal and hydrological properties. Furthermore, the routes of the cable circuits may include various types of native soils. An existing approach is to conservatively assume that the region (surrounding the cable) that falls into the 50°C boundary is considered dry and that outside is wet. Standard soil thermal resistivities and ambient temperatures are appropriately assigned for each month [1]. Over the whole year, the actual ambient soil temperature may not be as high as the standard value. This leads to under utilisation of cable ampacity and it is likely that circuits could reliably operate at levels of 5 to 10 percent higher [2].

The need to look at moisture migration and its ultimate consequence of thermal runaway, due to the heating from underground cables became important after a catastrophic failure of the power supply system occurred at Bostal Heath, London during the summer period in 1962. An investigation that followed revealed failures on two 132kV cable feeders. The feeders had been highly loaded and therefore, the soil surrounding the cables had continuously been hot and dry. Increased thermal resistance of the soil became inevitable due to moisture migration in regions adjacent to the high voltage cable surfaces. Increased moisture migration away from the region had therefore caused the soil to overheat and thermal runaway occurred.

Thermal runaway pertaining to underground cables is a term describing the process whereby thermal resistivity of the soil starts to increase exponentially as the surrounding soil dries. This process occurs when additional or prolonged heating drives any remaining moisture away until the return of moisture flux under the moisture gradient is no longer available. Failure of cables will therefore become inevitable especially when the heating is prolonged and surplus moisture from precipitation so as to replenish the moisture influx is absent. The outflow of moisture away from the area around the cable and under the thermal gradient is often referred to as moisture migration.

Thermal runaway is generally avoided by de-rating the carrying capacity of the cable; optimising the thermal resistivity of the medium the cable is embedded in and/or ensuring that the maximum operating current is not exceeded at all times. The latter has been described as under-utilising the full capacities of cables under all ranges of condition when a conservative approach is undertaken. Controlled thermal backfills are often used as the bedding material for cable burials because they provide low thermal resistivity for good thermal dissipation. However, when backfills are used surface troughs need to be considered. Surface troughs are exposed to diurnal changes in surface ground temperatures and in cases of cyclic

loadings over a long period of time or highly loaded emergency loadings whereby moisture could possibly be driven out of the trough area, small sized troughs may be exposed to the possibility of impeded immediate moisture return due to the concrete walls acting as barriers [3]. This is because following an extensive drying period, once the moisture capillary is broken it could take a considerable long time for equilibrium moisture to be achieved unless immediate, heavy precipitation occurs and moisture slips underneath the concrete lids of the trough. The trough thus may be exposed to the possibility of the onset of thermal runaway. The threat of possible causes to thermal runaway provides the purpose in understanding the hydrological effects on bedding materials, be it backfills or native soils. In this project, the bedding material that is of interest is sand. Over the years, sand has been the bedding material due to its inexpensive cost, its reasonable thermal properties and the fact that it is easily available.

Investigation into the phenomenon of thermal runaway is essential in order to understand its behaviour so that it could be avoided in the future. To achieve this, it is necessary to understand the physical, thermal and the hydrological properties of the bedding material of cables, which typically is sand. High quartz sand is usually used as an alternative to crushed stone backfill for cable burials in United Kingdom, Norway and some other parts of the world. In countries of semi-arid climates, sand is vastly used, and to compensate for the occurrence of thermal runaway, it is used to ensure that bedding materials are properly compacted.

Ultimately, the relationship between the thermal properties and the behaviour of moisture and heat distribution must be established. The most important part of the investigation is to distinguish the physical conditions whereby thermal runaway could actually occur. This is achieved by investigating the behaviour of soil drying using the heat and moisture transfer model developed by Philip and de Vries [4].

A literature review on thermal drying and the associated moisture migration is documented in Chapter 2 and the mechanisms of heat transfer that are possible in heated soils are explained. Existing approaches in solving heat and moisture transfers are discussed. This chapter includes the comparison and discussion to justify the chosen analytical approach, the finite element method. Also, how other researchers have tackled the problem of heat and moisture transfer and identifying thermal runaway are discussed.

Soils are characterised by their physical nature and each soil has different thermal and hydraulic properties. Soils are classified according to characteristics such as texture, shape and size. Thermal properties are the properties associated with the ability of the soil to contain thermal energy and describe whether it is a good or bad thermal conductor. Hydraulic properties describe the retention and transmission quality of water in soils. An insight into this subject is detailed in Chapter 3.

Chapter 3 also describes the properties/characteristics of the bedding material of interest that have been studied and their relationship with temperature and moisture obtained semi-empirically. The soil/backfill properties that are essential to heat and moisture transfer are the thermal conductivity, thermal diffusivity, isothermal diffusivity and hydraulic permeability. Thermal conductivity is the main factor for thermal transfer whereas isothermal diffusivity is for moisture transfer. Accurate determination of soil suction is crucial because it holds the key in empirically determining both isothermal diffusivity and hydraulic permeability. Temperature and moisture are strongly interdependent in the process of heat transfer within a porous medium, and in this project the unsaturated state of soil/backfill is of interest. This is because the unsaturated state of soil/backfill is susceptible to extensive drying. Another point worth mentioning is that the type of moisture referred to in the thesis is water only. This promotes simplicity and thus neglects mass in the form of chemical or mineral solutes.

A controlled, simple experiment has been conducted in observing heat transfer with respect to moisture transfer and this is described in Chapter 4. A soil sample with pre-defined volumetric moisture content is placed within a cylindrical apparatus whereby a hot plate is placed at one end and a cold plate at another. The induced heating upon the hot plate creates temperature gradient within the volume of soil and moisture migration is initiated. The experiment has been conducted with soil samples of several different initial volumetric moisture contents. Results show that the rate of heat transfer increases with the intensity of the heating and becomes prominent in low initial moisture contents. Moisture migration occurs inevitably to cause the increase of temperature of drier regions and decrease of temperature of the neighbouring wetter regions. The volume of the cylindrical apparatus can be divided into several horizontal layers or regions and by assuming that temperature at each measuring location has reached its time constant, 'local' thermal conductivity can be determined. The dry front that formed within the sample has also been observed after each experiment.

The results obtained in Chapter 4 have been compared to the solution obtained using the Philip and de Vries heat and moisture transfer model in Chapter 5. The heat and moisture transfer model developed by Philip and de Vries consists of two highly non-linear partial differential equations. The finite element method has been used to solve these partial differential equations. These are solved using the exclusive MATLAB® -incorporated finite element software called FEMLAB. Soil properties that have been used in FEMLAB are those that are obtained and estimated in Chapter 3. Both thermal and hydraulic soil properties that have been used in FEMLAB are dynamically calculated in each of its iteration. The calculated experimental 'local' thermal conductivity of each region in the cylindrical apparatus has been compared to those obtained from FEMLAB. The performance of the simulated temperatures in both transient and steady state and those obtained experimentally from Chapter 4 have also been extensively

compared and discussed. The effectiveness of the model has been investigated in this chapter.

A laboratory experiment on a simulated cable has been conducted to study the heating behaviour imposed on the surrounding soil as it would on real cables. The absence of external environmental factors during the commission of the experiment has allowed the recorded temperatures to be compared to that obtained from the finite element simulations. This is documented in detail in Chapter 6.

Finally, conclusions and further work are presented in Chapter 7.

CHAPTER 2

2.0 THERMAL DRYING AND MOISTURE MIGRATION

Introduction

As far as buried power cables are concerned, the thermal drying of the medium in which they are embedded is inevitable. The distribution of power via these cables leads to power losses that heat the medium. The effect of temperature gradient between the cable conductor and its adjacent material within the cable allows heat flow. As the heat front progresses outwards from the cable, a temperature gradient is formed between the cable and its adjacent surroundings. The heat flow continues radially outwards until a point is reached when a temperature gradient no longer exists to allow for significant flow of heat flux.

The effect of heat escaping from the heat source causes, to some extent, the loss of the moisture content of the bedding material. This could simply be the native soil or the backfill that is usually used to provide better thermal conditions. The effect of thermal drying physically generates heat and moisture flow. The degree to which the bedding material loses its moisture depends on the magnitude of the cable thermal losses and the physical, thermal and hydraulic properties of the other materials involved.

The processes of heat and moisture flow impose no danger until excessive drying occurs. Excessive drying technically commences when these flows no longer equate to each other. When this stage is achieved, the likelihood of cable failure is greatly increased.

2.1 HEAT TRANSFER MECHANISM IN SOILS

Transfer of heat generally involves heat energy flowing from a region of high temperature to a region of lower temperature. The mechanism of heat transfer in soils is predominantly by conduction although heat transfer by convection and radiation are also possible. Heat transfer by conduction involves heat contact by soil solids. In unsaturated soils, the process of heat transfer between moving moisture and soil solid is heat convection. Whereas radiation heat transfer is attributed from the emission of heat from the sun.

2.1.1 Heat Transfer by Conduction

Heat transfer by conduction in soils/backfills takes place at the contact points of solid particles. This process may also take place at paths that consist of solid particles; water or air space and paths where only water and air spaces are present. However, heat transfer by conduction limits the effective overall conduction irrespective of the high intrinsic thermal conductivity that the solid particles may have [5]. Conduction depends on three quantities. These are the soil thermal conductivity, the contact area between soil solids and heat flow; and temperature gradient. The greater the temperature gradient and the thermal conductivity, the faster the heat flows.

When a power cable is loaded and heats up, heat is transferred by conduction from the cable to the adjacent soil. This creates a temperature gradient in the direction of the heat being transferred. The region that is closest to the cable being the hottest and cooler at radial regions away from the cable [6]. The rate at which heat is transferred depends on the thermal properties of each individual component within the cable, such as the thermal conductivity and resistivity of the sheath and armour of the cable. Heat conduction is continuous throughout the soil to the

ground surface. The rate of heat conduction at this stage depends on the thermal properties of the individual components of the soil medium.

Heat transfer by conduction is described by Fourier's Law and is given by

$$q = -k\nabla T \tag{2.1}$$

Where q is heat flux, (Wm^{-2}); k is thermal conductivity, ($Wm^{-1}°C^{-1}$) and ∇T is temperature gradient.

2.1.2 Heat Transfer by Convection and Radiation

Heat transfer by convection in soils occurs in two stages. First, heat from soil solids is transferred to moisture adjacent to its surface. Near the soil solids, velocity of moisture flow is low and heat transfer in diffusion mode dominates. In the next stage and away from the surface, bulk motion increases and heat is transferred by moisture flow. Convection heat transfer is divided into two types; forced convection and free convection. The latter occurs when temperature variations causes moisture density in soil pores to change and induce buoyancy forces. Convection heat transfer in unsaturated soil occurs not only when moisture is present, but also when moving air exists in soil pores.

Typical values for convective heat transfer coefficients for air and water fall in the following ranges

- Air – 10 to 100 $Wm^{-2}K^{-1}$
- Water – 500 to 10 000 $Wm^{-2}K^{-1}$

As heat progresses from the cable surfaces towards the ground surface, it eventually escapes to the ambient air. The form of energy transfer between the ground surface and ambient is convection and radiation. This is due to the fact that the ground surface inevitably absorbs radiation from the sun and the temperature difference between the ground surface and ambient, whereas, air motion above the ground surface initiates energy transfer by convection. However, these effects are less acute for ground surfaces that have grass/vegetation because they act superficially as a layer of insulation, reducing the heat flux that is being transferred to the ambient [7].

Vegetation may also be incorporated in the moisture migration analysis as it extracts moisture at root depth [8]. Cables deeply buried are affected by vegetation roots at greater depth, cables buried near to surface ground affected by the surface vegetation having small and short roots. Surface trough cables are not affected by moisture extraction from vegetation due to their concrete surrounds.

Radiation from the sun is mostly short wave and heat penetrates into the sub-layers of soil via the ground surface. While some heat is absorbed some are also reflected. Soil temperature by depth is generally affected more by the radiation of the low frequency cycle (annual) rather than the high frequency cycle (daily) [7,9]. Due to annual cycles, the variations in interior temperature of soil are about 60% of that on the surface and are delayed whereas diurnal cycles do not greatly affect thermal conditions at cable depths of $0.7\text{m} < h_d < 1\text{m}$, where h_d is the depth of cable axis from ground surface [10].

2.1.3 Condensation and Evaporation

The increased temperature from power cable heating leads to evaporation in pores of unsaturated soils/backfills. The moisture present within these pores absorbs the

latent heat of vaporisation and therefore evaporates to vapour, which is then driven to regions of lower vapour pressure. At this point the released vapour gives up the latent heat and thus condenses. The counteraction of these heat transfer processes partly contributes to the equilibrium of heat flow towards and away from the power cables.

2.2 MOISTURE MIGRATION

To explain the phenomenon of moisture migration in the vicinity of a cable buried underground, it is necessary to consider energy transfer and physical processes that are involved along with the physical properties of soils, water and vapour under the influence of a temperature gradient.

2.2.1 Basic Concept

The factors affecting moisture migration under temperature gradients are the amount and duration of heat flow from the cable, soil temperature, type of soil and/or backfill, soil moisture content, hydrostatic pressure, depth of buried cable and soil surface conditions [11].

The driving force that induces moisture or soil water migration towards a cooler region throughout the soil is the temperature gradient. By Fourier's Law, the greater the temperature gradient and the shorter the heat transfer path towards the ground surface, the faster the rate of heat conduction. This means that the depth at which a cable is laid also plays an essential role in determining the behaviour of any moisture migration. The whole process must be investigated as a transient phenomenon as the temperature or heat flux at any fixed point within the soil medium varies with time. The transient heat transfer may be analysed as being one,

two- or three- dimensional depending on the level of the accuracy and the direction desired [12]. However, owing to the cable radial heat transfer and its symmetry, the heat transfer along the cable and along the circumference of its cross section can be presumed negligible.

By nature, heat is conducted in the direction of decreasing temperature. The migrated moisture becomes warm due to heat transfer by conduction and as it migrates/flows towards the cooler region, heat is then lost by convection to solid particles and air voids of lower temperature than the moisture. The interaction between solid and liquid water within the soil under this temperature gradient causes liquid water to flow by capillary conduction.

Capillary flow depends on the suction pressure and soil liquid permeability. Whereas suction pressure is dependant upon particle shape and size. Suction pressure can be expressed as a function of both moisture content and temperature whilst the soil liquid permeability as a function of moisture content [13]. However, an allowance must be made for the rate of moisture flow. During heat convection, it is restricted by the friction exerted by the solid particles that are present within the vicinity of the flow path. Another form of heat transfer that takes place is vapour migration in the form of latent heat of vaporisation.

The quantity of dissolved air in soil moisture decreases as temperature increases [14]. Therefore, soil moisture may not just flow away from the cable but also evaporate under the temperature gradient as it migrates. This vapour is diffused through air filled voids to the cooler region and the extent to which moisture migrates in this form depends on its vapour permeability and the pressure gradient. The smaller the soil vapour permeability, the more moisture migration in the form of vapour is impeded [15]. Migration of vapour towards the cooler region initiates condensation, returning an inflow of liquid water to counterbalance the

outflow of heat. Under unstable conditions, the net outflow of vapour is greater than the net inflow of the condensed vapour [16]. Hotspots are then created within the medium where the cable is buried and at this stage, lack of moisture to conduct away heat may lead to cable breakdown through overheating [17, 18]. Bladowski [19] showed that the thermal analysis of a buried cable could be tackled by representing the whole system by an electrical circuit. This is an alternative to site observations and laboratory experiments.

2.2.2 Philip and de Vries Model

Several researchers have constructed mathematical models to visualise the behaviour of the temperature and moisture transfer in regards to the heating of unsaturated porous mediums. Models vary with certain assumptions taken to suit the matter of interest and also the specified conditions under considerations. The most popular approach is of that of Phillip and de Vries [4], who used Fick's and Darcy's Law for the flow/diffusion of vapour and moisture flux respectively, in the unsaturated porous medium.

Fick's Law describes the passive movement of molecules down its concentration gradient. According to Fick's Law, diffusion of gas or vapour only occurs when there is a concentration gradient. The characterisation of the diffusion transport basically relates the diffusion of vapour flux to its diffusion coefficient as outlined by the following equation,

$$j = -D\nabla c \tag{2.2}$$

Where j is rate of the diffusive vapour flux, ($kgm^{-2}s^{-1}$); D is diffusion coefficient of its flux, (m^2s^{-1}) ; c is gradient of concentration of vapour flux, (kgm^{-3}) and ∇ represents gradient.

In 1856, a French hydraulic engineer named Henry Darcy was the earliest to develop a quantitative description of water flow through a porous medium [20, 21]. Through his experiment on water flow, he concluded that the rate of fluid flow through a porous medium is proportional to the potential energy gradient within that fluid. This is known as Darcy's Law. The constant of proportionality is the hydraulic conductivity; the hydraulic conductivity is a property of both the porous medium and the fluid moving through the porous medium.

Darcy's Law is described by the following relationship

$$v = -K_c \nabla \phi \tag{2.3}$$

Where v is velocity of moisture flux, (ms^{-1}); K_c is the proportionality constant and measure of hydraulic conductivity, (ms^{-1}) and $\nabla\phi$ is the difference of hydraulic potential, (m), at two points separated by a distance, l, (m). $\nabla\phi$ is defined as

$$\nabla\phi = \phi_2 - \phi_1 \tag{2.4}$$

Where ϕ_2 is greater than ϕ_1 .

Philip and de Vries made an extension to the 'simple theory' of vapour transfer. It was based on the review made by Carman [22] on the determination of liquid isothermal adsorption in a porous medium. The phenomenon is dependent on the physical adsorption and capillary condensation. Physical adsorption was observed to dominate at low relative humidity and on the other hand, capillary condensation dominates at high relative humidity. The simple theory of vapour diffusion neglects the interaction of vapour, liquid and solid phases and also the

difference between average temperature gradient in the air-filled pores and soil as a whole.

Based on Fick's Law, their extended theory leads to the separation of vapour mass flux to components of moisture and temperature gradients. Whereas, liquid/moisture transfer was described extensively based on Darcy's Law, which leads to separation of liquid flux density to components of temperature and moisture gradients and an extra component due to gravitation. Integrating the relationship between liquid and vapour flux density, total moisture flux density is obtained. Therefore, rate of moisture distributions can be determined.

The developed relationships are expressed in (2.5) and (2.6).

For liquid flux density, the equation is

$$\frac{q_L}{\rho_w} = -D_{TL}\nabla T - D_{\theta L}\nabla\theta - k_{unsat}i \qquad (2.5)$$

Where q_L is the liquid flux density, ($kgm^{-2}s^{-1}$); ρ_w is density of liquid water (kgm^{-3}); D_{TL} is thermal liquid diffusivity, ($m^2s^{-1}°C^{-1}$); $D_{\theta L}$ is isothermal liquid diffusivity, (m^2s^{-1}); k_{unsat} is unsaturated hydraulic conductivity, (ms^{-1}); T is temperature (°C); θ is volumetric moisture content and i is the unit vector in the positive z direction.

For vapour flux density, the equation is

$$\frac{q_v}{\rho_w} = -D_{TV}\nabla T - D_{\theta V}\nabla\theta \qquad (2.6)$$

Where q_v is the vapour flux density, ($kgm^{-2}s^{-1}$); D_{TV} is thermal vapour diffusivity, ($m^2s^{-1}°C^{-1}$) and $D_{\theta V}$ is isothermal vapour diffusivity, (m^2s^{-1}).

By integrating (2.5) and (2.6), the total moisture flux, q_m, ($kgm^{-2}s^{-1}$), can be found:

$$\frac{q_m}{\rho_w} = -D_T\nabla T - D_\theta\nabla\theta - k_{unsat}i \tag{2.7}$$

Where the thermal diffusivity, D_T, is

$$D_T = D_{TL} + D_{TV} \tag{2.8}$$

And the isothermal diffusivity, D_θ, is

$$D_\theta = D_{\theta L} + D_{\theta V} \tag{2.9}$$

The differential equation for moisture transfer is

$$\frac{\partial\theta}{\partial t} = \nabla.(D_T\nabla T) + \nabla.(D_\theta\nabla\theta) + \frac{\partial k_{unsat}}{\partial z} \tag{2.10}$$

Where z is the z plane of the cartesian coordinate system, and t is time, (s). The isothermal vapour diffusivity obtained from the moisture gradient component of the vapour flux density is used in the heat distribution equation as shown in (2.11).

$$C\frac{\partial T}{\partial t} = \nabla.(\lambda \nabla T) + L\nabla.(D_{\theta V}\nabla\theta) \qquad (2.11)$$

Where C is volumetric heat capacity of soil ($kJm^{-3}°C^{-1}$); λ is soil thermal conductivity, ($Wm^{-1}°C^{-1}$); and L is volumetric latent heat of vaporisation, (Jm^{-3}).

Experimental observations undertaken by Rose [23] has verified that at low moisture contents, vapour diffusivities of isothermal and non-isothermal components become dominant and as moisture content increases to much higher values, liquid diffusivities dominate in return.

2.2.3 Other Theories

In 1960, a theory on moisture migration under temperature gradient based on irreversible thermodynamics by Taylor and Cary was proposed but was later modified due to its restriction to require heat flux through soil [24]. A general flow law was developed which could be applied to simultaneous heat movement and any matter by using appropriate functions of that matter. The manipulation of coefficients of soil water diffusivities within the 'Taylor and Cary' theory is common with the developments of Philip and de Vries.

An extended observation by Cassel and Nielsen [25] to distinguish the validity of theories was individually developed using Fick's Law, the extended version of Fick's Law and irreversible thermodynamics. Net moisture flux was proven to be under-predicted by use of Fick's Law and the use of Taylor-Cary theory was proven to further under-predict by doubling that produced using Fick's Law [26, 27]. The only good and acceptable agreement was with Philip-de Vries theory. This gives an explanation why many researchers have preferred Philip-de Vries model to analyse thermal and moisture behaviour of moisture migration in porous media. Field

observations have established that maximum net moisture migration exists for values of moisture content, $\theta < 0.077$ or possibly for $0.077 < \theta < 0.101$ [25].

Like Cassel et al [25], Rose [23] justified Philip-de Vries theory in estimating the isothermal vapour diffusivity. Part prediction by Philip-de Vries theory states that a discontinuous liquid phase enhances water movement by transmitting vapour flux and hence acting as a 'short circuit' path for vapour flow. This was confirmed by investigating isothermal vapour transfer [23].

Another attempt to look at the effects of liquid and vapour conductivities on moisture migration by Rose [26] showed that the former decreases continuously from saturation to complete dryness whereas the latter rises slowly from zero saturation to maximum near dryness and after which, (at complete dryness) decreases rapidly. This has lead Rose to establish a distinguishable concept on porous wetting having six stages (Figure 2.1).

Dakshanamurthy and Fredlund [27] proposed a model that suits compressible or deformable mediums in which Darcy's Law was used to describe migration in the liquid phase and Fick's Law in air phase. The model also takes into account the effect of pore air and water pressures under hydraulic and temperature gradients. Application of Philip and de Vries model was neglected since it is invalid for incompressible conditions. However, thermal analysis under moisture migration seldom assumes the medium or soils are compressible and this is because, with extensive computational work involved, simplification is inevitable.

Milly [28] and Sophocoleous [29] have both generalised the theory developed by Philip and de Vries. The objective for this was to facilitate the complicated presence of hysteresis and in-homogeneity of soil/porous media. They have converted the original theory by replacing the formulation based on moisture

content to that of matric head. One of the differences in their approach is the numerical method each used to solve the problem. Milly used the finite element method whilst Sophocoleous used the finite difference method. However, the simplification made on the temperature dependence of the relative humidity and the liquid thermal diffusivity by Sophocoleous was criticised by Milly. The latter simplification erroneously doubled the temperature effects on the liquid flow.

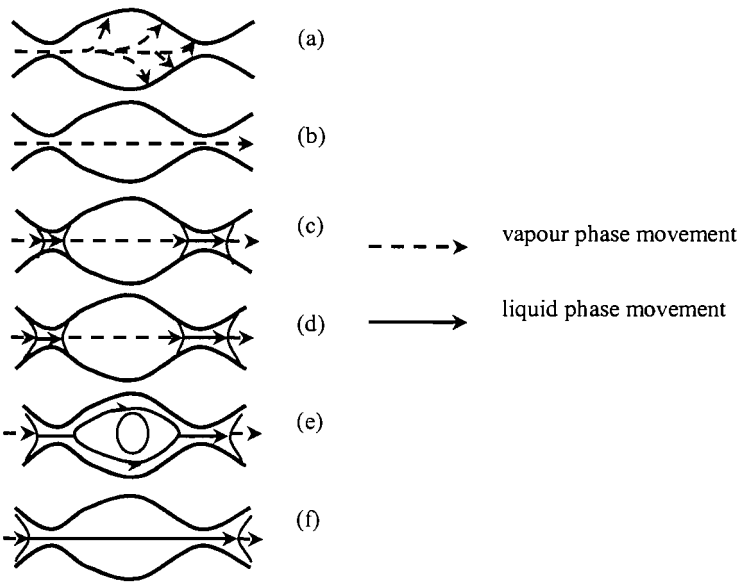

Figure 2.1 – Water movement at various stages in the wetting of porous material [26]. a)adsorption, b)vapour transfer, c)distillation, d)surface creep, e)unsaturated hydraulic flow and f)saturated hydraulic flow.

Milly has included in his numerical method the advection of wetting due to the pressure head gradient, an aspect which has been neglected by Phillip and de Vries. The effect of the generalisation taken was to develop a model for hysteresis non-isothermal conditions. Despite the simplifications made, Sophocoleous concluded that the non-isothermal formulation is suitable for a long term study on the seasonal influences on water transport involving extended drying conditions; whereas the isothermal formulation is suitable for predicting pressure head and temperature profiles.

2.3 ANALYSING THERMAL DISTRIBUTION OF POWER CABLES - EXISTING METHOD

The original approach taken by researchers in analysing thermal distribution around buried power cables has been solving the partial differential of heat conduction equation of the surrounding mediums (backfills and surrounding soils) only. El-Kady [30]; Hanna and Chikhani [31]; Hanna, Chikhani and Salama [32, 33, 34]; Tarasiewicz and Grzybowski [35]; and Flatabo [36] have done extensive thermal analyses for trench cables but unfortunately this analysis does not include the influence of moisture migration. The solution of the moisture transfer differential equation (2.10) and heat distribution equation (2.11) are therefore useful in improving their analyses. El-Kady and Hanna [32, 33, 34] used the finite difference method to solve the thermal transfer model. Whereas Tarasiewicz and Flatabo had used finite element methods. Both models neglect the influence of moisture migration on the thermal distribution around the power cables.

2.3.1 Consideration of Moisture Migration

Realising moisture migration is a serious influence on cable failure, more recently researchers have included moisture migration effects to account for the occurrence of thermal runaway. Some of the approaches that had been taken were to use different limiting temperatures for different soil beddings and using soil suction to predict extensive thermal drying.

Arman, Cherry and Gosland [37] were among the first to include the influence of moisture migration in analysing thermal distribution of power cables and thermal runaway. Discovering that moisture migration depends very much on the nature of the bedding material, particle shape and size, its density and moisture content, they applied dryness-zone boundary temperatures of 50°C and 35°C for loamy or clayey

soils and sandy soils, respectively. These temperatures are believed the maximum temperature that can be maintained in each respective soil, without allowing further increase in its thermal resistivity. However, this approach was found inflexible in adjusting the resistivity values of dry zone and could only be applied to a limited number of cases.

An approach in determining the occurrence of drying-out soil was done by Koopmans, van de Wiel, van Loon and Palland [38] whereby soil suction at cable depth is used to identify the presence of thermal drying. Hydraulic conductivity is estimated using the model proposed by Childs and Collins-George [39]. By using the estimated hydraulic conductivity, the vegetation factor model developed by Feddes, Kowalik and Zaradny [40] and a water balance model, soil suction is estimated at cable depth. The minimum soil suction at cable depth, at which drying-out have occurred (during the 9-year data collection period) had been identified. This value was set as the critical soil suction (pF_{crit}). Then, if observed suction at cable depth (during cable loading) is found below the critical value, drying out is expected to have occurred. This method, however, was found to have underestimated the ambient soil suction at drying out and therefore resulted in over-estimating the maximum temperature of cable surface.

Nahman and Tanaskovic [41] have included the drying out phenomenon in analysing maximum cable ampacity for underground cables around the Belgrade urban area, using the finite element method. They used iterative steps whereby when drying out did occur, a new calculated soil thermal resistivity is inserted into the model. Drying out due to extensive moisture migration is assumed to have taken place by assuming a boundary that separates two regions of different moisture intensity that have reached an isothermal temperature, calculated using a formula given by Mainka [42]. Unfortunately, this approach neglected the influence of moisture distribution, which is an important element of the drying out phenomenon.

2.3.2 Heat and Moisture Transfer Approach

Analytical models have improved by the contribution of scientists in the study of mass flow in temperature-induced porous media and the determination of soil thermal and hydraulic properties by geophysical engineers. The inclusion of moisture migration in thermal distribution analyses, which has now become a popular approach, means that modelling drying-out problems are a step closer to realistic solutions [43, 44, 45]. Heat and moisture transfer equations are also important not only to electrical engineers but also to geopyshics engineers [46] and civil engineers, whom find it useful when considering problems of underground moisture damaging the quality of buildings [47, 48, 49].

There have been several experiments to model heat and mass transfer to verify Philip-de Vries theory. Moya, Prata and Cunha [44] have investigated the moisture migration by modelling a system with a parallel-piped container (1.2m x 0.87m x 0.64m) filled with well-graded crushed granite stone and heat source of 25.4mm external diameter. Instrumentation was provided to measure the cable surface temperature, soil moisture content and heat flux measure along a tangential temperature gradient. The experimental results were validated against a numerical model by solving a one-dimensional analytical solution using finite volume methodology.

Greater heat flux causes a greater drying out in the soil at close proximity to the heated source and suffers a more severe reduction in its saturation degree than regions away from it. Cyclic simulation revealed a gradual decrease in the repeatable increase and decrease of saturation degree [44]. This is due to moisture outflow due to vapour flux and inflow by capillary action.

With experiments similar to those conducted by Hartley and Black [45], Moya et al [44] have found that the boundaries of the container affects the soil temperature and hence the temperature and moisture distribution. They had used the solution of finite difference method of dimensionless equations derived from Philip and de Vries equations. Moya et al [44] concluded that it was not a dominant effect since the conductor temperature was well above that of the soil and the boundaries. However, Hartley et al [45] treated this differently by altering their numerical model to suit the disturbed problem due to the local boundaries.

Analysis has shown that:-

- Moisture migration is in two stages. Its rate decreases until a critical moisture content is achieved after which it increases rapidly.
- Critical moisture content (at which minimum rate of moisture migration occurs) is independent of rate of surface heat flux and is a function of the soil initial moisture content of given porosity.
- It is possible to predict soil behaviour under a larger heat source, provided the same porous medium is used.

Ewen and Thomas [50] have included sensible heat transfer into the heat and moisture transfer equations by which, observation shows that vapour flow is a powerful process at high temperatures but is the opposite under a moisture gradient. It involved a numerical solution using the finite difference algorithm that included up-winding differencing of convective terms and central differencing of the spatial analogues. The main argument was made towards the effective specific area for vapour flow, which Philip and de Vries implied and related to air content. Ewen et al [50] observed that this is not true as it is equal to porosity, not a function of air content.

Thomas [51] showed that non-linear coupling of heat and moisture transfer is important in unsaturated soil and if neglected, will significantly affect the variations of moisture content in soils. Unlike those numerically solved by finite difference methods [49, 50, 51], the equations of conservation of water and heat was solved by finite element method using the Galerkin formulation. The solution was compared to an uncoupled non-linear model and linear model of the same problem. It was concluded that modelling non-linearity of isothermal moisture diffusivities is important, as large variations in moisture content appear with low overall moisture content.

Assuming soil is incompressible, Radhakrishna, Lau and Crawford [52] utilised integrated finite differences that promise a good flexible solution for a variety of linear and non-linear boundary conditions. It dealt with material properties of both granular and fine-grained media whilst having some other advantages. Their solution was validated against a field test by Abdel-Hadi [53]. The shortcoming of this work however is the over-simplification of the assumptions - the surface volumetric moisture content is assumed zero – and unrealistic boundary conditions were simplified such as to ignore totally rainfall infiltration. This caused discrepancies between measured and predicted temperature and moisture values in one of their test cases [52].

2.4 METHODS OF PROBLEM SOLVING

The most popular methods in solving coupled moisture and heat differential equations over the years are to use either a finite element or a finite difference method. Either method has been proven to provide successfully results for the investigation of moisture and heat distributions around buried power cables.

A general partial differential equation that can be solved either by the finite element or finite difference method is

$$L_{diff}\mathbf{u} = \mathbf{f} \tag{2.12}$$

Where L_{diff} is the differential operator, **f** is a given function and **u** is the unknown function with appropriate boundary conditions.

In general, the finite difference method discretises the operator L_{diff} and the boundary conditions. Therefore as a solution, values of the function in the discrete points of the mesh as a solution are obtained. However, boundary conditions in the finite difference model are complex as compared to that of a finite element model.

Finite element analysis requires the integral formulation of (2.12). Therefore, the appropriate linear space of the finite element is discretised instead of the operator L_{diff}. Unlike the finite difference method, the solution obtained is a continuous solution in the whole area and not only at the nodes. In general, the finite element method can easily handle complicated boundary shapes and discontinuities in material properties. Accuracy can easily be obtained by reducing the size of the mesh elements. Boundary conditions in the finite element model are handled in a much simpler manner and therefore, the numerical solution obtained is more accurate.

From Table 2.1, it is obvious that finite element formulation is favoured more than the finite difference method regardless whether the soil under analysis is deformable or non-deformable.

RESEARCHERS	THEORY/APPROACH	COMPUTATIONAL METHOD
Dakshanamur-thy and Fredlund [27]	Temperature changes in soil converted to change in pore air pressure. Uses Darcy's and Fick's Law. Case: soil is compressible.	Forward finite difference. Two-dimensional.
Milly, [28]	Matric/potential based formulation. Hysteretic and inhomogeneity case.	One-dimensional. Galerkin finite element method.
Sophocleous, [29]	Matric based formulation. Moisture and heat flow in unsaturated-saturated porous media.	One dimensional solution using Crank-Nicholson implicit method
Moya et al [44]	Ignoring sensible and convection heat in energy balance equation; (original model of Philip and de Vries);Dimensionless time and radial distance	2-dimensional continuum model using finite volume methodology.
Hartley and Black, [45]	Case: homogenous and isotropic medium. Uses Darcy's Law and Fick's Law.Uses non-dimensionless time and radial coordinate	Implicit finite difference.
Thomas and Ewen, [50]	Included flow factor area in the moisture gradient term of the Philip and de Vries vapour flow equation.	Two-dimensional. Implicit finite difference.
Thomas, [51]	Included gravitational effect in moisture flow equation; Ignoring sensible heat transfer, convection effects in heat balance equation.	Galerkin finite element coupled with finite difference time-stepping scheme
Radhakrishna et al, [52]	Based on original Philip and de Vries model.	Integrated finite difference
Anders and Radhakrishna [43,54]	Ignoring sensible and convection heat in energy balance equation; uses original model of Philip and de Vries	2-dimensional triangular Galerkin finite element method.
Freitas and Lima, [55]	Phillip and de Vries model. Interpolation and extrapolation of soil properties.	Finite volume methodology.
Thomas and Sansom, [103]	Potential based formulation. Included air pressure as independent variables, effect of vapour flow due to bulk air flow. Uses Darcy's Law.	Finite element using finite difference time-stepping scheme. Galerkin residual approach.
Thomas and Li, [104]	Case: Non-deformable medium. Conduction, convection and latent heat of vaporisation are included in the Philip and de Vries heat balance equation.	Self-implicit finite difference by parallel processing.

Table 2.1 – Methods used by most researchers in solving heat and moisture transfer.

By comparison, the finite element approach is a more widely applied tool compared to the use of finite differences [54]. This may be the reason why finite elements are preferred when solving the highly non-linear coupled heat and moisture equations. Based on this knowledge, the approach of using finite elements has been used in this research.

2.4.1 The Employment of Soil Properties and Boundaries

Most researchers have opted to use constant thermal and hydraulic properties in solving simultaneous heat and moisture transfer problems. The use of constant values does not result in accurate temperature and moisture distributions. Dynamic soil properties are necessary in order to obtain accurate results.

Freitas and Lima [55] have used the non-linear dependence of temperature and moisture content of soil properties in their approach. Finite volume methodology is used instead of the general finite element or finite difference method. Soil properties are obtained from literature reviews, assuming that the soil is of the same category or kind as the one in the model. However, due to restrictions on computational time, they assigned soil properties at 20°C and 70°C, then interpolated and extrapolated the desired values at each iteration. This approach may not accurately represent soil properties at different soil moisture contents. A more accurate approach is to interpolate and/or extrapolate the values not only using assigned values at two temperature ends but also to account for the interpolation/extrapolation of values at two assigned values of two temperature and moisture ends.

Preece and Hitchcock [56] have investigated the effects of using constant and variable soil properties in solving heat and moisture transfer equations. It was found that simulations using constant soil properties lead to moisture changes at cable

surfaces in excess of the initial moisture content, which is invalid. Solving the heat and moisture equations using variable soil properties showed that extensive moisture migration occurs at temperatures well below 50°C. Although the Philip and de Vries model had been explicitly extended in their study, the incorporation of dynamic soil properties had not been fairly described. In their work, only the soil thermal conductivity that is variable to both temperature and moisture. Soil hydraulic properties that are used are variable only to moisture.

Buonanno, Carotenuto, Dell'Isola and Villacci [57] have included the effects of radiative and convective transfer on the boundary of their finite element model (single buried cable). This is to account for the environmental effects such as wind speed and solar radiation. However, the moisture distribution equation is neglected and soil thermal conductivity used in the model is constant, although three types of soil conditions are considered (dry sandy soil, vegetable soil and clayey soil).

Like Buananno et al [57], Kjellgren [58] had included the same environmental effects on the boundary to study ground surface temperatures of bare soil. Evaporation is used to describe the coupled moisture distribution boundary. The soil hydraulics and thermal properties are included in the problem as a function of moisture content. Simulated ground temperatures at depths of up to 15cm have shown agreeable results to measurements. However, there was increased uncertainty of surface temperatures at times of high solar radiation. This may be due to the fact that the moisture distribution equations considered have neglected the vapor phase of moisture transfer, which at low moisture contents, plays a major role in moisture migration. And unlike the Philip and de Vries equations, he had not separated the hydraulic conductivity induced moisture gradient term into both temperature and moisture terms. An improvement to this approach would be to use similar boundary conditions but with Philip and de Vries model and with the presence of a heated power cable.

2.4.2 FEMLAB

Over the last decade, researchers have benefited from the development of various, advanced finite element software packages in order to tackle real-world problems. Generally, these packages incorporate an automatic mesh generator, pre-processing and post-processing tools. Two well-known finite element software packages currently available are ANSYS and FEMLAB. At the beginning of this study, it was found that ANSYS does not easily allow the solution of simultaneous partial differential problems. However, this facility has now been developed although the application is indirect. It was decided to solve the simultaneous heat and moisture transfer equations using FEMLAB.

FEMLAB is an alternative that provides a better graphics-user-interface (GUI) environment. This package is used in conjunction with MATLAB. It has the flexibility in addressing the needs of users at different levels. Therefore, problems of simultaneous interactions of various physical phenomena can be easily tackled and visualised.

2.5 CONCLUSIONS

This chapter has presented a review on the processes of thermal drying and moisture migration. Possible modes of heat transfer within the porous medium are heat conduction, radiation and heat convective. Philip and de Vries have developed a model that explicitly describes the heat and moisture transfer phenomena in a porous medium. Heat transfer is attributed by the thermal conductivity of the heated porous medium under a thermal gradient and heat produced by latent heat of vaporisation under a moisture gradient. Whereas the moisture transfer is attributed by thermal moisture diffusivity under a thermal gradient and isothermal moisture

diffusivity under a moisture gradient. Moisture transfer occurs in two phases, liquid and vapour.

Other theories have also been discussed and although other scientists have made further extensions to the model, it has been decided that only the original Philip and de Vries equations will be used to promote simplicity and reduce computational time. This is due to the fact that the coefficients of the thermal and moisture gradients are highly non-linear.

In conclusion, it has been decided that the best way to understand the problem of moisture migration from buried cable circuits is to solve the Philip and de Vries theory of heat and moisture transfer equations simultaneously, using a two-dimensional finite element method. By solving the equations simultaneously, transient and steady state temperature and moisture are interactively determined between the equations. This gives the advantage of re-calculating the values of thermal and hydraulic properties concerned. Thus, accurate temperatures are achieved and the phenomena of thermal runaway and moisture migration can be accurately predicted.

For simplification, assumptions that the soil/backfills are homogenous, incompressible and a constant pressure have been applied. The presence of a chemical solute within the soil structure and the effect of mineral matter on the moisture/water movement have also been assumed negligible.

CHAPTER 3

3.0 SOIL PROPERTIES

Soil is basically comprised of solid particles, water and air. The particles are a product of physical and chemical weathering. Properties of soil depend on its shape, size, its distribution size within the whole mass and also the interaction between phases that form the soil. The factors determining its physical properties are shown in Table 3.1.

Characteristic	Physical properties
Shape, size of particles and its distribution	Classification, organic constituents, specific gravity
Soil phase composition	Water content, void ratio, saturation, degree of compaction, consistency
Deformation characteristics	Compression, shrinking, swelling, structure collapse
Hydraulic characteristics	Water movement, capillarity, thermal movement, permeability, gravitational movement

Table 3.1 - Soil characteristics and its physical properties.

A unit volume of unsaturated soil is depicted in Figure 3.1(a) and theoretically, can be rearranged as shown in Figure 3.1(b) [105]. The total volume of unsaturated water is defined as

$$V_T = V_s + V_w + V_a \tag{3.1}$$

Where V_T is the total unit volume of an unsaturated soil, constituted of water, air and solid particles; V_s, V_w and V_a are the unit volumes of solid particles or soil solids, water and air, respectively.

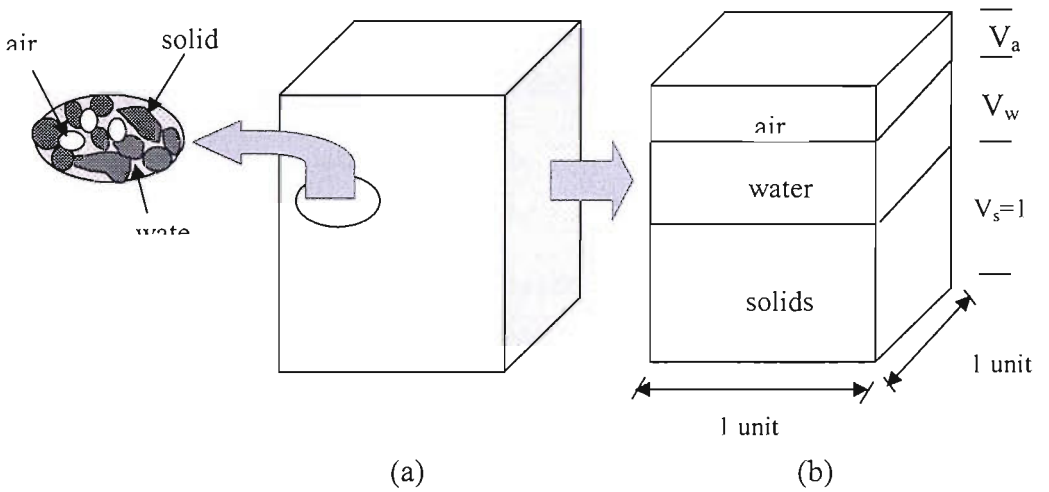

Figure 3.1 – Basic understanding of soil composition [105]. (a) Elementary volume of soil. (b) Soil composition.

Volume of voids, V_v, in a unit volume of an unsaturated soil is the total of those of water and air. This is as given in (3.2).

$$V_v = V_w + V_a \tag{3.2}$$

If V_T is selected such that Vs corresponds to one unit, the following basic soil properties can be determined [105] by referring to Figure 3.1(b).

- Void ratio, e, is defined as

$$e = \frac{V_v}{V_s} \tag{3.3}$$

- Degree of saturation, S, is defined as

$$S = \frac{V_w}{V_v} \tag{3.4}$$

- Gravimetric moisture content, θ_g is defined as

$$\theta_g = \frac{V_w}{V_v}\frac{1}{G_s} \tag{3.5}$$

Where G_s is a dimensionless unit called specific gravity, which represents the relative density of solid particles, ρ_s , with respect to that of water, ρ_w. G_s is defined [105] as

$$G_s = \frac{\rho_s}{\rho_w} \tag{3.6}$$

- Soil porosity, P_{or} is the ratio of volume of voids to the total unit volume of an unsaturated soil. This property is further explained briefly in Section 3.3. It is defined as

$$P_{or} = \frac{V_v}{V_T} = \frac{e}{1+e} \tag{3.7}$$

- Soil bulk density, ρ_b , is defined as

$$\rho_b = \frac{M_s+M_w}{V} = \frac{G_s(1+\theta_g)}{1+e}\rho_w \tag{3.8}$$

- Soil dry density, ρ_d , is defined as

$$\rho_d = \frac{G_s}{1+e}\rho_w = \frac{\rho_b}{1+\theta_g} \tag{3.9}$$

- Soil saturated density, ρ_{sat} , is defined as

$$\rho_{sat} = \frac{G_s}{1+e}\rho_w \tag{3.10}$$

3.1 SOIL CLASSIFICATION

Soils are classified according to the size distribution of their constituent particles. This is achieved with particle size analysis whereby soil is screened with sieves of different apertures. The amount of the soil passing each aperture is taken as a percentage of the total soil being analysed. The result is usually presented as a cumulative curve on a logarithmic graph showing the percentage of soil in each fraction. Prior to analysing, the soil is oven-dried and only the amount passing through a sieve with mesh size of 2mm is considered as representative of data medium. Reports are presented separately if gravels or larger sized particle are present.

British Standard 1377 (1975) gives a standardised procedure of the laboratory size distribution analysis. This method outlines that the oven-dried soil is shaken through a nest of sieves, manually or mechanically. The masses retained on each sieve are determined and used to calculate the percentages passing each sieve.

An example of size distributions for sand, clay, silt and gravel obtained from software package SoilVision are as shown in Figure 3.2. Details of the soils are listed in Table 3.2.

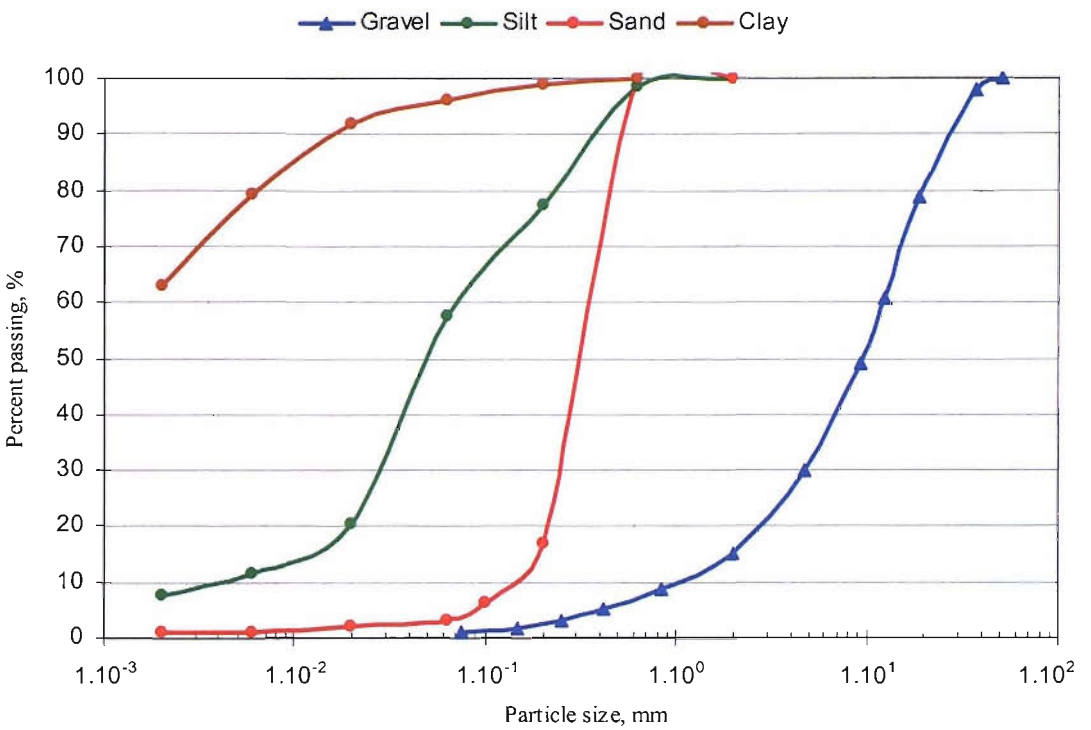

Figure 3.2 - Particle size distribution of typical soils taken from SoilVision.

SOIL	SOIL	DESCRIPTION
Clay	10982	Seelow clay. Tested by U. Schindler, Inst. of Hydrology, Centre for Research on Agricultural Landscapes and Land Use (ZALF), Muncheberg, Germany.
Silt	10844	Muenchehagen II. Tested by W. Ehlers, Inst. Agronomy and Plant Breeding, Goettingen, Germany.
Sand	11477	Berlin medium sand. Tested by E. Vetterlein, Inst. fuer Bodenkunde, Germany.
Gravel	11555	Waste rock. Tested by Greg Herasymuik (origin unknown)

Table 3.2 - Details on type of soils taken from SoilVision software package.

Based on the analysis, one could then class the soil under investigation using the classification scale set by The British Standard Institute (Table 3.3). The categories for silt and sand are subdivided into three other classes; fine, medium and coarse. Those which fall into the fraction of less and more than 2μm, are classified as clay and gravel respectively.

TYPE OF SOILS		EFFECTIVE DIAMETER
Clay		Less than 2μm
Silt	Fine	Between 2μm and 6μm
	Medium	Between 6μm and 20μm
	Coarse	Between 20μm and 50μm
Sand	Fine	Between 50μm and 200μm
	Medium	Between 200μm and 500μm
	Coarse	Between 500μm and 2000μm
Gravel		More than 2000μm

Table 3.3 - Soil classification according to British Standard Institute.

A term to describe the quality of the soil gradation is called the coefficient of uniformity. This is a ratio of weight of particles being 60% finer (or also known as D_{60}) to that of 10% finer (D_{10}). According to a general specification for civil engineering work in Hong Kong, a well-graded material consists of material that has a coefficient of uniformity exceeding 10 whilst a uniform-graded material consists of material that has a coefficient of uniformity of 10 or less [60].

3.2 MINERAL MATTER IN SOIL

Quartz (SiO_2) usually dominates the non-clay fraction because of its resistance to weathering and its abundance in certain parent materials such as granite, sandstone and surface deposits. Other constituents are feldspar, calcite and mica. The main minerals of the clay fraction are secondary products of weathering. The clay minerals are namely 'flaked' kaolinite, illite and 'needled' halloysite crystals or montmorillonite. These minerals have large surface area per unit volume. The surfaces of these crystalline particles have negative charges, therefore attracting water molecules for adsorption. This leads to swelling of clay in the presence of water.

The amount of mineral consisting in a sample soil contributes to the determination of its overall thermal and physical properties. For example, sand consists mainly of quartz. Quartz has a high thermal conductivity compared to other soil constituents. Therefore, sand has better thermal properties than silt or clay.

3.3 SOIL POROSITY

Porosity is defined as ratio by volume of voids to the total volume of the soil sample. Typical values for sand ranges from 0.3 to 0.5 and for clay, porosity is greater than 0.9. Since clay has finer particles, it could be concluded that fine grains have greater porosity. Therefore, soil porosity is often associated with the shape of soil particles. Fine sand usually consists of a greater proportion of flat, plate shaped particles than bulky ones whereas clay consists of sheeted crystal structure and needle shaped particles. Soil porosity has a large influence on the magnitude and rate of moisture migration. A property that is closely related to porosity is known as voids ratio. It is defined as the ratio of voids by volume to the volume of solids in a sample soil or aggregate. Soil porosity is as defined earlier in (3.7).

3.4 SOIL WATER

Moisture content is defined as the ratio of the weight of water present in the soil to the weight of dried soil. Higher moisture content helps to reduce the thermal resistivity of the soil/backfill as a whole as water has a high thermal conductivity compared to air. Changes of moisture content are seasonal as evaporation increases when the ambient temperature increases during the summer [11, 61]. Fluctuations occur as moisture is lost to evaporation to the atmosphere and moisture is regained by rainfall. Soil moisture content increases with increasing depth. Due to variations in moisture content according to seasons, a 'moisture control' season is established and in the UK it is from 1st of April until 31st October. This is a period when evaporation is expected to be crucial to the cable environment [17].

Optimum moisture content will permit greatest compaction. This is due to the fact that moisture provides the lubrication needed to overcome the friction that keeps particles from sliding into empty spaces.

Effects of moisture content on soil properties include [62] :-

- Thermal conductivity. An increase in moisture content results in a further increase in thermal conductivity.
- Heat capacity. Steadily increases with moisture content. This is due to the fact that water has a high capacity for storing heat.
- Thermal diffusivity. Maximum at relatively low moisture content and after certain moisture content is reached, decreases with increasing moisture content.

3.4.1 Phenomenological and structural basis

Soil water shares a large amount of interfacial area with the solid phase and gas phase. Interaction between these phases has a great influence on the moisture movement and water retention of the soil. There are two perspectives in which soil water is present although they are more generally classified to hygroscopic, adsorbed, capillary and combined water [63, 64]. These are known as phenomenological and structural basis. Phenomenological basis is described by the following.

- Ground water: It fills voids only at its subsurface and is subjected to no other forces but gravity. This water would be first to be removed under the influence of temperature.

- Capillary water: Water is lifted from the ground water table by surface tension. Two zones are created, a zone of capillary saturation where water fills pores and a zone of open capillaries where larger pores contain air and smaller ones hold water connected to ground water by a network of pores.

- Adsorbed water: This type is held on grain surfaces. This would be the last to be removed under influence of temperature.

- Film water: This forms thin films of ordinary water surrounding grains due to surface tension.

Structural basis is described by the following.

- Pore water: Pore water is mobile under hydrodynamic forces. They exhibit physical and chemical properties of ordinary water.

- Solvate water: Solvate water is subjected to polar, electrostatic and ionic binding forces.

- Adsorbed water: Surrounding surfaces of particles, it is immobile or cannot be removed by hydrodynamic forces.

- Structural water: It can only be driven off at high temperatures such to cause destruction of the soil structure.

A phenomenon that involves changes in soil moisture content is associated with pore water and solvate water. Under normal variations in temperature and pressure, adsorbed and structural water are constant. These categories are illustratively described in Figures 3.3 and 3.4. The capillary forces determine moisture content in soil in the absence of gravitational rain and surface evaporation. This action of capillary forces is more pronounced in loamy soils compared to other soils.

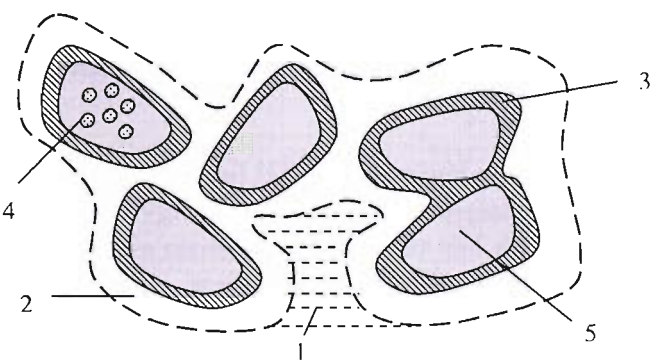

Figure 3.3 – Structural water forms [107] .1-pore water. 2-adsorbed water. 3-solvate water. 4-structural water. 5-solid particle

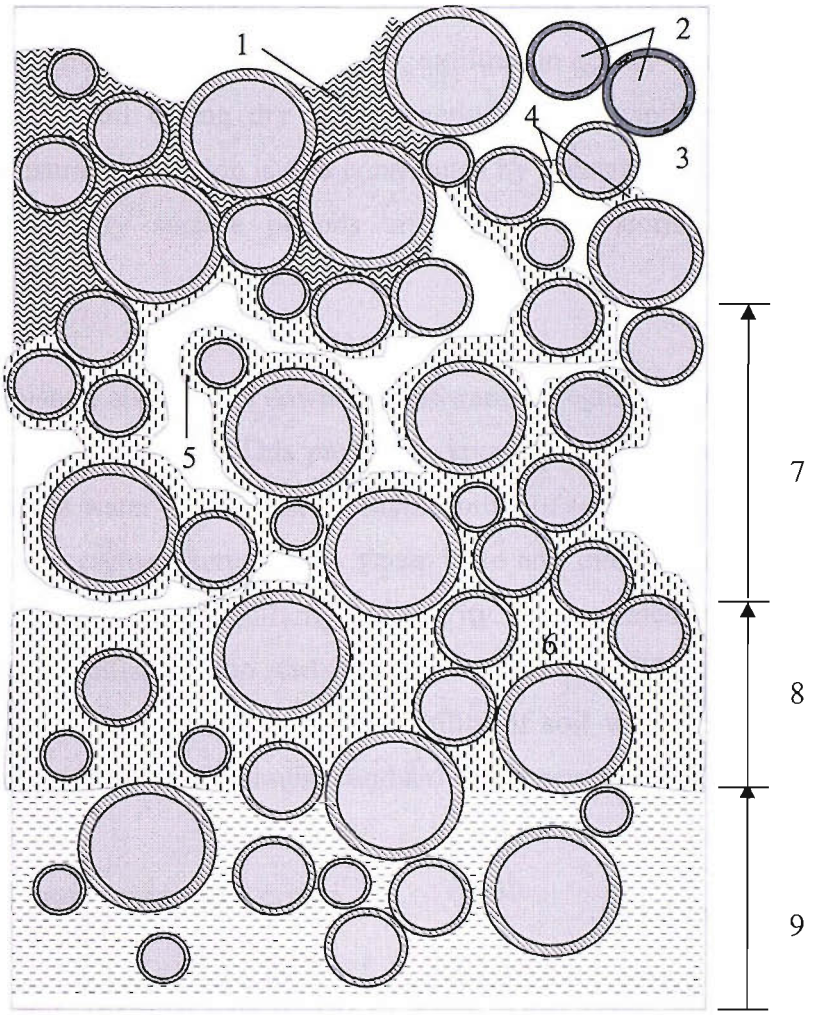

Figure 3.4 – Water forms in soil [107]. 1-perched gravitational water. 2-solid particle surrounded by hygroscopic water. 3-saturated water vapour. 4-contact water. 5-water film. 6-open capillary water. 7-air and water. 8-capillary saturation zone. 9-ground water.

3.5 SOIL WATER/MOISTURE MOVEMENT

There are three predominant factors in the movement of the liquid phase in soil, the interaction between infiltration and exfiltration, percolation and capillary rise. Infiltration is an occurrence when liquid moisture diffuses into soil during wet surface periods under capillary action and gravity. Moisture content reduces with

increasing depth of penetration and hence capillarity is reduced, this process is dominated by gravity. On the other hand, exfiltration occurs when liquid moisture diffuses out of soil during dry surface periods when capillary action opposes gravity. Moisture exfiltration is also contributed by vegetation extract at root depth. Both wet and dry surface periods are known as 'storm' and 'interstorm' respectively.

Soil moisture also travels downwards towards a region almost saturated above the water table by gravity. This process is known as percolation. The downward speed of surplus water depends on the permeability of soil and the rate of rise of the water table. At regions between the water table and intermediate zone, moisture movement is governed by capillarity and gravity. The intermediate zone is the zone where upward capillary action starts to oppose percolation. There are two hydraulic properties that are used to quantify the ability of soil water movement in soils. These are soil suction and hydraulic conductivity or permeability.

3.5.1 Soil water retention curve

The relationship between the quantity of water at any given point in a soil profile and its equivalent potential energy is known as the water retention curve. This property depends on the texture and structure of soil as the water content changes with pore size as water is lost or gained. For example, sand releases water more quickly than clay. Water hysteresis occurs in soil due to the different behaviour of wetting and drying of within soil structure. Wetting of soil takes a different curve than drying of soil and it is a complex process. However, in this study the effect of hysteresis on moisture migration has been ignored for reasons of simplification. Only the drying part of the hysteresis curve is considered since it is associated with moisture migration during thermal runaway. Soil water retention curves for typical sand, silt, clay and gravel taken from SoilVision are as shown in Figure 3.5.

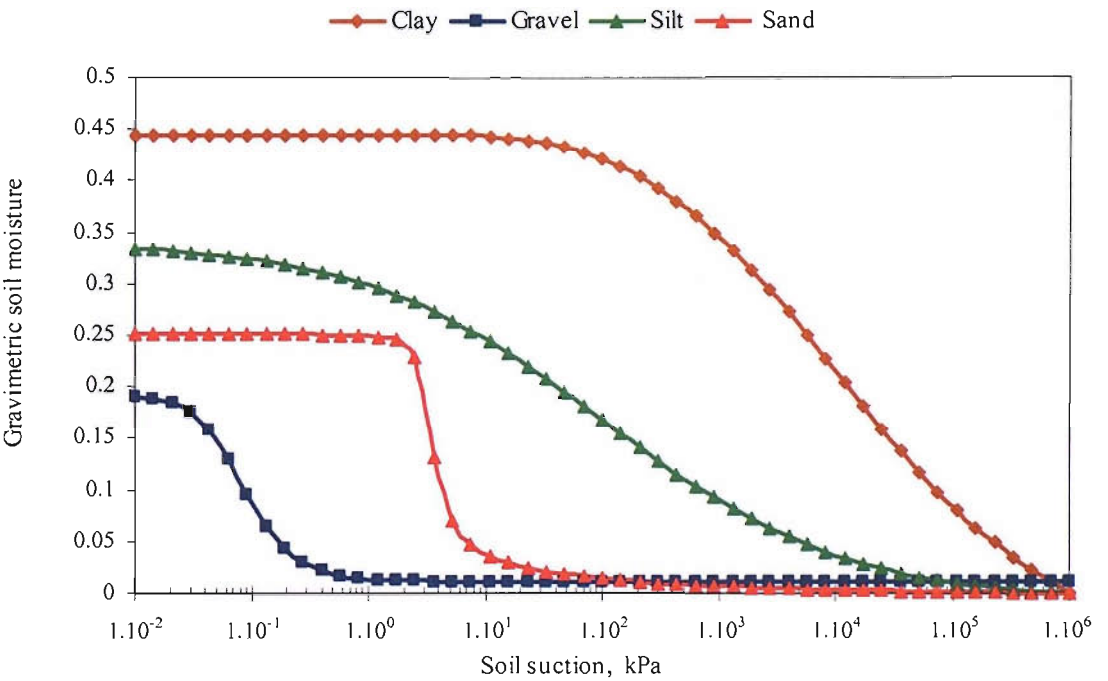

Figure 3.5 - Soil water retention curve for typical soils (taken from SoilVision) described in Table 3.2.

3.5.2 Hydraulic permeability

Hydraulic permeability is closely related to soil suction. It measures how easily the water moves under capillary action and it differs for various types of soil. In heat and moisture transfer, hydraulic permeability is influenced by gravity. Soils with large particle size generally have greater hydraulic permeability compared to those with smaller particle size. For example, sand has a higher hydraulic permeability than clay or silt at high moisture contents.

Hydraulic permeability for the types of soils (taken from SoilVision) mentioned in Table 3.2 is as shown in Figure 3.6.

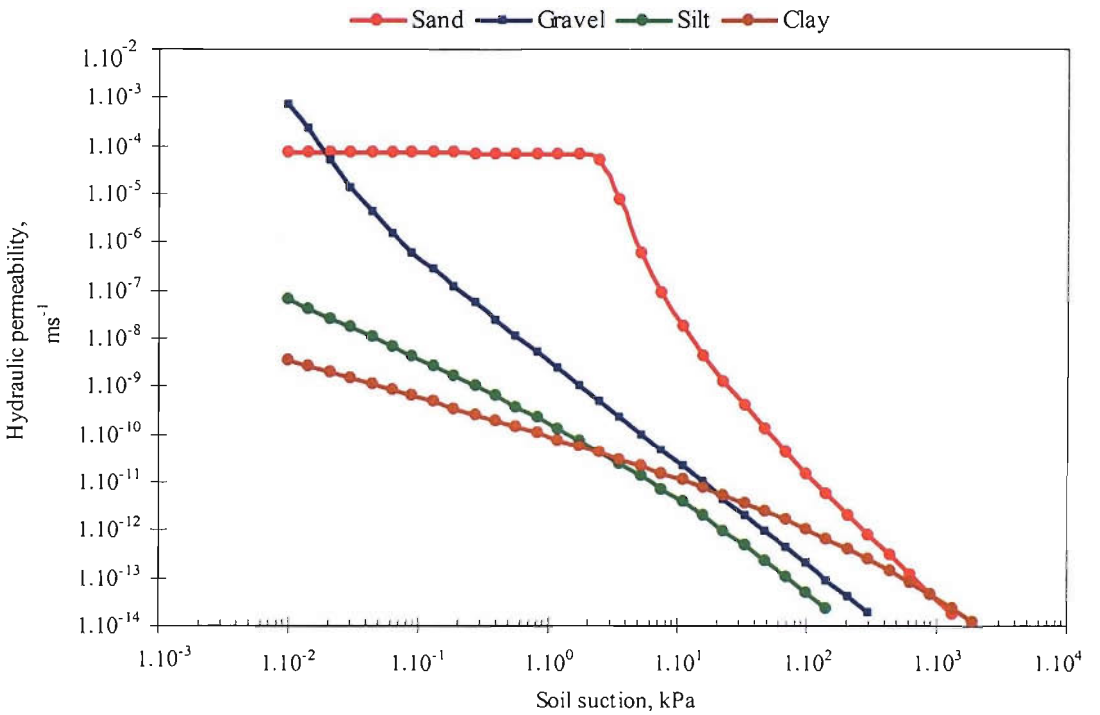

Figure 3.6 - Hydraulic permeability for typical soils (taken from SoilVision) described in Table 3.2.

3.6 SOIL THERMAL RESISTIVITY

The thermal resistivity of the soil depends on the thermal resistivity of its single components and their relative volume and the soil mineral composition. Considering the constituents of soil, the thermal resistivity of minerals such as quartz and granite are the lowest, followed by that of water, organic matter and air. Low thermal resistivity in soil is achieved by containing the maximum amount of quartz and the minimum amount of air as possible. Although thermal conductivity of water is less than that of soil solid particles, water soil increases the thermal conductivity of the soil as a whole [62]. Table 3.4 shows the value of typical thermal conductivity of various soil constituents.

	SPECIFIC HEAT CAPACITY $kJkg^{-1}°C^{-1}$	DENSITY $(10^3)kgm^{-3}$	VOLUMETRIC HEAT CAPACITY $MJm^{-3}°C^{-1}$	THERMAL CONDUCTIVITY $Wm^{-2}°C^{-1}$
Air (20 °C)	1	0.0012	0.0012	0.025
Water	4.2	1.0	4.2	0.6
Ice (0 °C)	2.1	0.9	1.9	2.2
Quartz	0.8	2.7	2	8.8
Clay minerals	0.8	2.7	2	2.9
Organic	2.5	1.1	2.7	0.25

Table 3.4 - Thermal properties of soil constituents.

An experiment conducted at the Ontario Hydro Research Laboratory on particles of 1mm and larger showed that grain shape and size influences thermal properties. The latter being more significant than the former [65]. Thermal resistivity increases with decreased particle size. Saturation moisture content increases with decreased dry density because the amount of space to be filled by moisture increases when dry density is decreased. Therefore, the density of the soil more or less affects the thermal resistivity. Soils with coarser components that are individually dispersed in a matrix of cohesive components have lower thermal resistance than that of soils with continuous granular skeleton and finer materials at its interstices; at the same dry density and moisture content.

Using a 'soil thermal tester' in investigating moisture migration in cable backfills, Halfter et al [6] concluded that maximised dry density with better compaction does not result only in a decrease in soil thermal resistivity, but also a decrease in average rate of growth of overall thermal resistivity and lessens the susceptibility of the material towards moisture migration considerably. Halfter et al

[6] looked at two types of backfill; decomposed granite (red earth originating from decomposed granite) and decomposed rhyolite. The granite backfill is a clayey coarse-grained soil whereas the rhyolite backfill is fine-grained clayey silt with sand.

It was observed that although clayey silt backfills have low average rates of growth in overall thermal resistivity and good affinity to moisture, they only show good thermal properties under very wet conditions. Its thermal resistivity becomes unacceptable for lower moisture contents. As for coarse-grained soils, with the sufficient moisture content, they possess favourable thermal properties for cable trench backfill performance.

3.6.1 Methods of Measurement

The method of measuring thermal conductivity of soil falls into two basic categories; steady state and transient methods. The steady state method employs an apparatus whereby a volume of sample soil is tested with its two ends maintained at hot and cold temperatures. This is to initiate a temperature gradient. When thermal equilibrium is reached, the thermal conductivity is calculated from the temperature gradient and the heat flux employed. However, the reliability of this method is questionable as moisture content of the soil experiences redistribution at the region near the hot end/plate. Therefore, the moisture content at that region appears to be much lower than the average bulk moisture content and the opposite of the region near to the cold end/plate.

Measuring thermal conductivity using the common thermal probe method is a transient type method. Careful consideration given to the design of the ideal probe can result in obtaining a very reliable result. This is because steps taken in the design stage can guarantee that the measurement will not suffer from moisture

redistribution. Unlike the steady state method, the thermal probe is robust and therefore, measurements can be performed outside laboratory.

3.6.2 Specific Heat Capacity of Soil

Heat capacity of soil can be estimated from the total weighted mean of volumetric heat capacities of its constituents. This is because by nature, soil is heterogeneous containing water, air, organic material and minerals in various proportions.

Referring to Table 3.4, an example can be taken in calculating say, a soil with 0.1, 0.35, 0.02 and 0.53 by volume of air, water, organic matter and clay mineral respectively. Based on weighted mean of the volume of each constituent, the soil is calculated to have a volumetric heat capacity of 2.6×10^3 kJ m^{-3} $°C^{-1}$.

3.7 PROPERTIES OF SOIL UNDER INVESTIGATION

The soil used in this project is a sand taken from a quarry in Swindon. It is a typical sand used by the National Grid plc in trough cable bedding. This soil is referred to in this thesis as soil SWN1. A series of experiments and calculations have been undertaken in order to characterise SWN1. Obtained results are described in the following sections.

3.7.1 SoilVision

A software package called SoilVision has been used to assist in obtaining a thorough understanding of soil properties. It is also a database of almost 3,000 different soils ever reported and therefore it is useful in comparing properties of different types of soils. Dr. Murray D. Fredlund whom is a well-known researcher

in soil physics from University of Saskatchewan, Canada developed the package in 1999. Realising that definition to soil properties for input to computer-based models often proves to be a difficult problem, he combines knowledge-based systems with geotechnical engineering.

With SoilVision, estimations of several properties whereby experimental apparatus are unavailable can be obtained. This is made possible using curve fitting of pseudo-transfer functions (PTF) reported in several relevant journals. The method that offers the best fitting is chosen to estimate the property of interest. Therefore, the advantage of using the software is that it combines experimental data with the ability to predict unsaturated soil properties when several essential data are unknown or missing. Apart from allowing estimation of missing soil data, it also provides indication of the likely variability of the estimated data.

3.7.2 Grain Size Distribution

Grain size distribution of SWN1 is determined using the dry-sieve method, BS1377-1975, part 7B. The equipment used is an electromagnetic sieve shaker called 'analysette-3' that consists of a number of different apertures of woven mesh sieves [66]. The mesh sieves are compliant to BS 410/3310. The schematic of the mechanical shaker is as shown in Figure 3.7. The final distribution is taken as an average of three test results. The average is shown in Table 3.5 and its distribution on the logrithmatic graph is shown in Figure 3.8.

The result is entered into the SoilVision database and a distribution graph is obtained. It is classified by the United States Department of Agriculture, USDA standard as sand. Its coefficient of uniformity, C_u is 2.19, with D_{10} and D_{60} equals to 0.3309 and 0.7246 respectively. The coefficient of uniformity indicates that soil

SWN1 is fairly uniform-graded sand. The lower this value, the more uniform the size of the particles of the soil.

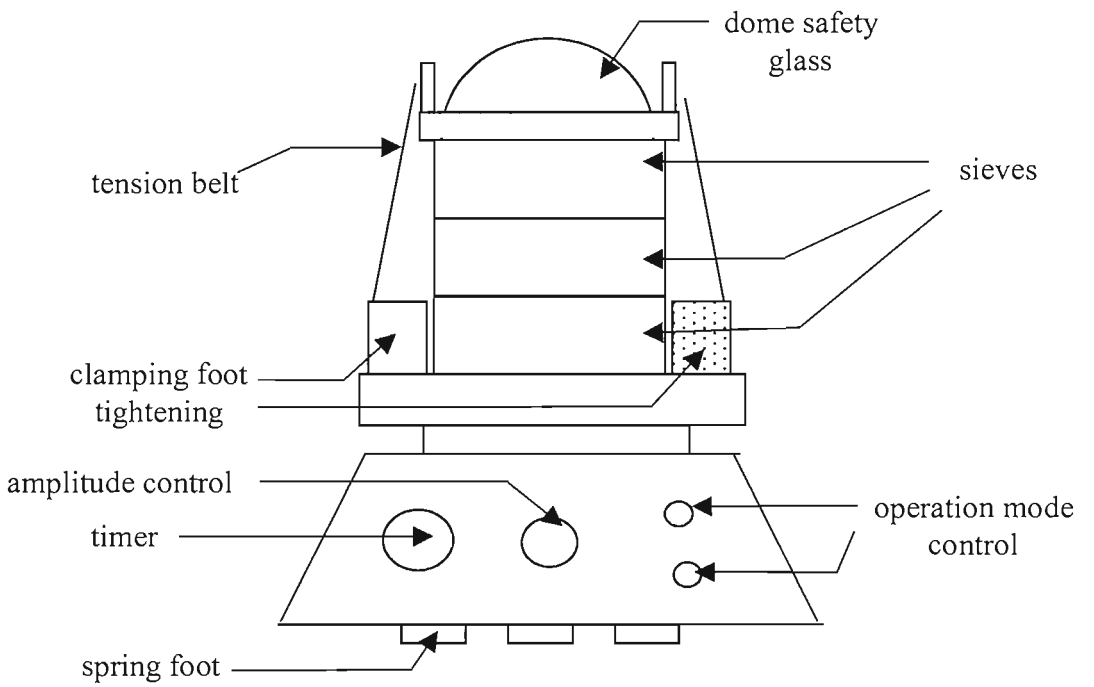

Figure 3.7 - Schematic diagram of the mechanical shaker.

According to the Unified Soil Classification System (USCS), soils can be classified into 15 different groups. The groups are well-graded gravel, poorly graded gravel, gravel with sand, clayey gravel, well-graded sand, poorly graded sand, silty sand, clayey sand, peat, silts of low and high compressibility, clays of high and low liquid limits and organic soils of high and low plasticity. The categorisation is based on the textural basis of the soils; coarsely grained, finely grained and highly organic. It can be seen from Figure 3.7 that SWN1 consists mainly of almost sand, without the presence of gravel. Its particle size ranges from 0.03mm to 2.36mm.

APERTURE SIZE	PERCENTAGE (%)
75 μm	1.76
150μm	7.18
300μm	33.29
600 μm	48.76
1.18 mm	7.69
2.36 mm	1.27
4.75 mm	0

Table 3.5 – Percentage retained per aperture size soil SWN1.

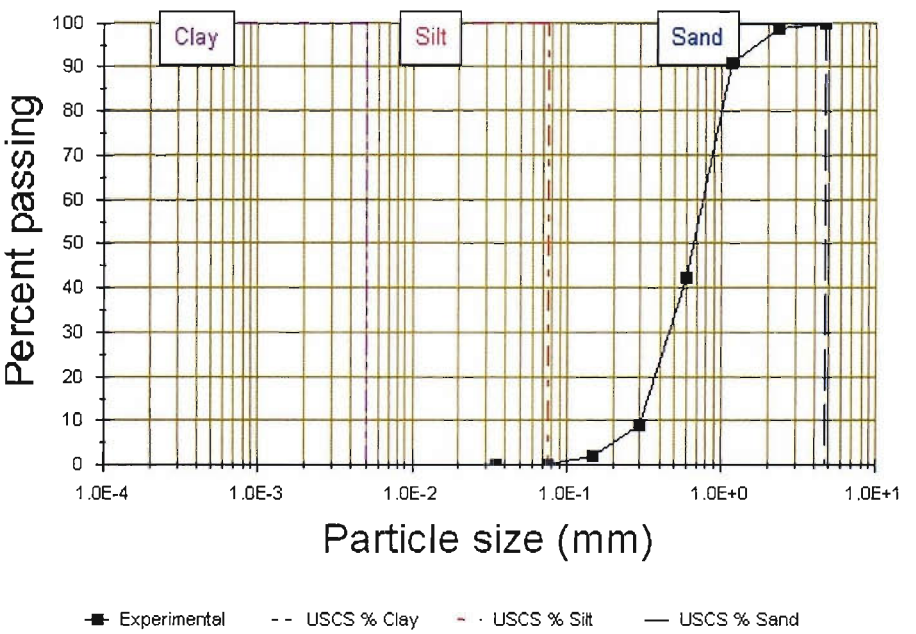

Figure 3.8 - Grain size distribution of SWN1. USCS : Unified Soil Classification System.

3.7.3 Experimentally Determined Property – Soil Suction

The water-holding or soil suction characteristics of soil SWN1 have been determined experimentally using a 5 bar pressure plate extractor (Figure 3.9).

Figure 3.9 - Pressure plate extractor.

This equipment consists of a porous ceramic plate, covered on one side by a thin neoprene diaphragm, sealed to the edges of the ceramic plate such as shown in Figure 3.10. There is a screen between the plate and the diaphragm. This screen provides a route for water flow. The route of the water flow is connected to an outlet tube fitting via an outlet stem, which connects to the outside of the equipment.

On the surface of the ceramic plate, soil samples retained by plastic rings are placed. These are then saturated with water and mounted on the pressure vessel. Excess water is forced out of the outlet tube as air pressure in the chamber is increased. The outflow will flow through the microscopic pores of the ceramic plate and then, the screen before flowing out through the outflow stem.

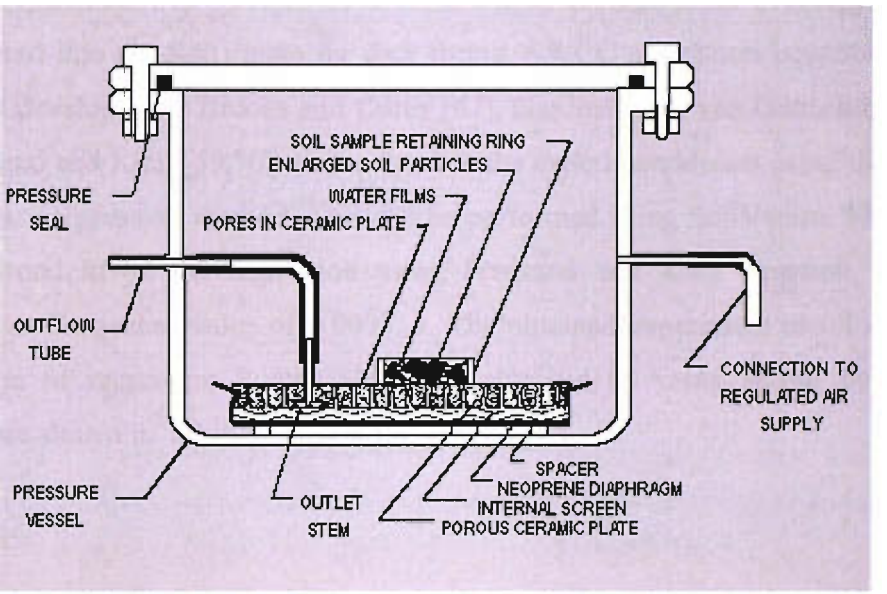

Figure 3.10 - Cross section of the pressure plate extractor.

Pore size determines the maximum air pressure that a wetted ceramic plate can support before letting air pass through its pores. The smaller the pore size, the higher the air pressure that the pore can support without draining. The pressure value capable of breaking down the meniscus formed by water surface tension is called the bubbling pressure or the air entry value for the porous plate.

Pressure plate cells must be used at air pressure values below the air entry value for the cell. At any given air pressure in the extractor, water flows through the pores in the soil sample and the ceramic plate until the effective curvature of the water films in the soil are the same as the pores in the plate. At that time, water flow ceases since equilibrium is reached between the air pressure in the extractor and the soil suction. Hence, there is an exact relationship between air pressure in the extractor and the moisture content in the soil samples. The result obtained is therefore, the soil water characteristic curve (SWCC) and it represents the ability of the soil to store water.

The experiment was repeated three times and an average of the obtained results were entered into the SoilVision for data fitting. SWCC estimation equations that have been developed by Brooks and Corey [67], Gardner [68], van Genuchten [69] and Fredlund and Xing [59,70] can be fitted to the experimental data using the non-linear square regression method. This can be performed using SoilVision. The best fit was found to be the regression using Fredlund and Xing equation, which produced an R-squared value of 0.999714. The obtained experiment result and its comparison of regression R-squared values obtained by using fitting by other methods are shown in Table 3.6 and 3.7 respectively.

SUCTION, KPA	GRAVIMETRIC MOISTURE CONTENT, θ_g
1.38	0.220
2	0.054
6	0.018
7	0.011
10	0.009
14	0.016
50	0.010
200	0.007
300	0.003
400	0.004

Table 3.6 - Experiment result of the soil suction experiment.

Fitting the experimental data using the Fredlund and Xing SWCC equations gives an advantage of employing the estimation in the Philip and de Vries heat and transfer equations, which shall be discussed in the next chapter.

SWCC FITTING METHODS	R-SQUARED
Fredlund and Xing [70]	0.999714
Brooks and Corey [67]	0.9923654
Gardner [68]	0.9983
Van Genuchten [69]	0.9519367
Van Genuchten/Burdine [69]	0.9983213

Table 3.7 - Comparison of SWCC data fitting with regression R-squared value.

The relationship between soil suction and gravimetric moisture content according to Fredlund and Xing formula of SWCC is given by (3.11).

$$\theta_g=\theta_s\left[1-\frac{\ln\left(1+\frac{\psi}{h_r}\right)}{\ln\left(1+\frac{1\times10^6}{h_r}\right)}\right]\left[\frac{1}{\left(\ln\left(e^1+\left(\frac{\psi}{a_f}\right)^{n_f}\right)\right)^{m_f}}\right] \tag{3.11}$$

Where θ_g is gravimetric moisture content, θ_s is saturated gravimetric moisture content, ψ is soil suction, (kPa), h_r is suction at which residual moisture content occur, (kPa); a_f is soil parameter, primarily a function of air entry value of soil, (kPa); n_f is a soil parameter, primarily a function of the rate of moisture extraction from the soil once air entry value is exceeded; m_f is a soil parameter, primarily a function of residual moisture content of soil. Values of the constants obtained from SoilVision are available in Table 3.8 and the water retention curve is as shown in Figure 3.11.

CONSTANTS	VALUE
m_f	0.7523522
h_r	1.895168 kPa
a_f	1.442746 kPa
n_f	21.8698
θ_{sat}	0.2546

Table 3.8 - Value of SWN1 constants for (3.11).

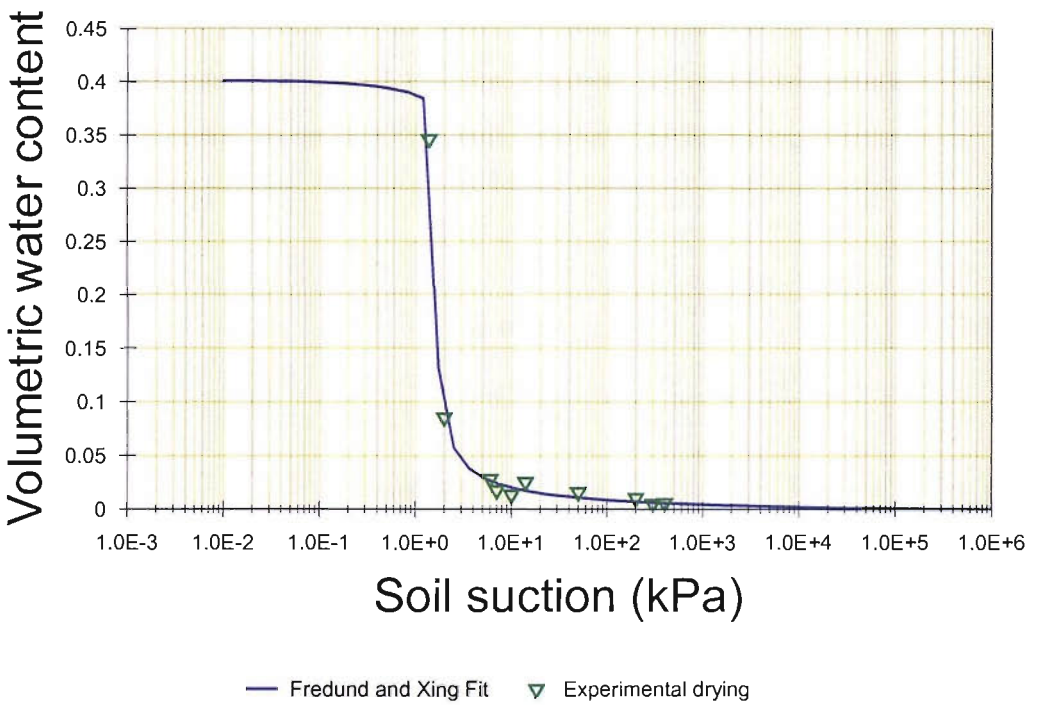

Figure 3.11 - Soil water retention for soil SWN1.

The fitted SWCC data can be expressed in terms of soil suction as a function of volumetric moisture content, θ. If this is preferred, θ_g is replaced with θ and the saturated volumetric moisture content, θ_{sat}, for SWN1 obtained from SoilVision is 0.4. A 95% confidence interval is calculated for the fitted data.

Assuming a t-distribution of errors, the result is as the following

$$\theta = 0.4x\left[1-\frac{\ln\left(1+\frac{\psi}{h_r}\right)}{\ln\left(1+\frac{1\times10^6}{h_r}\right)}\right]\left[\frac{1}{\left(\ln\left(e^1+\left(\frac{\psi}{a_f}\right)^{n_f}\right)\right)^{m_f}}\right] \pm 7\% \qquad (3.12)$$

Soil suction is proportional to water surface tension, σ (3.13). Given this relationship and manipulating (3.12) for a given reference temperature (room temperature is assumed to be at 20°C), soil suction at different temperatures can be determined [71, 72].

$$\psi \alpha \sigma \qquad (3.13)$$

$$\psi(\theta,T) = \frac{\sigma_{ref}}{\sigma_T}\psi(\theta)_{ref} \qquad (3.14)$$

Where σ is water surface tension, (Jm^{-3}), σ_{ref} is water surface tension at reference temperature, (Jm^{-3}), σ_T is water surface tension at temperature T, (Jm^{-3}), $\psi(\theta)_{ref}$ is suction at reference temperature, (kPa).

Obtaining data from Mayhew and Rogers [73], water surface tension, σ, can be expressed in terms of temperature, T (°C) using

$$\sigma(T) = 0.1171\text{-}0.0001516(T+273) \quad (3.15)$$

3.7.4 Saturated hydraulic permeability, k_{sat}

The saturated hydraulic permeability of soil SWN1 can be estimated using the algorithms provided in SoilVision. This parameter is essential in calculating unsaturated hydraulic permeability, k_{unsat}. The applicability of most of these estimation methods on a wide range of soils is explicitly defined. Therefore, a method that calculates the most reasonable value has to be chosen. Referring to a value possible for any typical sand, the estimation produced by the USBR method [74] seems to be the most reasonable value. (USBR formula is the formula recommended for materials comprising the medium-grain sands with a coefficient of uniformity of less than 5). It also gives a smaller confidence limit since the applicability is narrowed to only soils that have a coefficient of uniformity less than 5% and medium grained sands, criteria that SWN1 readily satisfies.

The USBR formulation is

$$k_{sat} = 0.36 D_{20}^{2.3} \quad (3.16)$$

Where D_{20} is grain diameter, with 20% coverage on the grain size distribution curve, (mm); k_{sat} is saturated hydraulic permeability, (ms^{-1}).

D_{20} for SWN1 is 0.4384 mm. Therefore, the estimated saturated hydraulic permeability is 5.403×10^{-4} ms^{-1}.

3.7.5 Unsaturated hydraulic permeability, k_{unsat}

The k_{unsat} of SWN1 can also be estimated using SoilVision. The estimation equations available in SoilVision for predicting soil k_{unsat} are reliable because they are chosen for their better prediction and application capabilities [59]. This is the only reasonable alternative for determining k_{unsat} when laboratory measurements are not possible.

The estimation equations available include those from Kunze [75], Fredlund and Xing [76], Campbell [77], Mualem [78], modified Campbell [79], van Genuchten [69] and Brooks and Corey [67]. All of the methods require Fredlund/Xing, van Genuchten or Brooks/Corey SWWC curve as an input. However, only methods that use Fredlund SWCC are considered in the process of selecting the best estimation for k_{unsat}. This is due to the fact that Fredlund/Xing SWCC curve-fitting method provides the best fit for SWN1. The k_{unsat} estimation methods under consideration are that given by Campbell [77], modified Campbell [79] and Fredlund/Xing [76].

Since the unsaturated hydraulic property of SWN1 is not experimentally determined, there should be a guideline to which fitting would give the best and most realistic estimation. Using the SoilVision soil database, a query was made to look for soils that are sand and have almost the same physical characteristics as SWN1. The specific criteria are soil that has effective grain diameter between 0.2mm and 0.5mm, percent of coarse grained less than 1% and has its k_{unsat} experimentally determined. The experimental data has to be more than 3 and determined over a fairly wide range of soil suction for reliability of estimation.

There are four possible soils that fit the pre-determined criteria and their unsaturated hydraulic permeability are compared with that from the SWN1 estimation of k_{unsat}. Details of the sands obtained from the query wizard are tabulated in Table 3.9 and the comparison of experimentally determined, unsaturated hydraulic permeability of these soils with that estimated for SWN1 is as shown in Figure 3.12.

SOILS SIMILAR TO SWN1	DETAILS
11062	Hard sand. Tested by P. Luescher, Eidgenoessische Forschungsanstalt, Switzerland
11187	Ulen sand from frigid Aeric Calciaquoll family. Tested by W.M. Schuh, State Water Commission, Russia.
11474	Berlin coarse sand 1. Tested by E. Vetterlein, Instituet fuer Bodenkunde, Germany.
11477	Berlin coarse sand 4. Tested by E. Vetterlein, Instituete fuer Bodenkunde, Germany.

Table 3.9 - Details of soil used for unsaturated hydraulic permeability comparison.

It was shown in Figure 3.11 that estimation using Fredlund and Xing pseudo-transfer functions (PTF) has the best curve for sands that are similar to SWN1. Estimations using PTFs developed by van Genuchten, Brooks and Corey and Campbell seem to have large predicting error for soil suctions greater than 1 kPa. The curves fitted by these methods seem far off from the permeability curves of any of the soils. Therefore, it was decided that estimation of k_{unsat} using the Fredlund and Xing method would be the best one to describe SWN1 unsaturated hydraulic permeability.

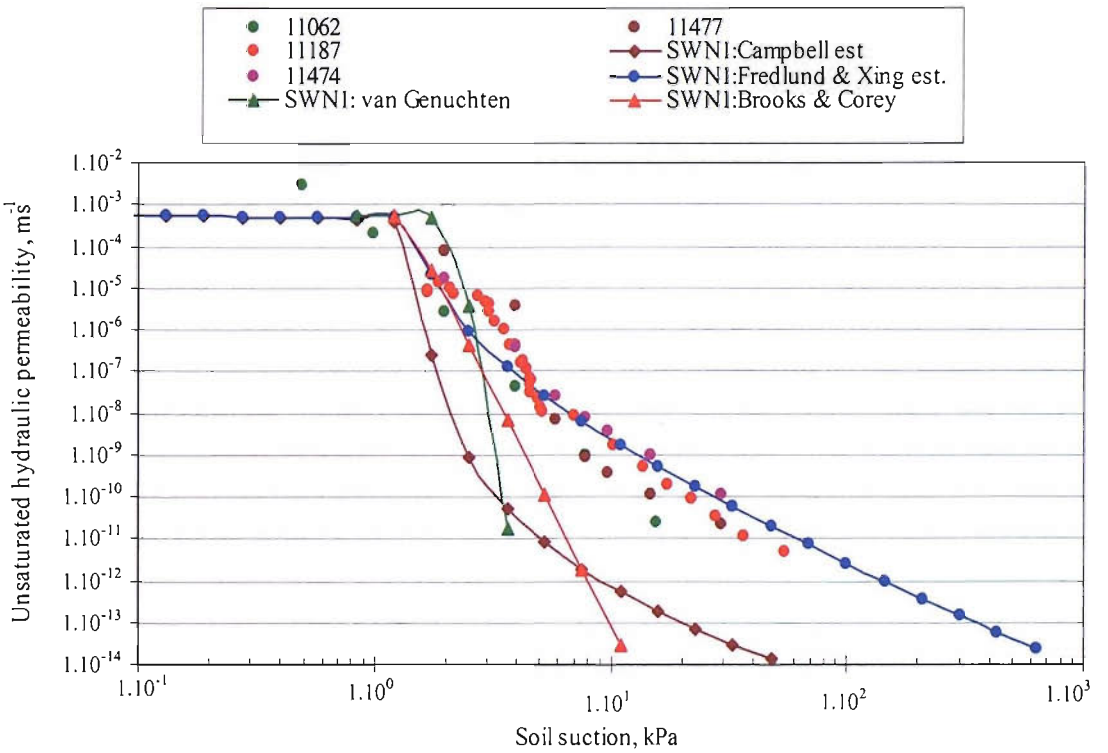

Figure 3.12 - Unsaturated hydraulic permeability of soils similar to SWN1.

The Fredlund and Xing formulation in estimating k_{unsat} is as shown in the following equation.

$$k_{unsat} = k_{sat}\left(\frac{\theta}{\theta_{sat}}\right)^{2+\frac{2}{b}} \tag{3.17}$$

Where k_{sat} is saturated hydraulic permeability, (ms^{-1}), obtained from USBR estimation method and b is parameter used to vary the estimation. b = 0.41.

Hence, for a 95% confidence limit, k_{unsat} estimation for SWN1 is obtained and as shown in (3.18).

$$k_{unsat} = k_{sat}\left(\frac{\theta \pm 7\%}{\theta_{sat}}\right)^{2+\frac{2}{b}} \tag{3.18}$$

Similar to the development of soil suction in terms of volumetric water content and temperature, k_{unsat} at different temperatures can be determined using the principles of Darcy's Law. This law states that water flow velocity is linearly proportional to the water potential gradient.

The unsaturated hydraulic permeability, k_{unsat}, which is a ratio of this velocity, is therefore inversely proportional to the dynamic viscosity of water, η, (3.19).

$$k_{unsat} \propto \frac{1}{\eta} \tag{3.19}$$

The above $k_{unsat}(\theta)$ would be the k_{unsat} values at reference temperature. Therefore, the expression is defined in (3.20).

$$k_{unsat}(\theta, T) = \frac{\eta_{ref}}{\eta_T} k_{unsat}(\theta)_{ref} \tag{3.20}$$

Where η_{ref} is water dynamic viscosity at reference temperature, (Nsm^{-1}) and η_T is water dynamic viscosity at temperature T, (Nsm^{-1}).

Obtaining data from International Critical Tables [80], η, is expressed in terms of temperature, T, (°C), such as in (3.21).

$$\eta(T) = 0.0014e^{-0.0177.T} \tag{3.21}$$

3.7.6 Liquid Diffusivities, $D_{\theta L}$ and D_{TL}.

The equation in (2.5) is also known as liquid water velocity equation [71]. Alternatively, it can be described as

$$\underline{U} = -D_{TL}\nabla T - D_{\theta L}\nabla\theta - a\underline{i} \tag{3.22}$$

Where $\underline{U}$ is equivalent liquid velocity, (ms^{-1}) and a is a constant.

Using the Darcy's Law (2.3) and

$$\gamma = \frac{1}{\sigma}\frac{d\sigma}{dT} \tag{3.23}$$

the liquid water velocity can be expanded and implicitly described in terms of temperature and moisture gradients [71] using

$$\underline{U} = -k_{unsat}\ \gamma\ \psi\nabla T - k_{unsat}\ \frac{d\psi}{d\theta}\nabla\theta \tag{3.24}$$

Hence from (3.22) and (3.24), it can be seen that thermal liquid diffusivity, D_{TL}, ($m^2s^{-1}°C^{-1}$) and isothermal liquid diffusivity, $D_{\theta L}$, (m^2s^{-1}) are given respectively by (3.25) and (3.26). The third term of (3.22) is described by (3.27).

$$D_{TL}(\theta,T) = k_{unsat}(\theta,T)\,\gamma\,\psi(\theta,T) \tag{3.25}$$

$$D_{\theta L}(\theta,T) = k_{unsat}(\theta,T)\,\frac{d\psi}{d\theta} \tag{3.26}$$

$$a = gk_{unsat} \tag{3.27}$$

Where g is acceleration due to gravity, 9.81 ms^{-2}.

The values of the liquid diffusivities, $D_{\theta L}$ and D_{TL} of soil SWN1 are calculated using the values of unsaturated hydraulic permeabilities and soil suction, which are obtained using (3.18) and (3.20). The results are plotted in Figures 3.13 and 3.14. In order to consider the significance to buried cables, the values plotted are those at temperatures of 20°C, 40°C, 60°C and 80°C.

It can be seen that the diffusivities of soil liquid varies, depending on its gradients. Thermal liquid diffusivities are larger in magnitude than the isothermal term. This means that temperature gradient plays a greater role than moisture gradient in displacing moisture. The difference in the order of magnitude is about 3.

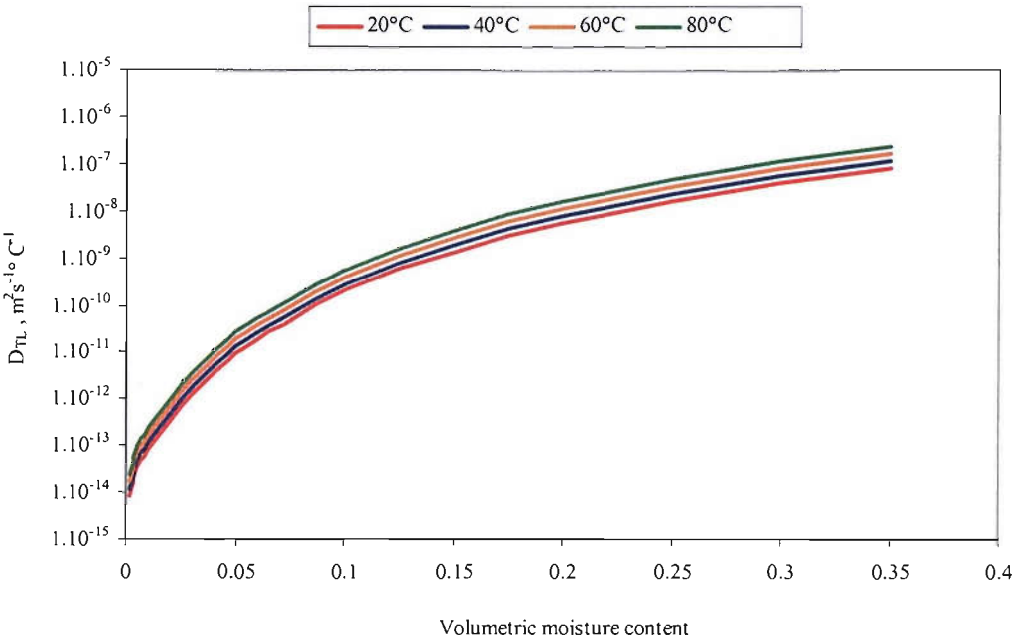

Figure 3.13 - Thermal liquid diffusivity of SWN1 at different temperatures.

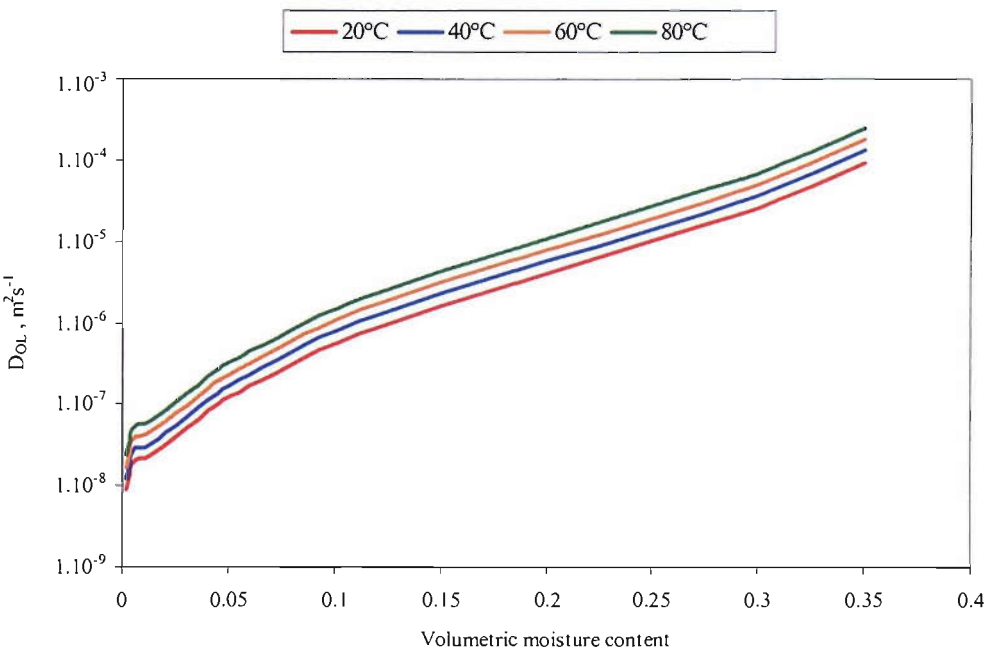

Figure 3.14 - Isothermal liquid diffusivity of SWN1 at different temperatures.

3.7.7 Vapour Diffusivities, $D_{\theta V}$ and D_{TV}.

Similar to (3.22), the water vapour diffusivities are denoted from the expression of the vapour velocity, $\underline{V}$, (ms^{-1}), which is described in terms of temperature and moisture gradients [4].

$$\underline{V} = -D_{TV}\nabla T - D_{\theta V}\nabla\theta \tag{3.28}$$

The isothermal vapor diffusivity, $D_{\theta V}$, (m^2s^{-1}) is defined as (3.19).

$$D_{\theta V} = k_{v\theta}\,\rho_v \frac{\dfrac{\partial\psi}{\partial\theta}}{\rho_{ref}} \tag{3.29}$$

Where $k_{v\theta}$ is isothermal vapour permeability, (m^2s^{-1}); ρ_v is vapour density, (kgm^{-3}) and ρ_{ref} is liquid water density at reference temperature, (ρ_{ref} = 998 kgm^{-3}) and the thermal vapor diffusivity, D_{TV}, ($m^2s^{-1}{}^{\circ}C^{-1}$) defined as (3.20) [71].

$$D_{TV} = k_{vT}\,R\mathrm{T}h\,\frac{\beta_s}{\rho_{ref}} \tag{3.30}$$

Where k_{vT} is thermal vapour permeability, ($m^2s^{-1}{}^{\circ}C^{-1}$); R is gas constant, at 461.5 $Jkg^{-1}K^{-1}$, h is relative humidity, T is absolute temperature, (K) and β_s is the temperature derivative of saturated water vapor density, ρ_o.

The temperature derivative of the saturated vapour density is given by

$$\beta_s = \frac{d\rho_o}{dT} \tag{3.31}$$

The isothermal and thermal vapour permeability [71] are defined in (3.22) and (3.23).

$$k_{v\theta} = D_{atm}\, \upsilon \frac{\Lambda}{RT} \tag{3.32}$$

$$k_{vT} = D_{atm}\, \upsilon \Lambda \frac{\frac{(\nabla T)_a}{\nabla T}}{RT} \tag{3.33}$$

Where D_{atm} is the molecular diffusivity of water vapor in air, (m^2s^{-1}), and Λ is the equivalent vapor flow area, $\frac{(\nabla T)_a}{\nabla T}$ is the ratio of the average temperature gradient in air-filled pores to overall gradient temperature and υ is the mass flow factor. The mass flow factor [71] is defined as (3.34).

$$\upsilon = \frac{P}{(P-p)} \tag{3.34}$$

Where P is air pressure, a fixed value at 1 x 10^3 kPa and p is the partial pressure of water vapour, (kPa). D_{atm} is taken from Krischer and Rohnalter [81] and quoted by Ewen [71] as

$$D_{atm} = 5.89 \times 10^{-6}\left(\frac{T^{2.3}}{P}\right) \tag{3.35}$$

Data for the equivalent flow area, Λ, is derived from the equation quoted from Philips and de Vries [4] and the experimental data on water-vapor transfer in soils by Gurr, Marshall and Hutton [82] and Rollins, Sprangler and Kirkham [83]. This is best fitted to a linear equation in terms of volumetric air content [71], such as shown in (3.36)

$$\Lambda = 0.3 + 1.32a_v \tag{3.36}$$

Where a_v is volumetric air content expressed in percentage, %.

The soil sample SWN1 has been taken from a large disturbed bulk source, which has the porosity of 0.4. It is assumed that the state of the cable bedding also has the same porosity. This value is taken as constant. The equation in (3.36) therefore can be rearranged in terms of volumetric water content, θ.

$$\Lambda = 0.3 + 1.32\ (0.4 - \theta) \tag{3.37}$$

The term $\frac{(\nabla T)_a}{\nabla T}$ in (3.33), is derived by Philip and de Vries and used by Preece [84] and Hitchcock [56, 106] in their work.

$$\frac{(\nabla T)_a}{\nabla T} = \frac{1}{3}\left(\frac{2}{1+\left(1-\frac{\lambda_i}{\lambda_o}\right)G_a} + \frac{1}{1+\left(1-\frac{\lambda_i}{\lambda_o}\right)(1-2G_a)}\right) \tag{3.38}$$

Where λ_i is thermal conductivity of individual material in soil, ($Wm^{-1}°C^{-1}$), λ_o is thermal conductivity of pore medium in soil, ($Wm^{-1}°C^{-1}$), G_a is the air shape factor.

Estimation of G_a requires knowledge of volumetric moisture content at wilting point (a point at which relative humidity of soil falls significantly from unity) or critical moisture content, $\theta_{critical}$. (Critical moisture content is a point when a soil starts to be deprived of moisture in order to maintain at least 75% of its field capacity). Volumetric moisture content at wilting point and field capacity of soils are usually estimated at 1500 kPa and 30 kPa respectively. Critical moisture content can be estimated at 75% of its field capacity. 1500 kPa is the limit for most plants to remove water from soil and beyond which permanent wilting is achieved.

The wilting point of soil SWN1 is found to be at θ = 0.005. However, estimating field capacity at 30 kPa resulted in a moisture content value that is too low for soil SWN1. Referring to Figure 3.10, the field capacity can be roughly estimated at about 0.07 and therefore the critical moisture content, being at about 75% of its field capacity, is 0.05. As the soil dries up from wilting point to θ=0, the multiplier to term G_a has air and moisture as its medium. Hence, λ_o is the sum of thermal conductivity of air, λ_a and thermal conductivity of water or moisture, λ_w. The region where the moisture starts to build up from wilting point to saturation, the G_a has moisture or water as its medium. Using this technique similarly used by Kimball [86], the air shape factor, G_a for soil SWN1 is obtained.

Linear and exponential interpolations has been used for determining the G_a from the region of wilting point,θ_{wilt} to saturation, θ_{sat}. It is assumed that the shape of the solid grains are mostly spheres and hence, G_a =0.333. Kimball has found that the latter shows a better result compared to his experimental data. Therefore, in this attempt, only exponential interpolation is considered. For the region from θ=0 to

θ_{wilt}, a linear interpolation is used. The determined values of G_a at θ_{wilt} and $\theta=0$ are then expressed in terms of temperature, T (°C). Kimball had also suggested that the critical point could be used to replace the wilting point in calculating the air shape.

Both methods have been calculated and the result showed that there is not much difference in the values of G_a either after the wilting or critical point, except that the point, where G_a starts to increase exponentially occurs obviously at different moisture contents. Therefore, it would be important to start to evaluate the air shape linearly at the critical point rather than at the wilting point.

At $\theta=\theta_{critical}$,

$$G_a = -1e^{-5}T^2 + 0.0017T + 0.0046 \tag{3.39}$$

At $\theta = 0$,

$$G_a = 2e^{-7}T^2 - 7e^{-6}T + 0.0129 \tag{3.40}$$

The values of λ_a , $(Wm^{-1}{}^{\circ}C^{-1})$, used is taken from Table A-11 of [12], expressed in terms of temperature, T , (°C).

$$\lambda_a = 7e^{-5}T^2 + 0.0242 \tag{3.41}$$

Effective thermal conductivity of air consists of thermal conductivity of air, λ_a, and thermal conductivity of vapour, λ_v. The latter term is calculated using (3.40), derived by Krischer et al [81] and later modified by Philips et al [4] for humidity lower than saturation.

$$\lambda_v = D_{atm} hL\upsilon \left(\frac{d\rho_o}{dT} \right) \tag{3.42}$$

Where L is latent heat of vaporisation, taken as 2.4 x 10^6 Jkg^{-1} and ρ_o is taken from that quoted by Ewen [71], deriving from Mayhew and Rogers [73] data,

$$\rho_o^{-1} = 194.4 \exp\left[-0.06374T + 0.1634 \times 10^{-3} T^2 \right] \tag{3.43}$$

For moisture contents below the wilting point, the thermal conductivity of air is taken only as λ_a, otherwise the effective thermal conductivity of air is calculated by adding (3.42) to (3.41).

Values of λ_w are dependent of temperature and these are taken from Table A-9 of [12] and fitted to a polynomial expression, obtaining

$$\lambda_w = -1e^{-5} T^2 + 0.0021T + 0.5599 \tag{3.44}$$

The result of air shape factor, G_a obtained for the volumetric water content up to saturation is as shown in Figure 3.15.

Figure 3.15 shows that at 20°C, the air shape factor increases as θ increases up to saturation point. There is a pronounced increase in the air shape factors at 40°C, which gradually increases at subsequent temperature increase. The physical explanation to this is that as water fills up the air-filled pores, air pores get contorted and smaller. When there is the influence of the rate of temperature, loss of

water mass increases due to presence of heat and therefore the air pores get even smaller, leading to a greater air shape factor. However, the values for air shape factors at 80°C are less than that at 60°C. This is due to the fact that as the temperature rises and exceeds a certain degree above 60°C, the air shape gets larger as water releases its latent heat. This leads to smaller values of air shape over the range of saturation.

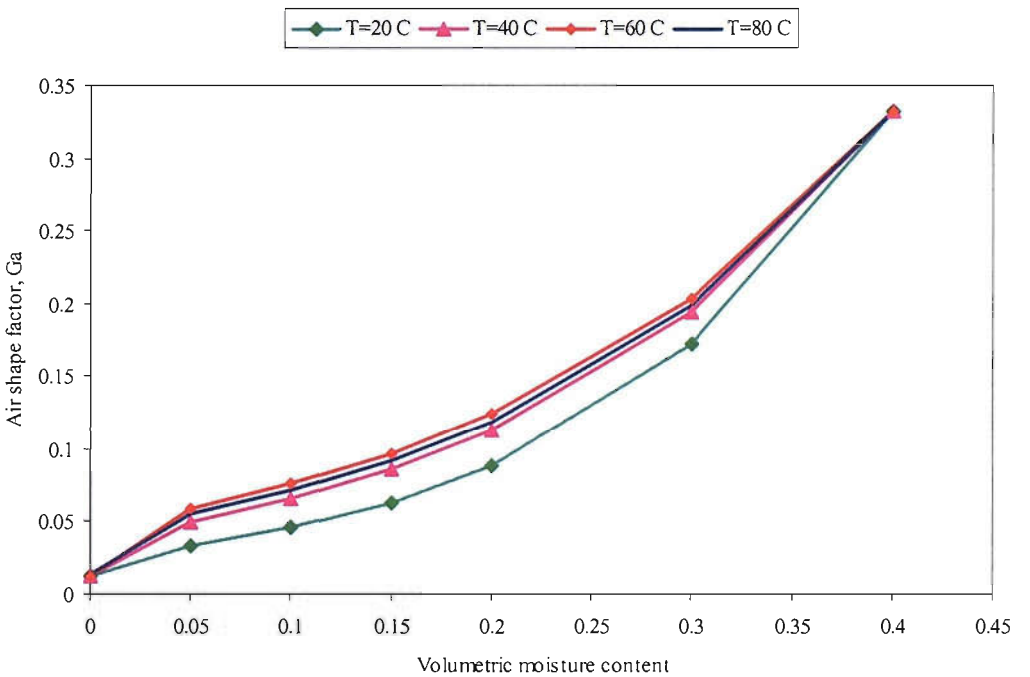

Figure 3.15 - Air shape factor, G_a curve .

The essential parameters needed to calculate the vapour diffusivities have been outlined and explained. The calculated values for the vapour diffusivities are plotted in Figures 3.16 and 3.17. Figures 3.13, 3.14, 3.16 and 3.17 show that all diffusivitives, in each respect, increase as temperature increases. The increase is more significant in vapor diffusivities than in liquid diffusivities.

Figures 3.18 and 3.19 clearly show the significance of each diffusivity. Referring to Figure 3.19, the thermal diffusivities for both liquid and vapour cross approximately at $\theta = 0.07$, which is approximately the field capacity of SWN1. Therefore, one would expect that below field capacity, vapour migration dominates over that of liquid under the influence of temperature and vice versa above it. On the other hand, liquid diffusivity dominates over the whole range of the moisture content under the influence of moisture gradient. There is a gradual and significant reduction in isothermal vapour diffusivity as θ increases. This is because as moisture fills up the air filled pores, there are fewer paths for vapour to diffuse away as the air shape factor increases. However, it may dominate isothermal liquid diffusivity at very low moisture contents (well below 0.01).

The calculated diffusivities are also compared to those values calculated by Ewen on his Garside sand sample, also calculated at 20°C [71]. Isothermal diffusivities of SWN1 appeared to be greater than that of the Garside sand. There is a maximum of about 1 order of magnitude difference in the isothermal vapour diffusivities, calculated at not more than 16% difference. Whereas Figure 3.17 shows that unlike the isothermal properties, SWN1 has its magnitude of thermal liquid diffusivity lower than that of Garside sand. Their difference is 12% at the maximum. However, its thermal vapour diffusivity is in good agreement with that of Garside sand with less than 3% difference.

Inspection revealed that the differences in the magnitude of isothermal diffusivities between SWN1 and Garside sand is due to the term $d\psi/d\theta$ in (3.26) and (3.29). The soil suction curve obtained by Ewen shows that suction decreases exponentially with very low moisture contents and trails off constantly at about $\theta=0.2$. Whereas for the values interpolated using the Fredlund and Xing method, suction continues to decrease gradually at this θ value. This results in a significant

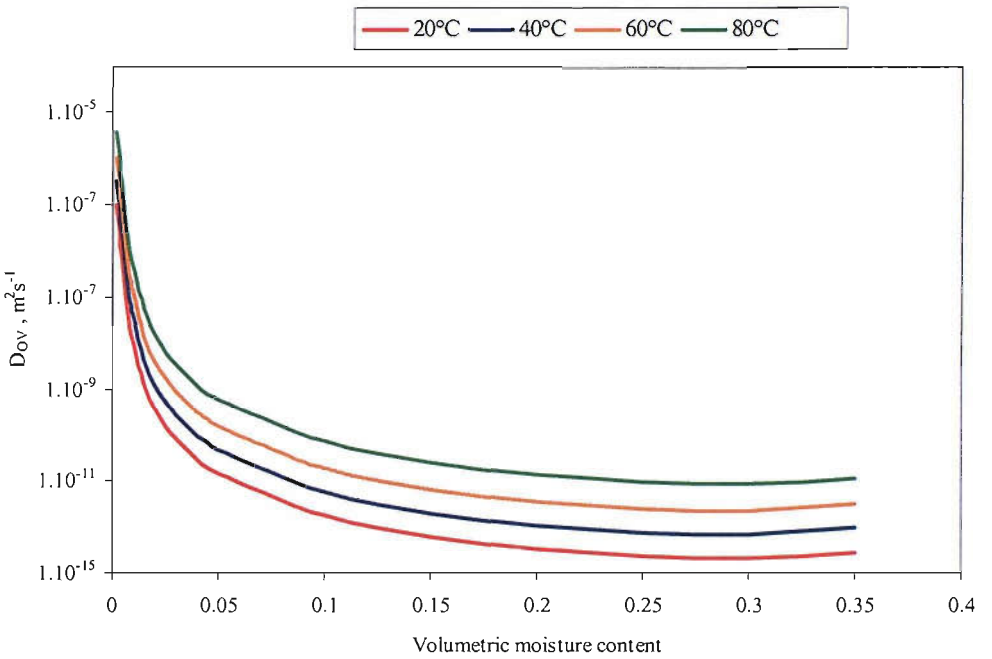

Figure 3.16 - Isothermal vapour diffusivity of SWN1 at different temperatures.

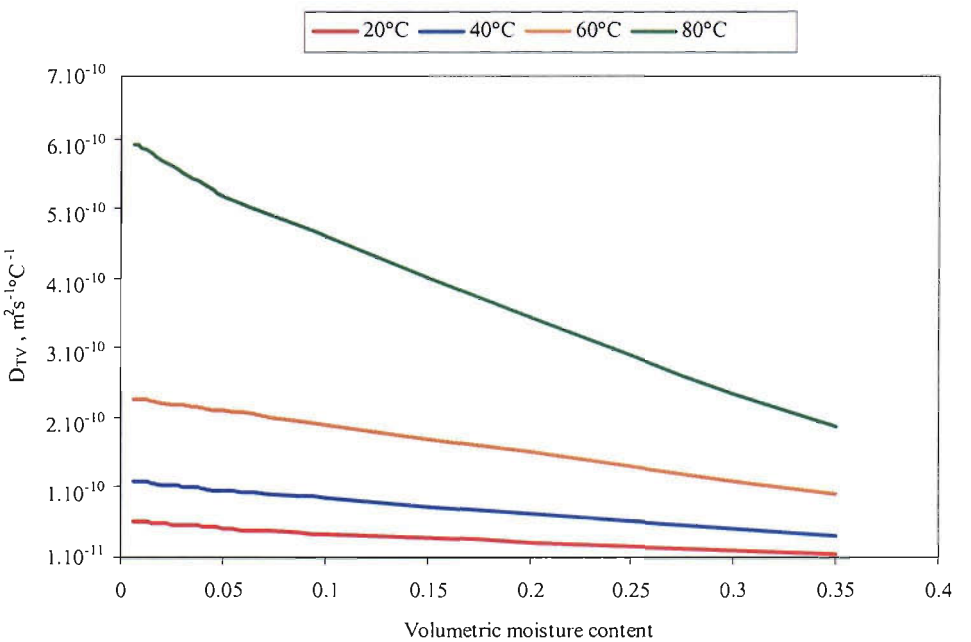

Figure 3.17 - Thermal vapour diffusivity of SWN1 at different temperatures.

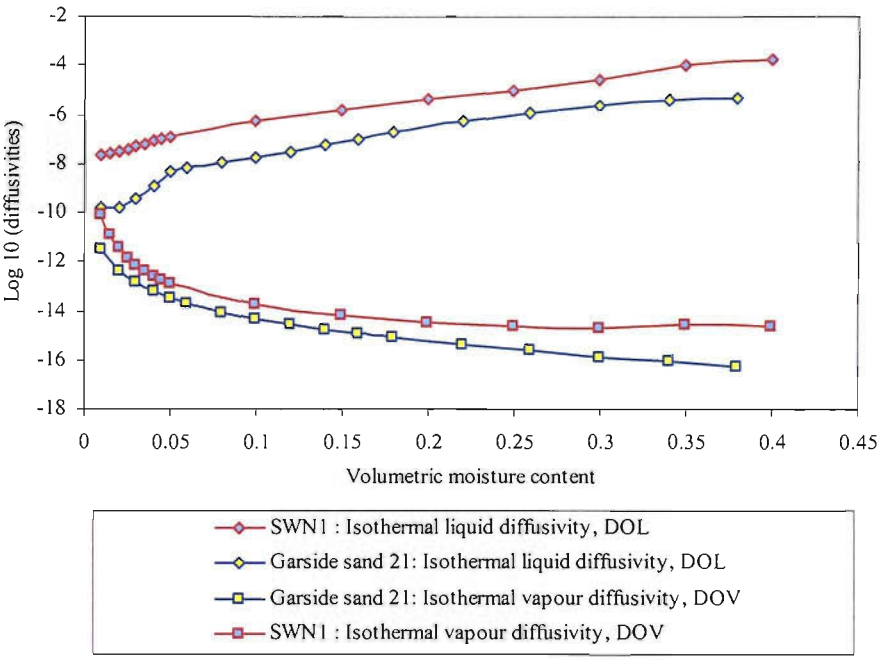

Figure 3.18 – Isothermal diffusivities at 20 °C.

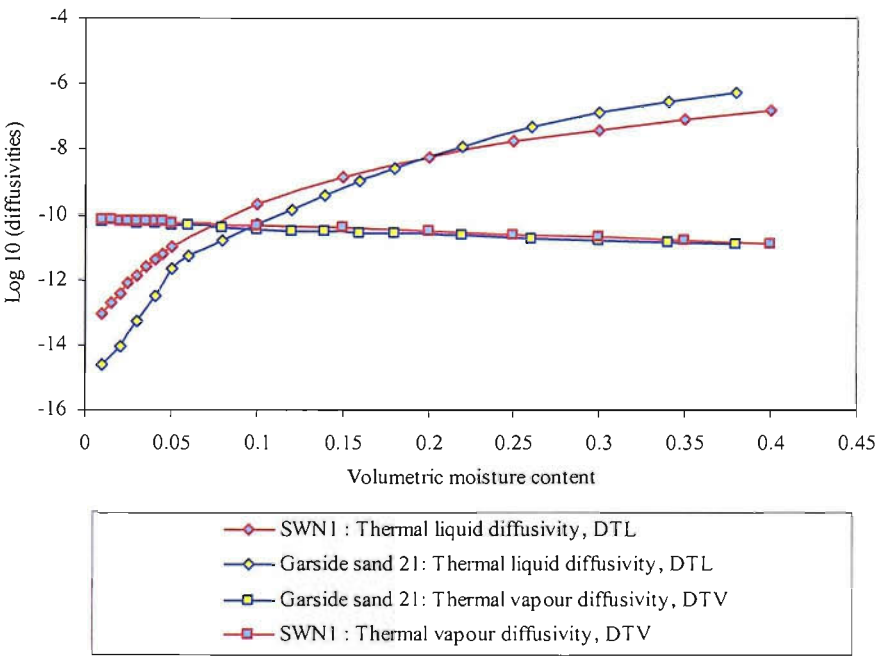

Figure 3.19 – Thermal diffusivities at 20 °C.

difference in the calculation of $d\psi/d\theta$, that of SWN1 appearing to be slightly greater than that calculated by Ewen.

3.7.8 Thermal Conductivity

There are three essential parameters needed for analysis of the thermal distribution using the Philip and de Vries equation (2.11). These are the volumetric heat capacity, C, thermal conductivity, λ, and the isothermal vapour diffusivity, $D_{\theta v,}$ of the soil. The isothermal vapour diffusivity has been defined, calculated and described in the previous section.

The thermal conductivity of soil SWN1 has been determined using the thermal probe method. This method is commonly used due to its simplicity and had been used by many researchers; Sepashkah and Boersma [86], DaPonte, DiPippo and Fowler [87] and others [88, 89, 90, 91], whose scope of interest ranges from geophysics to electrical power.

A heating probe with good thermal conductivity is inserted into a soil sample contained within a cylindrical container. The soil sample is initially oven-dried and prior to the probe insertion, the dry sample is given the desired water content by adding a percentage weight of water. In order to avoid or reduce the presence of air pockets within the soil, the sample is carefully packed into the container. It is essential that the thermal probe is only inserted after the container has been packed with the sample (to achieve minimal disturbance). The probe temperature is recorded while heating the sample. Once a steady state temperature is achieved, the heating is stopped.

The thermal conductivity is obtained from the following equation.

$$\lambda = \frac{Q}{4\pi\Delta T} \ln\left(\frac{t_2}{t_1}\right) \tag{3.45}$$

Where λ is thermal conductivity, ($Wm^{-1}°C^{-1}$), Q is heating rate, ($Wm^{-1}s^{-1}$), and ΔT is temperature change from time t_1 to t_2, (°C).

The dry density of the soil tested is 1575 kgm^{-3}. The result of the thermal conductivity result is plotted against θ in Figure 3.20.

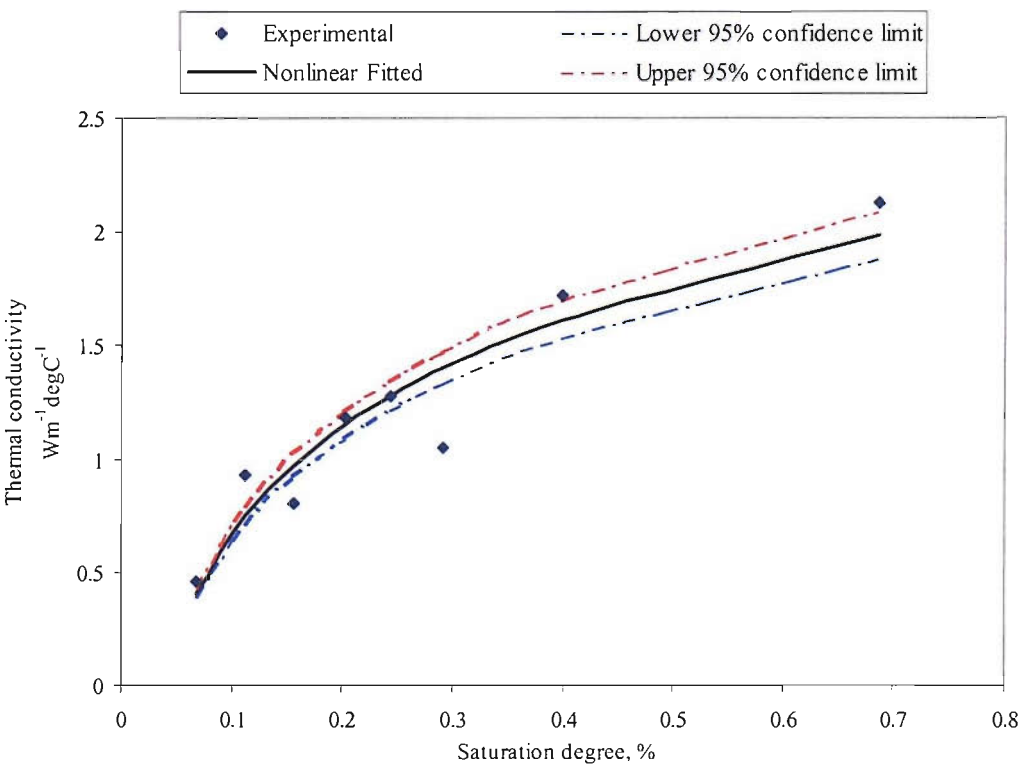

Figure 3.20 - Thermal conductivity of SWN1 at dry density 1575 kgm^{-3}

The data obtained shows that as θ increases, the thermal conductivity increases gradually. Therefore, the thermal conductivity data is fitted to a logarithmic expression using a non-linear regression fitting (3.46) as a function of saturation degree. The R-squared error is found to be 0.8886.

Assuming a t-distribution, 95% confidence interval is calculated for the fitted data and the following equation is obtained.

$$\lambda\left(\frac{\theta}{P_{or}}\right)=0.6857\ln\left(\frac{\theta}{P_{or}}\right)+2.2447\ \pm 5\ \%\ (Wm^{-1}{}^{\circ}C^{-1}) \tag{3.46}$$

Where $\frac{\theta}{P_{or}}$ presents saturation degree, $\%, P_{or}$ is porosity of medium, λ is thermal conductivity of soil, $(Wm^{-1}{}^{\circ}C^{-1})$.

Johansen [92] model in predicting thermal conductivities of unsaturated soils employs a linear interpolation between saturated and dry thermal conductivities (3.47). It also involves a multiplier that acts as a slope to the whole equation which, is better known as the Kersten's number, Ke. The Ke number is described in relation to the saturation degree of the soil. A relationship between the linear interpolation of saturated-dry thermal conductivities and Ke for SWN1 can be obtained by fitting (3.46) to the following equation.

$$Ke=\frac{\lambda-\lambda_{dry}}{\lambda_{sat}-\lambda_{dry}} \tag{3.47}$$

Where S is the saturation degree, expressed in %, λ_{sat} is the thermal conductivity of soil at saturated state, ($Wm^{-1}°C^{-1}$) and λ_{dry} is the thermal conductivity of soil at dry state, ($Wm^{-1}°C^{-1}$). The saturation degree is also defined as (3.48).

$$S = \frac{\theta}{P_{or}} \tag{3.48}$$

The Ke obtained for SWN1 is found to be,

$$Ke = (0.3236 \ln(\frac{\theta}{P_{or}}) + 0.9497) \pm 5\% \tag{3.49}$$

The Kersten number obtained differs from that estimated by Johansen. He suggested the following equation for the estimation of Ke.

For coarse soils, the Kersten number is given by

$$Ke = 0.68 \log_{10} S + 1 \tag{3.50}$$

For fine soils, the Kersten number is given by

$$Ke = 0.94 \log_{10} S + 1 \tag{3.51}$$

Using SoilVision, the experimental thermal conductivities can be fitted and and/or compared to the Johansen model. The fitting to the Johansen model gives an R-squared of 0.6193533 (Figure 3.21).

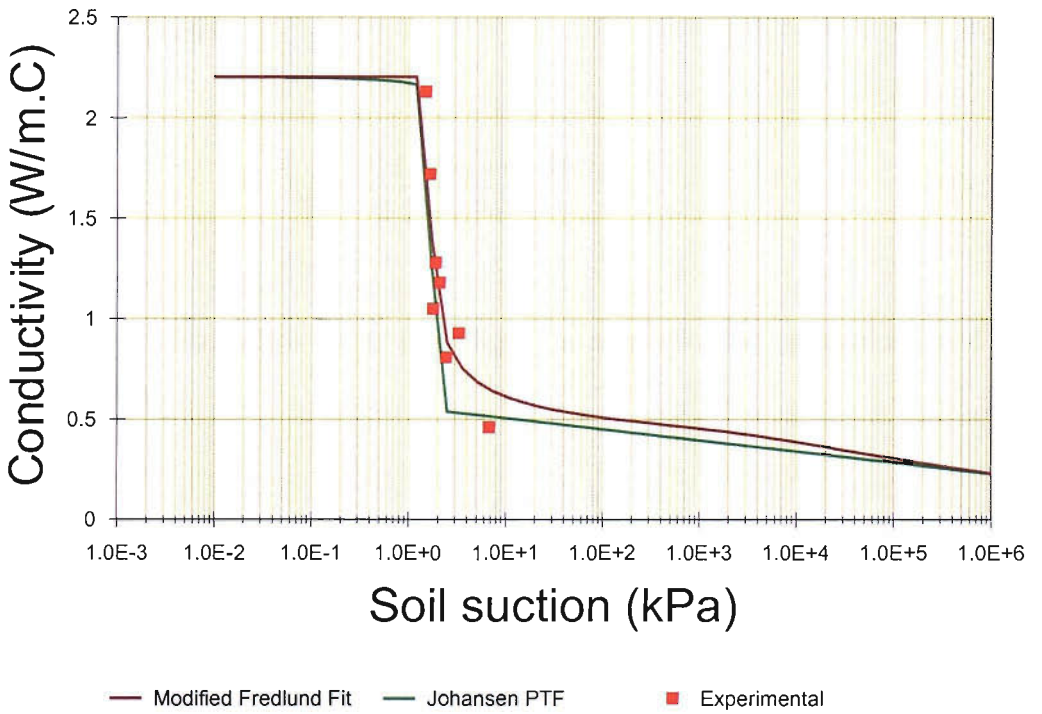

Figure 3.21 - Thermal conductivity of SWN1 against soil suction.

One of the factors affecting thermal conductivity is dry density, ρ_{dry} of the soil. The greater the dry density, the greater is its thermal conductivity at the same moisture content [93]. Johansen [92] has developed the relationship between dry density and the thermal conductivity of soils at its dry state, λ_{dry}, ($Wm^{-1}°C^{-1}$), and saturated state, λ_{sat}, ($Wm^{-1}°C^{-1}$). Using the same approach suggested by Ewen [71], thermal conductivity of soil with respect to its dry density can be estimated by interpolating the formula given by Johansen. The typical minimum and maximum dry density of uniform sand is 1330 and 1890 kgm^{-3} respectively, hence, using this

information and the calculation obtained for the $\rho_d = 1575$ kgm^{-3}, the expression for λ_{dry}, (Wm^{-1}°C^{-1}), as a function of dry density is found to be (3.52) and (3.53).

From Johansen, thermal conductivity of soil between dry densities of 1550 and 1750 kgm^{-3} is given by

$$\lambda_{dry} = \frac{0.137\rho_d + 64.7}{2.7 - 0.947\rho_d} \tag{3.52}$$

Using (3.52) to interpolate ρ_d at 1575 kgm^{-3} a simplification is obtained and as shown in (3.53)

$$\lambda_{dry} = 0.232(1 + 1.29(\frac{\rho_d}{1000} - 1.575)) \tag{3.53}$$

Also, from Johansen, thermal conductivity of soil at its saturated state is given by

$$\lambda_{sat} = \lambda_w^{P_{or}} \lambda_s^{(1-P_{or})} \tag{3.54}$$

Where λ_w is thermal conductivity of soil of water that is dependant of temperature, (Wm^{-1}°C^{-1}) and λ_s is thermal conductivity of solid soil, (Wm^{-1}°C^{-1}).

The conductivity of solid soil is defined as

$$\lambda_s = \lambda_{quartz}^{q_c} \lambda_{min}^{(1-q_c)} \tag{3.55}$$

Where λ_{quartz} is thermal conductivity of quartz, λ_{min} is thermal conductivity of minerals, taken as 2.2 ($Wm^{-1}°C^{-1}$), q is quartz content percentage over solid content, assumed to be at 0.6.

Using data taken from [94], thermal conductivity of quartz can be estimated using (3.56).

$$\lambda_{quartz} = 0.00008T^2 - 0.0347T + 9.207 \tag{3.56}$$

And the values of λ_w are calculated from (3.44).

The Kersten number formulated by Johansen can only predict for saturation degree greater than 10%. The prediction of thermal conductivity is therefore discontinuous because the thermal conductivity is linearly approximated for saturation degree less than 10%. Using the formulation developed by Fredlund [41], continuous representation of the thermal conductivity can be achieved. However, unlike the Johansen model, the Fredlund model of thermal conductivity is equated as a function of soil suction. The basis of the Fredlund formula is to determine empirically the Kersten number using experimental data. Fitting the experimental result to his formulation, the required parameters can be obtained.

Fredlund formulation of Kersten number, Ke is defined as

$$Ke = \left(1 - \frac{\ln\left(1 + \frac{\psi}{3000}\right)}{\ln\left(1 + \frac{1\times10^6}{3000}\right)}\right)\left(\frac{1}{\ln\left(e^1 + \frac{\psi}{a_{fi}}\right)^{n_{fi}}}\right)^{m_{fi}} \tag{3.57}$$

Where a_{fl} is the fitting parameter related to the breaking point of the curve, m_{fl} is the fitting parameter related to the curvature of the curve, n_{fl} is the fitting parameter related to the maximum slope of the curve.

FITTING PARAMETER	VALUE
a_{fl}	1.5638
m_{fl}	0.3896
n_{fl}	36.3383

Table 3.10 Values of fitting parameters for (3.57)

The estimation by Fredlund method gives a regression R-squared value of 0.9768444. This comparison can be seen in Figure 3.20. Rearranging the whole expression for thermal conductivity by using (3.50), (3.51), (3.52), (3.53) and (3.54) gives equations that can be used to calculate the thermal conductivities at different temperatures. Using the Johansen formula, the thermal conductivity of soil is,

$$\lambda = \lambda_{dry} + Ke\,(\lambda_{sat} - \lambda_{dry}) \tag{3.58}$$

Assuming a student's t-distribution, a 95% confidence limit is calculated and hence,

$$\lambda(\psi) = \lambda_{dry} + (\lambda_{sat} - \lambda_{dry})\left(1 - \frac{\ln\left(1+\frac{\psi}{3000}\right)}{\ln\left(1+\frac{1\times10^{6}}{3000}\right)}\right)\left(\frac{1}{\ln\left(e^{1}+\frac{\psi}{1.5638}\right)^{36.3383}}\right)^{0.3896} \pm 4\% \tag{3.59}$$

Comparison on the quality of the curve fitting and the estimation plot of the experimental thermal conductivity is as shown in Table 3.11 and Figure 3.22 respectively. Referring to Figure 3.22, it can be seen that both log regression and Johansen method give poor estimates at low saturation degrees. Furthermore, these methods do not provide estimation at other temperatures. Unlike these methods, Tarnawski provides a method to estimate thermal conductivities at other temperatures. However, it underestimates the experimental thermal conductivites. Therefore, it is concluded that Fredlund method gives the best estimation. Estimation of the thermal conductivities at other temperatures can be obtained by applying the temperature dependance of the soil suction.

KERSTEN NUMBER FITTING METHOD	R^2 VALUE
Johansen (3.48)	0.6914
Log regression (3.39)	0.8886
Fredlund (from SoilVision)	0.9768
Tarnawski et al [95, 96]	0.7135

Table 3.11 Quality of the regression fit on the experimental thermal conductivity.

The Kersten number in (3.57) is a function of soil suction, and it can be rewritten in a simpler form as a function of volumetric moisture content. Since the field variables that would be used in Philips and de Vries equations are temperature and volumetric moisture content, the transformation is essential and this is given by (3.60).

$$Ke = \frac{0.128052 - 0.0012T + 0.75S + 1.167329S^{.2}}{1 - 0.0074T - 0.84135S + 2.098585S^2} \qquad (3.60)$$

Where S is the saturation degree, expressed in %. It is a function of volumetric moisture content and obtained when volumetric moisture content is divided with soil porosity.

For low saturations, (S<0.125), an interpolation is applied to estimate the Kersten number, such suggested by Tarnawski [95]. Saturation at 0.125 marks a volumetric moisture content of 0.05 for soil SWN1. Hence, for θ less than 0.05, Ke is calculated using

$$Ke = Ke_{0.125}\frac{\theta}{\theta_{0.125}} \tag{3.61}$$

Where $\theta_{0.125}$ is θ at 0.125 and $Ke_{0.125}$ is the Kersten number at $\theta_{0.125}$.

$Ke_{0.125}$ calculated from (3.60) can be simplified in terms of temperature as shown in (3.62)

$$Ke(T)= 0.000034T^2 - 0.000921T + 0.282531 \tag{3.62}$$

Thermal conductivities at other temperatures are plotted as shown in Figure 3.23. It can be seen that thermal conductivity at the same moisture content increases as temperature is increased. Curvature of the curve becomes much pronounced as the temperature is increased. It also can be seen that thermal conductivities at high temperatures increase to an almost constant value at an earlier saturation degree than that at lower temperatures. These trends are fairly similar to the experimental data predicted by Campbell [97], Kimball [85], Sepashkah [86] and Tarnawski [95,96].

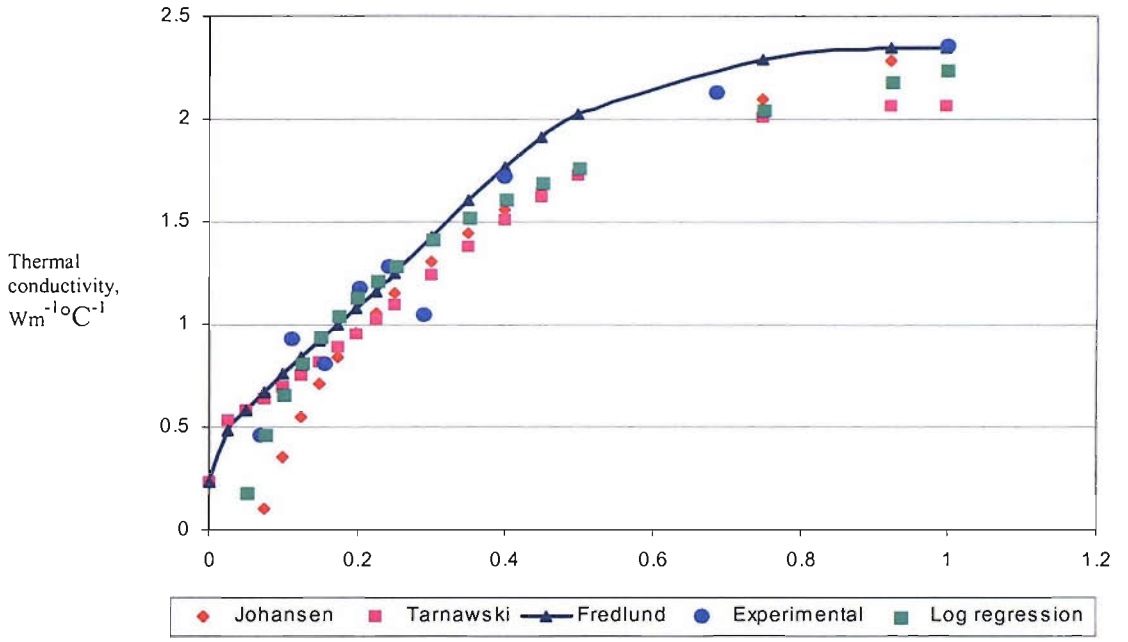

Figure 3.22 - Quality of regressions on thermal conductivity of SWN1.

There are no available thermal conductivity data for any type of sand in the SoilVision database for comparison purposes. Most soils of sand-type that are included in the database have only their hydraulic properties available. However, comparison can still be made with that of Garside sand.

The comparison of the thermal conductivity between the two soils is as shown in Figure 3.23. From this graph, one would expect that soil SWN1 would not behave like the Garside sand in thermal drying. Alternatively, this provides us with a benchmark for SWN1 thermal behaviour.

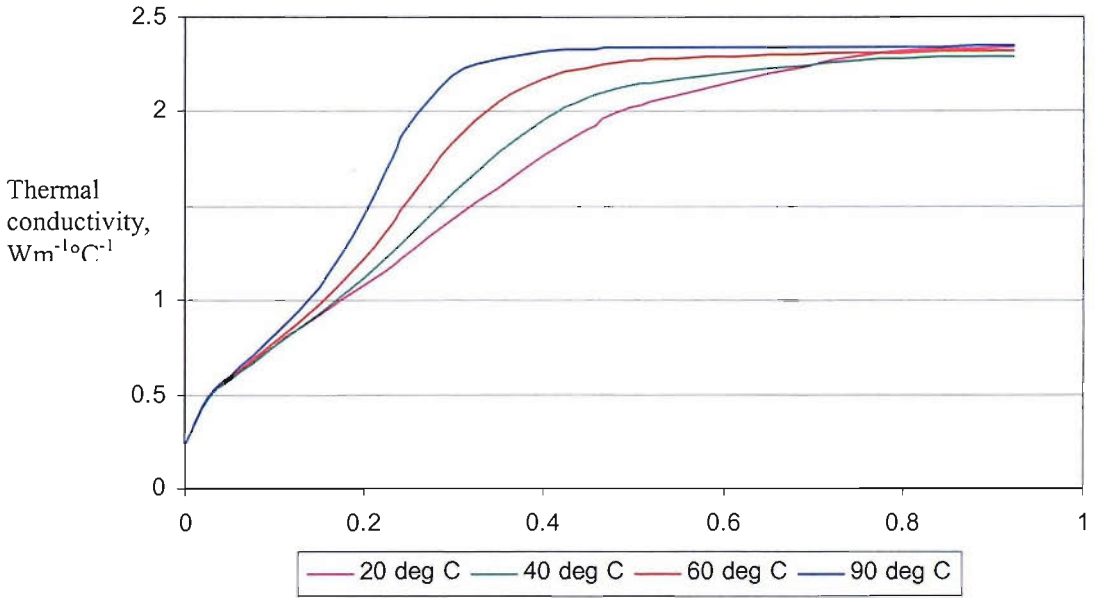

Figure 3.23 - Fredlund estimation on thermal conductivity of soil SWN1 at other temperatures.

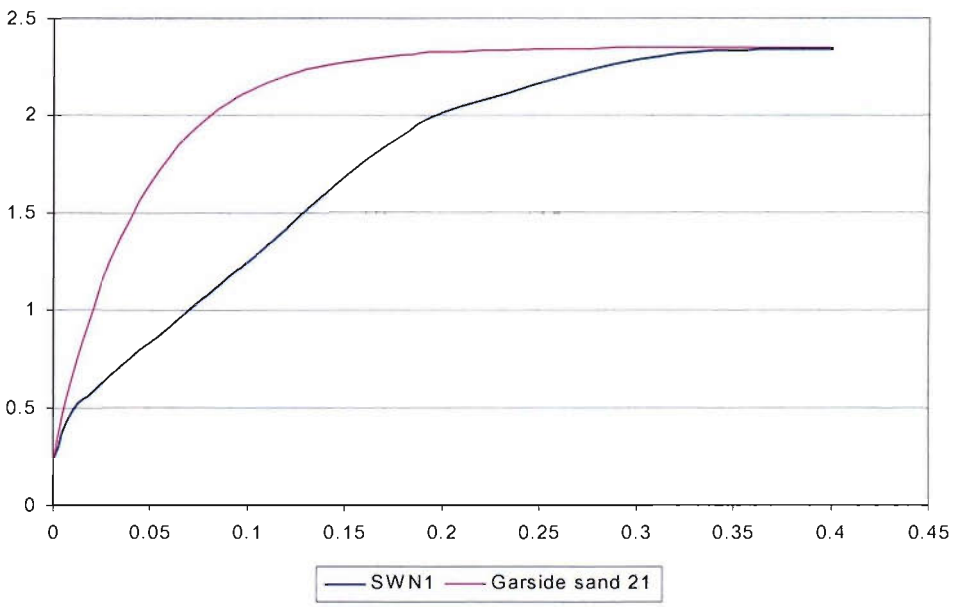

Figure 3.24 - Thermal conductivity comparison at 20°C.

3.8 VOLUMETRIC SPECIFIC HEAT

The volumetric specific heat of soil, C, can be obtained by calculating the sum of the volumetric heat capacities of the individual soil constituents weighted by their volume fractions [98].

$$C = C_s\Phi_s + C_a\Phi_a + C_o\Phi_o + C_w\theta \tag{3.63}$$

Where C_s, C_a, C_o and C_w is volumetric heat capacity of soil solids, air, organic matter and water, respectively ($kJm^{-3}\ °C^{-1}$); Φ_s, Φ_a and Φ_o is volume fraction of soil solids, air and organic matter respectively, expressed in percentage. Volumetric heat capacity of soil that is contributed by soil air is negligible and assuming that the sum of $C_s\Phi_s$ and $C_o\Phi_o$ can be replaced with the volumetric heat capacity of quartz soil, (3.53) can be further simplified. This is given in (3.64).

$$C_s = C_{qs}(1-\theta_s) + C_w\theta \tag{3.64}$$

Where C_{qs} is the volumetric heat capacity of quartz soil, ($kJm^{-3}\ °C^{-1}$) and θ_s is the saturated volumetric moisture content. C_{qs} is calculated using (3.65) with the specific heat of quartz soil, c_{qs} taken from [99] as 295 ($Jkg^{-1}\ °C^{-1}$).

$$C_{qs} = c_{qs}\rho_{dry} \tag{3.65}$$

3.9 CONCLUSIONS

The essential soil parameters of the Philip and de Vries equations are the thermal conductivity, hydraulic permeability, isothermal and thermal moisture diffusivities.

When laboratory equipment for determining all soil hydraulic properties is not readily available, only one hydraulic property needs to be experimentally obtained, which is soil suction. Other hydraulic properties can then be estimated using values for soil suction.

SoilVision provides a means of determining other hydraulic properties by the use of pseudo-transfer estimations. Comparison of SWN1 to other similar soils is also possible and the selection of estimation method can be easily decided.

The variations in the liquid diffusivities with temperature are not as great as that of vapour diffusivities. Both isothermal and thermal liquid diffusivities increase with increased moisture content. Whereas both isothermal and thermal vapour diffusivities decrease with increased moisture content. As temperature increases, isothermal vapour diffusivities over the whole range of moisture content increase. The incremental change is fairly constant for every 20 °C increment. However, this is not the same for thermal vapour diffusivities over the whole range of moisture content. The change of thermal vapour diffusivities is greater at higher temperatures, especially at low levels of moisture contents.

At a constant temperature, thermal conductivity increases as moisture content increases. For intermediate moisture contents, thermal conductivity also increases as temperature increases.

The study of each component of moisture transfer is possible by obtaining the diffusivities over the whole range of moisture contents. All soil properties that are described in this Chapter are highly non-linear and highly dependent of both temperature and moisture. Therefore, it is important to look at variable coefficients when employing Philips and de Vries equations in order to solve heat and moisture problems. This approach has been employed and is discussed in Chapter 5.

CHAPTER 4

4.0 MOISTURE MIGRATION EXPERIMENT

Moisture migration has been investigated experimentally and the results are presented in this chapter. The apparatus used to induce moisture migration under the influence of a thermal gradient in soil is presented in the first section. In the second section the results obtained from the experiment are detailed. The validation of the Philips and de Vries equations using these results are then discussed in the next chapter.

The objective of the moisture migration experiment is to study experimentally the behaviour of moisture migration under a thermal gradient, especially for backfill having low moisture content. Since it is known that soils or backfills having regions of low moisture content are susceptible to drastic moisture migration and hotspots, it is useful to investigate the behaviour of heating on soils having low moisture content by use of the moisture migration apparatus (MMA).

4.1 MOISTURE MIGRATION APPARATUS

Moisture migration apparatus is used to observe the behaviour of moisture migration under a temperature gradient. It is an apparatus used by Pirelli Cables Ltd. in order to investigate hydrological instability in soils [16]. The experiment has a cylindrical hollow container, in which a sample of soil is placed. The bottom plate of the test cell contains a hot plate and the upper plate is water-cooled. They are referred to as the 'hot' and 'cold' plates respectively, and are used so that a temperature gradient is induced within the medium.

Seven thermocouples are placed at incremental distances from the bottom plate to record the temperature during the heating period. This container has an inner diameter of 0.28m and height of 0.35m, thus having a volume of about 0.0216 m^3. Figure 4.1 shows the cross-section of the MMA. Thermocouples are labelled as T_1, T_2, T_3, T_4, T_5, T_6 and T_7.

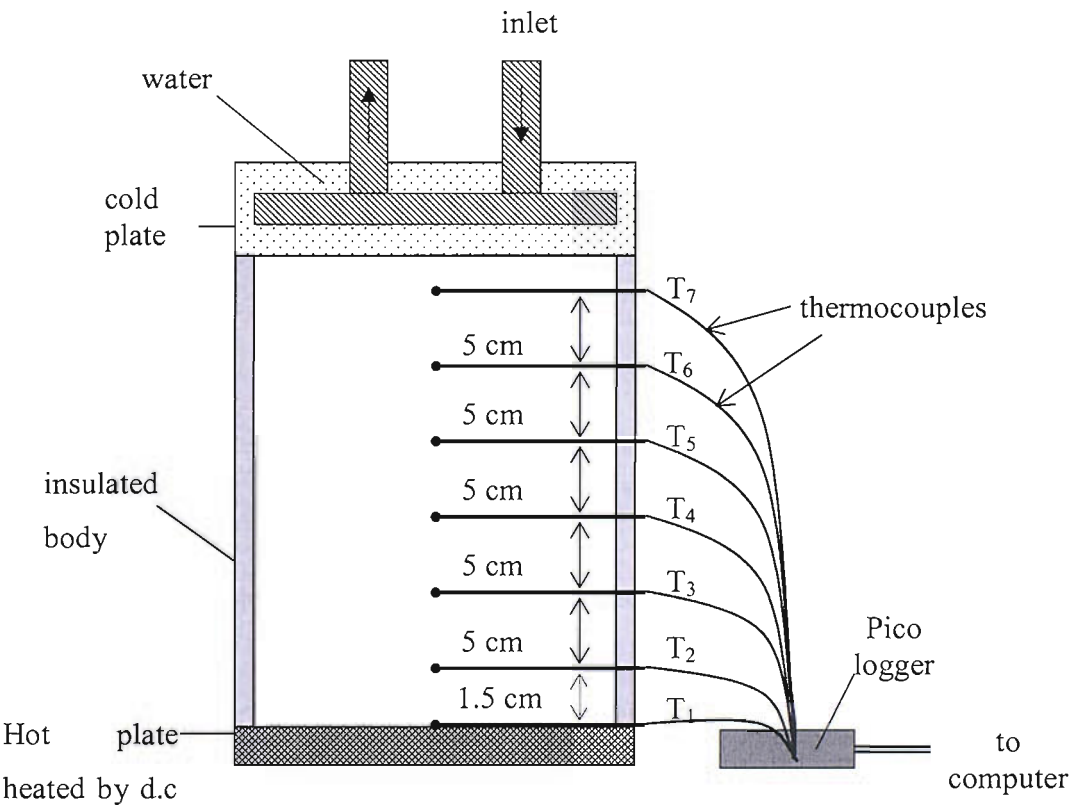

Figure 4.1 - Cross section of the MMA.

The outer jacket of the MMA is insulated to ensure that heat flow is not influenced by ambient temperature, in order to achieve ideal parallel heat flow between the plates.

For this research, MMA was filled with soil SWN1, layer by layer, carefully placing each thermocouple at the centre. Prior to this procedure, the soil was prepared to the desired gravimetric moisture content. The predefined moisture content was the initial state of the soil used in the experiment. Gravimetric and volumetric moisture contents are calculated using (4.1) and (4.2) respectively.

$$\theta_g = \frac{M_{wet} - M_{dry}}{M_{dry}} \tag{4.1}$$

Where M_{wet} is weight of the wet sample, (kg), and M_{dry} is weight of the dry sample, (kg).

$$\theta = \theta_g \frac{\rho_b}{\rho_w} \tag{4.2}$$

Where ρ_b is bulk density of soil, (kgm^{-3}) and ρ_w is density of water, (kgm^{-3}).

The height of the soil was recorded so that the bulk density of the soil could be calculated. Experiments were carried out using heating powers of approximately $40Wm^{-2}$ and $80Wm^{-2}$. Each experiment was conducted with different initial moisture content. The values selected were low volumetric moisture contents ranging from 1% up to approximately 5%. Respective temperatures were recorded every minute during the experiment. Experiments ran for between two to seven days. Soil samples at each thermocouple location were then taken after each experiment in order to determine the moisture content distribution.

4.1.1 Sources of Error

The experiment has been carried out only once in each case. This is because even if an experiment is repeated, exact bulk density may not be successfully attained as that which had been attained previously. This is due to the difficulty in preparing a sample for such a large volume as required by the MMA. Furthermore, the locations of thermocouples are easily displaced in the process of preparing the sample into the MMA. Hence, the result of the repeated experiment is unlikely to be similar as the same experiment that was carried out previously.

Recorded temperatures were subject to errors from the ± 1°C resolution of the J type thermocouples. Whereas thermocouples were located at their appropriate positions accurate to 5mm, unless if these are largely displaced during soil compaction, which may increase the discrepancy to more than 5mm.

4.2 EXPERIMENTAL RESULTS

The 40 Wm^{-2} and 80 Wm^{-2} heating resulted in a maximum hot plate/soil average temperature of 52°C and 80°C, respectively. The results of the heating are as shown in Figures 4.2, 4.3, 4.4 and 4.5. For each case, it can be seen that temperature profiles of the soil located near to the cold plate shows a gradual decrease, a period of time after the heating started. This shows that this region gained a considerable amount of moisture such that the 'local' thermal conductivity of the soil was increased leading to a lower local temperature.

Indirectly, the graphs generally indicate the location of the dry/wet interface during each experiment. They also provide information such as the length of time required for the dry-moist boundary or interface to start to form. After a period of

time, the dry-moist interface is located between two neighbouring thermocouples because temperatures recorded by one thermocouple increase whilst those recorded by the other decrease progressively over time. The time at which this starts to occur indicates the total time taken for moisture from cooler regions to migrate completely to the neighbouring region.

For instance, from Figure 4.3 (a) it can be seen by examination that dry/moist interface is formed in the area between T_3 and T_4 approximately after 41 hours and later in the area between T_4 and T_5 approximately after 97 hours. Figure 4.4(b) also roughly indicates that the dry/wet interface is formed in the area between thermocouples T_3 and T_4 approximately after 50 hours. Approximately after time 97 hours, the dry/wet interface started to form between T_4 and T_5. This shows moisture has migrated across the distance between 50 hours and 97 hours. Similar details for other experiments are tabulated in Table 4.1.

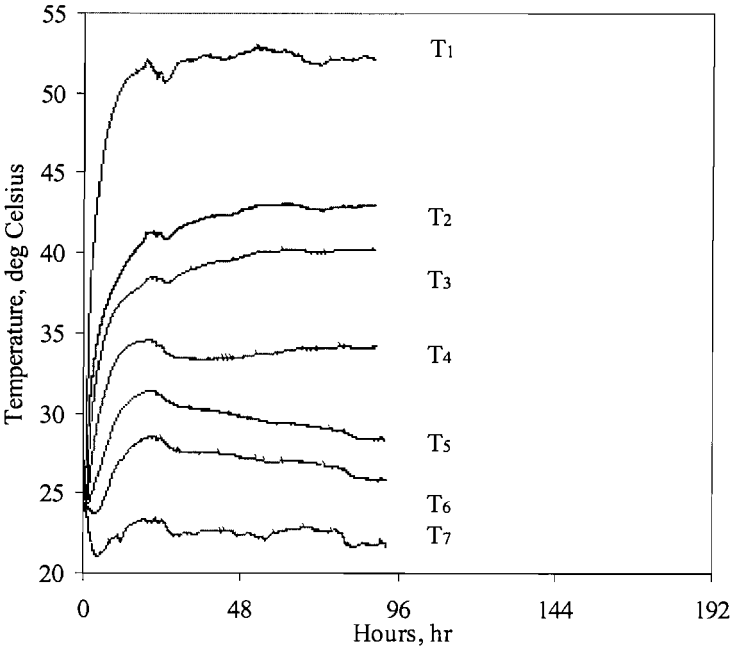

Figures 4.2 - MMA experiment: Initial volumetric moisture content of 1% with 40Wm^{-2} heating.

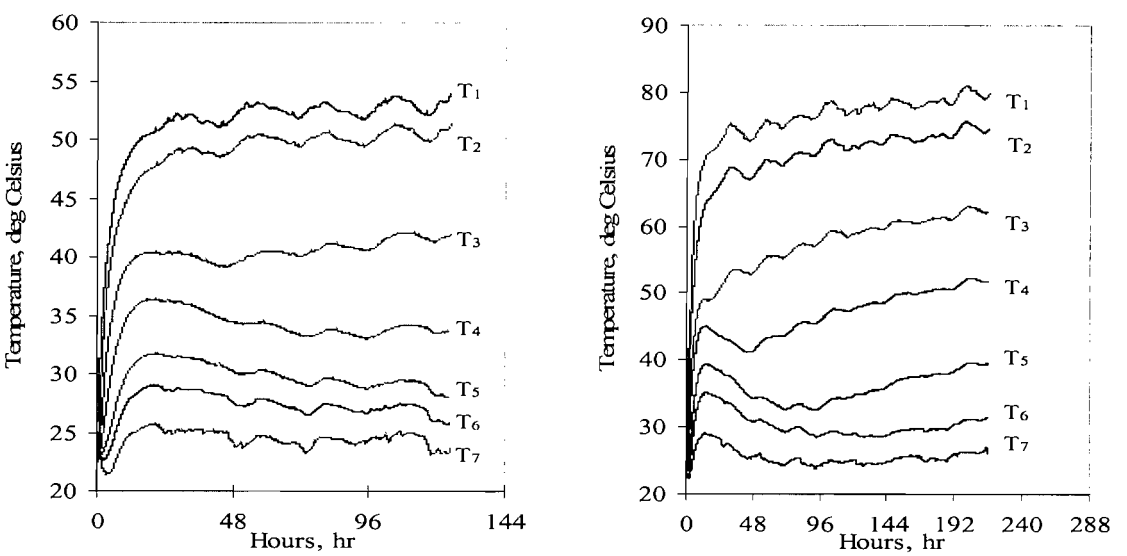

(a) (b)

Figures 4.3 - MMA experiments: Initial volumetric moisture content of 1.6% with (a) 40Wm^{-2} and (b) 80Wm^{-2} heating.

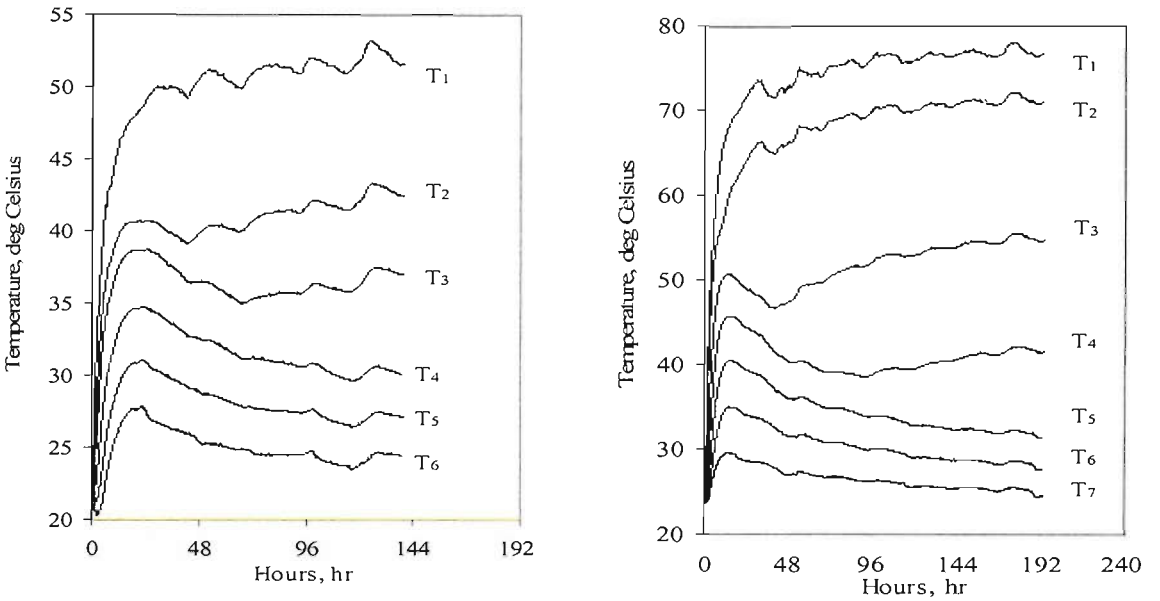

Figures 4.4 - MMA experiments: Initial volumetric moisture content of 3% with (a) 40Wm^{-2} and (b) 80Wm^{-2} heating.

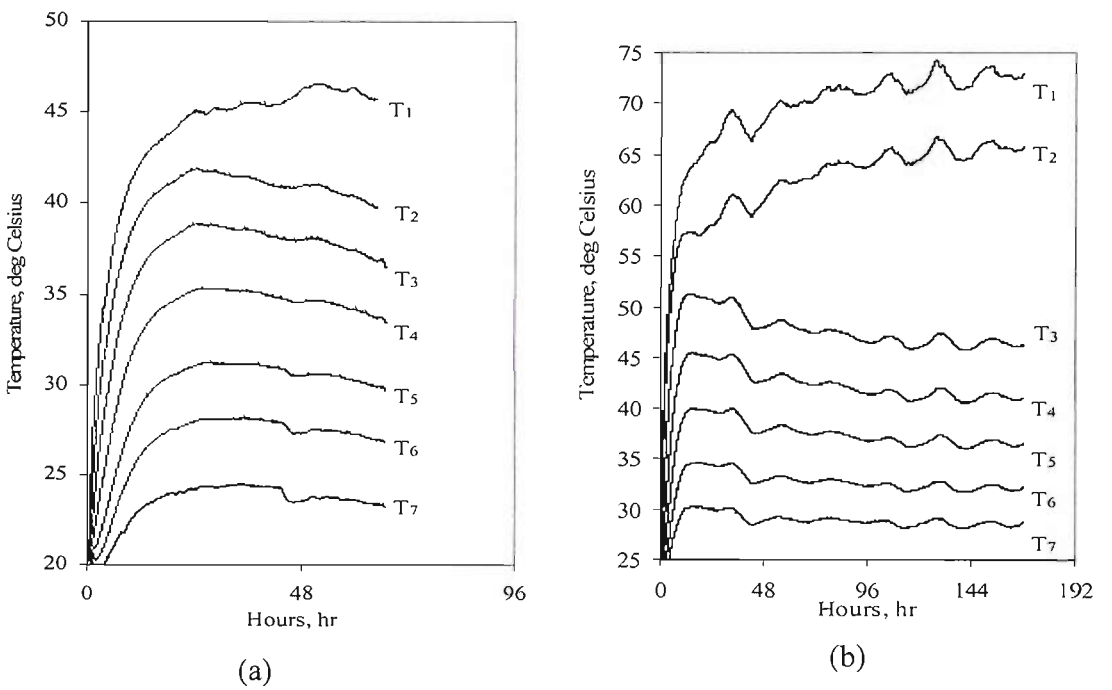

Figures 4.5 - MMA experiments: Initial volumetric moisture content of 5% with (a) 40Wm^{-2} and (b)80Wm^{-2} heating.

Initial moisture content	Experiment no.	Bulk density (kgm^{-3})	Heating, (Wm^{-1})	Time, (hours (approximately)	Interface location	
					Ti_1	Ti_2
1%	1	1690	40	55	T_4	T_5
1.6%	2	1630	40	42	T_3	T_4
				97	T_4	T_5
	3	1660	80	14	T_3	T_4
				55	T_4	T_5
				83	T_5	T_6
3%	4	1696	40	42	T_2	T_3
				67	T_3	T_4
	5	1623	80	50	T_3	T_4
				97	T_4	T_5
5%	6	1414	40	28	T_1	T_2
	7	1460	80	28	T_2	T_3

Table 4.1 - Details on time after which dry/moist interface starts to form and its location for different initial volumetric moisture contents and heating.

Experiments 1 and 6 were only undertaken for a short time compared to the others. Although extensive observations are therefore limited, the temperatures recorded are sufficient to be used for comparison with simulations obtained using the finite element analysis model (which will be discussed in the next chapter).

With reference to Figure 4.1, the close proximity of T_2 and T_1, it is expected that their respective temperatures during the experiment are fairly close. This is seen in Figures 4.3(a), 4.3(b), 4.4(b) and 4.5(b). However, it is not seen in Figures 4.2, 4.4(a) and 4.5(a). It was found by inspection that there was a considerable displacement of T_2, T_3 and T_6 from their original locations in experiment 1, as seen in Figure 4.2. This has resulted in large temperature differences between locations

T_1 and T_2; also between T_6 and T_7. The distance between T_1 and T_2 was more than 1.5cm and that between T_5 and T_6 was less than 5cm. These may have been caused either by the process of compaction or careless placement. Similar situations were detected in experiments 4 and 6 between T_1 and T_2, as seen in Figure 4.4(a) and 4.5(a), respectively. T_7 of experiment 4 was not operational during the experiment and thus there are no recorded temperatures of T_7.

It could not be determined what causes the oscillation although there are two possibilities. One possibility is poor hot plate insulation with respect to ambient temperature. Although the hot plate is capable of achieving temperatures of above 60°C, the heat flux produced might not have been great enough to eliminate the influence of ambient temperature fluctuation. The other possibility is that the soil sample within the MMA might have not been ideally compacted and the presence of air pockets in the soil affected the temperature measurement.

4.2.1 Moisture Content

At the end of each experiment, soil samples at the vicinity of each thermocouple end had been taken by excavating the soil, a layer after another. It was ensured that samples were taken particularly at the centre point of the soil layer because it was where the thermocouples were placed. Moisture contents were (at the vicinity of each thermocouples' end) then determined using these soil samples using (4.1) and (4.2). These data provide direct indication of the moisture condition throughout the heat path and, therefore, moisture profile of the soil, after each experiment.

Obtained data is tabulated in Table 4.2, with experiment number referred to Table 4.1. These are also presented in Figures 5.19 - 5.22 in Chapter 5.

	VOLUMETRIC MOISTURE CONTENTS (m^3m^{-3})							
Exp. no.	T_1	T_2	T_3	T_4	T_5	T_6	T_7	Top soil
1	0	0	0	0	0.001	0.029	0.057	n/a
2	0	0	0	0	0.003	0.005	0.018	0.065
3	0	0.002	0.003	0.010	0.008	0.050	0.042	0.060
4	0	0	0.0006	0.0004	0.001	0.012	0.036	0.051
5	0	0	0.0009	0.014	0.016	0.030	0.050	0.065
6	0	0	0.020	0.058	0.05	0.05	0.05	0.065
7	0	0.002	0.031	0.040	0.036	0.039	0.052	0.080

Table 4.2 - Moisture content at each location after each experiment.

4.2.2 Discussion

Referring to Table 4.1, experiments 2 and 3 reveal that the time at which dry/moisture interface enters the area between T_3 and T_4 is earlier for $80Wm^{-2}$ than for $40Wm^{-2}$. Similar behaviour is observed for the area between T_4 and T_5 of the same experiment. However, unlike experiment 2, the dry/moisture interface in experiment 3 is found to be entering the area between T_5 and T_6 at an earlier time, approximately after 83 hours. Similar behaviour is also observed in experiments 4 and 5.

Temperatures for T_1 and T_2 of each experiment (except experiment 1 and 4 due to thermocouple displacement error) differ by about 1 to 2°C and continue to increase over time. In experiment 6, although the displacement between T_1 and T_2 was merely 3cm, the temperature of T_2 decreases indicating that moisture is

migrating very slowly and that thermal conductivity within the particular area increases, thus decreasing temperature.

The behaviour of the recorded temperatures in Figures 4.2, 4.3, 4.4 and 4.5 proves that due to the imposed gradient temperature, moisture migrates towards cooler regions. This results in decreased 'local' thermal conductivity and increased thermal conductivity of the cooler/wetter region due to the high conductivity of the accumulated moisture. Higher heating power/heat flux increases the rate of migration. This can be seen in Figures 4.3(a) and 4.3(b) where $80Wm^{-2}$ heating caused temperatures of T_3, T_4 and T_5 to increase at a much faster rate.

As expected, $80Wm^{-2}$ heating on initial volumetric moisture content of 0.016 caused a greater temperature increase at T_3, T_4 and T_5 compared to the results obtained for initial volumetric moisture content of 0.03. Whereas in experiment 7, no temperature increase has occurred to T_3, T_4 and T_5. This shows that initial moisture content is crucial in determining the behaviour of soil heating especially under high power heating. This also indicates that in certain circumstances, critical measures should be taken in order to determine the actual, dynamic thermal conductivity of a certain medium due to prolonged heating.

From these results, the conservative approach of assuming constant thermal conductivity in solving thermal problems must be misleading, especially in cases where prolonged drying under extreme environmental conditions occurs. A good example of this case is the situation of a heavy loaded underground cable operating under high ambient temperatures in areas of low rainfall.

4.3 THERMAL CONDUCTIVITY ESTIMATION

The temperatures obtained from the MMA experiments were manipulated to extract the approximate thermal conductivity of the regions in the MMA using the basic law of conductive heat transfer. Only data or temperatures that are recorded after the initial transient time are used. This is because only during this time, the intended power supplied has stabilised or reached its final steady state. The full volume is divided into several regions, each region being the area located between two neighbouring thermocouples. Where region 1 is the volume between T_1 and T_2, region 2 is the volume between T_2 and T_3 and so on up to region 6, which is the volume between T_6 and T_7. It is assumed that heat flux is distributed evenly across the cross section area throughout the experimental time. It is also assumed that the heat flux supplied remains constant after a steady state is obtained. The results are shown in Figure 4.6 to Figure 4.9.

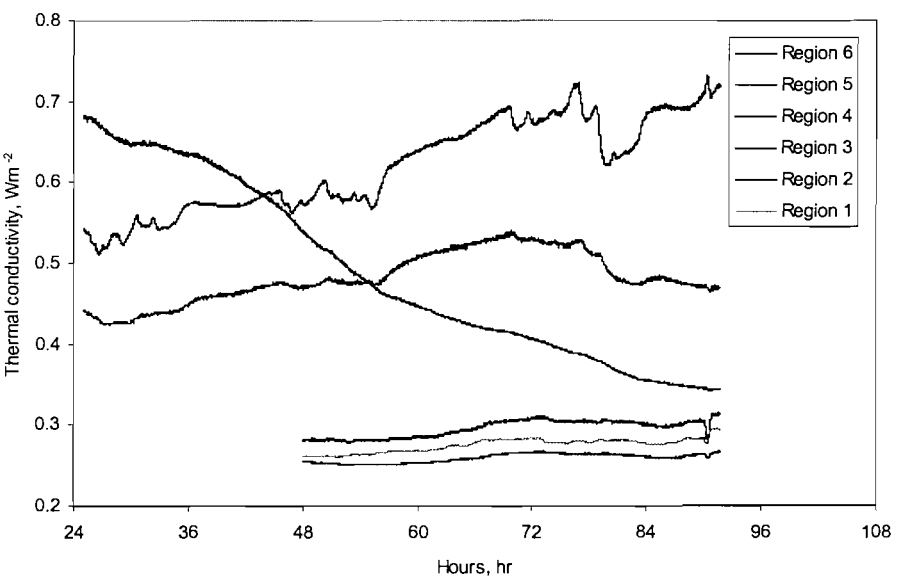

Figure 4.6 - Thermal conductivity variations on $40Wm^{-2}$ heating, initial volumetric moisture content of 1 %.

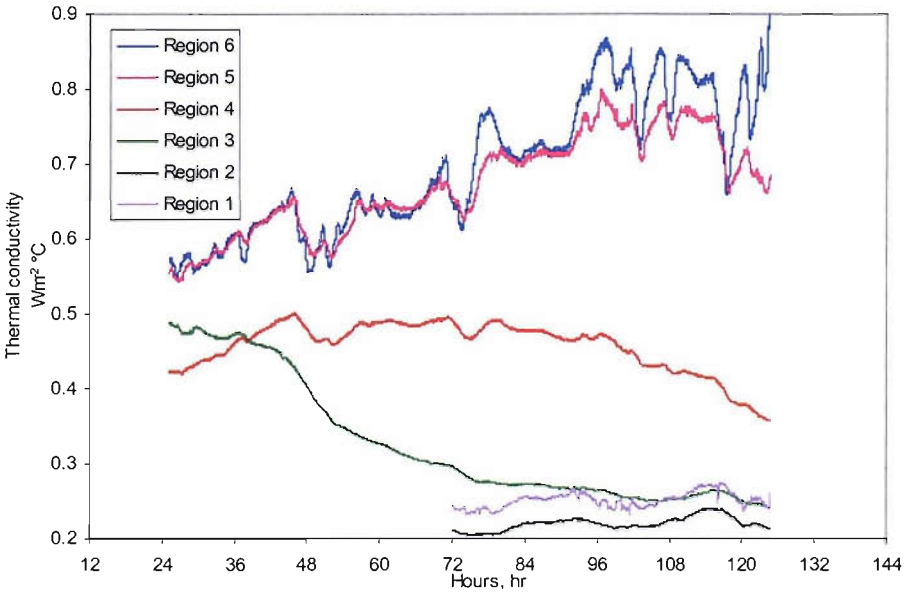

Figure 4.7 (a) - Thermal conductivity variations on 40Wm^{-2} heating, initial volumetric moisture content of 1.6%.

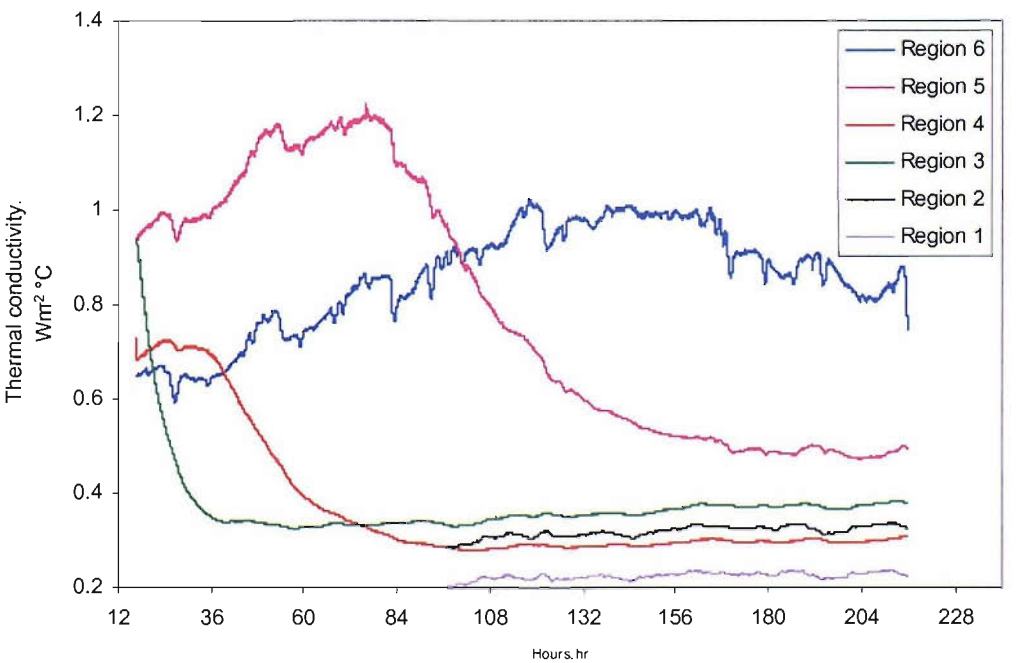

Figure 4.7 (b) - Thermal conductivity variations on 80Wm^{-2} heating, initial volumetric moisture content of 1.6%.

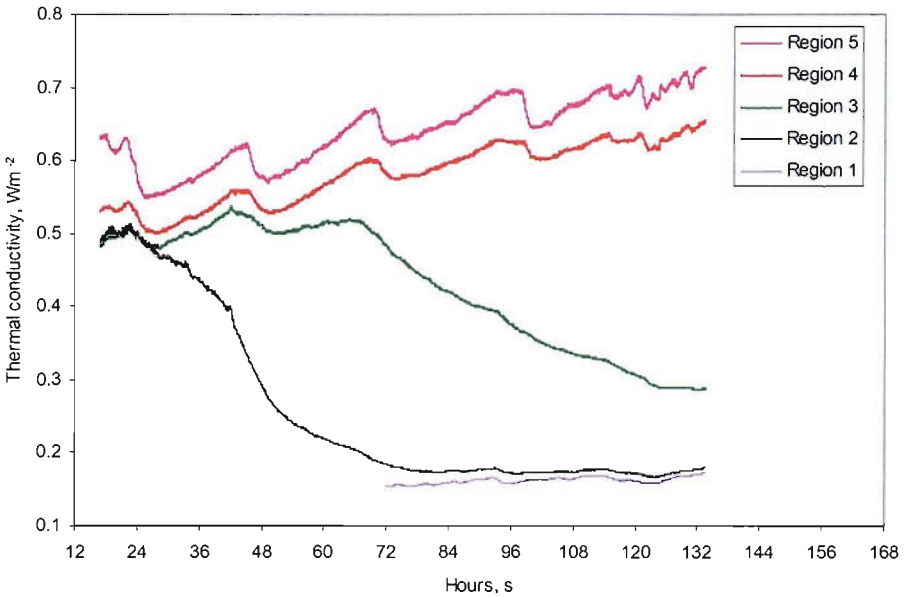

Figure 4.8 (a) - Thermal conductivity variations on 40Wm^{-2} heating, initial volumetric moisture content of 3%.

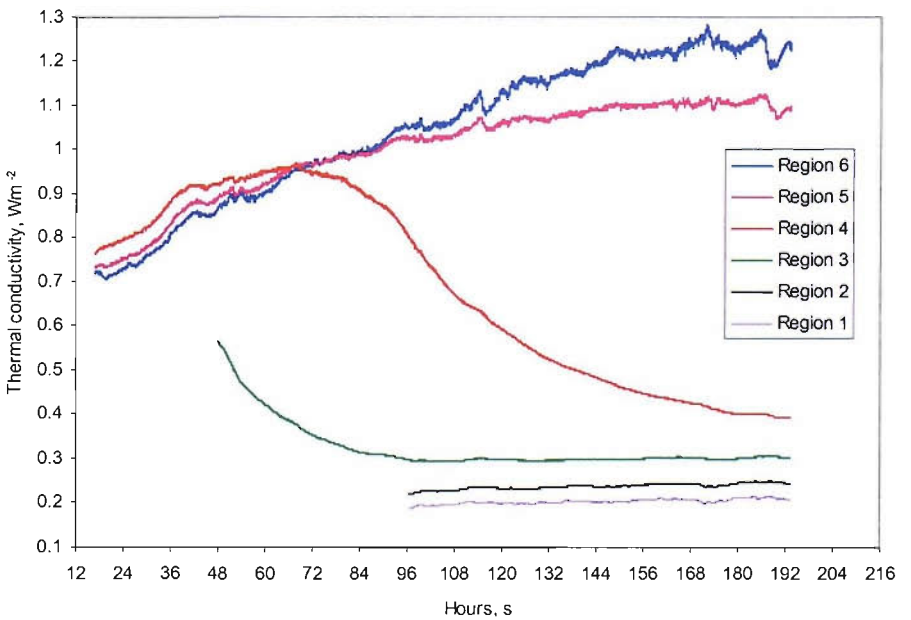

Figure 4.8 (b) - Thermal conductivity variations on 80Wm^{-2} heating, 0.03 initial volumetric moisture content of 3%.

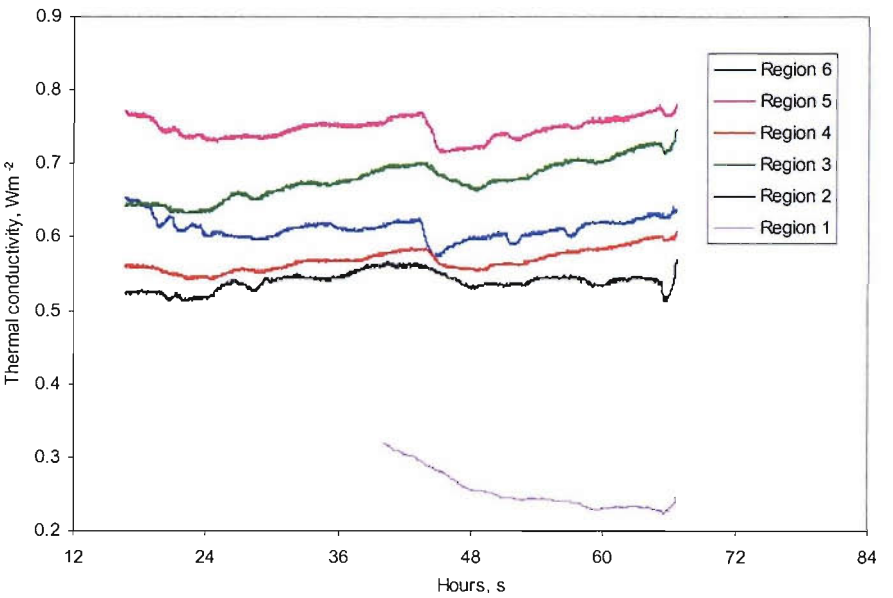

Figure 4.9 (a) - Thermal conductivity variations on 40Wm^{-2} heating, initial volumetric moisture content of 5%.

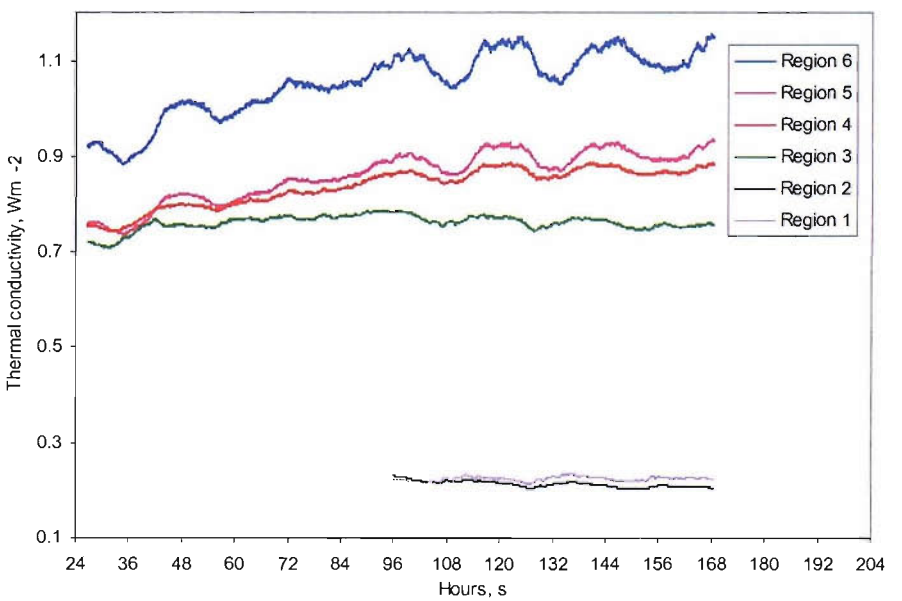

Figure 4.9 (b) - Thermal conductivity variations on 80Wm^{-2} heating, initial volumetric moisture content of 5%.

4.3.1 Discussion

It can be seen from the $40Wm^{-2}$ heating of Figures 4.6, 4.7(a), and 4.8(a), that regions 1 and 2 are practically dry at the end of each experiment. The thermal conductivity of these regions is the lowest compared to that of other regions and remain fairly constant until the end of each experiment (note that any fluctuation in thermal conductivity is due to temperature variations). This suggests that these regions may have attained dry thermal conductivities. Moisture also seems to have migrated from these regions before the steady state temperature is reached. Whereas thermal conductivities of regions 5 and 6 continually increase until the end of experiment suggesting that moisture accumulates in the cooler region and acts to increase thermal conductivity. Region 3 of Figure 4.6 and 4.7(a) also has a low thermal conductivity and this remains fairly constant throughout the experiment. However, the low thermal conductivity in regions 1, 2 and 3 are attained earlier in Figure 4.6 compared to Figure 4.7(a). This is as expected as 1% as this experiment had the lowest initial volumetric moisture content and therefore the drying rate is faster.

Thermal conductivity remains low only in region 1 of Figure 4.9(a). This is because for this experiment the initial volumetric moisture content is greatest. From Figure 4.9(a), it can be seen that the thermal conductivity in region 5 is higher than that of region 6. This may be due to the influence of gravity. Since the temperature gradients in regions 5 and 6 are not high, the distance of these regions away from the hot plate may have caused the influence of gravity to become significant. Referring to the Philip and de Vries heat and moisture transfer equations, hydraulic permeability is a gravity dependent term. At high moisture contents, water flow is higher and therefore, in the case of 5% initial volumetric moisture content (Figure 4.9(a)), accumulation of moisture in higher regions is affected by gravity causing a net downwards migration.

The thermal conductivity in region 3 of Figure 4.9(a) is also higher than region 4. This could be explained by the migration of moisture away from the lower regions but the accumulated moisture may not quite reach region 4, and will not increase the thermal conductivity significantly.

For initial volumetric moisture contents of 3% and 5%, by the end of the experiment, using $80Wm^{-2}$ heating shows that regions 5 and 6 attain thermal conductivity as high as 1.2 - 1.4 $Wm^{-2}C^{-1}$. This is not seen in experiment 3, which at the end of the experiment had its thermal conductivity of region 5 decreasing indicating that the dry/wet interface is approaching.

The drying at lower regions using $80Wm^{-2}$ heating is more extensive than the $40Wm^{-2}$ experiments. More regions are found to attain low thermal conductivity at the end of each experiment, which means the dry volume is greater than that of $40Wm^{-2}$. The gravity effect as described earlier for Figure 4.9(a) was however, not attained in Figure 4.9(b). This may be due to the stronger heat flux induced when using the $80Wm^{-2}$ heating thus net moisture flow upwards is more significant than hydraulic permeability.

With the information obtained from these graphs, it is possible to compare the predicted location of the dry/wet interface with the actual location. For example, for $80Wm^{-2}$ heatings on 0.016 and 0.05 initial volumetric moisture contents, visual inspection at the end of each experiment revealed that interface is approximately at 15 and 8 cm away from the hot plate respectively. Referring to Figures 4.8(b) and 4.9(b), the location of the dry/wet interface could be predicted between regions 4 - 5 and between regions 2 - 3 respectively. The measurements recorded (approximately 18 cm and 8 cm away from the hotplate) lie in these regions. Therefore, it is possible to predict the dry/wet interface by determining the behaviour of the changing 'local' thermal conductivity.

Results have also shown in Figures 4.2-4.9 that dry/wet interface is possible to form at temperatures well below 50°C. It is also evident that initial volumetric moisture content has an influence on the temperature and distance (away from the heat source) at which dry/wet interface starts to form. It is observed in Figures 4.3(b), 4.4(b) and 4.5(b) that at 96 hours, dry/wet interface started to form at about 34°C, 40°C and 60°C for 0.01, 0.016 and 0.05 initial volumetric moisture contents, respectively. (Temperature at which dry/wet interface started to occur is taken as the greater temperature recorded by the thermocouple nearest to the dry/wet interface) . Also, at 96 hours, each of these interfaces is formed within Regions 4, 5 and 2 for 0.01, 0.016 and 0.05 initial volumetric moisture contents, respectively. This shows that lower initial moisture contents are susceptible to greater rate of thermal runaway with possibility of dry/wet interface forming at temperatures well below 50°C.

4.4 CONCLUSIONS

Migration of moisture shown in the MMA experiments shows that heat is transferred at a faster rate when the initial moisture content of soil is lower and of course, when the heating power is higher. Prior to cable energisation, it is important to ensure that the initial moisture content of soil or backfill is above a defined minimum level so that possible rapid and extensive drying of the backfill is prevented.

The imposed temperature gradient forces moisture to flow away from hotter regions and therefore, influences the thermal conductivity of sub-regions to alter; ie. to decrease when losing moisture and to increase when gaining moisture. The influence of gravity at moderate heating power starts to become significant when the initial volumetric moisture content is approximately greater than 5%.

The experiment has also shown that excessive dryings occur at temperatures well below 50°C for low moisture contents (that of less than 5%). Therefore, if conservative approach of assigning 50°C isotherms to dry/wet interface are to be applied in solving heat transfer problem around underground cables, it would only be valid for backfills (if similar to SWN1) with initial volumetric moisture content of 5% or maybe greater.

CHAPTER 5

5.0 FEMLAB: HEAT AND MOISTURE DISTRIBUTION

The finite element method (FEM) has been chosen to simulate the MMA results described in chapter 4 using the mathematical equations describing the heat and moisture relationship developed by Philip and de Vries [41]. This method has advantages over finite difference methods [41]. Unlike the finite difference method, the solution obtained is a continuous solution in the whole area of the elements and not at the nodes. Hence it is preferable to many researchers, especially, in this field of interest [42, 43, 44, 45]. Complex geometries can be easily handled with computer written programs. Finite element programs could be written in any computing language such as Borland C, Microsoft C++ or MATLAB. However, now that computing power has greatly increased specialist tools for mathematical modelling that are mainly graphical user interface (GUI) handled have been developed. These tools exploit computing power to tackle complex problems and solve partial differential equations (PDEs). Identified common tools that are capable of solving PDEs using the finite element method are ANSYS and the increasingly popular software, FEMLAB.

After much familiarising with ANSYS during the early stages of the project, it was found that its capability in handling or solving several PDEs simultaneously is both complex and tedious. FEMLAB is more robust, flexible and capable of solving PDEs simultaneously and allow interactions of various physical phenomena. This makes FEMLAB indeed a unique tool and almost all of its applications are straightforward. It also offers computer aided design (CAD) facilities and covers the employment of automatic mesh generation, equation solving, visualisation and

post-processing in one integrated environment. Hence, it has been preferred over ANSYS as the tool to solve the heat and moisture equations proposed by Philip and de Vries.

5.1 FINITE ELEMENT - GENERAL FORM

Linear, nonlinear and eigenvalue PDEs can be solved in FEMLAB using the coefficient, general or weak form of the finite element method. It is convenient and simple to solve a 2D problem (of Philips and de Vries equations) using the coefficient form. Although simplicity is introduced in coefficient form solutions, the analytical Jacobian matrix is not necessarily computed correctly and thus will lead to slow convergence.

However, an exact Jacobian matrix is calculated when the general form solution is used and therefore, a faster convergence is achieved. Therefore, since the nature of the problem is highly non-linear and coefficients are dependant on the field variables, namely temperature and volumetric moisture content, the general form is more suitable for this application.

A time dependant PDE problem, in general form and in a bounded region Ω is given by [102],

$$d_a \frac{\partial u}{\partial t} \nabla . \Gamma = F \tag{5.1}$$

Where d_a, Γ and F are coefficients. d_a and Γ are also known as the mass coefficient and flux vector, respectively. u is the dependent field variable and t is time.

The generalised Neumann boundary condition [102] on the region boundary $\delta\Omega$ are given by (5.2)

$$-\mathbf{n}\Gamma = G + \left(\frac{\partial R}{\partial u}\right)^T \mu \tag{5.2}$$

Where G and R are also coefficients. μ is an unknown new function called the Lagrange multiplier, **n** is the outward unit normal vector. The superscript ^{T} to coefficient $\frac{\partial R}{\partial u}$ is the transpose of $\frac{\partial R}{\partial u}$.

The Dirichlet boundary condition on the region boundary $\delta\Omega$ [102] is given by (5.3),

$$0 = R \tag{5.3}$$

Since there are two variables involved, temperature (T) and volumetric moisture content (θ), it is necessary to generate the PDE in a coefficient form that is capable of accommodating two variables.

The general form of (5.1) in 2 dimensional space in a bounded region Ω [102] is given by (5.4) and (5.5).

$$d_a \frac{\partial u_1}{\partial t} + \nabla.\Gamma_1 = F_1 \tag{5.4}$$

$$d_a \frac{\partial u_2}{\partial t} + \nabla.\Gamma_2 = F_2 \tag{5.5}$$

And the generalized Neumann boundary condition on $\partial\Omega$ [102] is given by,

$$-\mathbf{n}\Gamma_1 = G_1 + \left(\frac{\partial R_1}{\partial u_1}\right)^T \mu_1 + \left(\frac{\partial R_2}{\partial u_1}\right)^T \mu_2 \tag{5.6}$$

$$-\mathbf{n}\Gamma_2 = G_2 + \left(\frac{\partial R_1}{\partial u_2}\right)^T \mu_1 + \left(\frac{\partial R_2}{\partial u_2}\right)^T \mu_2 \tag{5.7}$$

Therefore the Dirichlet boundary condition on $\partial\Omega$ [102] is given by,

$$0 = R_1 \tag{5.8}$$

$$0 = R_2 \tag{5.9}$$

5.1.1 Linearisation

Due to the soil parameters being highly dependant on changes in volumetric moisture content and temperature, simulation times are lengthy. Therefore, an alternative approach has been taken. A faster convergence is achieved by performing a linearisation process on the non-linear Philips and de Vries equations. The linearisation involves transforming the equations into coefficient form. The linearisation used in FEMLAB [102] is as given in (5.10), (5.11) and (5.12).

$$d_a \frac{\partial u}{\partial t} + (-c_b \nabla \tilde{u} - \alpha \tilde{u} + \gamma_b) + \beta . \nabla \tilde{u} + a_b \tilde{u} = F \tag{5.10}$$

$$\mathbf{n}(c_b \nabla \tilde{u} + \alpha \tilde{u} - \gamma_b) + q_b \tilde{u} = g_b - h_b{}^T \mu \tag{5.11}$$

$$h_b \tilde{u} = r \tag{5.12}$$

Where c_b is the diffusion coefficient, α is the conservative flux convection coefficient, γ_b is the conservative flux source term, β is the convection coefficient, a_b is the absorption coefficient, q_b is the boundary absorption coefficient, f is the source term, g_b is the boundary source term, h_b is the scalar coefficient for Lagrange multiplier, μ and r is the boundary term. (5.10) is the general linearisation in bounded region Ω; (5.11) is the Neumann boundary on the bounded region $\partial\Omega$ and (5.12) is the Dirichlet boundary on the bounded region $\partial\Omega$.

And $\tilde{u}$ is defined [102] as

$$\tilde{u} = u - u_0 \tag{5.13}$$

Where u_0 is the linearisation point, which usually is the initial value of u. The coefficients in (5.10), (5.11) and (5.12) are, therefore, transformed into (5.14)-(5.23) [102].

$$c_b = \frac{\partial \Gamma}{\partial \nabla u} \tag{5.14}$$

$$\alpha = \frac{\partial \Gamma}{\partial u} \tag{5.15}$$

$$\beta = \frac{\partial F}{\partial \nabla u} \tag{5.16}$$

$$a_b = \frac{\partial F}{\partial u} \tag{5.17}$$

$$q_b = \frac{\partial G}{\partial u} \tag{5.18}$$

$$h_b = \frac{\partial R}{\partial u} \tag{5.19}$$

$$\gamma_b = \Gamma \tag{5.20}$$

$$f = F \tag{5.21}$$

$$g_b = G \quad (5.22) \qquad r = R \quad (5.23)$$

For the simulations the time step that has been used is 10 minutes. Through observation of trial and error, the interval was found to be fairly reasonable in optimising the length of simulation time and minimising required memory. Too small a step size requires large memory space and may overload the workspace. Furthermore, a greater amount of time steps increases the length of simulation time since variable coefficients are computed at each time step. Therefore, optimising the size of the time step is crucial especially when meshes are subsequently refined to larger amounts of elements and nodes.

5.2 MMA SIMULATION

The use of FEMLAB starts with finalising the geometry and dimension of the MMA experiment into the FEMLAB environment. Due to high non-linearity of the soil properties and the cylindrical symmetry of the MMA apparatus, it is wise to reduce the 3-D problem into a 2-D problem. Since it is originally a cylindrical-geometry problem, reducing to a 2-D problem requires a transformation of the solution equations. This is practical because the solutions would be independent of the cylindrical coordinate, θ. Therefore, reduction to a 2-D problem means the cylindrical coordinate r and z is transformed to x-y plane coordinates of the 2-D environment. It is assumed that the soil is homogeneous and that the stress-strain effect is negligible.

Since the nature of the problem is symmetrical, only half of the domain needs to be solved. The truncated part of the half-geometry is placed along the y-axis where x=0. This axis is not a boundary in the original problem but due to the transformation of the problem into a 2-D case, an artificial Neumann boundary

condition is essential. The initial values of temperature and volumetric moisture content are set as zero at this boundary. Since the solutions involve the physics of conduction heat transfer and water diffusion, the model to be developed is multi-physical. The unknown components are temperature, T and moisture content (volumetric), θ. These are also the terms that couple the heat and moisture equations. Heat transfer and diffusion modes are selected and the geometrical problem employed is as shown in Figure 5.1. Bold numbers shown are the assigned edge/boundary numbers. The geometry is divided into two subdomains. One is to represent the hotplate and the other is the SWN1 soil. Prior to solving, these are meshed using the automatic mesh generator and the hotplate subdomain is made inactive for the moisture solution.

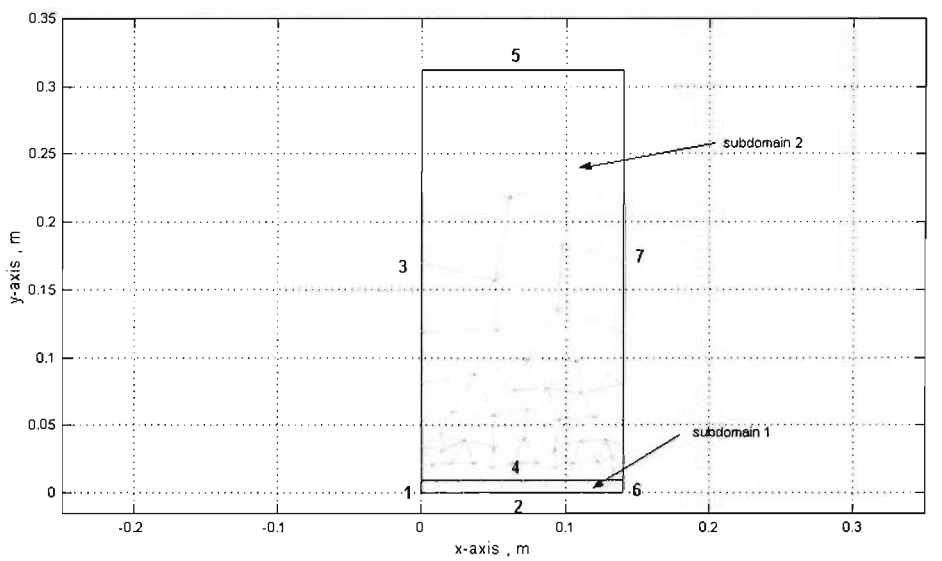

Figure 5.1- Mesh S1: meshed geometry for 40Wm^{-2} experiment on initial volumetric moisture content of 1.6%.

5.2.1 Mesh

For each of the MMA experiments, the cylindrical apparatus was prepared and refilled. For example, an 80 Wm^{-2} experiment was not repeated on the compacted sample that had been used for a 40 Wm^{-2} experiment and vice versa. This is because the moisture displacement after a completion of any particular experiment would require redistribution as it may not be uniform. Therefore, due to the difficulty in maintaining similar compaction for the same initial volumetric moisture content, the volumetric compaction for each experiment varies and this alters the geometry used in FEMLAB for each simulation. In consequence, the total elements and nodes employed vary from one experiment to another. However, in order to maintain similar quality of the meshes in every case, four mesh parameters are set. These are the maximum general-edge size, maximum element size for the surface in contact with the hot plate (edge 4 in Figure 5.1), mesh growth rate and mesh size expression. The value for the maximum general-edge size is set to 0.075 and maximum element size for edge 4 is set to 0.015. Whereas the mesh size expression is set as

$$x^2 + y^2 + 0.14 \tag{5.24}$$

A finer mesh has been accommodated at the region where intense heat flux is expected in order to achieve accurate results. Therefore, for the refined mesh near the hotplate, a growth rate of 1.35 is used. Mesh details for each simulation are as shown in Table 5.1. This pre-defined mesh is named mesh S1. Further mesh refinement has been done using FEMLAB default settings, which divide each element into four further elements. Details on the refined mesh for each experiment are also shown in Table 5.1. This refined mesh is named mesh S2. Figure 5.2 shows an example of an S2 mesh for the 40Wm^{-2} experiment on initial volumetric moisture content of 1.6% (refined version of mesh in Figure 5.1).

EXPERIMENT		NO. OF ELEMENTS		NUMBER OF NODES	
INITIAL θ	HEATING, Wm^{-2}	S1	S2	S1	S2
0.01	40	119	476	74	266
0.016	40	121	484	75	270
	80	119	476	73	264
0.03	40	129	516	79	286
	80	126	500	78	278
0.05	40	123	492	76	274
	80	123	492	76	274

Table 5.1 - Mesh details of the geometry of all experiments.

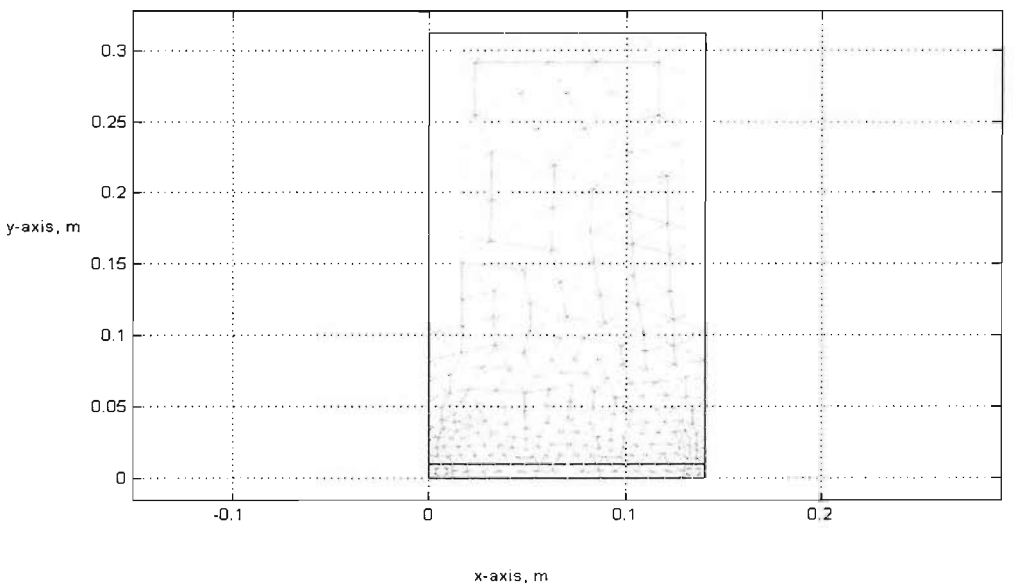

Figure 5.2 - Mesh S2 : refined meshed geometry for $40Wm^{-2}$ experiment on initial volumetric moisture content of 1.6%.

5.2.2 Coefficients and Boundaries

Heat flux per area could be assigned at the soil/hotplate edge (and therefore the hotplate domain is totally neglected) but since the time constant of the soil heating depends on the interaction between specific heat capacity of the soil and the hotplate, it is practical to assign the hot plate with the equivalent heat source in $Wm^{-3}°C^{-1}$.

Constants are not used for soil parameters but instead they are made variable, as functions of both temperature and moisture. These are the thermal conductivity, hydraulic permeability, moisture and thermal diffusivities of the soil. Each of these parameters is saved as MATLAB editor files that are accessible during the simulation in FEMLAB. The specific heat capacity and the thermal conductivity of the hot plate are constant. Details of the parameters used are shown in Table 5.2 and conditions at the boundaries (as defined in Figure 5.1) detailed in Table 5.3.

PROPERTIES	SOIL (EDITOR)	HOTPLATE
Specific heat capacity, $Jm^{-3}°C^{-1}$	Cp.m	$0.2e^{6}$
Thermal conductivity, $Wm^{-1}°C^{-1}$	Thermcon.m	12
Moisture diffusivity, m^2s^{-1}	Diff_O.m	-
Thermal diffusivity, $m^2s^{-1}°C^{-1}$	Diff_T.m	-
Hydraulic permeability, ms^{-1}	Kunsat.m	-
Isothermal moisture diffusivity, $m^2s^{-1}°C^{-1}$	Diff_OV.m	-

Table 5.2 - Variable coefficients used in FEMLAB.

Boundary with respect to Figure 5.1	1	2	3	5	6	7
θ						
Initial	inactive	inactive	0	θ_i	inactive	θ_i
Type	-	-	Neumann	Neumann	-	Neumann
q_b	inactive	inactive	0	0	inactive	0
g_b	inactive	inactive	0	0	inactive	0
h_b	inactive	inactive	0	0	inactive	0
r	inactive	inactive	0	0	inactive	0
T						
Initial	0	T_i	0	T_i	T_i	T_i
Type	Neumann	Neumann	Neumann	Dirichlet	Neumann	Neumann
q_b	0	0	0	0	0	0
g_b	0	0	0	0	0	0
h_b	0	0	0	1	0	0
r	0	0	0	T_c	0	0

Table 5.3 - Boundary conditions with q_b, g_b, h_b and r as defined in equations 5.18, 5.19, 5.22 and 5.23 respectively.

Ti and θ_i are the initial temperature and volumetric moisture content, respectively. T_c is temperature of the cold plate. The hotplate is impermeable to moisture and therefore, simulation time has been alternatively reduced by setting this particular subdomain inactive. Since boundary 4 is the interface boundary between the hotplate and soil, it has been disabled and therefore not included in Table 5.3.

5.3 RESULTS

There are three sets of simulation results for each experimental case. These are the simulations using soil properties (as described in Table 5.2) on mesh S1, modified soil properties on mesh S1 and modified soil properties on mesh S2. These simulations are named simulation FEM-OS1, FEM-MS1 and FEM-MS2.

5.3.1 FEM-OS1

The term FEM-OS1 is used to label the simulations that resulted from using the soil properties on coarse mesh S1. Results are as shown in Figures 5.3 - 5.6. Each simulation is referred to in the following text by its moisture content/heat power.

It can be seen from Figures 5.3 and 5.4(a) that FEM-OS1 simulations on 0.016/40 Wm^{-2} and 0.01/40 Wm^{-2} have produced results that are in reasonable agreement with the experimental results. This indicates that the soil properties that used are accurate for volumetric moisture contents of 0.01 and 0.016 when in conditions of moderate heat flux.

Simulated steady state temperatures T_2 - T_7 of Figures 5.3 and 5.4 are in good agreement with the experimental values. These simulated temperatures successfully reflect that hydrological effects do occur such that the local thermal conductivity of the hotter region is decreased and vice versa due to moisture migration. In consequence, the temperatures (T_1 and T_2) near the hottest region continue to increase and those away from the hotplate (T_5, T_6 and T_7) continue to decrease.

The greatest absolute error generated by FEM-OS1 on 0.01/40 Wm^{-2} and 0.016/40 Wm^{-2} during the transient state is about 14% for both. Whereas during the

steady state, greatest absolute error generated on 0.01/40 Wm^{-2} and 0.016/40 Wm^{-2} are about 6% and 8% respectively.

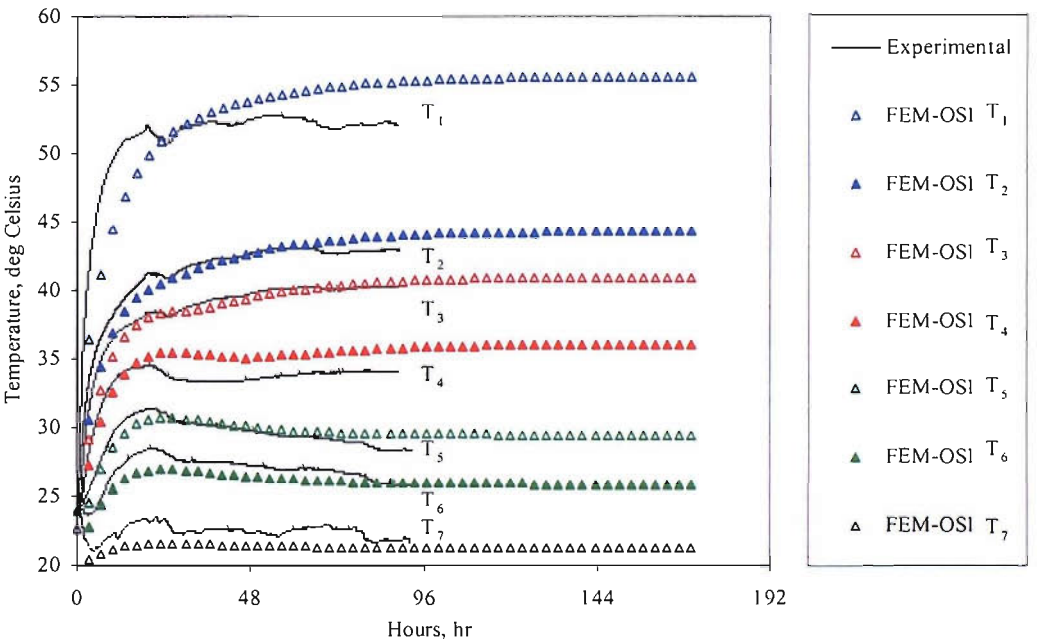

Figure 5.3 - FEM-OS1 result for 40 Wm^{-2} heating on initial volumetric moisture content of 1%.

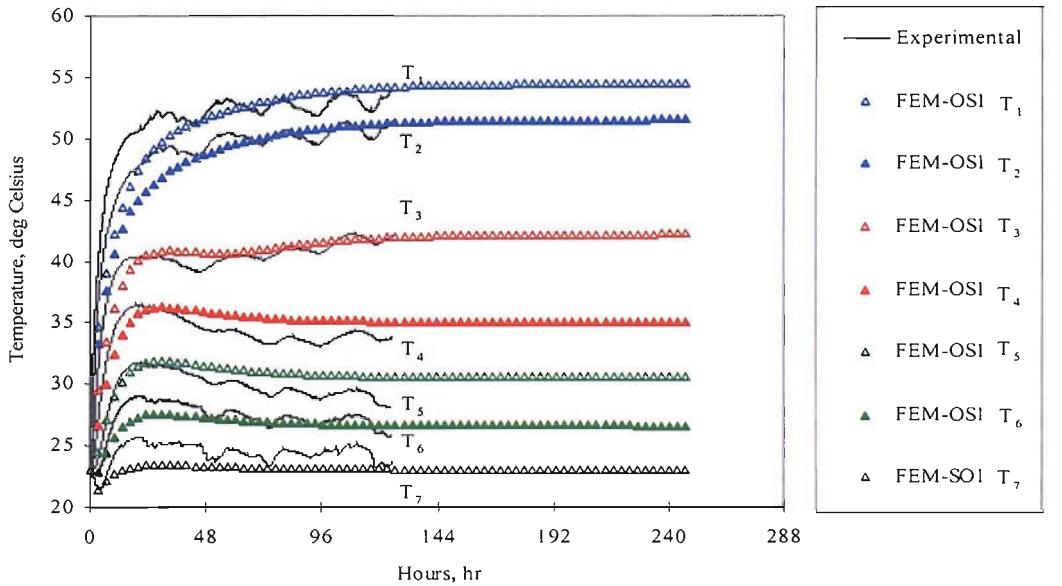

Figure 5.4(a) - FEM-OS1 result for 40 Wm^{-2} heating on initial volumetric moisture content of 1.6%.

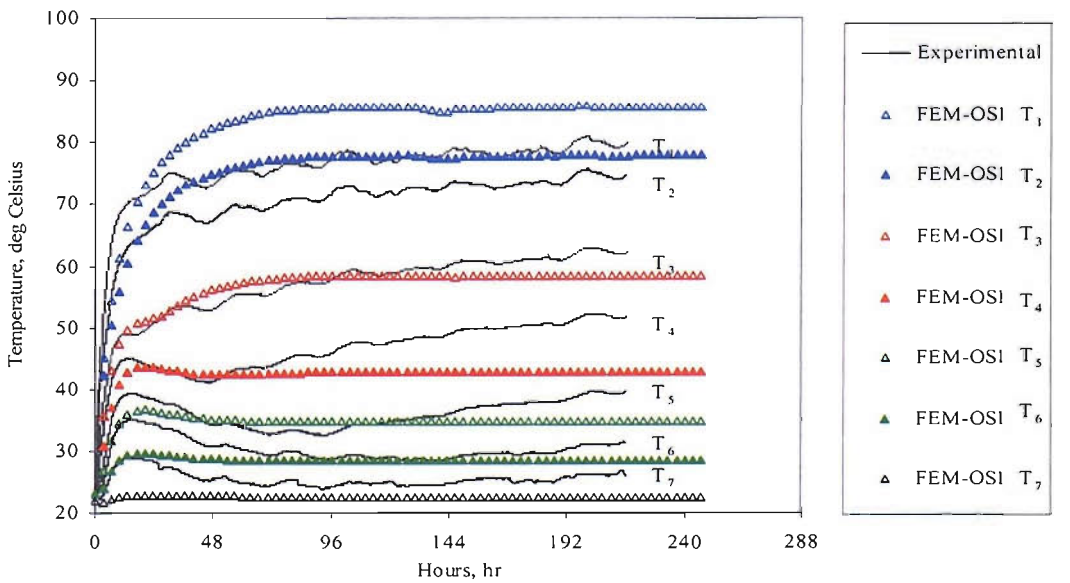

Figure 5.4(b) - FEM-OS1 result for 80 Wm^{-2} heating on initial volumetric moisture content of 1.6%.

On the other hand, FEM-OS1 simulations on 0.016/80 Wm^{-2}, 0.03/40 Wm^{-2}, 0.03/80 Wm^{-2} and 0.05/80 Wm^{-2} have less satisfactory results. Most simulated temperatures have been underestimated and remain constant once a steady state value has been reached. This behaviour shows that the FEM-SO1 simulations in these cases fail to reflect the actual hydrological effects that are occurring. Figures 5.4 – 5.6 show that each simulated temperature does not vary over time and therefore does not represent any changes in thermal conductivity due to moisture migration.

The FEM-OS1 simulated temperature of the hot plate for 0.03/40 Wm^{-2} and 0.05/40 Wm^{-2} cases is about 45 °C and 42 °C respectively. Although it is as expected (ie the hotplate temperature is greater for the 0.03/40 Wm^{-2} case than that for 0.05/40 Wm^{-2}), these values have actually been under estimated by at least 10% over the duration of the experiment. When the simulation time increases beyond the experiment time length, the error can be expected to increase as the actual temperature of the hotplate continues to rise while that of the simulation remains constant.

The time-extended FEM-OS1 simulation shown in Figure 5.5(a) reveals that although simulated temperatures on 0.05/40 Wm^{-2} are in good agreement to those of the experimental values, the simulated temperatures fail to show any decrement due to increased local thermal conductivity as the result of moisture migration from region 1. FEM-OS1 simulations for 0.016/80 Wm^{-2}, 0.03/80 Wm^{-2} and 0.05/80 Wm^{-2} have resulting errors as great as 18%, 16% and 24% respectively. The simulated steady state temperature of T_1 and T_2 in Figure 5.4(b) has been over estimated by about 8-9 °C, whereas the transient simulated temperatures of T_1 and T_2 in Figures 5.5(b) and 5.6(b) have been underestimated and vary from the actual experimental temperatures by about 20%.

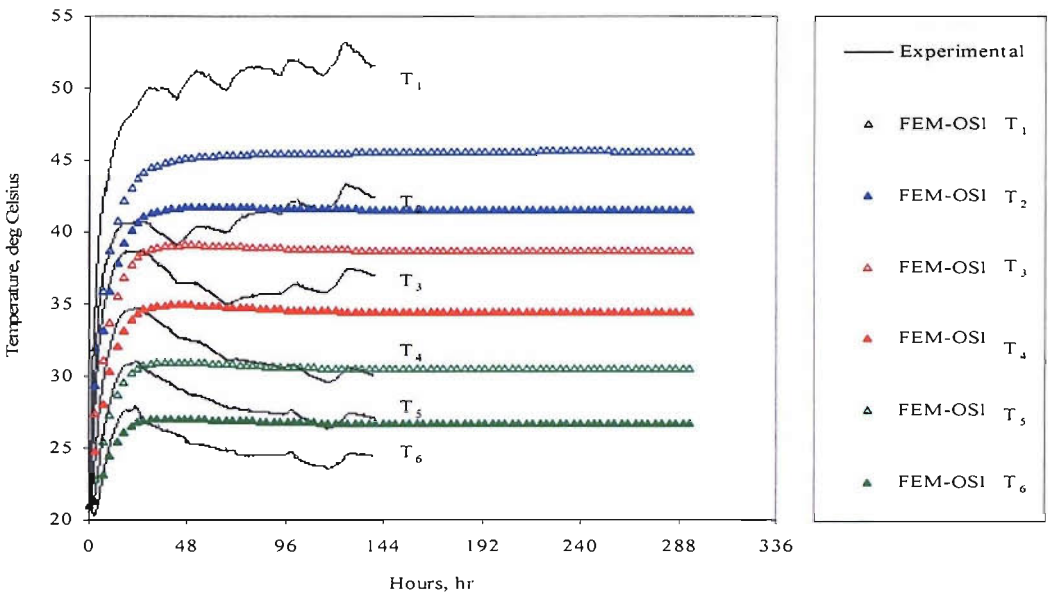

Figure 5.5(a) - FEM-OS1 result for 40 Wm^{-2} heating on initial volumetric moisture content of 3%.

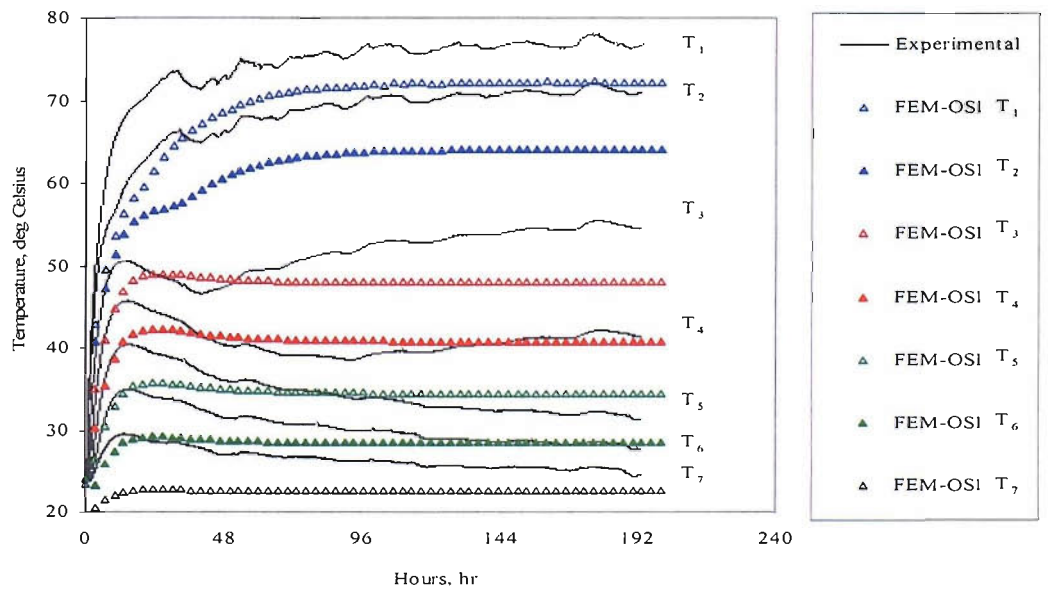

Figure 5.5(b) - FEM-OS1 result for 80 Wm^{-2} heating on initial volumetric moisture content of 3%.

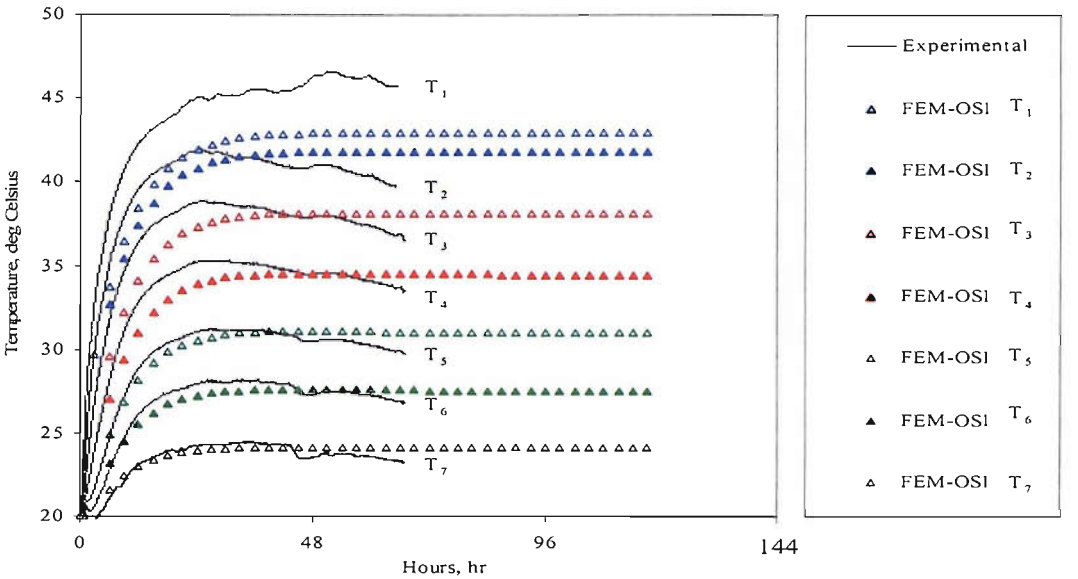

Figure 5.6(a) - FEM-OS1 result for 40 Wm^{-2} heating on initial volumetric moisture content of 5%.

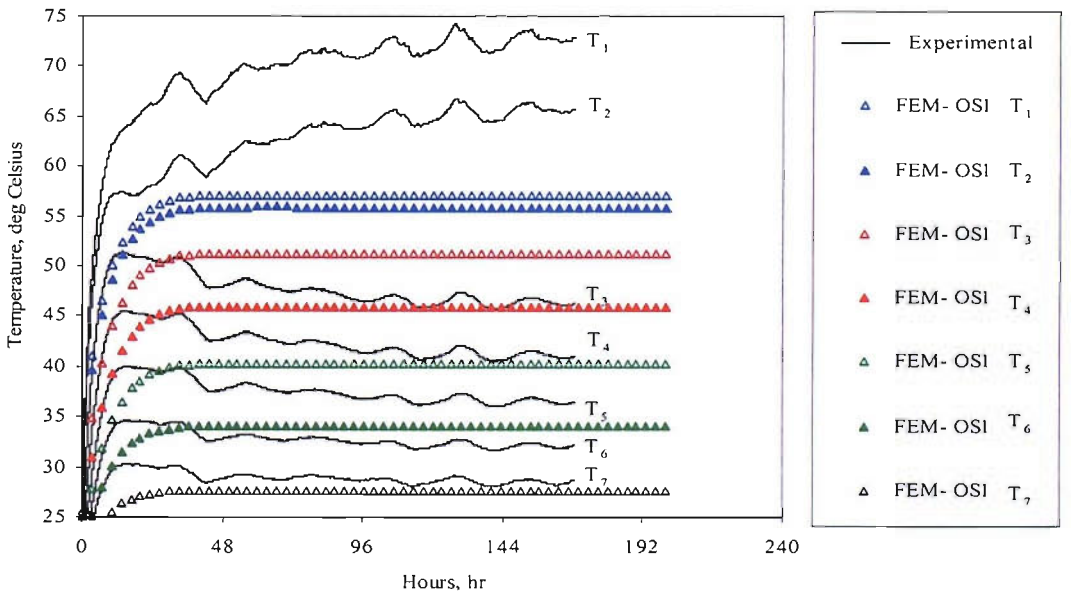

Figure 5.6(b) - FEM-OS1 result for 80 Wm^{-2} heating on initial volumetric moisture content of 5%.

FEM-OS1 simulations on all experiments have shown that the soil properties used do not always reflect the actual variations in temperature due to the hydrological effect modelled using the Philip and de Vries equations. Only FEM-OS1 simulations on 0.01/40 Wm^{-2} and 0.016/40 Wm^{-2} have actually shown the temperatures of T_2 - T_7 responding to moisture migrating across the hotter region towards the cooler region. It is worth investigating which coefficients significantly influence the discrepancies occurring in these simulations.

Although thermal conductivity is the most influential factor in thermal distribution, it was not the factor that has the greatest effect on the simulation results. This is because thermal conductivity of SWN1 has been both experimentally and analytically determined and for t-distribution of 95%, the confidence interval is fairly small.

When thermal conductivity is altered by a factor and used in the FEM-OS1 simulations, the simulated temperatures increase or decrease accordingly by a constant displacement. The temperature response fails to show immediate changes in temperatures wherever possible when moisture migration is present. In other words, the simulation is still insensitive to the moisture distribution. For example, FEM-OS1 has been repeated on the 80 Wm^{-2} MMA experiment of the initial volumetric moisture content of 0.03. The same thermal conductivity editor file has been used to provide the necessary calculation but it was reduced to a factor of 0.85. The results of this simulation are shown in Figure 5.7.

Results that are obtained with the reduced thermal conductivity are indicated by the FEM-SO1-R legends. The gradual reduction in experimental temperatures of T_2, T_3, T_4, T_5, T_6 and T_7 in Figure 5.6 clearly indicate that substantial amount of moisture has migrated from the hotter region such that the local thermal conductivity is increased hence the temperature decrement. Both FEM-SO1 and

FEM-SO1-R simulations have shown that temperatures of these locations did not gradually decrease as a consequent of the moisture migration.

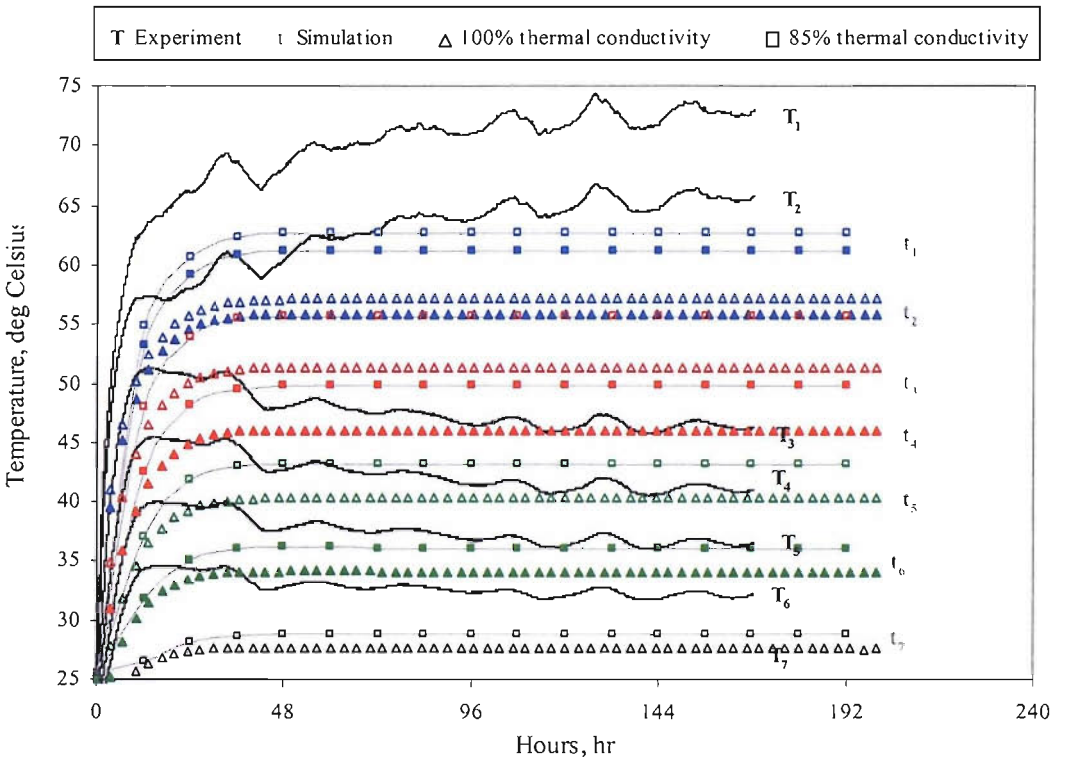

Figure 5.7 – Comparison of results for 80 Wm^{-2} heating with initial volumetric moisture content of 5%.

Through further investigation using FEMLAB, it was found that temperature and moisture distributions are sensitive to changes in isothermal moisture diffusivity, isothermal vapour diffusivity and hydraulic conductivity ie model parameters. It is fair to conclude that if these properties are accurately determined, the moisture distribution that would be calculated will ensure correct calculation of local thermal conductivity and hence temperature distribution.

After many attempts in simulating each case by trial and error (using similar approach to other soil hydraulic properties - properties are increased and decreased by a certain factor), it was found that isothermal vapour diffusivity, unsaturated hydraulic conductivity and moisture diffusivity interactively play a great role in influencing the simulated temperature response under conditions of moisture migration. Therefore, this proves that these properties are as important as thermal conductivity in determining a dynamic temperature distribution. This is further discussed in the next section.

5.3.2 FEM-MS1 and FEM-MS2

Investigation (applying constants to dynamic parameters by trial and error) has revealed that the isothermal vapour diffusivity, hydraulic conductivity and isothermal diffusivity have been overestimated and, therefore, may have caused previous FEM-SO1 simulations to produce erroneous results.

It was found that isothermal diffusivity has been overestimated by about two orders of magnitude for volumetric moisture contents below 0.05 and about 15 times more for that above 0.05. Whilst the isothermal vapour diffusivity has been overestimated by an order of magnitude for volumetric moisture contents below 0.05 and about 15 times more for that above 0.05. The unsaturated hydraulic permeability has also been overestimated by 2 to 3 orders of magnitude over all ranges of θ.

Modifications are applied by multiplying the appropriate fraction to each of the properties. These are as shown in (5.25), (5.26) and (5.27) for the isothermal vapour diffusivity, isothermal moisture diffusivity and hydraulic permeability, respectively. Modifications have been applied appropriately and simulations for all MMA experiments are repeated on meshes S1 and S2. These are labelled as FEM-MS1

and FEM-MS2 simulations respectively and the results can be seen in Figures 5.8 - 5.10.

With reference to the parameters defined in (3.19), (2.9) and (3.8), the following soil parameters are modified to be (5.25), (5.26) and (5.27) respectively.

$$\left.\begin{aligned} D_{\theta V\_mod} &= 0.01 D_{\theta V} \quad \text{for} \quad \theta \le 0.05 \\ &= 0.065 D_{\theta V} \quad \text{for} \quad \theta > 0.05 \end{aligned}\right\} \tag{5.25}$$

$$\left.\begin{aligned} D_{\theta\_mod} &= 0.1 D_{\theta} \quad \text{for} \quad \theta \le 0.05 \\ &= 0.065 D_{\theta} \quad \text{for} \quad \theta > 0.05 \end{aligned}\right\} \tag{5.26}$$

$$K_{unsat\_mod} = 1e^{-5}.\theta^{4.2345} \tag{5.27}$$

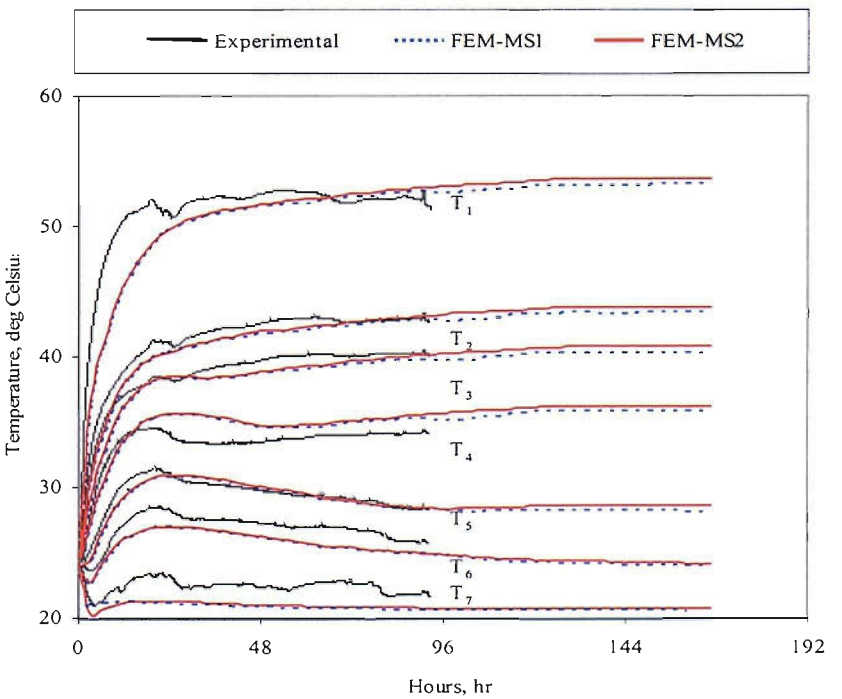

Figure 5.8–FEM-MS1 and FEM-MS2 results for 40 Wm^{-2} heating on initial volumetric moisture content of 0.01 as compared to experimental results.

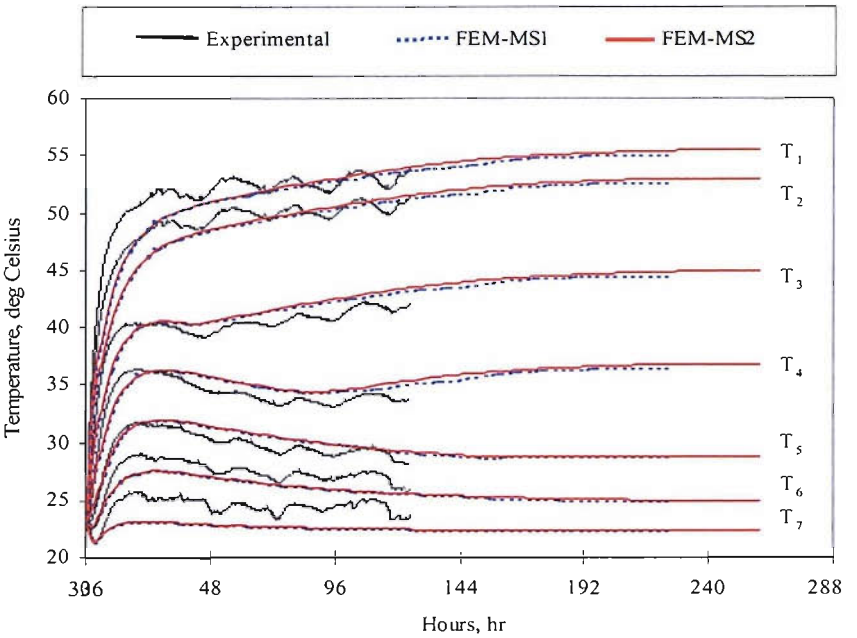

Figure 5.9(a)– FEM-MS1 and FEM-MS2 simulation results on 40 Wm^{-2} with initial volumetric moisture content of 1.6% as compared to experimental results.

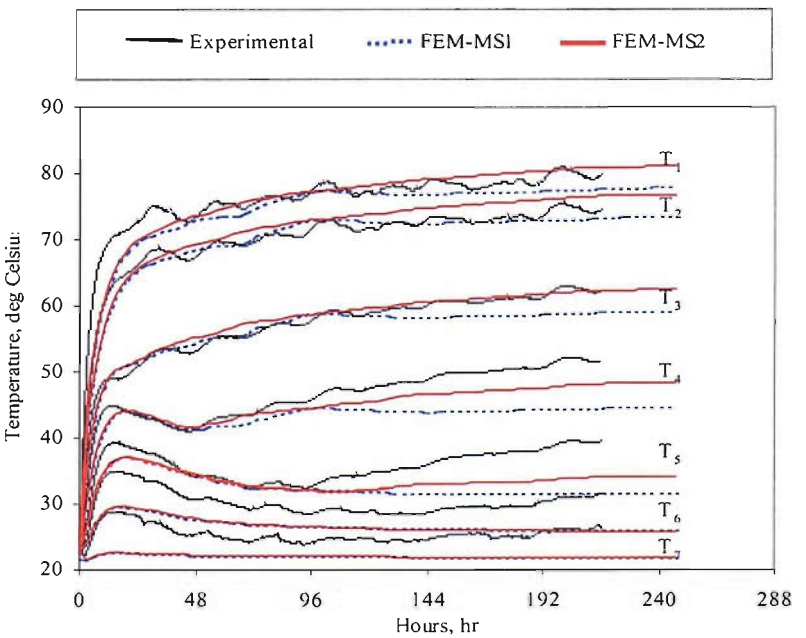

Figure 5.9(b)– FEM-MS1 and FEM-MS2 simulation results on 80 Wm^{-2} with initial volumetric moisture content of 1.6% as compared to experimental results.

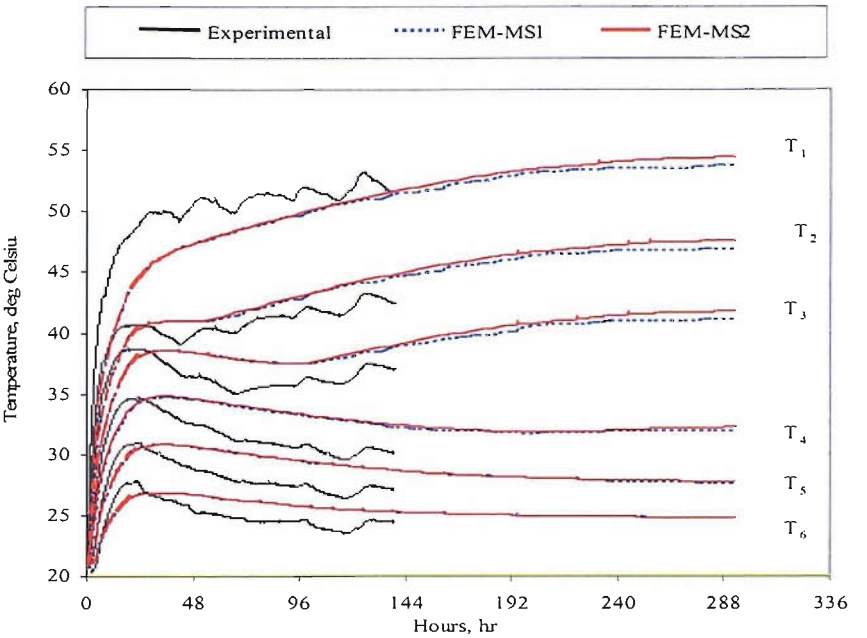

Figure 5.10(a)- FEM-MS1 and FEM-MS2 simulation results on 40 Wm^{-2} with initial volumetric moisture content of 3% as compared to experimental results.

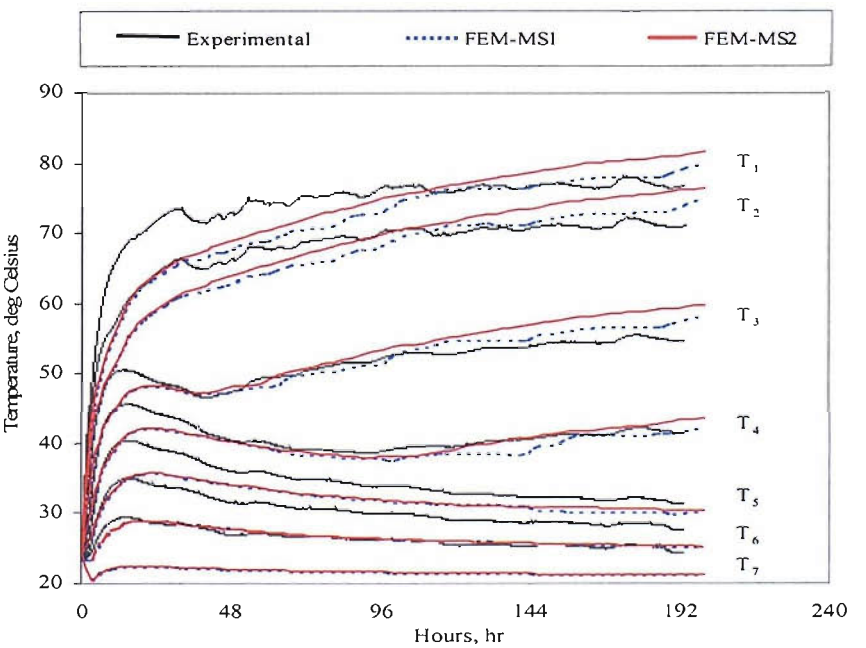

Figure 5.10(b) – FEM-MS1 and FEM-MS2 simulation results on 80 Wm^{-2} with initial volumetric moisture content of 3% as compared to experimental results.

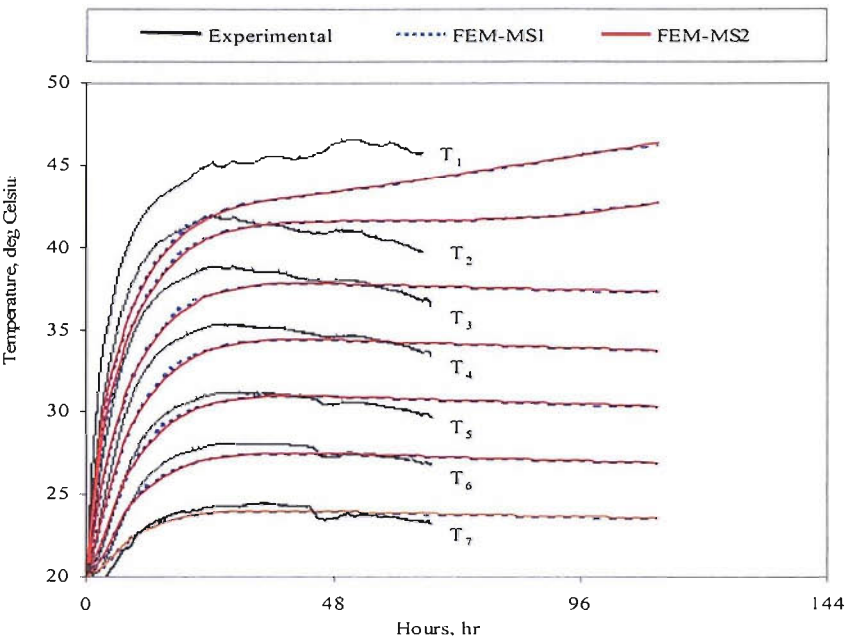

Figure 5.11(a) – FEM-MS1 and FEM-MS2 simulation results on 40 Wm^{-2} with initial volumetric moisture content of 5% as compared to experimental results.

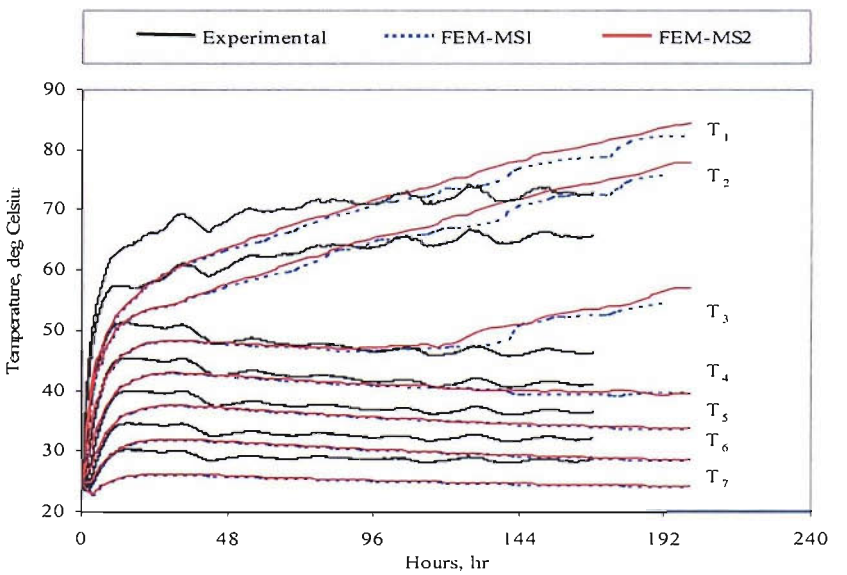

Figure 5.11(b) – FEM-MS1 and FEM-MS2 simulation results on 80 Wm^{-2} with initial volumetric moisture content of 5% as compared to experimental results.

a) Steady State Results

The simulated results of increasing temperature due to moisture loss at each thermocouple location have been improved greatly using the modified hydraulic soil properties. For example, these can be seen in the FEM-MS1 and FEM-MS2 results for T_3 shown in Figures 5.8 - 5.10. The simulated results of decreasing temperature due to increasing moisture from neighbouring hot regions have also been equally improved as shown in the simulated temperatures for T_5 in Figures 5.8 - 5.10.

Steady-state temperatures for T_1 and T_2 simulated using FEM-MS1 and FEM-MS2 are also in good agreement with experimental values. Error for steady-state T_1 has been reduced to an average of 1% and less than 5% for 0.01/40Wm^{-2} and 0.016/80Wm^{-2} respectively and that of T_2 to an average of 2% for 0.016/80Wm^{-2}. Towards the end of experimental time, simulated T_1 and T_2 has its error decreased to less than 5% for cases 0.03/40Wm^{-2}, 0.03/80Wm^{-2} and 0.05/80Wm^{-2}.

However, it can be clearly seen that for most of the FEM-MS1 and FEM-MS2 simulation results, temperature T_6 has been underestimated. The average percentage error for this simulated temperature is greater for the 80Wm^{-2} cases than the 40Wm^{-2} and ranges from 10% to 12%.

b) Transient Results

Thermal transient stage of all simulated temperatures has not been improved for either FEM-MS1 and FEM-MS2. This proves that the modified soil properties that are used within these two types of simulations do not affect the thermal transient response. Hence, it is fair to conclude that thermal transients are largely affected by

the volumetric heat capacity of the soil, since it is the thermal capacitive part of the heat distribution that influences the transient time constant.

Largest discrepancies have been found to be present at thermal transient stage of simulated T_1 and T_2 for all cases. Maximum percentage error for simulated T_1 that resulted from FEM-MS1 and FEM-MS2 simulations range from about 12% to 16% for all 40Wm^{-2} cases whilst range from 18% to 20% for all of the 80Wm^{-2} cases. Maximum percentage error for simulated T_2 at thermal transient stage range from 8% to 17% for all of the cases.

Discrepancies resulting from the FEM-MS1 and FEM-MS2 simulations at thermal transient stage may have been caused by the simplified formula that is used to calculate the volumetric heat capacity of the soil SWN1.

c) Mesh Factor

Results that are produced from FEM-MS1 simulations do not differ much than that with FEM-MS2, except for 0.016/80Wm^{-2} and 0.03/80Wm^{-2}, as can be seen in Figures 5.9b and 5.10b. Refining mesh S1 has improved the simulations for these locations because the drying front has reached the area that is coarsely meshed in FEM-MS1. Hence temperatures are more accurately determined. For example after 216 hours, with mesh S2, the simulated temperature of T_3 has its absolute error reduced from 6% to 2% for 0.03/80Wm^{-2} case. Whereas after 192 hours, with refined mesh S2, simulated T_4 has its absolute error reduced from about 7% to 3%.

Simulated T_4 for 0.03/80Wm^{-2} could be further improved with a finer mesh at and around the area. This may well be done by further refining the mesh or adjusting the mesh growth rate, which determines the rate at which edge length grows away from the hotplate (being the smallest part of geometry).

At time 168 hours, FEM-MS2 simulation for 0.05/80Wm^{-2} has shown a smooth temperature increase at T_3, which is not observed in FEM-MS1. Referring to the surface plot, the drying front has reached this location and, hence, the temperature increases due to loss of moisture. Therefore, sudden increases in temperature at the drying fronts can be easily detected by using a simulation with a refined mesh.

d) Thermal conductivity

Thermal conductivity of regions 1 – 6 as detailed in Chapter 4, in Figures 4.6 - 4.9 are compared to those estimated during the FEMLAB simulations. Only the thermal conductivity used in the FEM-MS2 (post-transient stage) is compared as it involves the finest mesh.

Values of thermal conductivity that have been extracted from all FEM-MS2 solutions are single point solutions. Each of these values is assumed to represent thermal conductivity at the vicinity of each measurement point. Provided that solutions of FEM-MS2 are in agreement with those of the experiment, it is expected that thermal conductivity of each region to fall within the range of those of two neighbouring thermocouple location points. For example, thermal conductivity of Region 2 shall be expected to be within the range of those simulated at T_2 and T_3. This practice is considered justifiable since thermal conductivity of the regions may not vary significantly between two neighbouring thermocouples, especially when the distance is about 0.05m away or less. Results are as shown in Figures 5.13 - 5.18.

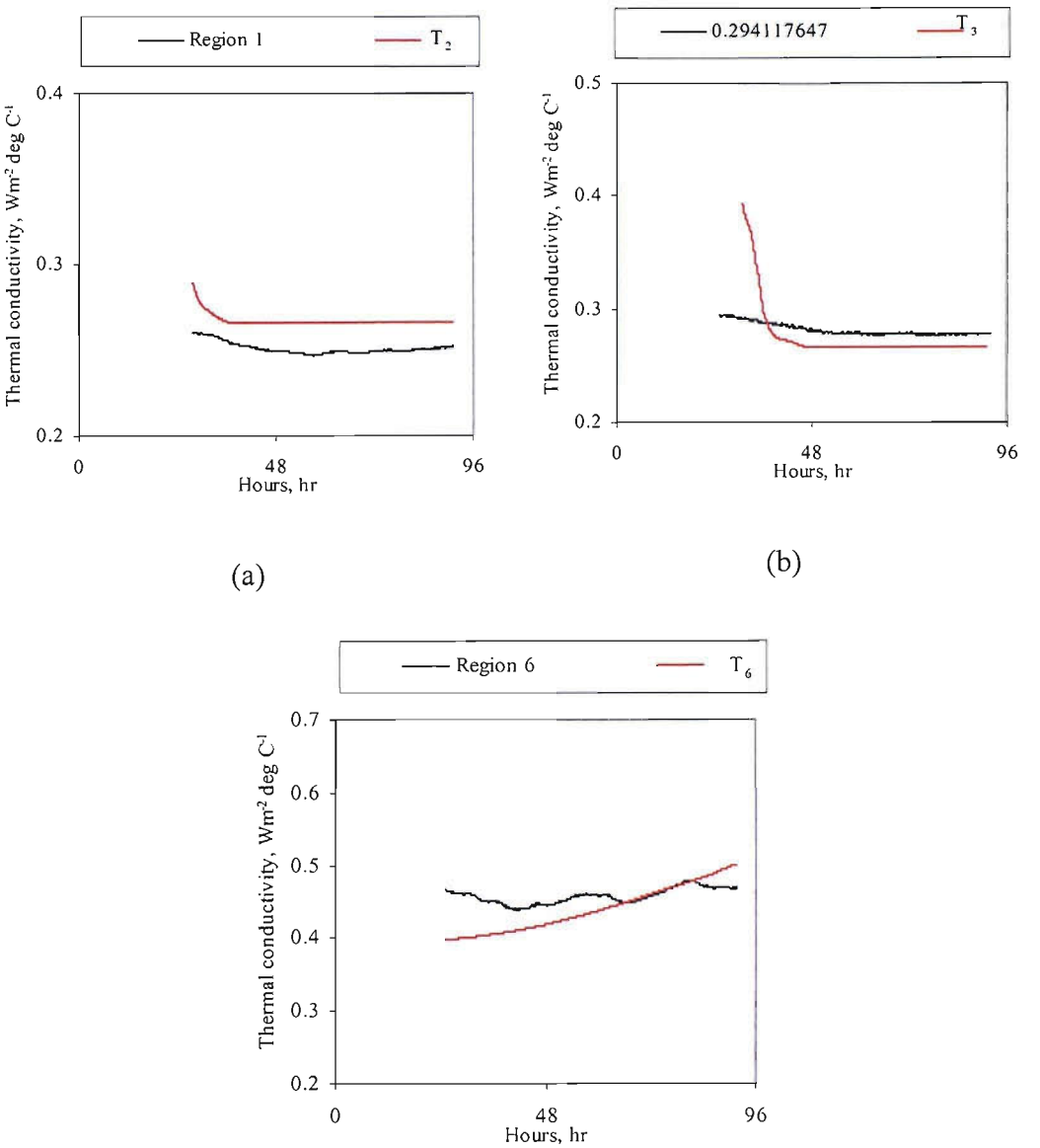

Figure 5.12 - Comparison between thermal conductivity at area (a) T_2 (b) T_3 and (c) T_6 from 0.01/40Wm^{-2} FEM-MS2 simulations with those of Regions 1, 2 and 6 from Figure 4.6.

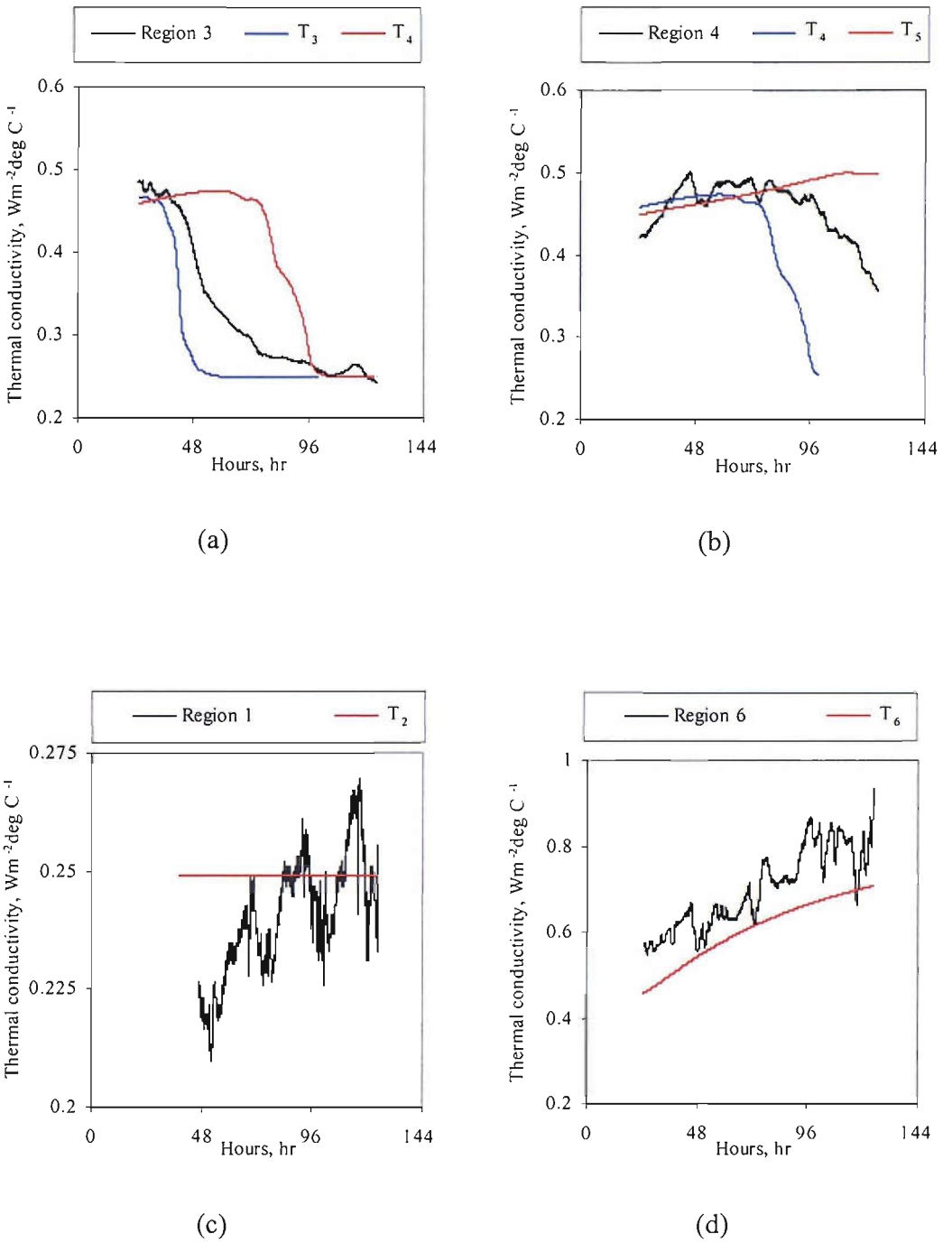

Figure 5.13 - Comparison between thermal conductivity at area (a) T_3 and T_4 (b) T_4 and T_5 (c) T_2 and (d) T_7 from 0.016/40Wm^{-2} FEM-MS2 simulations with those of Regions 3, 4, 1 and 6 from Figure 4.7(a).

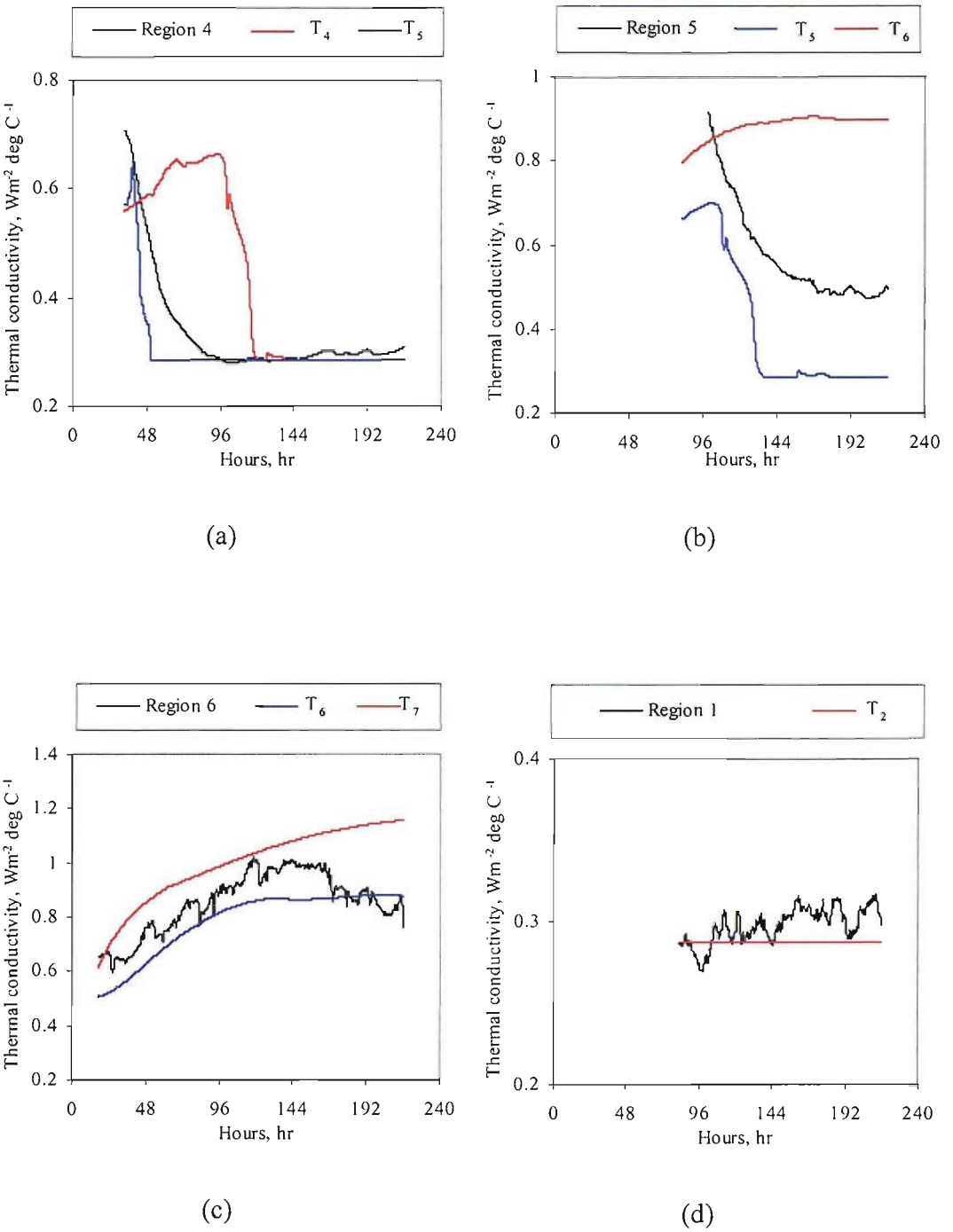

Figure 5.14 - Comparison between thermal conductivity at area (a) T_4 and T_5 (b) T_5 and T_6 (c) T_6 and T_7 (d) T_2 from 0.016/80Wm^{-2} FEM-MS2 simulations with those of Regions 4, 5, 6 and 1 from Figure 4.7(b).

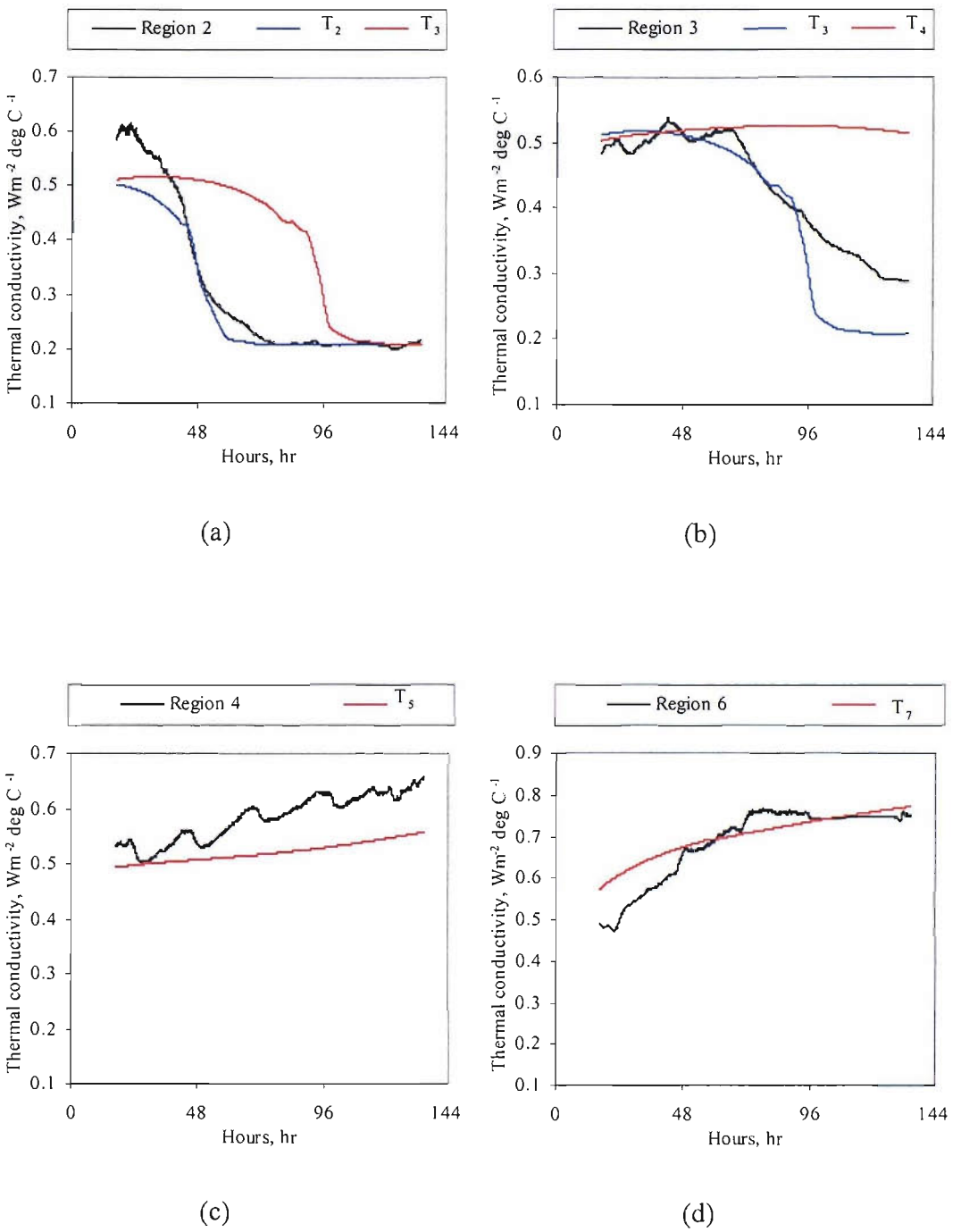

Figure 5.15 - Comparison between thermal conductivity at area (a) T_2 and T_3 (b) T_3 and T_4 (c) T_5 and (d) T_7 from 0.03/40Wm^{-2} FEM-MS2 simulations with those of Regions 2, 3, 4 and 6, respectively from Figure 4.8(a).

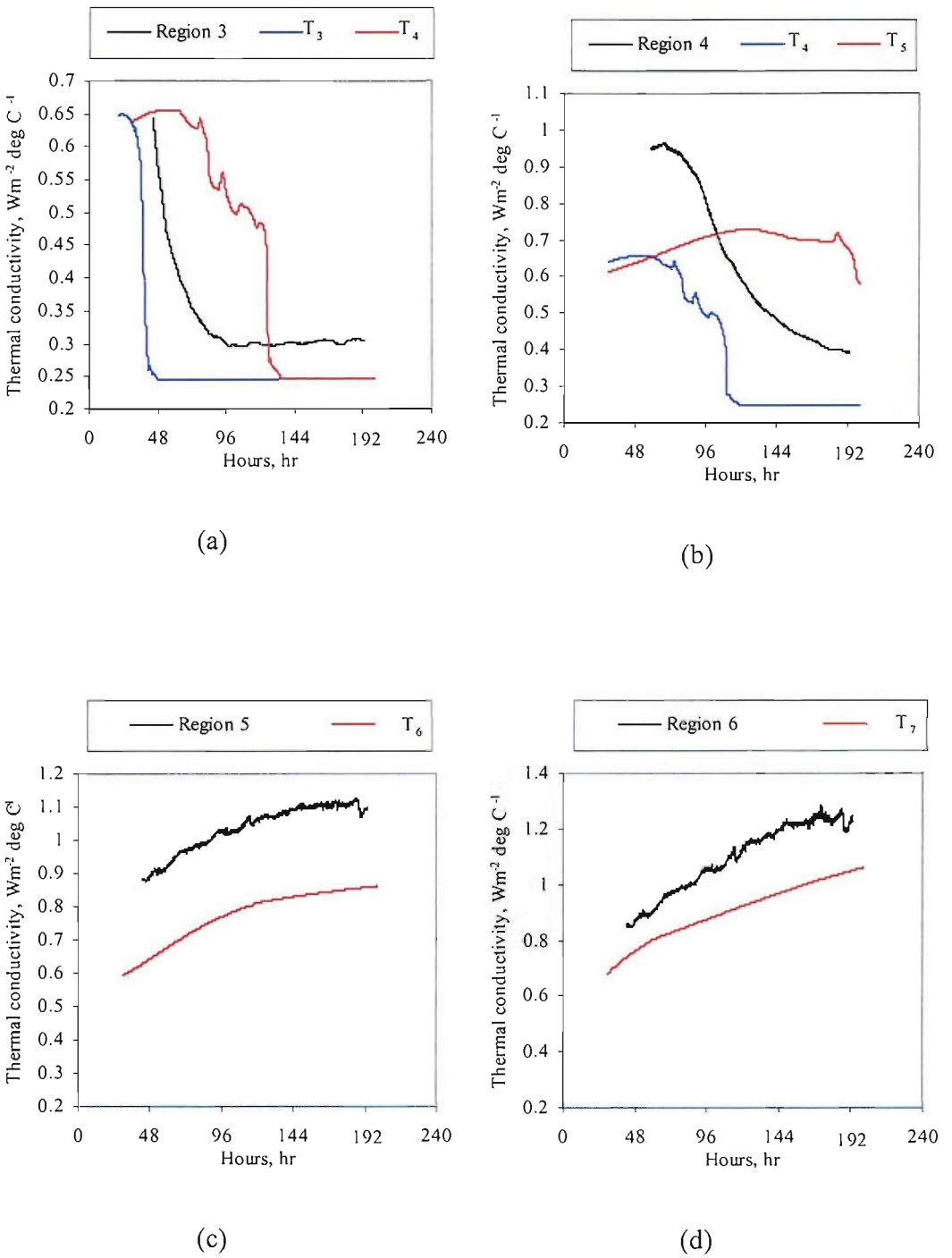

Figure 5.16 - Comparison between thermal conductivity at area (a) T_3 and T_4 (b) T_4 and T_5 (c) T_2 and (d) T_7 from 0.03/80Wm^{-2} FEM-MS2 simulations with those of Regions 3, 4, 2 and 6, respectively from Figure 4.8(b).

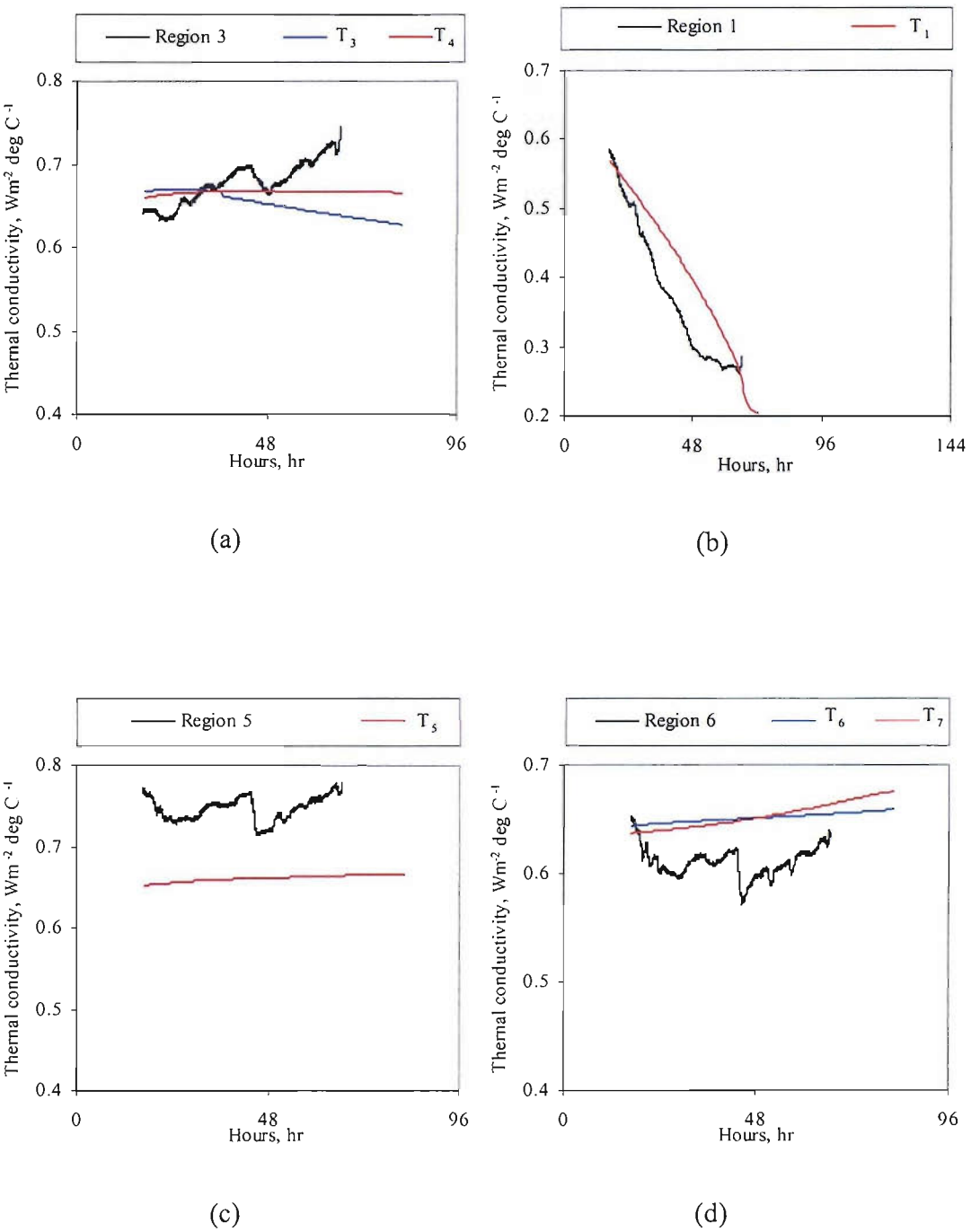

Figure 5.17 - Comparison between thermal conductivity at area (a) T_3 and T_4 (b) area at the vicinity of hotplate (c) T_5 and (d) T_6 from 0.05/40Wm^{-2} FEM-MS2 simulations with those of Regions 3, 1, 5 and 6, respectively from Figure 4.9(a).

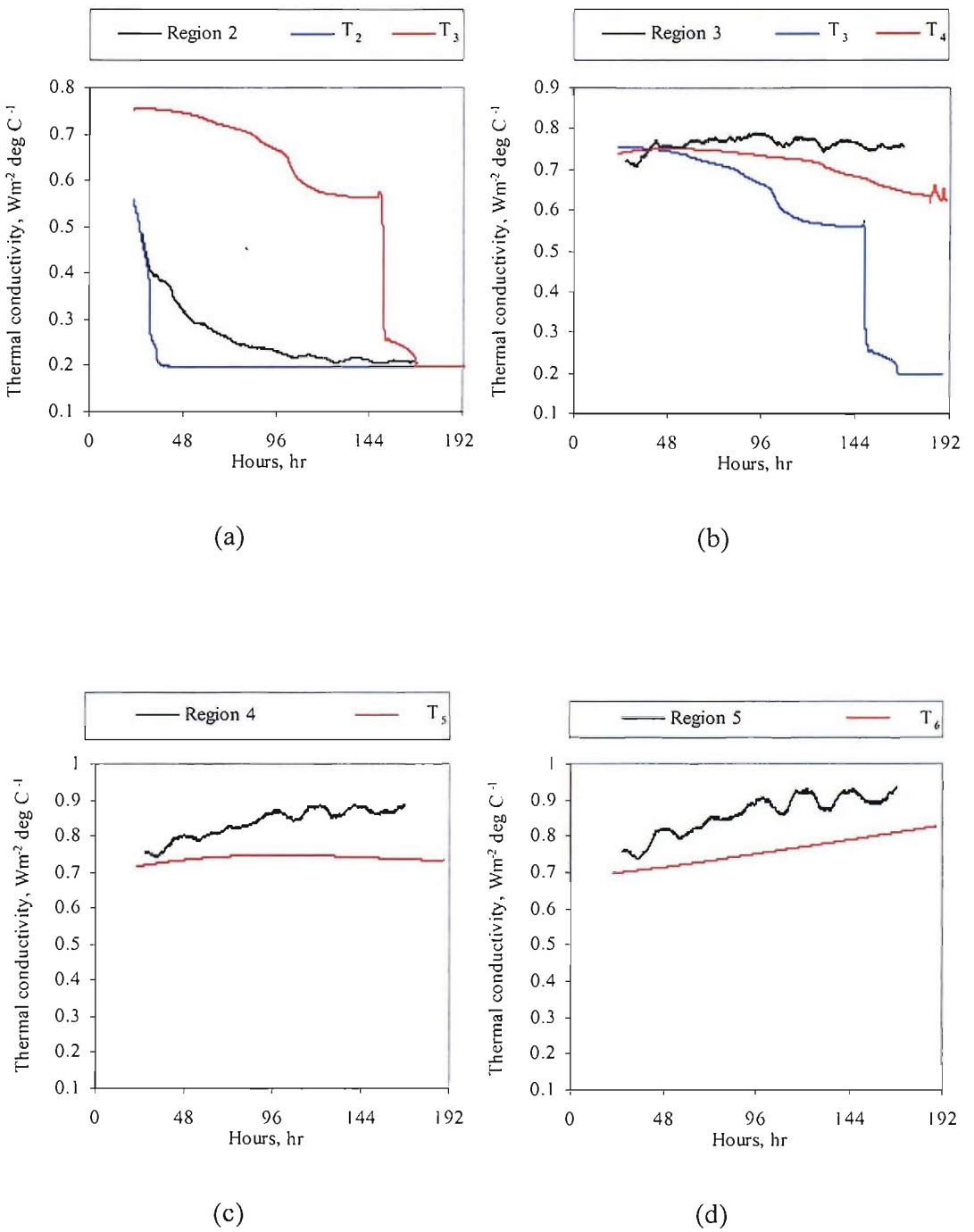

Figure 5.18 - Comparison between thermal conductivity at area (a) T_2 and T_3 (b) T_3 and T_4 (c) T_5 and (d) T_6 from 0.05/80Wm^{-2} FEM-MS2 simulations with those of Regions 2, 3, 4 and 5, respectively from Figure 4.9(b).

For 0.01/40Wm^{-2}, it was found that thermal conductivities of almost all regions do not fall within the range of those of their two neighbouring thermocouples (values are extracted from FEM-MS2 simulations). However, thermal conductivities of Region 1, Region 2 and Region 6 are found to be in reasonable agreement to those at T_2, T_3, and T_6, respectively. Although these values are not within the thermal conductivity range extracted from FEM-MS2, these are at least almost near the value of that of one neighbouring thermocouple. These results are as shown in Figures 5.12(a), (b) and (c). Figure 5.12(b) shows that thermal conductivities from these two different results exhibit similar behaviour; ie decrease over time before attaining a constant value.

For 0.016/40Wm^{-2} and 0.016/80Wm^{-2} there is reasonable agreement between the values of thermal conductivity in Regions 3,4 and Regions 4, 5, 6 respectively (Figure 5.13 and 5.14). For 0.03/40Wm^{-2} and 0.03/80Wm^{-2}, there is reasonable agreement between the values of thermal conductivity Regions 2, 3 and Regions 3, 4 respectively (Figure 5.15 and 5.16). Whereas for 0.05/80Wm^{-2}, reasonable agreement between the values of thermal conductivity are found to be in Regions 2, 3 (Figure 5.18). Regions 1 and 6 of 0.016/40Wm^{-2}; Region 1 of 0.016/80Wm^{-2}; Regions 4 and 6 of 0.03/40Wm^{-2}; and Regions 4 and 5 of 0.05/80Wm^{-2} only have reasonable agreement between experimentally estimated value for thermal conductivity and a simulation value at one neighbouring thermocouple location. Although some of these are slightly out of the thermal conductivity range, similar behaviour is detected between the value extracted from FEM-MS2 and those calculated from experimental results. For instance, thermal conductivity at point T_6 with that of Region 6 in Figure 5.13(d) increases over time at an almost similar rate. Also, thermal conductivity at point T_5 and T_6 increases over time and exhibits similar behaviour to thermal conductivity of Regions 4 and 5, respectively as seen in Figures 5.18(c) and 5.18(d).

Despite fluctuations, variation of thermal conductivity of Region 1 in Figures 5.13(c) and 5.14(d) are in agreement with that of T_2 indicating that dry thermal conductivity for initial volumetric moisture content of 0.016 was accurately used in FEM-MS2. The dry thermal conductivity (indicated by a red solid line) is about $0.25 Wm^{-2}°C^{-1}$ for the FEM-MS2 $0.016/40 Wm^{-2}$ case and about $0.28 Wm^{-2}°C^{-1}$ for the FEM-MS2 on $0.016/80 Wm^{-2}$ case.

5.3.3 Moisture profile

The moisture profile at the end of each experiment is shown in Figures 5.19 - 5.22. These profiles are compared to those results obtained using FEM-MS1 and FEM-MS2 simulations. At high temperature gradients, moisture profiles from FEM-MS2 simulations seem to be less than those from FEM-MS1. This is due to finer tuning in result provided by finer meshes in FEM-MS2. Therefore, finer solutions are more sensitive towards any changes in moisture at higher moisture gradients. However, moisture profiles from the finite element methods are overestimated for all cases except for that of $0.01/40 Wm^{-2}$ (Figure 5.19). Most of the overestimation is found to be at the region with the highest moisture gradient. The highly non-linear hydraulic characteristic of the soil may require a much denser and finer meshes at where the moisture gradient is the highest. It is difficult to determine where exactly the moisture gradient would be highest (along the path of moisture flux) since this moves along with the dry front as it moves toward the wetter region as time increases.

It is impossible to compare the severity of dryness caused by heating for different initial volumetric moisture contents. This is because each experiment has been compacted up to different heights within the MMA. This is in part due to large MMA volume and the difficulty in maintaining similar bulk density for all cases.

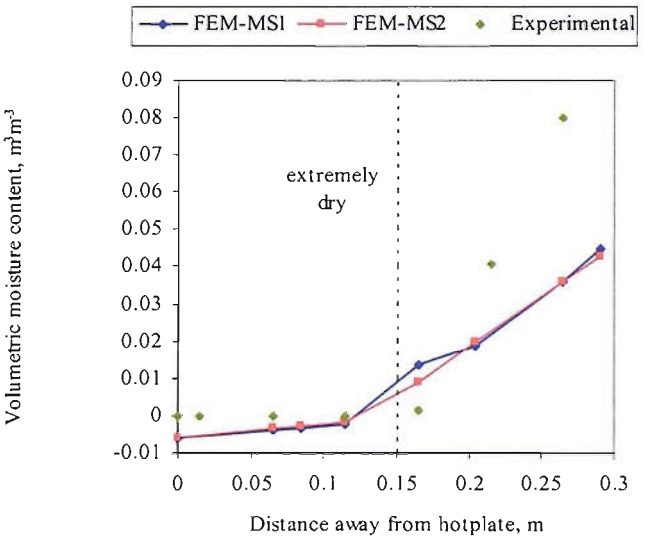

Figure 5.19 - Comparison on volumetric moisture contents from FEM-MS1 and FEM-MS2 simulations on 0.01/40Wm^{-2} at time t= 92.2 hours. Dash line indicates the point of dry front at the end of experimental time.

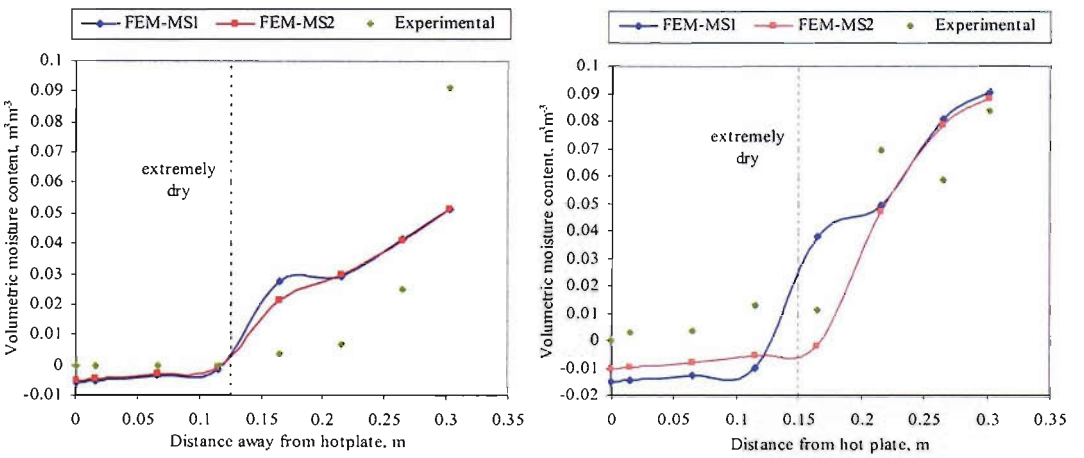

(a) (b)

Figure 5.20 - Comparison on volumetric moisture contents from FEM-MS1 and FEM-MS2 simulations on (a) 0.016/40Wm^{-2} and (b) 0.016/80Wm^{-2} at time t= 124.6 hours and t= 215.7 hours, respectively. Dash line indicates the point of dry front at the end of experimental time.

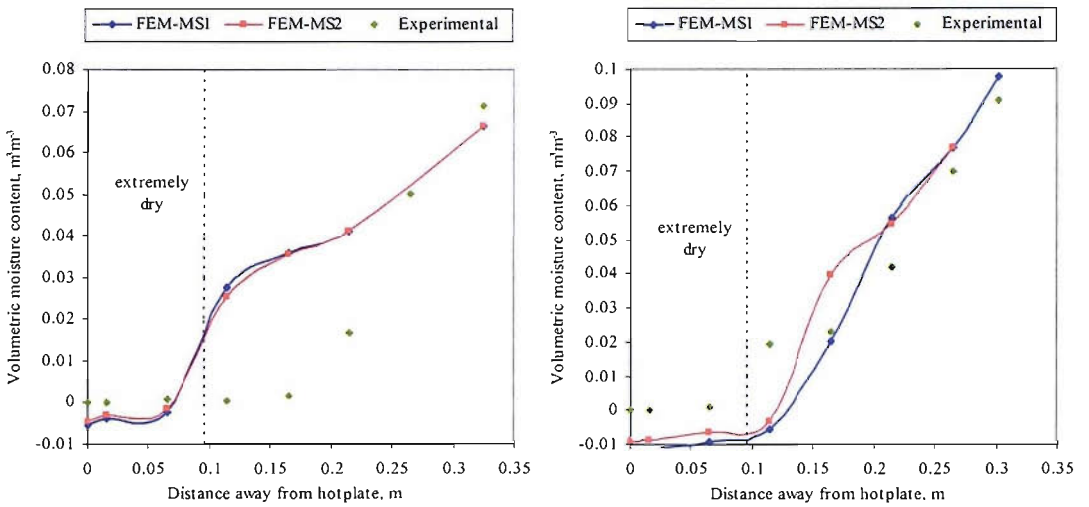

Figure 5.21 -Comparison on volumetric moisture contents from FEM-MS1 and FEM-MS2 simulations on (a) 0.03/40Wm^{-2} and (b) 0.03/80Wm^{-2} at time t= 163.9 hours and t= 193.3 hours, respectively. Dash line indicates the point of dry front at the end of experimental time.

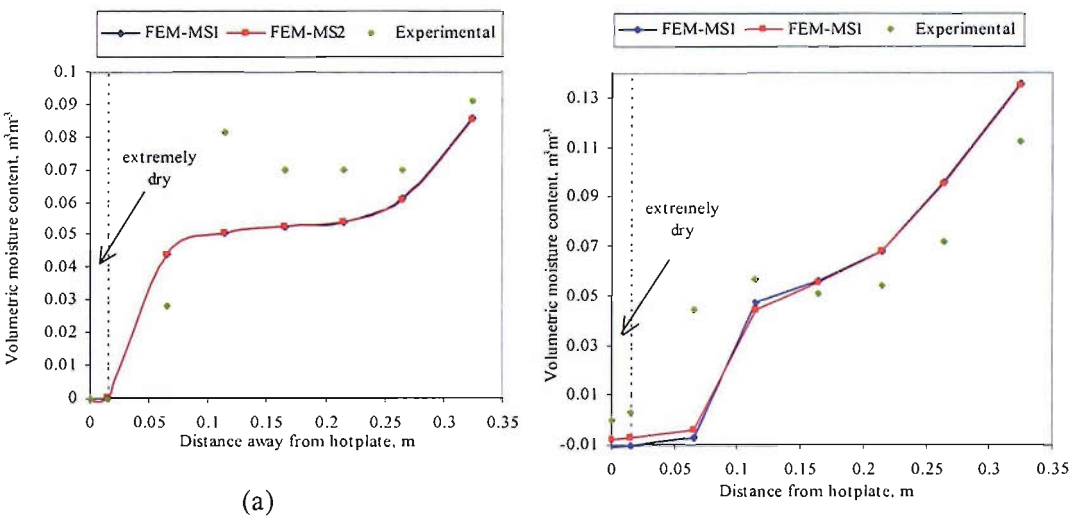

Figure 5.22 - Comparison on volumetric moisture contents from FEM-MS1 and FEM-MS2 simulations on (a) 0.05/40Wm^{-2} and (b) 0.05/80Wm^{-2} at time t= 115 hours and t= 168.4 hours, respectively. Dash line indicates the point of dry front at the end of experimental time.

Due to different bulk densities, dry and saturated thermal conductivity of the compacted soil may differ and hence result in different moisture profiles. Furthermore, the length of period that each soil is subjected to heating differs from one case to another. Therefore, from the experiments, no firm conclusion can be made to relate the severity of dryness with initial volumetric moisture content and length of time subjected to heating. However, moisture profiles that are obtained from these experiments are useful to compare results that are obtained from all FEM simulations.

Moisture profiles that are obtained from actual experiments show that the trend is exponential-like except for the 0.05/40 Wm^{-2} and 0.05/40 Wm^{-2} cases. Only the FEM solutions for 0.01/40Wm^{-2} successfully depict the exponential-like trend in moisture profile. Although the profiles obtained from the FEM simulations for the other cases are not exponential-like, they do estimate where the dry/wet interface is along the height of the MMA.

Due to the high non-linearity of the system used in FEM-MS1 and FEM-MS2 simulations, moisture results can easily become negative within regions that are extremely dry. However, this does not effect the dynamic calculations of the thermal conductivity since negative moisture values are assumed to be zero, ie the driest state possible.

5.4 CONCLUSIONS

As expected, finer meshes used in FEMLAB produced results that are closer to experimental results. Through observations using FEMLAB, finer meshes are crucial at areas where the heat flux is intense and as well as at areas where a dry/wet

interface is expected to form in order to gain accurate moisture migration predictions, which in turn acts as a mean in predicting thermal runaway.

Transient predictions produced greater error than those for steady state. This may be due to lack of information relating the soil thermal capacitance with its thermal conductivity. The accumulation and loss of moisture collectively at certain areas makes the prediction difficult as the capacitance and thermal conductivity of soil depends largely on moisture. However, it is the post-transient stage that is of more interest to cases such as overloading underground cables and underground cables embedded in low rainfall regions.

This chapter has demonstrated that post-transient thermal predictions are not impossible to attain fairly accurately if hydraulic and thermal properties of the backfill are characterised explicitly. Methods used to characterise hydraulic properties prove that it is possible to use them to verify the Philips and de Vries equations in order to estimate a temperature distribution.

Although there are discrepancies between the moisture profiles obtained from the FEM results and those observed experimentally, the simulated moisture distributions have been in good agreement and allow the 'local' thermal conductivity to be estimated reasonably accurately, and hence temperature variations due to changes in thermal and moisture gradients determined.

Most importantly, dynamic calculations of hydraulic and thermal properties used in finite element analysis of the Philips and de Vries equation have proven that fairly accurate temperature distribution is not impossible to simulate.

CHAPTER 6

6.0 TROUGH EXPERIMENT

A trough experiment that simulates heating of a power cable has been conducted under a controlled environment. The objective is to provide a means to compare the results obtained using finite element analysis with dynamic thermal and hydraulic soil properties with practical experimentation. It was also carried out in order to observe behaviour of a heated cable in a surface trough.

6.1 DESCRIPTION

The trough experiment consisted of a surface trough of 2 meters length, a hollow 2-meter long aluminium cylinder and networks of thermocouples attached to different locations within the surface trough. A cable is simulated using the aluminium cylinder (of 10 cm in diameter) with a length of heater tape helically wound around it in order to provide for a uniformly distributed heat. The trough used in the experiment set-up was a standard size cement trough that is widely used to embed surface trough cables. The trough experiment was designed and constructed to accommodate the purpose of investigating the behaviour of heated cable in this project; therefore it is new and original to the project.

The heater tape has a heating element within its length and it was wound around the cable and terminated at one end. The insulated ends are covered with a wooden sheet, one end is fitted with the heater tape termination, where it is connected to a regular D.C power supply. Two 1-meter long troughs were used to house the simulated cable, aligned side by side and gaps are sealed with foam sealant to ensure a continuous thermal boundary.

A network of thermocouples were installed using nylon fibre that holds them in position. There were nine networks of thermocouples altogether and three of these were located at three different points along the length of the simulated cable. The cross section of the trough and details on the thermocouple networks are shown in Figures 6.1 and Table 6.1, respectively.

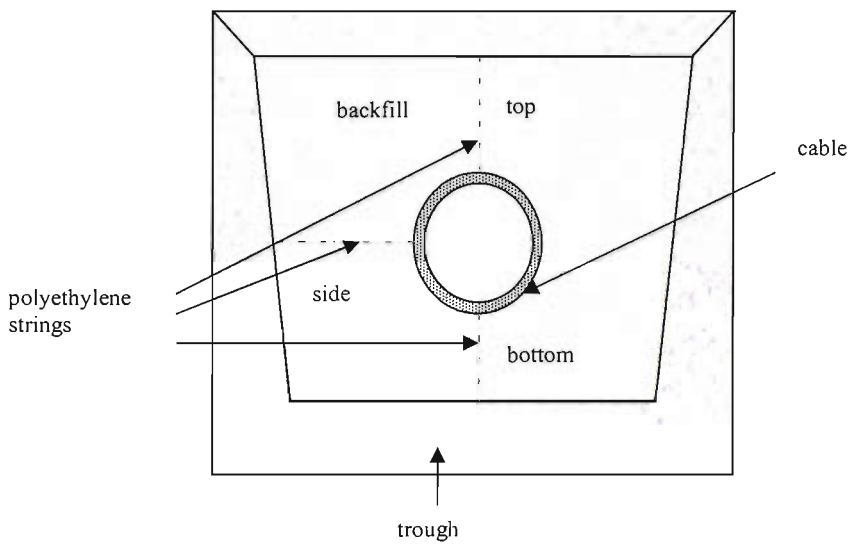

(a)

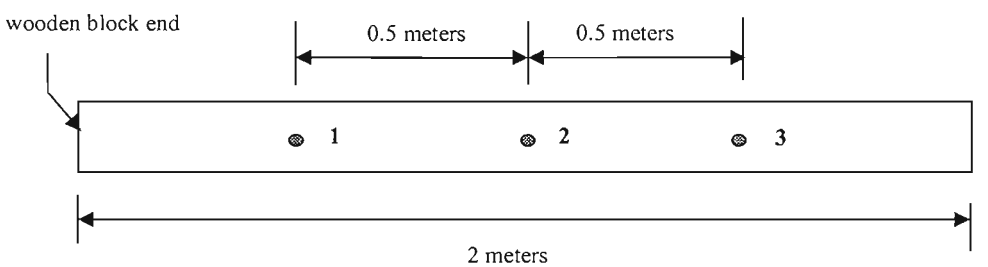

(b)

Figure 6.1 - (a) Cross section of the trough and simulated cable (b) Points along the cable length where nine thermocouple networks were placed.

Top			Side			Bottom		
Loc. as shown in Fig 6.1	Label	Dist. from cable (cm)	Loc. as shown in Fig 6.1	Label	Dist. from cable (cm)	Loc. as shown in Fig 6.1	Label	Dist. from cable (cm)
1	A1	0.5	1	D1	1.0	1	G1	1.0
	A2	1.5		D2	2.5		G2	2.0
	A3	3.0		D3	4.0		G3	3.0
	A4	4.5		D4	6.0		G4	4.5
	A5	6.0		D5	8.0		G5	6.0
	A6	7.0		D6	10.0		G6	8.0
	A7	8.0		D7	12.5		G7	10.0
2	B1	1.0	2	E1	1.5	2	H1	1.5
	B2	2.5		E2	3.0		H2	2.5
	B3	4.5		E3	5.5		H3	3.5
	B4	5.5		E4	7.5		H4	5.0
	B5	7.0		E5	9.5		H5	7.0
	B6	8.0		E6	11.5		H6	9.0
3	C1	0.5	3	F1	1.0	3	I1	1
	C2	1.5		F2	2.5		I2	2
	C3	3.0		F3	4.0		I3	3
	C4	4.5		F4	6.0		I4	4.5
	C5	6.0		F5	8.0		I5	6.0
	C6	7.0		F6	10.0		I6	8.0
	C7	8.0		F7	12.5		I7	10.0

Table 6.1 - Locations of thermocouples used in the trough experiment (with reference to Figure 6.1).

As indicated in Figure 6.1, positions 1, 2 and 3 were at 0.5 m, 1 m and 1.5 m from the wooden block end. At each position along the cable length, several thermocouples were placed between the surface of the cable and one side of the wall, the trough bottom and underneath the lid. Thermocouples were labelled both alphabetically and numerically according to their location along the cable length and the distance between the cable surface and inner boundary of the trough. Three

other thermocouples were placed at the inside surface of the cable at positions 1, 2 and 3 as shown in Figure 6.1. These are labelled J62, J63 and J64 respectively.

6.1.1 Data Acquisition System

Data acquisition system that was used comprised of one CR10X data loggers, two AM416 relay multiplexers, a power supply and a microprocessor. A workflow diagram of the system is as shown in Figure 6.2.

Relays were used to connect thermocouples to the data logger since the total number of thermocouples used was more than the number of channels available on the data logger. The CR10X in turn was connected to a SC32A optically isolated RS232 interface via an S12 cable. The SC32A was connected to the COM PORT of the computer via a 25-pin cable.

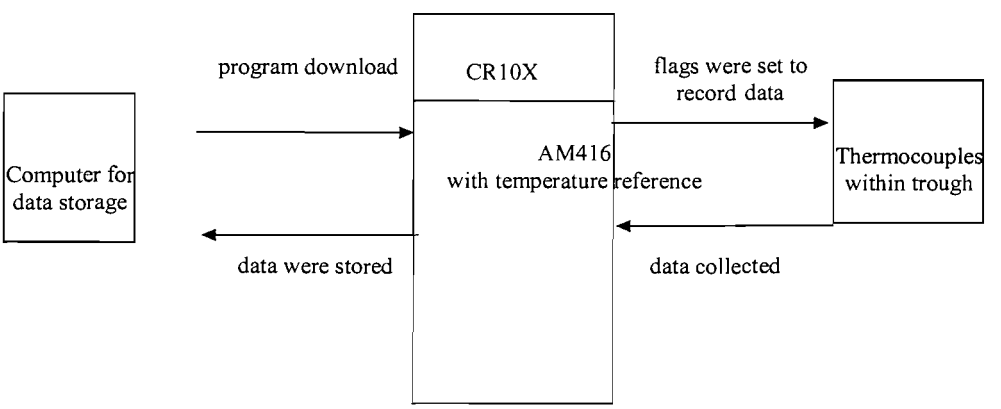

Figure 6.2 - Data acquisition system.

The multiplexers are powered using the datalogger battery. Two temperature reference junctions were used and these were connected to the system at both AM416 multiplexers. The reference junctions and the rest of the logger system are

kept in an enclosure to prevent the ambient conditions from influencing the thermal gradient near the reference junctions. When providing temperature reference, the standard for the data logger specifies that the typical polynomial linearisation error is $\pm 0.5°C$ over the temperature range -25°C to 50°C.

Data acquisition using the microprocessor was handled by PC208W Datalogger Support Software Package whereby a program was written, edited, compiled and downloaded to the datalogger. The software package was developed by Campbell Scientific Instruments, Inc. Instructions sequence for thermocouple readings were done in a programming format called Edlog, a program editor that contained in the PC208W Datalogger Support Software Package.

The program was written such that the temperatures are recorded every half an hour and collected to archive every 24 hours. Data recorded were saved to an archived directory. Data can also be viewed on-line using the same software.

6.1.2 Cable heat loss

The heat input to the simulated cable is obtained from the measured voltage and current. Hence the heat loss per meter length is calculated using

$$q_{loss} = \frac{V.I}{L_{cable}} \tag{6.1}$$

Where q_{loss} is the heat loss per meter length, (Wm^{-1}), V is the input voltage, (V), I is the input current, (A) and L_{cable} is the length of the simulated cable (m), which is 2 meters.

6.1.3 Sources of Error

The heater tape windings at the simulated cable ends were slightly more concentrated than its middle section in order to compensate for end effects. This is to ensure that ideally a cable with infinite length is simulated. In practice, the end effects would be a temperature difference between the ends and the centre of the cable that is caused by heat flowing axially. During all experiments that have involved heat loss per meter length ranging from 50 to 120 Wm^{-1}, temperature rise along the cable is found to be well within 10% of the maximum temperature rise.

The type of thermocouples used in the trough experiment were the same as those used in the MMA experiment described in Chapter 4. Thermocouple type K is specified to have maximum error of $\pm 3°C$ over the range of 0°C - 400°C and in practice, resolution of this type of thermocouple typically falls within $\pm 1°C$ of its readings. The resolution of the voltage and current readings are $\pm$ 10V and $\pm$ 0.2A.

6.2 FEMLAB SIMULATIONS ON SIMULATED CABLE

6.2.1 Mesh and Boundary Conditions

It is assumed that heat flux is uniformly distributed along the 2m length of the simulated cable when power is applied. Therefore, the radial heat distribution is of interest, and it is best to have it modelled at the cross section normal to length of the cable. Geometries for the trough cables are divided into three different subdomains, namely the trough walls, soil and the heated cylinder. As the cross section is symmetrical, only half of the geometry is considered. Mesh of the subdomains produced 472 nodes, 105 boundary elements and 879 elements whereas that of the subdomains with trough lids taken off produced 256 nodes, 78 boundary elements

and 461 elements. It was ensured that meshes at the cable and regions at its vicinity were denser. Details for the modelled trough cable with and without trough lid are shown in Figures 6.3 and 6.4.

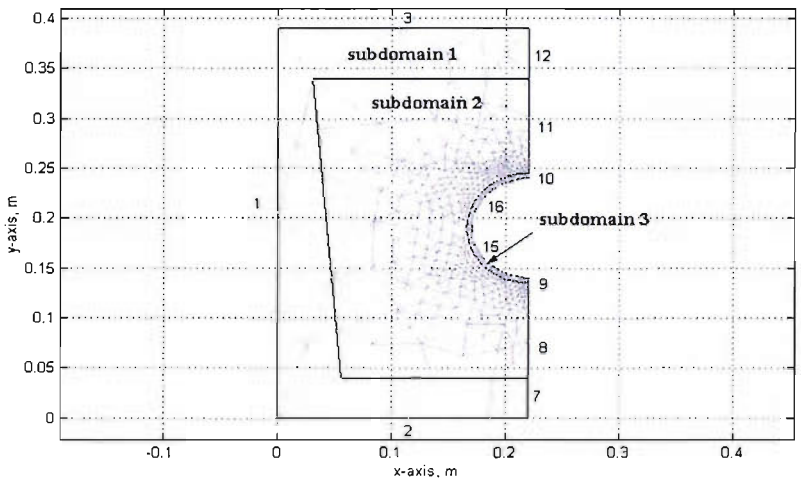

Figure 6.3 – Mesh and subdomains of the simulated trough cable. Numbers indicate edge numbers.

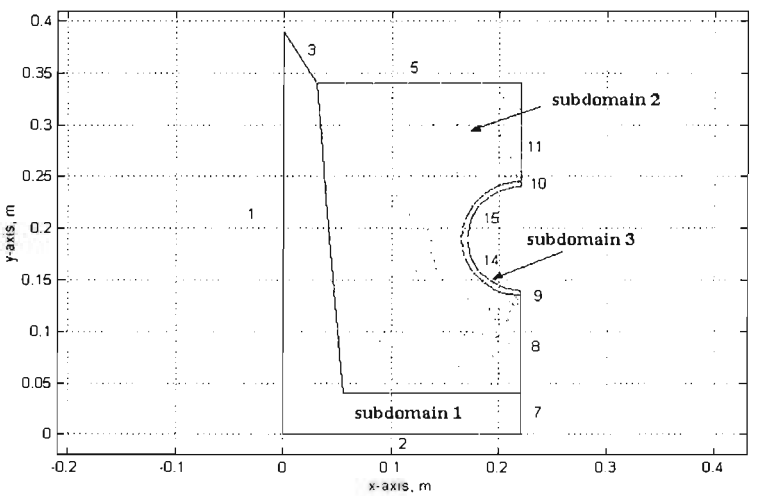

Figure 6.4 – Mesh and subdomains of the simulated trough cable without trough lid.

a) Boundary Conditions

Boundaries conditions for edges 7, 8, 9, 10, 11, 12 in Figure 6.1 and edges 7, 8, 9, 10, 11 in Figure 6.2 are Neumann type as these are symmetrical boundaries. The trough is seated on top of a wooden bench and hence the boundary for edge 2 for both Figures 6.1 and 6.2 is also Neumann type due to being insulated from the ambient temperature. Boundaries conditions for edges 1 and 3 in Figure 6.1 and edges 1, 3 and 5 in Figure 6.2 were subjected to convective heat transfer and therefore are defined as Dirichlet convective boundary. The assigned value for the convective heat transfer coefficient is 2 Wm^{-2} $°C^{-1}$. Fort [99] had used the following estimation of convective heat transfer coefficients, h_c for both horizontal and vertical surfaces in her work of simulating dynamic climate within a building.

For cooling of horizontal surfaces,

$$h_{cl} = A\Delta T^{0.31} \tag{6.2}$$

Where h_{cl} is the convective heat transfer coefficient, (Wm^{-2} $°C^{-1}$) and A is a constant that lies between 1.08 and 2.00.

For cooling of vertical surfaces,

$$h_c = 1.5\Delta T^{0.31} \tag{6.3}$$

Where the temperature difference, ΔT is defined as

$$\Delta T = T_s - T_{amb} \tag{6.4}$$

T_{amb} is the ambient temperature, (°C) and T_s is surface temperature, (°C).

The method used by Fort has been found to fall within reasonable values to the convective heat transfer coefficient experiments done by Hatton and Awbi [100]. Assuming that the temperature difference between the trough wall surfaces and the ambient temperature is about 2°C to 3°C, the value used for convective heat transfer coefficient in this work, 2 $Wm^{-2}°C^{-1}$ therefore is reasonably fair. Using the same method used by Theed [101] in modelling a simulated cable, edges 15 and 16 in Figure 6.1 and edges 14 and 15 in Figure 6.2 are subjected to a constant heat flux. In order to ensure constant temperature is effectively maintained at the surface of the cylinder, the constant heat flux is imposed on the inside surface of the hollow cylinder and material of the cylinder is ascribed with a large value of thermal conductivity.

The time step used is 1 hour. Considering that the time constant for similar size cable is much greater than three times of this, using 1 hourly time step seems reasonable. Furthermore, the size of the time step must not be too small since the total nodes involved in the simulation is very large.

b) Material Properties

All required material properties for soil (subdomain 2) were obtained simultaneously during simulations from Table 5.2 in Chapter 5. The bulk density of the soil filled within the trough is approximately 1578 kgm^{-3}. Thermal conductivity and volumetric heat capacity for materials in subdomains 1 and 3 (cylinder and trough) are used as constants. The thermal conductivities assigned for both aluminium cylinder and trough are 12 $Wm^{-1}°C^{-2}$ and 1 $Wm^{-1}°C^{-2}$, respectively. The volumetric heat capacity assigned for both aluminium cylinder and trough are 0.2 $MJm^{-3}°C^{-1}$ and 2 $MJm^{-3}°C^{-1}$, respectively. Assumptions have been made that the soil is homogeneous and isotropic.

6.2.2 Experimental Results & FEM Simulation (TR1)

The volumetric moisture content of the soil used in experiment TR1 is 0.045, which is reasonably damp to touch and not too dry. The simulated cable has been subjected to heat loss per meter length of 50 Wm^{-1} for about 7 days and then the heat loss per meter length was increased to 112 Wm^{-1} for another 14 days. During the heating of the trough cable, the trough had its lids on. Prior to FEM simulation, the temperature of the surface of the trough is assumed to be at 20°C and through inspection of the ambient temperature, the initial temperature is set to 18 °C. The temperatures recorded by thermocouples J62, J63 and J64 (at cable surface) are compared to the results obtained using FEMLAB simulation. The comparison is shown in Figure 6.5. The surface plots of both temperature and moisture, and heat and moisture flux plots in FEMLAB are shown in Figures 6.6 and 6.7.

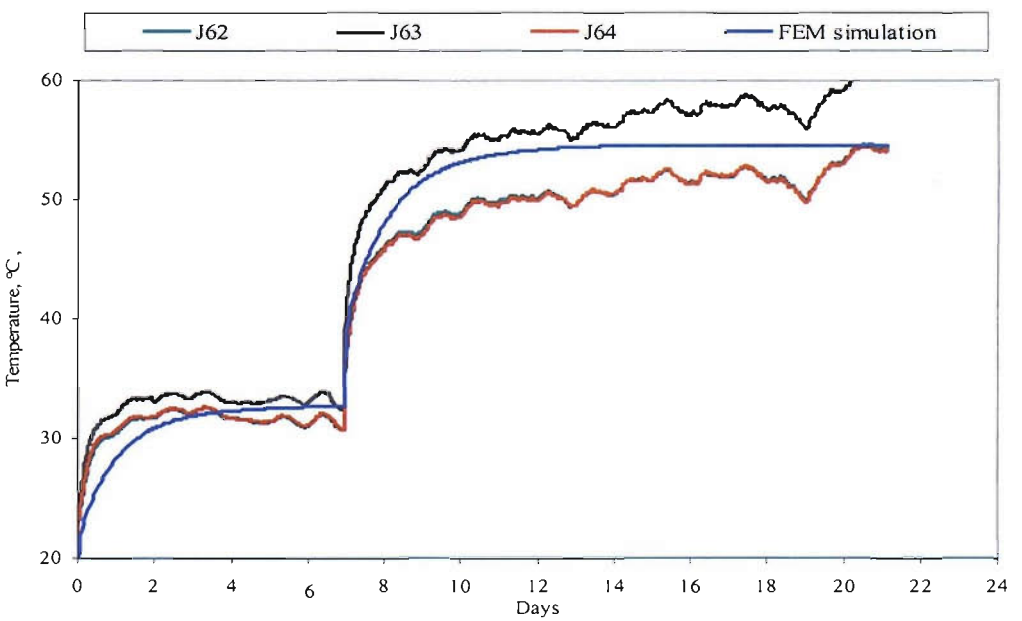

Figure 6.5 – Comparison between results obtained from FEM simulation and experiment for TR1.

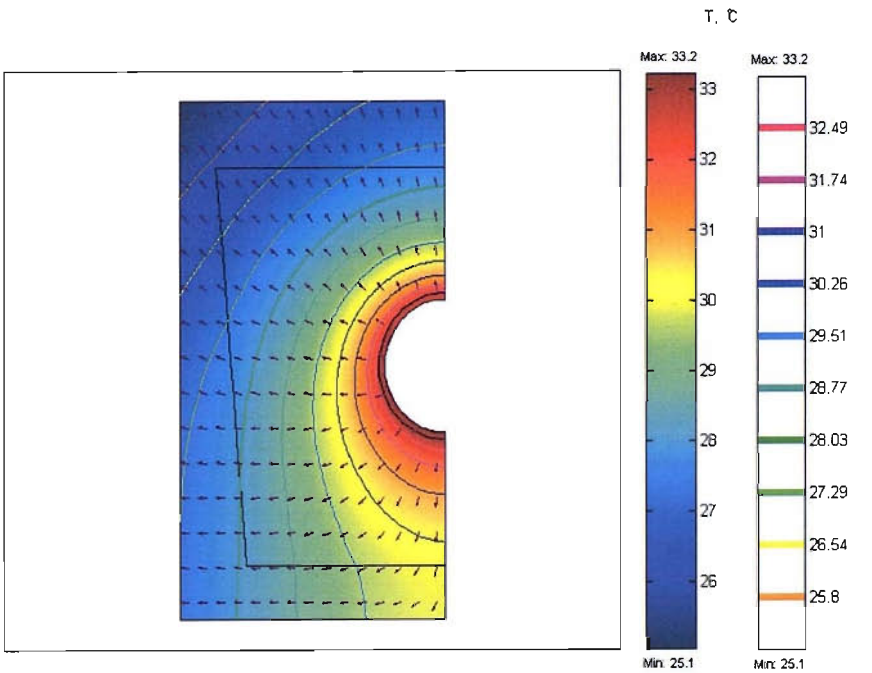

(a)

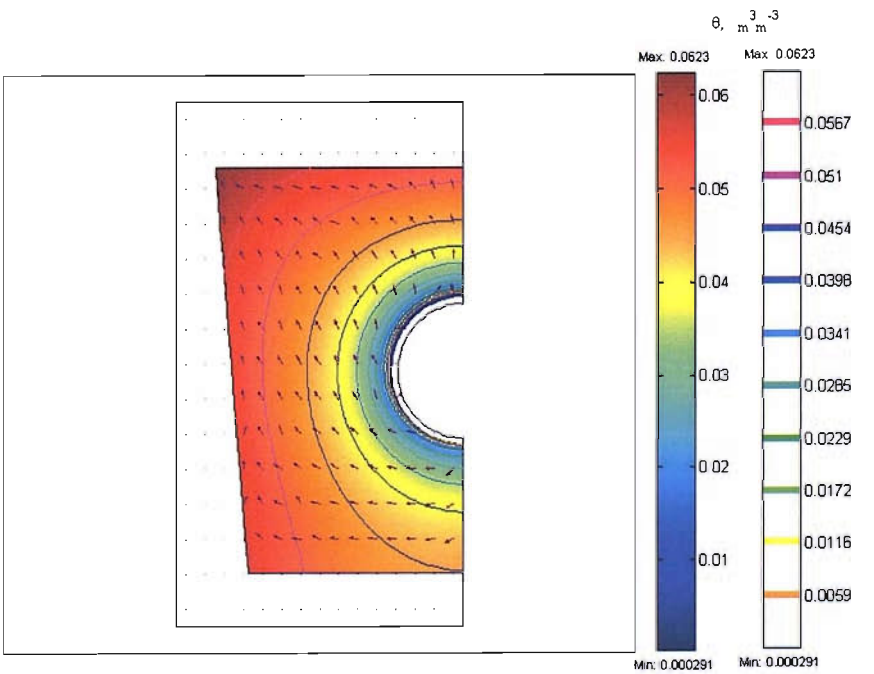

(b)

Figure 6.6 – Surface, contour and flux (arrows) plots of (a) temperature (b) moisture distributions of FEM simulation for TR1 at day 7.

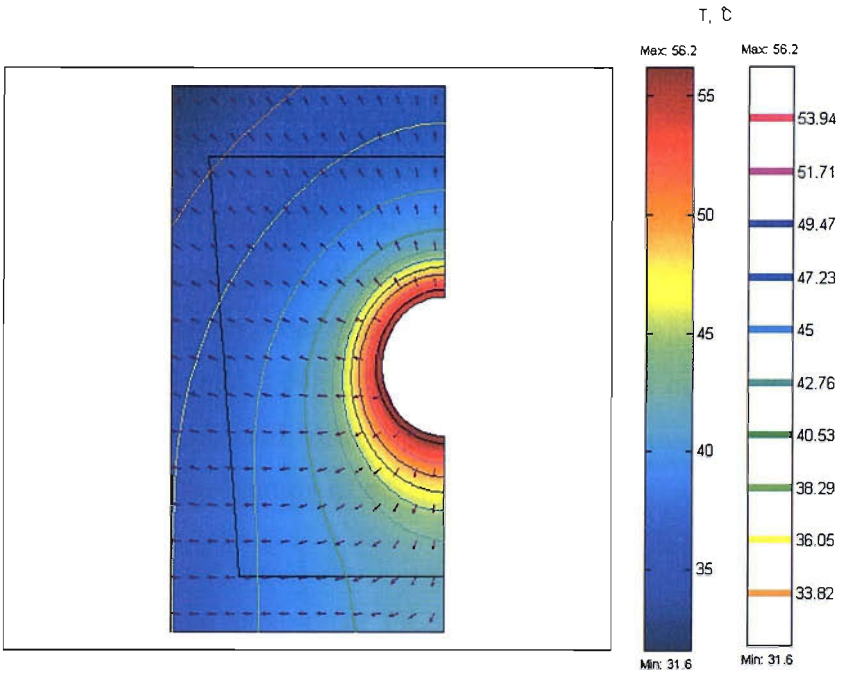

(a)

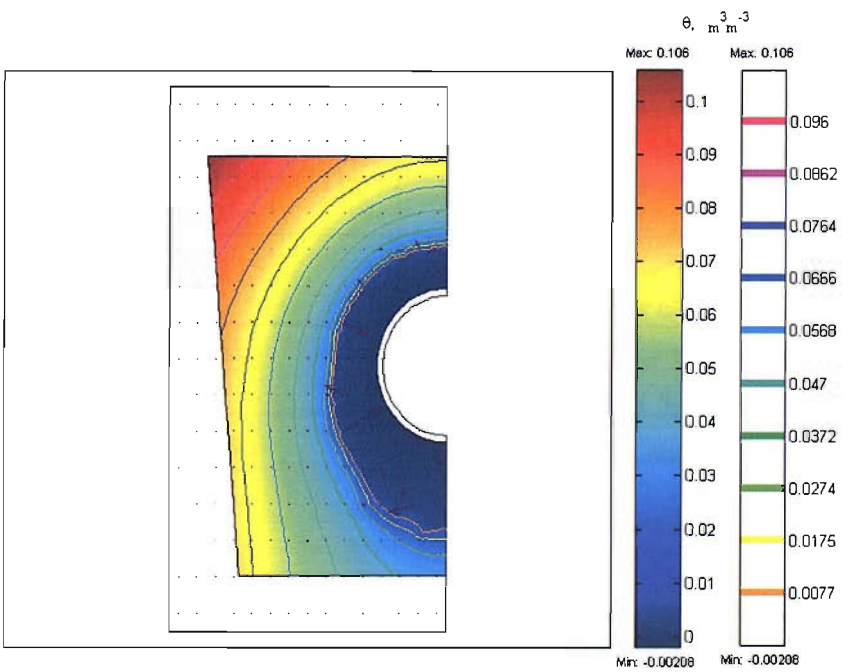

(b)

Figure 6.7 – Surface, contour and flux (arrows) plots of (a) temperature (b) moisture distributions of FEM simulation for TR1 at day 21.

6.2.3 Experimental Results & FEM Simulation (TR2)

After the heating to the trough cable in experiment TR1 had been stopped, the trough lids were taken off and the trough was allowed to cool. The heating to the cable trough remained idle for several weeks and the backfill is allowed to dry loosing moisture content through evaporation in still air, at room ambient temperature. This is done in order to set the trough running again with a volumetric moisture content lower than 0.045. This is much easier than having to excavate the soil and refill the trough with pre-prepared known moisture content because it would inevitably alter the location of the thermocouples.

Prior to commencing experiment TR2, volumetric moisture content of the soil was tested and it was found to be around 0.0008, which is very dry. The trough lids were placed back on the trough and the trough cable was subjected to a series of different heat losses per meter length as shown in Table 6.2.

SEQUENCE	HEAT LOSS PER METER LENGTH, (Wm^{-1})	DURATION AND DETAILS
1	115	One off heating, for 7 days and allowed to cool for almost 4 days
2	153	One off heating, for 3 days and allowed to cool for 4 days
3	50	8 hours of heating and 16 hours of cooling, repeated over a period of about 5 days; followed by cooling for about 3 days
4	100	8 hours of heating and 16 hours of cooling repeated for 2 days; followed by a brief cooling of 30 hours
5	100	Heating for about 3 days, brief cooling for 1 day.

Table 6.2 - Heating sequence for experiment TR2.

Since the volumetric moisture content is greatly reduced, the bulk density is also decreased due to the lower mass of retained moisture. Hence, assuming that the dry density remains unchanged, the reduced bulk density can be approximately calculated prior to commencing experiment TR2. The bulk density for experiment TR2 has been calculated to be 1511 kgm^{-3}. It is assumed that moisture has completely redistributed evenly within the volume of the trough. This time it has been assumed that the temperature surface of the trough for convective boundary is at 22°C. For the simulation, the initial temperature was set to 21°C. The comparison between simulation results of the temperature of the simulated cable and temperatures recorded by J62, J63 and J64 is shown in Figure 6.8.

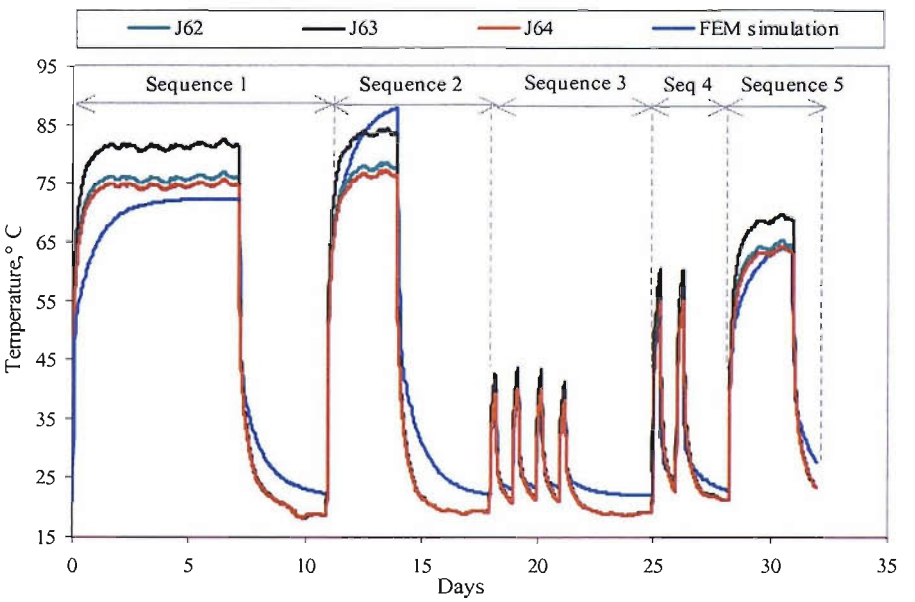

Figure 6.8– Comparison between results obtained from FEM simulation and experiment for TR2.

Figures 6.9 - 6.11 show the surface and contour plots of temperature and moisture distribution after heating in sequence 1, 2 and 5 obtained from the FEM simulations. Results of the simulation after the cooling session in sequence 1 is shown in Figure 6.12.

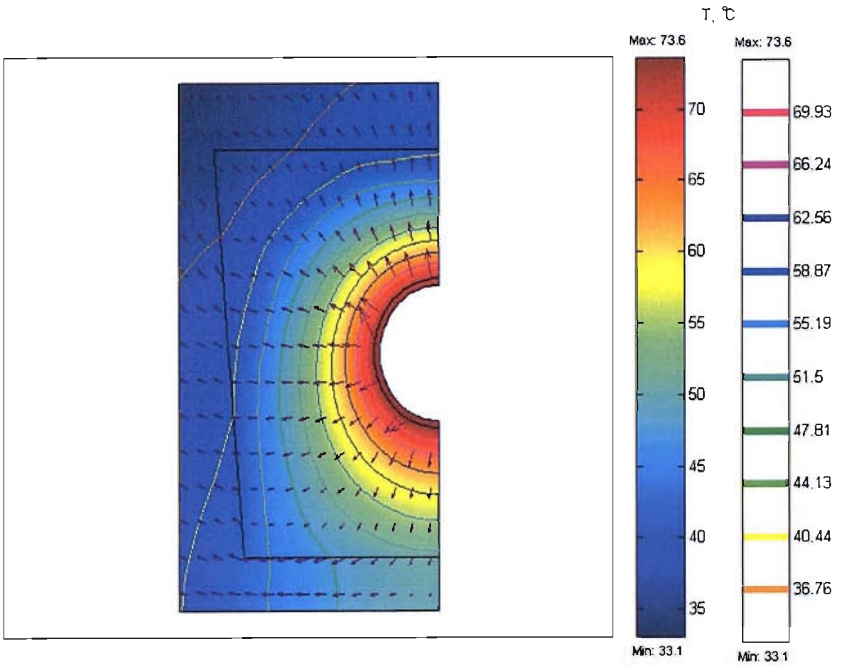

(a)

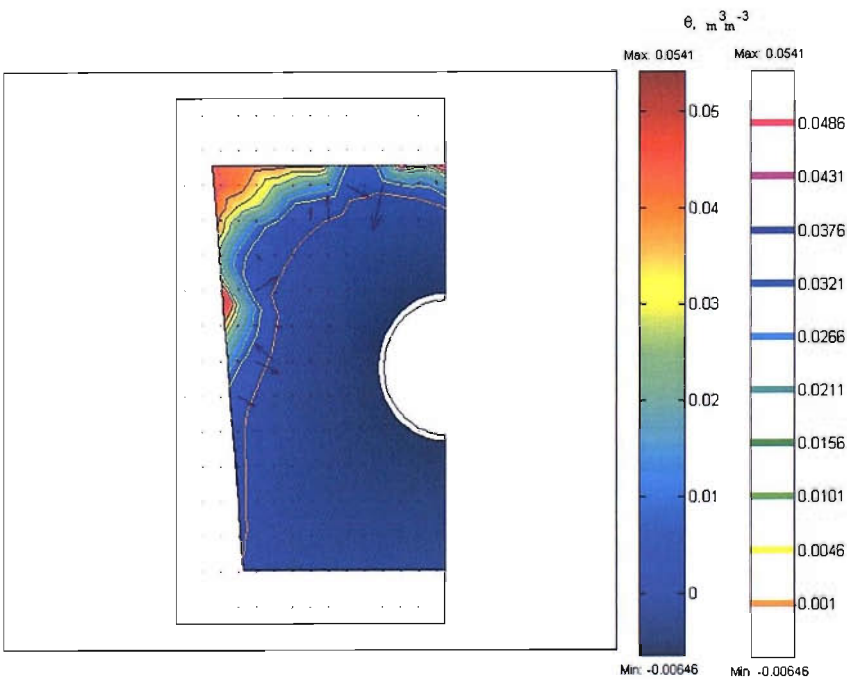

(b)

Figure 6.9 – Surface, contour and flux (arrows) plots of (a) temperature (b) moisture distributions after heating in sequence 1, experiment TR2.

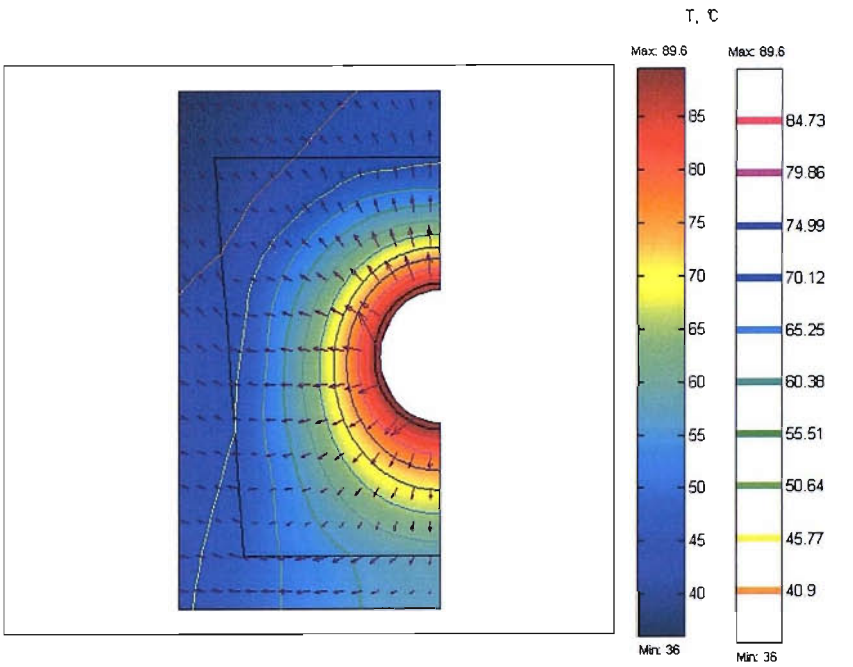

(a)

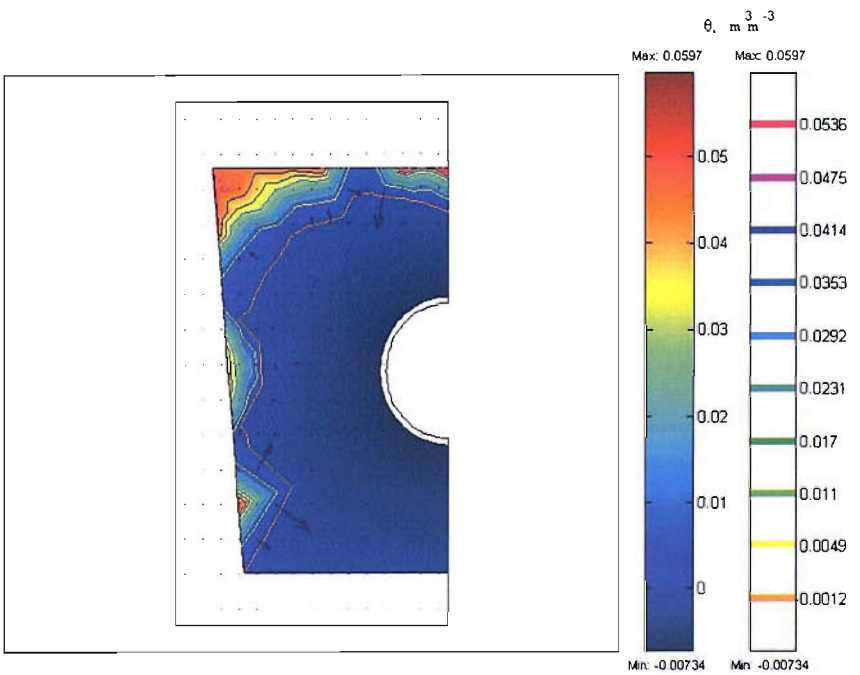

(b)

Figure 6.10 – Surface, contour and flux (by arrows) plots of (a) temperature (b) moisture distributions after heating in sequence 2, experiment TR2.

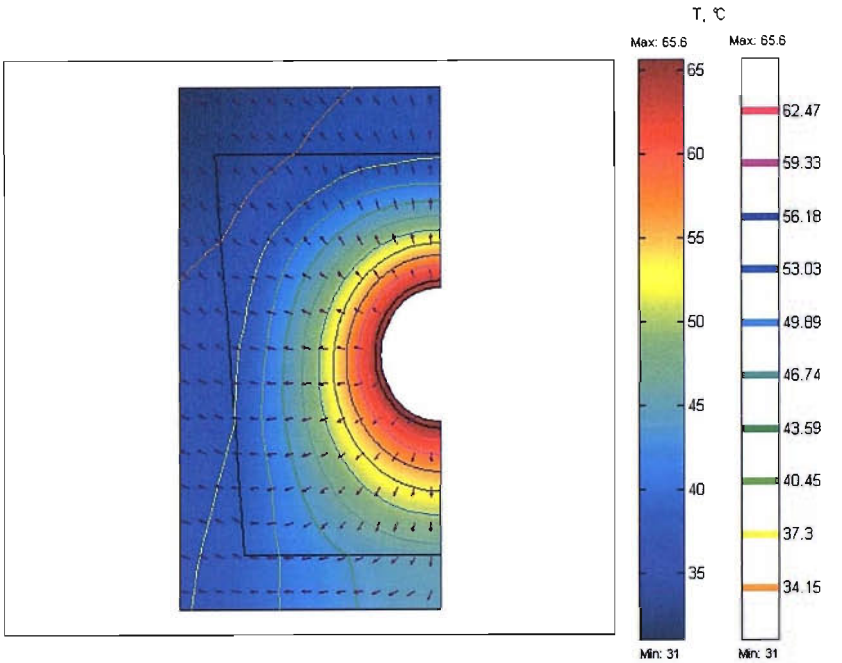

(a)

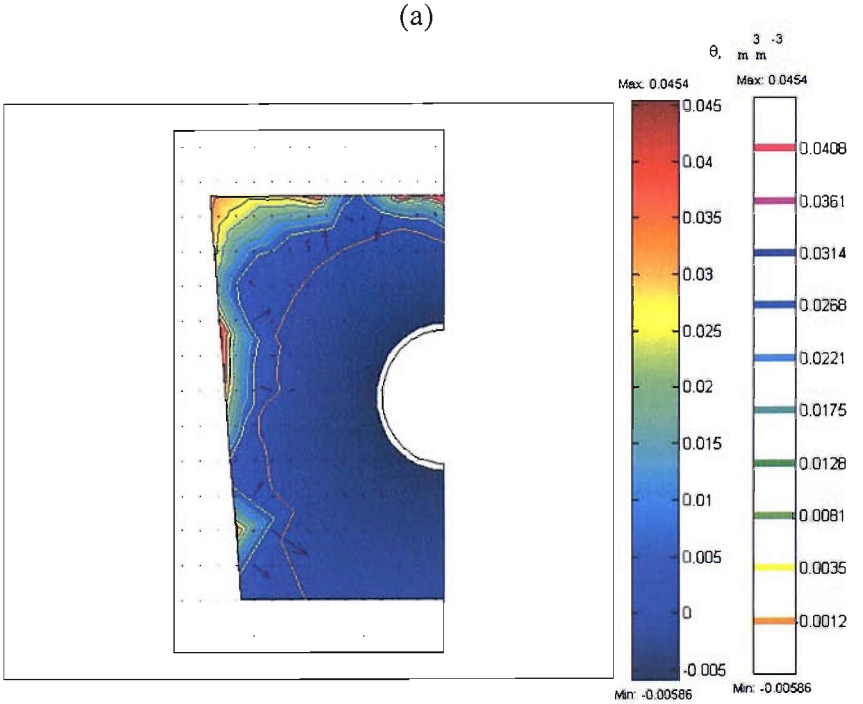

(b)

Figure 6.11 – Surface, contour and flux (by arrows) plots of (a) temperature (b) moisture distributions after heating in sequence 5, experiment TR2.

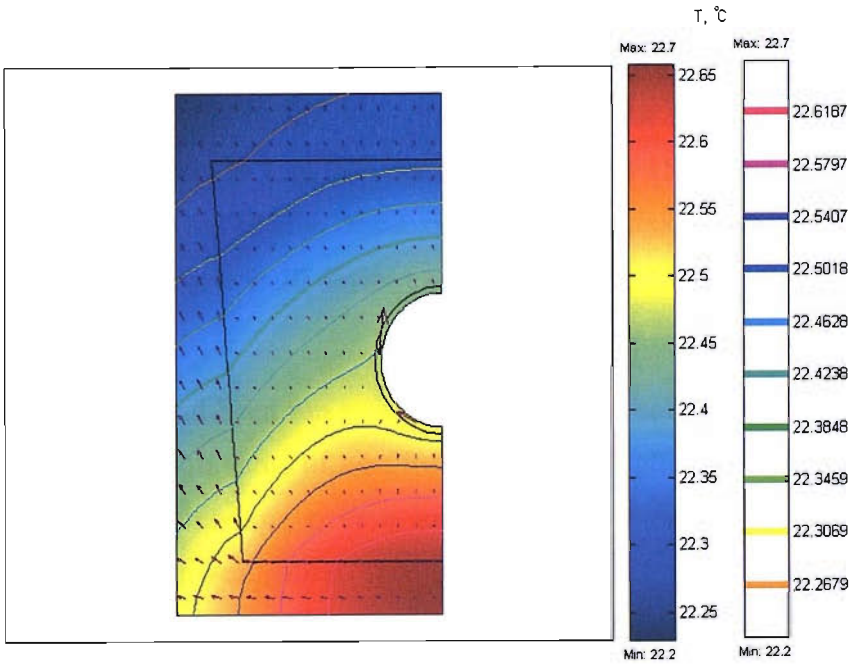

(a)

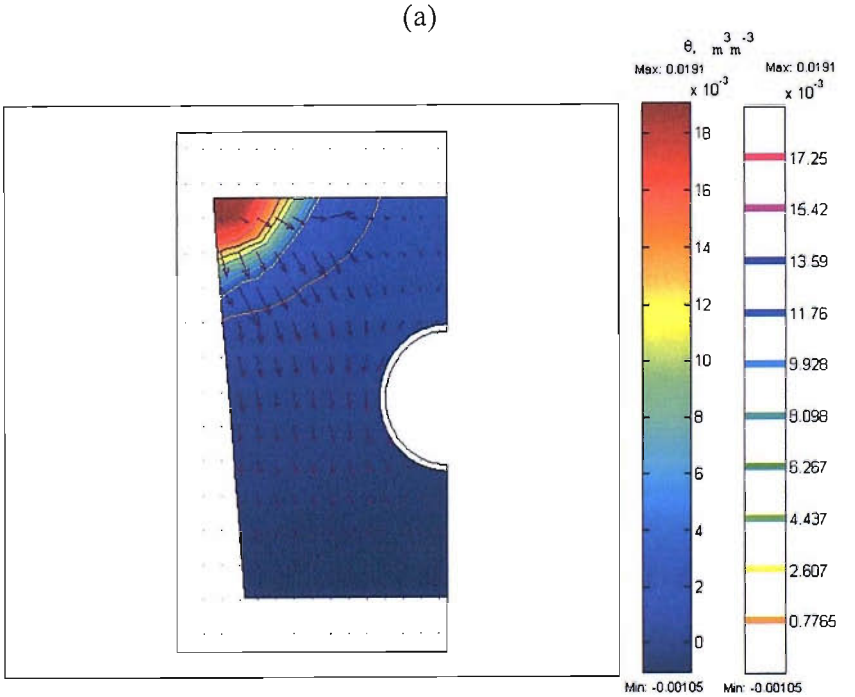

(b)

Figure 6.12 – Surface, contour and flux (by arrows) plots of (a) temperature (b) moisture distributions after cooling in sequence 1, TR2.

6.2.4 Experimental Results & FEM Simulation (TR3)

After experiment TR2, the trough was allowed to cool for about 2 days and the cable was subjected again to heat loss per meter length of 153 Wm^{-1}. The heating was only for a short period of time (approximately 7-8 hours) and the measurement of the subsequent cooling over 10 days was recorded.

This experiment had been run in order to investigate soil behaviour when the cable is subjected to high value of heat loss per meter length for a short period of time and followed by cooling over a longer period of time. This experiment provides a means in investigating how well moisture is redistributed under a thermal gradient after heating has ceased because in practice, it is often assumed (before cable heating is resumed) that moisture has evenly redistributed without knowing when exactly full redistribution is completed. Correct estimation of moisture redistribution leads to estimating accurate soil thermal conductivity and cable temperature and, therefore, improvement in the accuracy of a cable rating.

The temperature of the trough surface for the convective boundary had been assumed to be at 22 °C. Simulation for TR3 had been run using the solution that had been obtained previously in TR2 as its initial values.

Figure 6.13 shows the results of the cable temperature obtained from FEMLAB simulations and those from experiment TR3. Figure 6.13(a) and 6.13(b) are shown individually so that the simulation during heating would be visibly clearer. Plots (surface and contour) of both temperature and moisture distribution after each heating and cooling in experiment TR3 are shown in Figures 6.14 and 6.15, respectively.

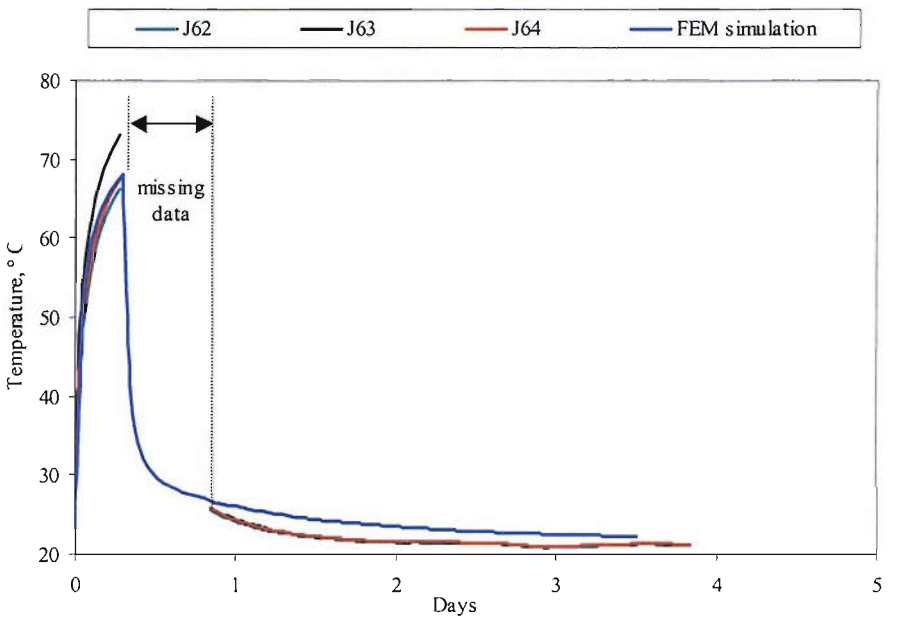

(a)

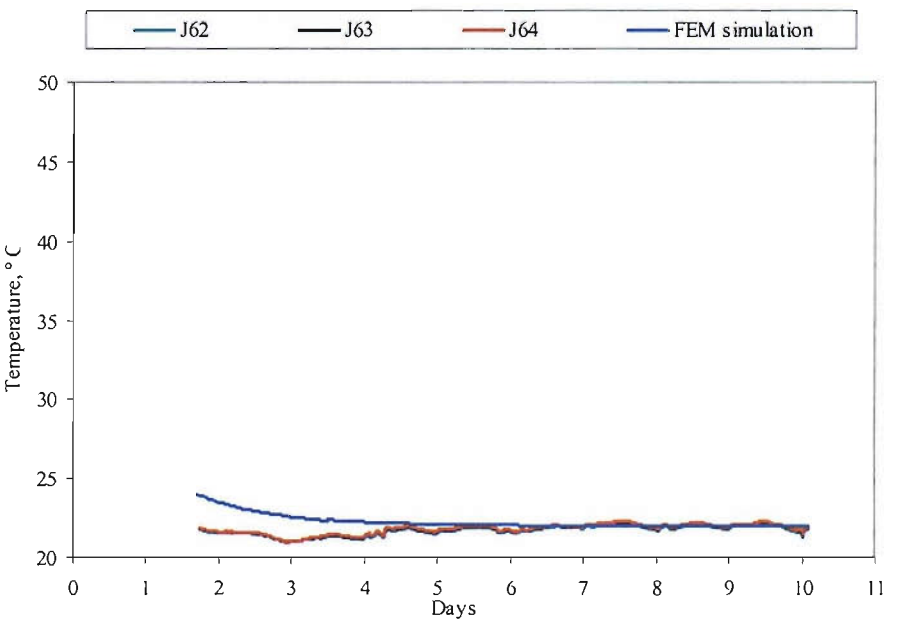

(b)

Figure 6.13 – Comparison between result obtained from FEM simulation and experiment for TR3 (a) during heating and approximately first 4 days of cooling (b) during cooling up to until 10 days.

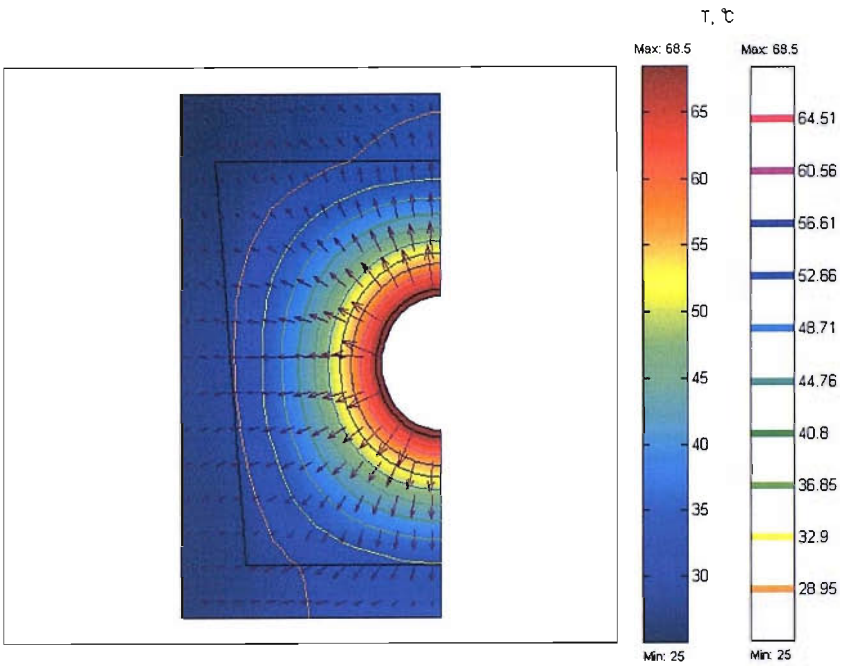

(a)

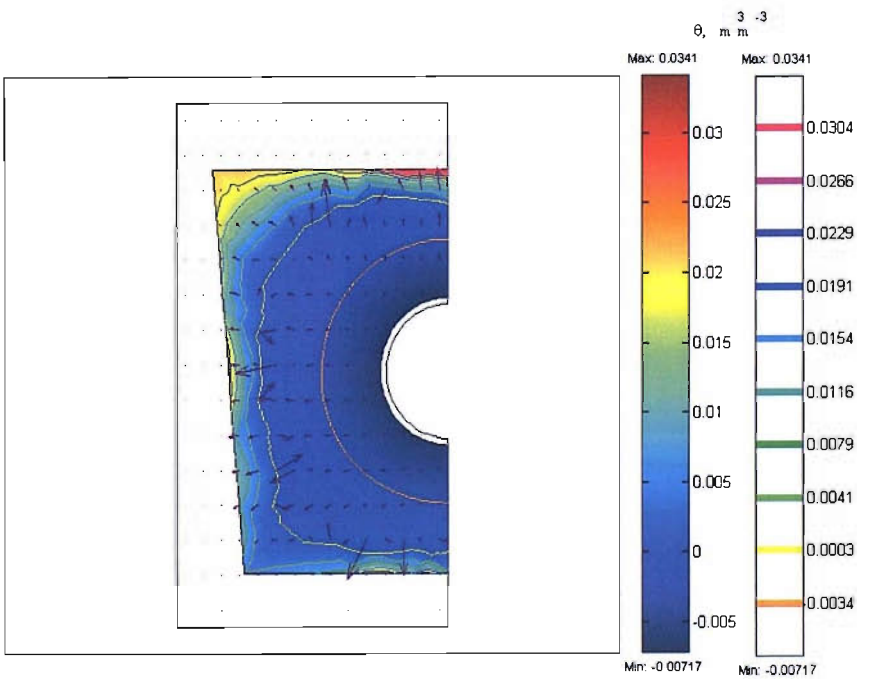

(b)

Figure 6.14 – Surface, contour and flux (by arrows) plots of (a) temperature (b) moisture distributions of FEM simulation for TR3 (after 7 hours heating).

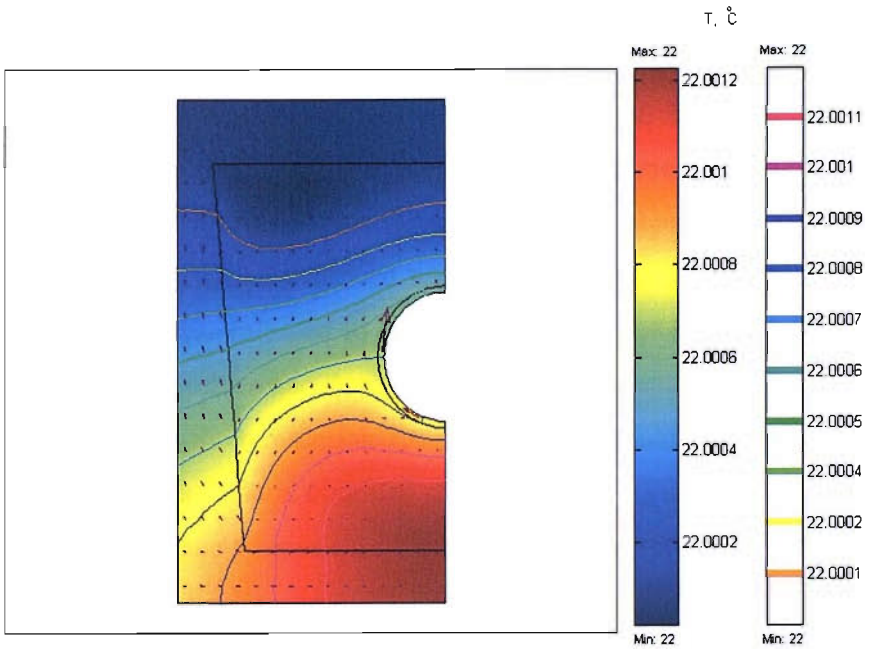

(a)

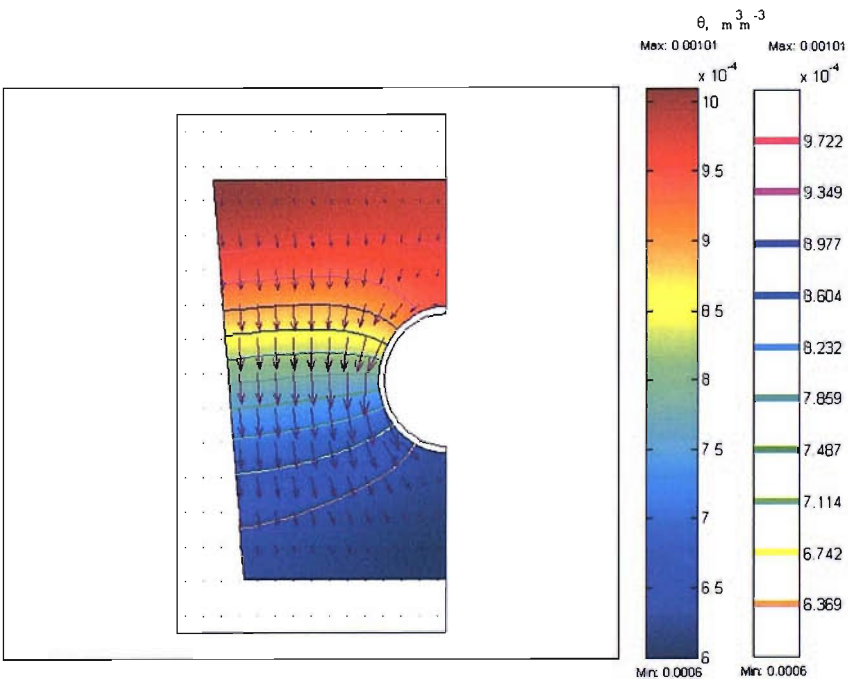

(b)

Figure 6.15 – Surface, contour and flux (by arrows) plots of (a) temperature (b) moisture distributions of FEM simulation for TR3 (approx. 10 days cooling).

6.2.5 Experimental Results & FEM Simulation (TR4)

Experiment TR4 has been conducted in order to investigate temperature rise when the cable is subjected to the highest available heat loss per meter length over a long period of time. In this experiment, the trough cable was subjected to 144 Wm^{-1} for an initial period of 2 days and followed with an increase to 153 Wm^{-1} for about 3 weeks. The increment was initiated to determine whether the FEM model is able to simulate the temperature increase due to increased cable heat loss when the soil is already dry. Similar to the simulation for TR3, the FEM simulation for TR4 had been carried out using solutions obtained previously from TR3 as its initial values and the convective surface temperature for the trough was set to 22 °C. The results obtained (cable temperature) using FEM simulation are compared to the experiment and is shown in Figure 6.16. Surface and contour plots of both distribution of temperature and moisture are shown in Figure 6.17. The cable was later allowed to cool for 52 days, with the first 8 days of cooling shown in Figure 6.16.

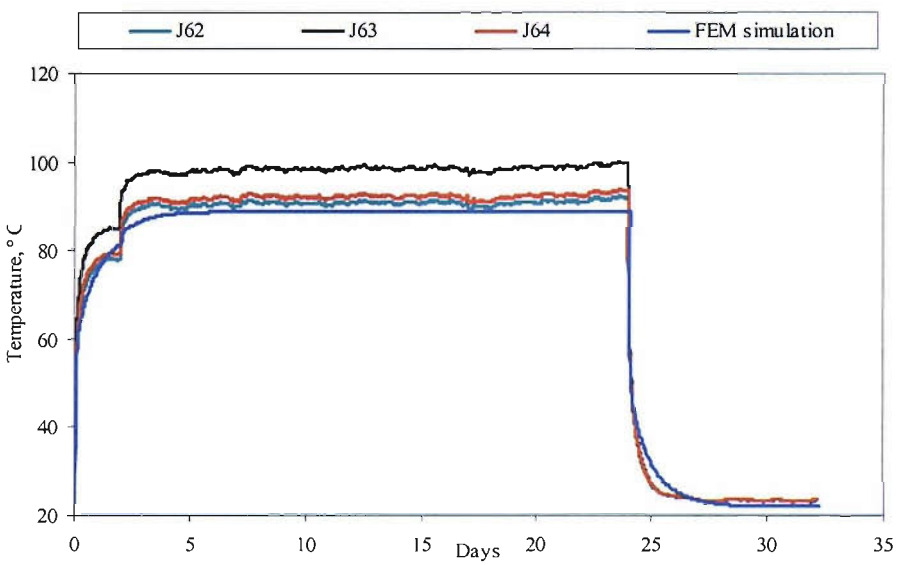

Figure 6.16 – Comparison between results obtained from FEM simulation and experiment for TR4.

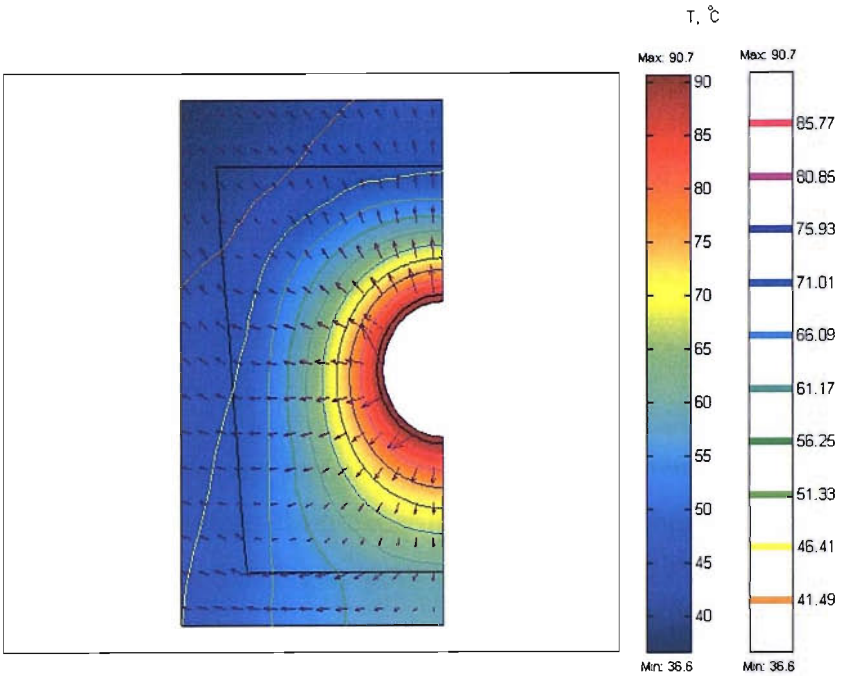

(a)

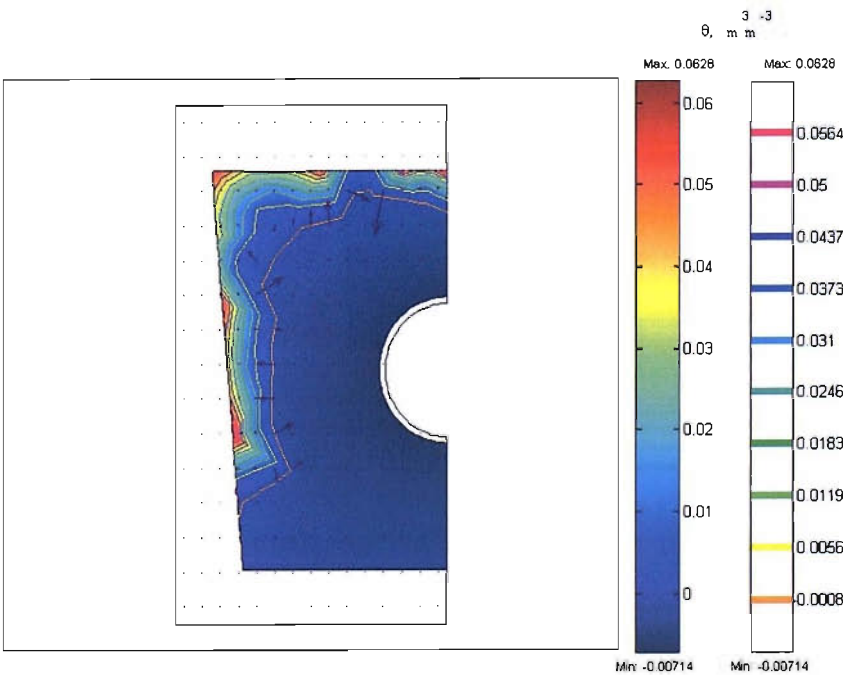

(b)

Figure 6.17 – Surface, contour and flux (arrows) plots of (a) temperature (b) moisture distributions of FEM simulation for experiment TR4 (after 24 days).

6.2.6 Experimental Results & FEM Simulation (TR5)

Experiment TR5 has been conducted by subjecting the cable to 112 Wm^{-1} heat loss per meter for about 93 days and then allowing it to cool for approximately 2 months. This experiment has been conducted to provide a means of comparing results obtained from FEMLAB when the trough cable is subjected to a cable heat loss per meter length that is slightly over 100Wm^{-1} over a long period of time.

All boundary conditions remained the same as previous simulation (TR4). Simulated cable temperatures from experiment TR5 are compared to that obtained from FEMLAB simulation in Figure 6.18. A large chunk of data has been lost due to an overwriting incident in retrieving data from the datalogger, however, data at the end of the experiment time has been obtained. Surface and contour plots, as well as heat and moisture fluxes after 93 days of heating are shown in Figures 6.19.

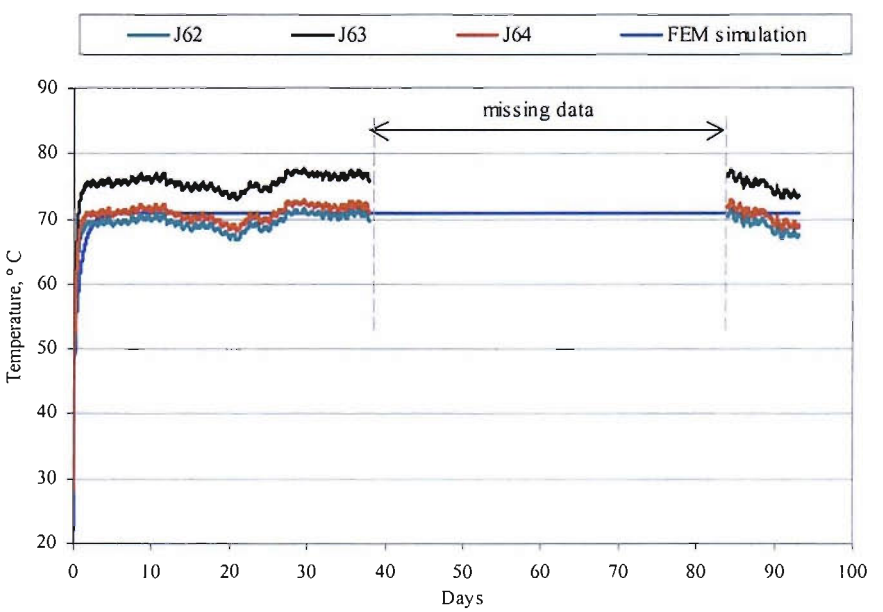

Figure 6.18 – Comparison between result obtained from FEM simulation and experiment for TR5.

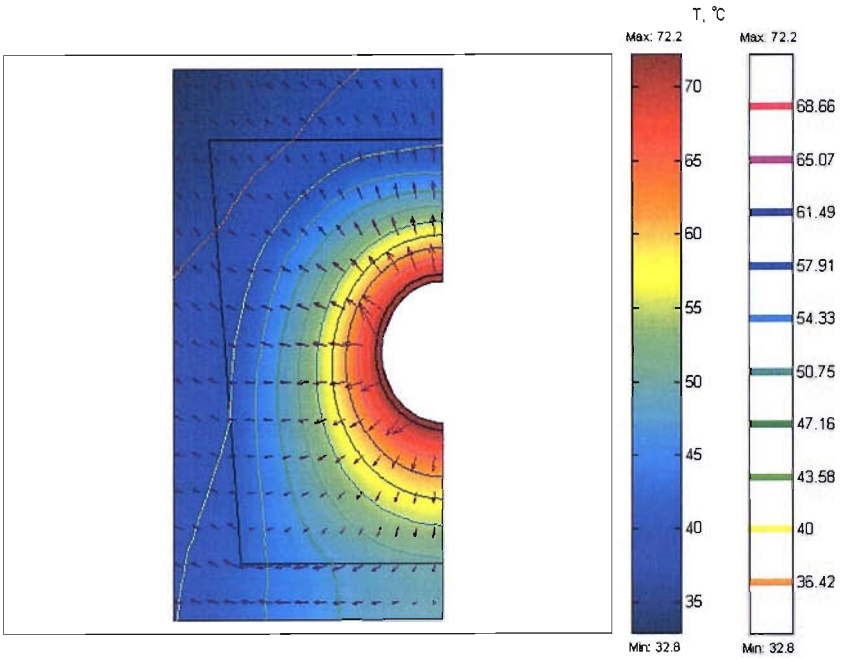

(a)

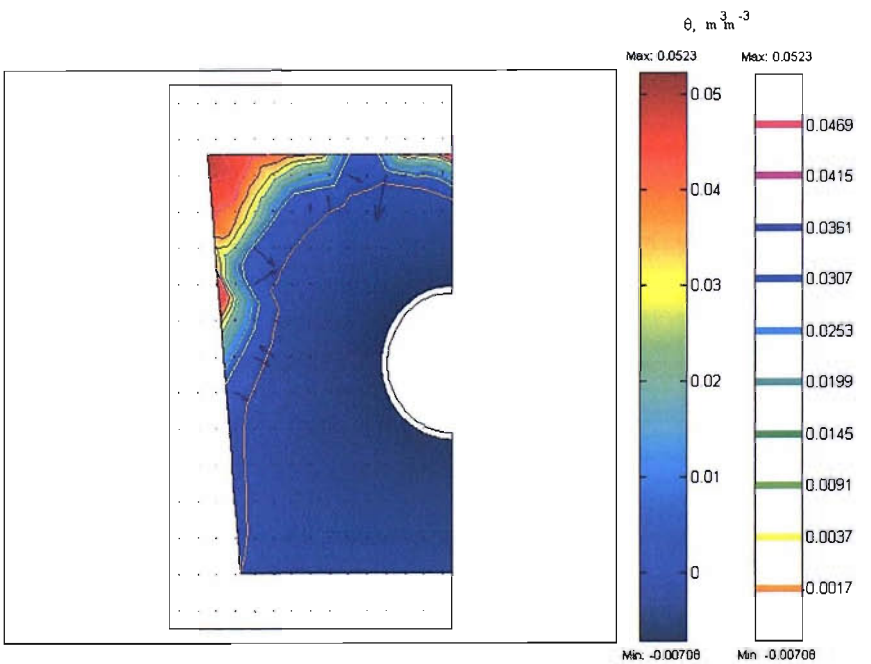

(b)

Figure 6.19 – Surface, contour and flux (by arrows) plots of (a) temperature (b) moisture distributions of FEM simulation for experiment TR5 (after heating).

6.2.7 Experimental Results & FEM Simulation (TR6)

In experiment TR6, the trough lids were removed while the cable was being heated. The simulated cable has been subjected to heat loss per meter length of $60Wm^{-1}$ for about 2 weeks and further increase to $120Wm^{-1}$ for another 59 days. FEM simulation for TR6 has used the meshes shown in Figure 6.4. Previous solutions obtained from FEM simulation of TR5 could not be used as initial values for TR6 due to the different meshes incorporated. There was a 60-day interval between the time that cable heat loss was removed during TR5 and the start of experiment TR6. The cooling of this interval has been simulated using FEMLAB, and it was found that both temperature and moisture are evenly redistributed over the whole region of subdomain 2; temperature at 22 °C and volumetric moisture at 0.0008. Therefore, the initial values for temperature and volumetric moisture content were set to 22 °C and 0.0008, respectively. The temperature of the surface trough for convective boundary was set to 26 °C. It is assumed that there is a constant moisture flux of $3.5x10^{-10}\,kgm^{-2}s^{-1}$ evaporating from the top surface. Results are shown in Figures 6.20 and 6.21.

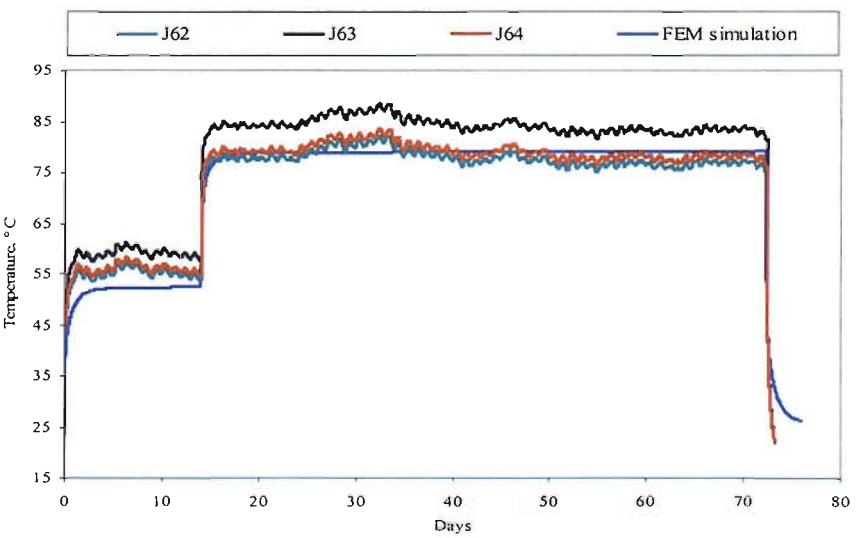

Figure 6.20 – Comparison between result (cable temperature) obtained from FEM simulation and experiment for TR6.

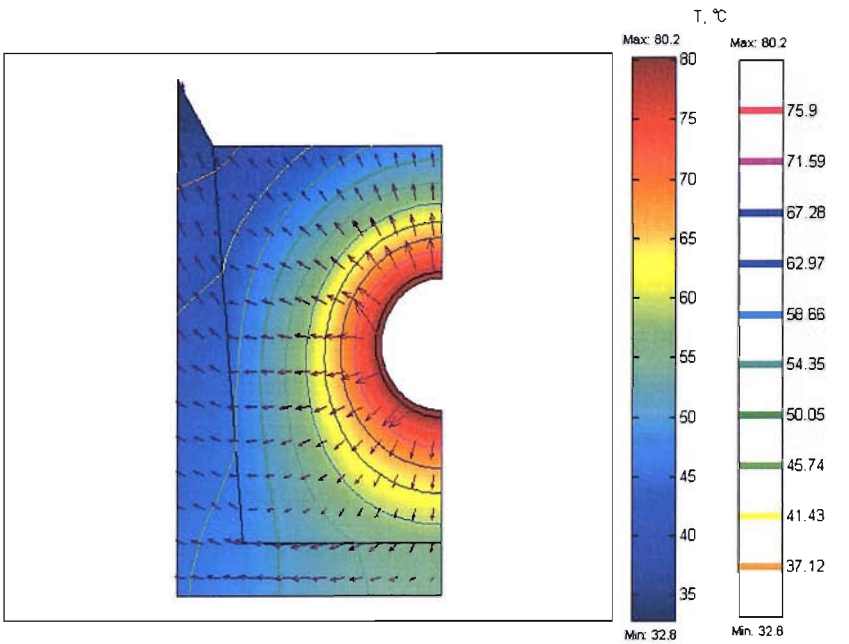

(a)

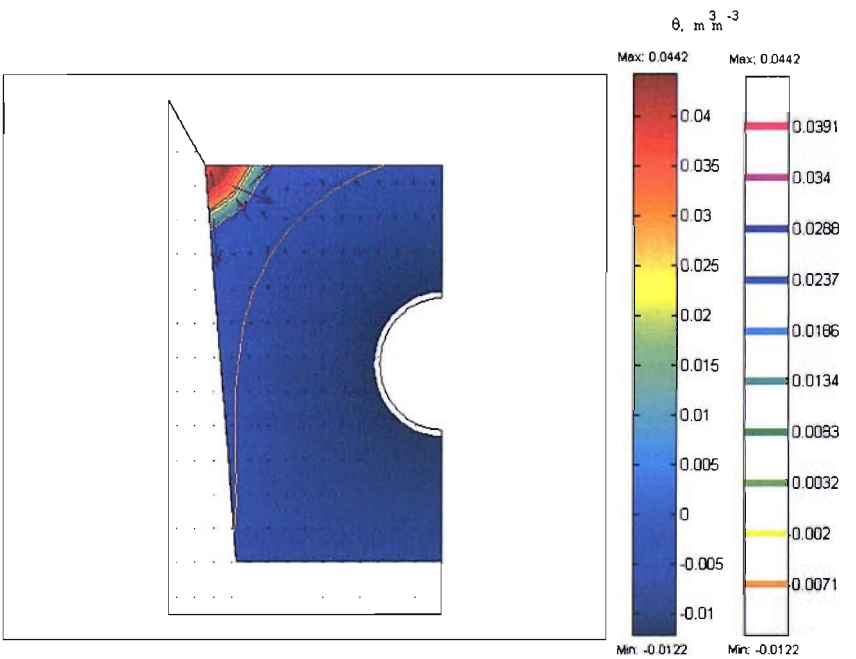

(b)

Figure 6.21– Surface, contour and flux (arrows) plots of (a) temperature (b) moisture distributions of FEM simulation for experiment TR6 (after heating).

6.2.8 Discussion

a) Experimental Results

Temperatures recorded by J63 in Figures 6.5, 6.8, 6.13, 6.16, 6.18 and 6.20 have shown that temperature at the middle length of the cable is about 4 – 6 °C greater than those at 0.5m away from the ends (J62 and J64). This is due to a slight discrepancy in the effective heat loss per meter length dissipated at the ends when compared to the middle of the simulated cable. The discrepancy in temperature is greater when the heat loss per meter length that was subjected to the simulated cable is greater. For example as seen in Figure 6.20, temperature of the simulated cable at mid-length is about 3 °C greater than those at the ends when the heat loss per meter is 60 Wm^{-1}, whereas when the simulated cable was subjected to 120 Wm^{-1} , the discrepancy is increased to about 6 °C. The temperature difference is well within 10% of the overall temperature rise and can, therefore, be assumed to be negligible. However, it is observed that these temperatures (recorded by J62, J63 and J63) attain similar steady state temperatures during each cooling.

Comparing experimental results in Figure 6.5 and 6.18, it can be seen that although the simulated cable was pre-heated to a heat loss of $50Wm^{-1}$ for a period of 7 days prior to being subjected to $112Wm^{-1}$, the steady state temperature of the simulated cable (after the $112Wm^{-1}$ heat loss has been initiated) in Figure 6.5 seems much less than that in Figure 6.18 (a difference of approximately 15 - 20°C). The time constant for the cable temperature to reach steady state is also longer than that in Figure 6.18. The difference is due to the fact that the initial volumetric moisture content in TR1 is relatively higher than that in TR5. This indicates that when a backfill is initially very dry, the steady state temperature of the cable can be expected to increase by approximately 33% when subjected to a constant cable heat loss. Backfills that are relatively dry have lower thermal capacitance due to a lack

of moisture or water that is needed to provide greater volumetric heat capacity within the backfill.

It can also be seen in experimental results shown in Figure 6.8 that soil thermal capacitive effect is detected after day 26, during cooling of sequence 4. The temperature of the simulated cable during final cooling of sequence 4 is about 3 °C higher than those during final cooling in sequences 1 - 3. This is because temperature of the simulated cable that had been attained after its first cyclic heating in sequence 4 had not been fully reduced to cooling temperature during the cooling period. Therefore, when the simulated cable was subjected to a further cyclic heat loss in sequence 5, the capacitive effect causes the cable surface to attain a temperature of about 3 °C higher (during cooling) when compared to the temperatures attained during cooling in previous sequences. However, this phenomenon was not detected in the final cooling of sequence 3. This may be due to the fact that value of the cyclic heat loss in sequence 3 ($50Wm^{-1}$) is half of that in sequence 4 ($100Wm^{-1}$) and would probably need greater number of similar cycles to achieve any capacitive effects.

Although there was a maximum difference of 4 - 6 °C in the temperatures recorded along the length of the simulated cable during heating, results in Figure 6.13 show that similar cooling temperatures of approximately 22°C had been attained by thermocouples J62, J63 and J64. The surface of the simulated cable started to attain a steady state cooling temperature about 2 days after the heating has ceased. As shown in Figures 6.16 and 6.8, a similar length of period has been observed to be needed for the temperature of the simulated cable to attain steady state cooling temperature (after heating has ceased). The experimental results shown in Figure 6.16 indicates that when a trough backfill with a very dry initial volumetric moisture content is subjected to a very high cable heat loss per meter length ($153Wm^{-1}$), the cable temperature could attain the boiling point of water.

It can be seen in Figure 6.16 (or Figure 6.22) that after about 20 days of heating, temperature of the cable surface slowly but steadily increases. It is suspected that if the experiment were to be prolonged over a longer period of time, breakdown may occur. A clearer observation may be achieved by looking at Figure 6.22.

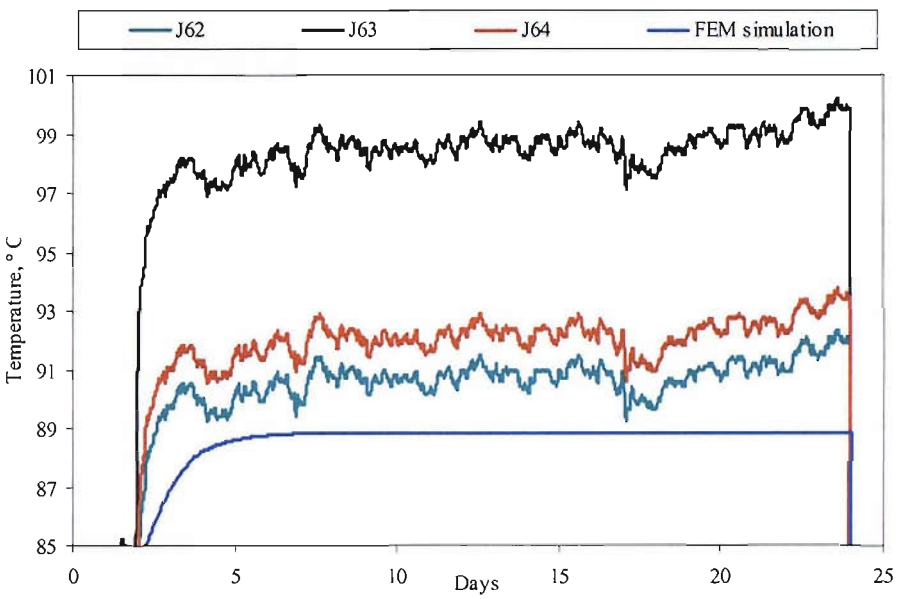

Figure 6.22 – Temperature of J63 slowly but steadily increases (TR4).

Although none of the results from other experiments are suitable for comparison with that from TR6 (the simulated cable with trough lids present in TR1 - TR5 had been subjected to heat loss per meter length that were not similar to that in TR6), results shown in Figure 6.20 can be used with the aid of further FEMLAB simulation in order to look at the effect of an exposed backfill surface on cable temperature. Results for comparison can be obtained by running a simulation that is similar to TR6 (but with the trough lids present, similar boundary conditions and initial values). This is further discussed in the next section.

b) Simulation

Figures 6.6 and 6.7 show that temperature and moisture move radially but not in a way that it is distributed concentrically. This is evident by looking at both contours. Since the top of the trough is subjected to convective boundary and bottom is insulated, the contours for both distributions look asymmetric. This may also be expected in buried underground cables where surface trough cables are situated quite near to the ground surface and has an infinite boundary below its base.

Figure 6.7 shows that the dry/wet interface is formed at the isotherm of 40 °C, whereby the areas within the boundary appears to be lacking moisture and areas outside are still attaining moisture. (Region indicated by blue in Figure 6.7(b) has zero moisture content). In order to observe if the isotherm differs if a different heating would have been used, a simulation is run with the 112 Wm^{-1} heating replaced with a lower heat loss, 80 Wm^{-1} (length of time subjected to the heat loss remained unchanged). The results in temperature and moisture surface plots are shown in Figure 6.23. The simulation results show that the dry/wet interface is found to be at 38 °C isotherm, 2 °C lower than that shown in Figure 6.7. A more obvious difference in the isotherms may be detected if the trough is simulated as if it is buried underground. This is because the trough boundaries would have not impeded temperature (or heat) that moves outwardly. Nevertheless, the isotherms obtained from results shown in Figures 6.7 and 6.23 show that it is possible to use Philip and de Vries equations in solving simultaneous heat and moisture transfer so that the location of the extremely dry and wet regions may be observed during cable loadings. This is useful in the sense that any possible thermal runaway may be predicted and, therefore, avoided.

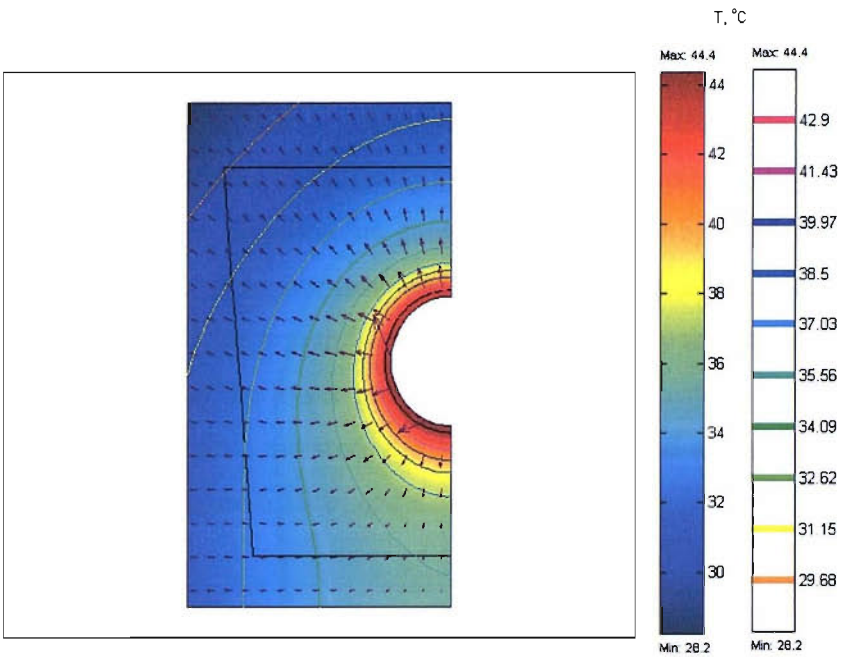

(a)

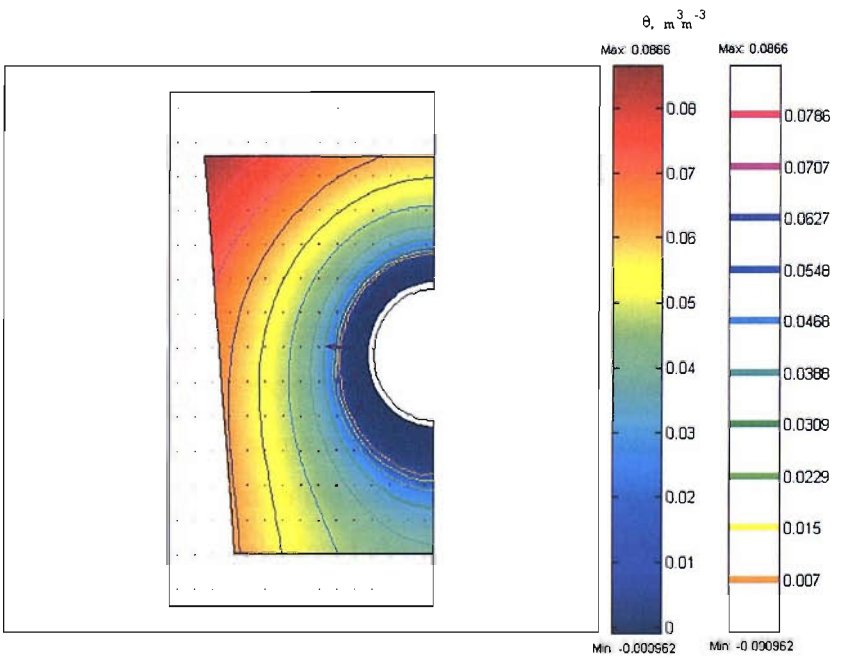

(b)

Figure 6.23– Surface, contour and flux (arrows) plots of (a) temperature (b) moisture distributions of FEM simulation at 80 Wm^{-1} to replace 112 Wm^{-1} in TR1 (after heating).

As moisture moves radially outwards, the volume near the vicinity of the cable surface becomes progressively dry and when constant heat flux is maintained over a period of time moisture is almost completely driven away from the rest of the volume towards the inner side of the trough walls and lid. These can be seen in the surface plots of moisture distributions shown in Figure 6.9(b), 6.10(b), 6.11(b), 6.14(b), 6.17(b), 6.19(b). A higher heat flux will have this effect occur at a faster rate and vice versa. Since the trough is constructed such a way that the half top part has a greater volume than the lower part and the fact that moisture moves radially outwards, highest cumulative moisture has been found located at the top corner of the troughs (as seen in Figure 6.19(b) and 6.21(b)).

Unlike Figures 6.13 and 6.16, results shown in Figure 6.8 reveal that the cooling temperatures of the simulation are higher than that of the experiment. This may be due to the fact that the trough surface temperature used for the convective boundary is higher. Therefore, if a lower convective temperature is assumed, cable temperatures can be expected to be slightly lower than that have been simulated in Figure 6.8.

Referring to Figure 6.8, it can also be seen that the simulated cable temperature in sequence 1 is about 2 °C less than the recorded temperatures of J62 whilst that in sequence 2 is about 2 °C more than the recorded temperatures of J63. Each simulation was run with the same corresponding experimental heat loss per meter length that had been subjected to the simulated cable. The experimental heat losses that have been used were calculated from values that had been taken from the voltage and current readings. Hence, the apparent discrepancies seen in sequence 1 and 2 in Figure 6.8 may be sourced from human error when the readings were taken. Furthermore, since the voltage analogue display was accurate to $\pm$10V, a human error in reading higher voltages (maybe more than 50V) inevitably would cause discrepancies in calculating the actual heat losses of the simulated cable. For

example, if the voltage reading is taken as 80V and that the current as 3A, the actual power has the marginal accuracy of about ±13% of the actual readings (voltage is 80V ±10V). Hence, it may be fair to say that the simulated temperature in sequences 1 and 2 in Figure 6.8 are in fact reasonable results since these lie less than ±9% of the average steady state temperatures recorded by J62, J63 and J64.

Experimental and FEM results in Figure 6.13 and 6.15 show that after cable heat loss had been removed for about 5 days, the cable temperature has reached its constant cooling temperature. However, moisture has not yet been evenly redistributed at this time. As the cable is allowed to cool for about 10 days, FEM simulation in Figure 6.15 shows that moisture flux is still moving towards the base of trough for redistribution. Hence, although moisture may be expected to wet very dry neighbouring volumes at a fast rate, redistribution of moisture does not take place as quickly as temperature over the same period of time.

Simulation results shown in Figures 6.12 and 6.15 were obtained using the mesh shown in Figure 6.3; whereby dense mesh is allocated near the cable surface in order to accommodate for possible high rates of change in temperature and moisture in this area. However, the mesh in Figure 6.3 was not suitable to be used for the simulation of the cooling periods because high rates of change of both temperature and moisture no longer form radially as both had been during the heating period. Better simulation results would have been achieved if a more suitable mesh were used.

The simulation results shown in Figures 6.16, 6.18 and 6.20 are fairly good when compared to the actual temperatures recorded by J62 and J64. The simulation results are also well below 7% of the average temperatures that had been recorded by J62, J63 and J64. In Figure 6.13, it can be seen that the simulation result of TR4

during cooling is in good agreement with the actual cooling temperatures. A similar result is also seen in Figure 6.16.

A simulation similar to that of TR6 has been simulated (but with lids present) in order to look at the effect of bare backfill on heating of a cable. Both simulations (with and without lids present) were then extended for cooling for about 12 days and further heating of $120Wm^{-1}$ for 25 days. Simulation results and comparisons are shown in Figure 6.24. For the first two heatings ($60Wm^{-1}$ and $120Wm^{-1}$), simulation results revealed that the simulated cable temperature is almost unaffected when the backfill is bare. Temperature of the simulated cable for the case of bare backfill is 0.5 °C greater than that for the case with the trough lids present when the cable is subjected to further heating of $120Wm^{-1}$.

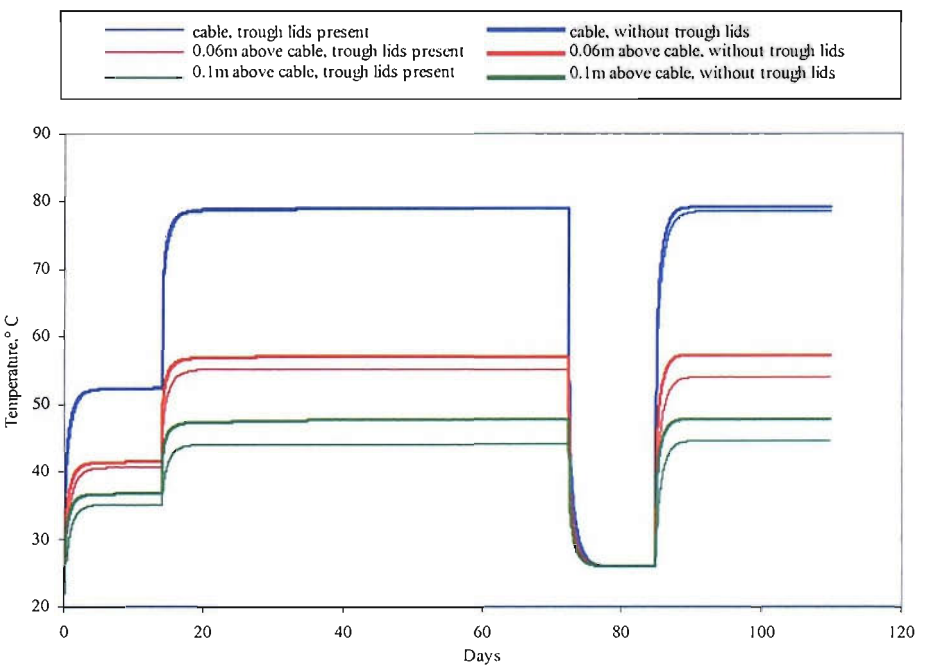

Figure 6.24 – Comparison of results (cable temperature) obtained from simulation of TR6 and that similar to TR6 with trough lids present.

For the case of bare backfill, temperatures at 0.06 m (perpendicularly) above the simulated cable and at the backfill surface are 1 - 3 °C and 2 - 4 °C higher than those for the case with trough lids present, respectively. The apparent temperature differences between the simulations for the two cases only appear during the second $120Wm^{-1}$ heating. This is partly because in the case with trough lids present, the cooling period allows moisture to be redistributed within the surface trough. In the case of bare backfill, moisture at the backfill surface is continuously lost through evaporation during the cooling process and moisture that has been lost through evaporation at the surface of the backfill could not be regained.

Generally, results obtained from FEM simulation for cable temperatures in experiments TR1, TR2, TR3, TR4, TR5 and TR6 are reasonably well within 2 to 3°C of the closest recorded temperatures, which is less than 5% of the closest actual cable temperatures, including sequence 2 shown in Figure 6.8. Overall, the simulation results are well less than 10% of the average recorded cable temperatures.

Moisture accumulation at the trough inner walls and lids as seen in all of the moisture distributions from FEMLAB simulation results may be more evenly distributed when meshes at these areas are further refined.

6.2.9 Conclusions

The results described in this chapter have proven that the implementation of Phillip and de Vries equation of simultaneous heat and moisture distribution using dynamic soil characteristics can produce accurate results in determining the heating behaviour of a cable placed in a surface trough.

It has been observed that moisture flux migrates away from the cable surface such as that of heat would dissipate from it. The contours normal to these fluxes are formed radially but not concentrically, due to the assumed boundary conditions. When a previously heated cable is allowed to cool, moisture of the backfill may not be evenly redistributed to its initial value as quickly as the temperature decreases to its initial value. Hence, in the case of cyclic loading of underground cables, the backfill capacitive heat effect may be caused by the fact that the return of moisture during unloading may not be fully redistributed. This consequently leads to the driest areas located near to the cable not returning to their original wet state at the beginning of the next loading cycle.

The time taken for cable surface to reach its constant temperature depends on the state of its surrounding backfill. If the backfill has a low initial volumetric moisture content, the time constant is slightly shorter than if it has higher initial volumetric moisture content. This is because moisture that is contained within backfill pores contributes to the heat capacity of the backfill as a whole.

A backfill surrounding underground cables that are contained within a surface trough may not be imposed to higher temperatures, as moisture that is driven away is not lost totally through evaporation to ambient as in the case where cables are buried directly. Hence, a surface trough acts as a safety barrier for loss of moisture especially when the cable is subjected to cyclic heating whereby driest region around it may be replenished by influx moisture during cooling, therefore decreasing the likelihood of thermal runaway.

Most importantly, FEM simulations on the simultaneous heat and moisture transfer made it possible to identify the dry/wet interface as well as the temperature at which it is formed, during a steady state heating. This is a useful tool in real

practice of cable loadings since progress of excessive drying may be detected in order to avoid thermal runaway.

CHAPTER 7

7.0 CONCLUSIONS

The avoidance of thermal runaway can be further investigated with thorough understanding of hydrological effects in backfills. In this study, heat and moisture equations in porous media that had been proposed by Philips and de Vries have been thoroughly studied. It has been shown that the behaviour of heating depends very much on the characteristics of the porous media.

Results obtained from the moisture migration experiments that have been carried out using the MMA show that heat is transferred at a faster rate when initial moisture of backfill is low, especially when the intensity of heat flux induced during heating is higher. Local thermal conductivity of a region within a backfill is altered when moisture is either lost or attained due to heating. Local thermal conductivity is decreased when moisture is lost and increased when moisture is attained. The influence of gravity upon backfill hydraulic permeability at moderate heating becomes significant when the initial volumetric moisture content is greater than 5%.

It has been identified that there are five soil properties that must be known for the distribution of heat and moisture to be modelled. These are the liquid diffusivities, vapour diffusivities, unsaturated hydraulic permeability and thermal conductivity. Each liquid and vapour diffusivity consists of two other elements that rely upon the gradient of temperature and moisture and divided into isothermal and thermal components. The four diffusivities are isothermal liquid diffusivity, thermal liquid diffusivity, isothermal vapour diffusivity and thermal vapour diffusivity. Moisture distribution within a backfill depends on these diffusivities and unsaturated hydraulic permeability. Whereas heat distribution

within a backfill depends on its thermal conductivity and isothermal vapour diffusivity.

In this work, both thermal and hydraulic properties of the backfill used have been investigated and obtained both experimentally and analytically. These characteristics have been incorporated in the Philips and de Vries equations and solved using the finite element method using FEMLAB®. Soil properties are made dynamically available within the FEMLAB simulation when the properties are recalculated at each iteration. This ensures reasonably accurate thermal and hydraulic behaviour during the investigation of drying of backfill during heating.

The Philips and de Vries equations have been implemented and tested against the practical experiments that have been carried out. Results show that simulations using these equations are in good agreement with those obtained from experiments indicating that Philips and de Vries equation can solve heat and moisture distribution problems accurately when soil properties under investigation are known with reasonable accuracy. It has been found that both isothermal diffusivity, isothermal vapour diffusivity and unsaturated hydraulic permeability of the backfill used have been overestimated. This may be partly due to the estimation obtained from the SoilVision software package, which have been overestimated. The most essential hydraulic characteristics needed for the accurate estimation of backfill hydraulic properties is the water retention curve and saturated hydraulic permeability.

It has been proven in this work that fairly accurate temperature distribution within a backfill due to heating can be determined when dynamic calculations of hydraulic and thermal properties are combined with finite element analysis. The changes in temperature fluctuations due to increasing and decreasing 'local'

thermal conductivity within regions can also be detected. The negative value in moisture distribution resulting from the finite element analysis is due to the imbalance mass conservation occurring within the Philips and de Vries equations. This is inevitable since the hydraulic properties of backfill itself are highly non-linear. However, this shortcoming does not greatly influence much of the thermal conductivity calculations since negative moisture values are always assumed to be zero, hence driest state attainable.

7.1 FURTHER WORK

The implementation of thermal and hydraulic properties of backfills within the simultaneous solution of the Philips and de Vries equations using the finite element method can be used to further investigate heating behaviour of power cables that are buried underground. Environmental effects such as convective ground surface, sun radiation, location of water table, percolation and neighbouring native soils have on the performance of buried power cables may also be further investigated using the method that has been used in this project. Results that are obtained from this practice may be studied to further improve the rating of buried power cables. This is achieved by estimating the external resistance between cable surface and the ambient as accurate as possible.

It is also useful to carry out an extension work following the achievement obtained in this project to look at heating behaviours of cables surrounded with different types of backfills and/or native soils, such as loam and clays.

REFERENCES

1. Cox, H.N; Holdup, H.W ;Skipper, D.J;' Developments in UK cable-installation techniques to take account of environmental thermal resisitivities', 1975, Proceedings of IEE, Vol 122, 11, pp 1253-1259.

2. Distributed Intelligence - underground transmission and distribution cable circuits, Transmission and Distribution World, June 1, 2001.

3. John Millar, R; Matti Lehtonen, Dec. 2002. The effect of moisture migration, native soil environment and trough cement quality on the steady state rating of HV power cables. TESLA report nr 66/2002, Helsinki University of Technology.

4. Phillips, J.R; de Vries, D.A; 'Moisture movement in porous materials under temperature gradients', Transaction of American Geophysical Union, 1957, **38**, (2), pp222-232.

5. Farouki, O.T; Physical properties of granular materials with reference to thermal resistivity, Highway Research Record, No. 128, pp 25-44.

6. Halfter, N.A; King, S.Y; 'Experimental investigation of moisture migration in power cable backfills', Electrical Engineering Transaction, The Instutition of Engineers, Australia, 1975, pp50-57.

7. Mochlinski, K; 'Assessing ground temperature', Electrical Times, 1971, pp 42-46.

8. Eagleson, P.S; 'Climate, soil and vegetation. 3: A simplified model of soil moisture movement in liquid phase', Water Resource Research, 1978, **14**, (5), pp722-730.

9. Kilmer, V.J; 'Handbook of soils and climate in agriculture', CRC Press, 1982, pg 445.

10. Bladowski, S; 'Heat transfer from cables laid in soil:Part I', Energetyka, 1965a, (2), pp36-39.

11. Orchard, R.S; Barnes, C.C; Hollingsworth, P.M; Mochlinski, K.; ' Soil thermal resistvity. A practical approach to its assessment and it influence on the current rating of buried cable', Conference Internaionale des Grands Electriques a Haufe Tension, 1960, **214**, pp1-34.

12. Cengel, Y.A, 'Heat transfer: A practical approach', International Edition, McGraw-Hill Publishing, 1998.

13. Radhakrishna, H.S; 'Heat flow and moisture migration in cable backfill', Ontario Hydro Reseacrh Quarterly, 1968, **120**, (2), pp10-20.

14. Elsevier Scientific Publishing Company, 'Handbook of soil mechanics, Volume I: Soil Physics', 1974.

15. Milne,A.G; Mochilinski, K.; ' Characteristics of soil affecting cable ratings' , Proc. IEEE, 1964, **111**,(5), pp1017-29.

16. Donazzi, F; Occhini, E. ; Seppi, A.; ' Soil thermal and hydrological characteristics in designing underground cables', Proc. IEE, 1979, **126**, (6), pp506-516.

17. Brooks,E.J; Gosling,C.H; Holdup,W.; 'Moisture control of cable environement with particular reference to surface troughs' , Proc. IEE, 1973, **120**, (1), pp51-59.

18. Arman, A.N; Cherry, D.M; Gosland, L; Hollingsworth,P.M; 'Influence of soil moisture migration on power rating of cables in H.V transmission systems', Proc. IEE, 1964, **111**, (5), pp1000-1016.

19. Bladowski, S; 'Heat transfer from cables laid in soil:Part II' , Energetyka, 1965b, (2), pp76-80.

20. Marshall, T.J, Holmes, J.W. Soil Physics. 1979. 1st Edition. Cambridge University Press.

21. David D. Introduction to Hydrogeology. 2002. 480 pages. Publication of EDGe Education,The University of Oklahoma.

22. Carman, P.C; 'Properties of capillary-held liquids', Journal of Physical Chemistry, 1953, **57**, pp56-64.

23. Rose, D.A; 'Water movement in porous materials. Part I: Isothermal vapour transfer', British Journal of Applied Physics, 1963a, **14**, pp256-262.

24. Taylor, S.A; Cary, J.W; ' Linear equations for the simultaneous flow of matter and energy in a continuous soil system', Soil Science Society of America Proceedings, **28**, 1964, pp167-172.

25. Cassel, D.K; Nielsen, D.R; Biggar, J.W; 'Soil-water movement in response to temperatue gradient', Soil Science Society of America Proceedings, **33**, 1969, pp 493-500.

26. Rose, D.A; Water movement in porous materials. Part2: The separation of the components of water movement', British Journal of Applied Physics, 1963b, **14**, pp491-496.

27. Dakshanamurthy, V.; Fredlund, D.G; A mathematical model for predicting moisture flow in an unsaturated soil under hydraulic and temperature gradient', Water Resources Research, 1981, **17**, (3), pp714-722.

28. Milly, P.C; 'Moisture and heat transport in hysteretic inhomogeneous porous media: A matric head formulation and a numerical model', 1982, Water Resources Research, 3, pp489-498.

29. Sophocoleous; ' Analysis of water and heat flow in unsaturated-saturated porous media', 1979, Water Resources Research, pp1195-1206.

30. El-Kady, M.A; 'Calculation of the sensitivity of power cable ampacity to variations of design and environmental parameters',1984, IEEE Transactionon Power Apparatus and Systems, vol PAS-103,8, pp2043-2050.

31. Hanna, M.A; Chickhani, A.Y; ' Effect of trench geometry, cable size and top layer thickness on the heat dissipation in buried cables' , 1992, Paper 92, PWRD, PES 1992 summer Meeting, pp 743-747.

32. Hanna, M.A; Chickhani, A.Y; Salama, M.M.A; ' Effect of geometry between cables on the heat dissipation from underground cable systems' , 1993, CCECE/CCGEI, pp 433-436.

33. Hanna, M.A; Chickhani, A.Y; Salama, M.M.A; ' Thermal analyses of power cables in multi-layered soil. Part 3:Case of two cables in a trench' , 1994, IEEE Transaction on Power Delivery, Vol 9, 1,pp 572-578.

34. Hanna, M.A; Chickhani, A.Y; Salama, M.M.A; ' Thermal analysis of power cables in a trench in multi-layered soil' , 1998, IEEE Transaction on Power Delivery, Vol 13, 2,pp 304-309.

35. Tarasiewicz, E.K; Grzybowski, S; 'Calculations of temperature distributions within cable trench backfill and the surrounding soil', 1985, IEEE Transactionon Power Apparatus and Systems, vol PAS-104,8, pp1973-1978.

36. Flatabo, N; 'Transient heat conduction problems in power cables solved by the finite element method', 1972, IEEE PES Summer Meeting, pp56-63.

37. Arman, A.N; Cherry, D.M; Gosland, L; Hollingsworth,P.M; 'Influence of soil moisture migration on power rating of cables in H.V trnsmission systems', 1964, IEE Proceedings, Vol 111, 5, pp1000-1016.

38. Koopmans, G; van de Wiel, G. M. L. M; van Loon, L. J. M and Palland, C.L; 'Soil physical route survey and cable thermal design procedure', 1989, IEE Proceedings, Vol 136, Part C, 6, pp 341-346.

39. Childs, E.C; Collins-George, N; 'Permeability of porous materials', 1950, Proceedings of Royal Society of London, Serial A, 201, pp 392-049.

40. Feddes, R.A; Kowalik, P.J; Zaradny, H.; 'Simulations of field water use and crop yield', 1978, Pudoc, Wageningen.

41. Nahman, J; M. Tanaskovic; 'Determination of the current carrying capacity of cables using the finite element method', Electric Power Systems Research, 2001, 61, pp109-117.

42. G. Mainka, 'Berechung der Belastbarkeit von in Erde verlegten Starkstromkabeln unter Beru¨cksichtigung von Belastungsfaktor und Bodenaustrocknung', 1971, ETZ-A 92, 3, pp125–130.

43. Anders, G.J; Radhakrishna , H.S; 'Power cable analysis with consideration of heat and moisture transfer in the soil' , IEEE Trans. on Power Delivery, 1988, **3**, 4, pp1280-1287.

44. Moya, R.E.S ; Prata, A.T ; Cunha Neto, J.A.B ; 'Experimental analysis of unsteady heat and moisture transfer around a heated cylinder buried into porous medium', International Journal Of Heat and Mass Transfer, **4**, 1999, pp2187-2198.

45. Hartley, J.G; Black, W.Z; 'Transient simultaneous heat and mass transfer in moist, unsaturated soils', Journal of Heat Transfer, Trans. ASME, **103**, 1981, pp 376-382.

46. Liou,Y; England, A.W; 'A Land Surface Process/Radiobrightness Model with Coupled Heat and Moisture Transport in Soil', IEEE Transactions on Geoscience and Remote Sensing, Vol 36, 1, pp 273-286.

47. Deru, M.P; Kirkpatrick, A.T; 'Ground-coupled Heat and Moisture Transfer from buildings. Part 1: Analysis and Modelling', 2001, NERL/CP-550-29693, American Solar Energy Society National Solar Conferences Forum 2001.pp1-9.

48. Deru, M.P; Kirkpatrick, A.T; 'Ground-coupled Heat and Moisture Transfer from buildings. Part 1: Application, 2001, NERL/CP-550-29694, American Solar Energy Society National Solar Conferences Forum 2001.pp1-7.

49. Xiaoshu, L; 'Modelling of Heat and Moisture Transfer in Buildings. 1.Model Program', 2002, Energy and Buildings, vol 34, pp 1033-1043.

50. Ewen, J.; Thomas, H.R; 'Heating unsaturated medium sand', Geotechnique, 1989, **39**, 3, pp455-470.

51. Thomas, H.R ; 'Nonlinear analysis of heat and moisture transfer in unsaturated soil', Journal of Engineering Mechanics, 1987, **113**, (8), pp1163-1180.

52. Radhakrishna, H.S; Lau, K.C; Crawford, A.M; 'Coupled heat and moisture flow through soils', Journal of Geotechnical Engineering, 1984, **110**, (12), pp1766-1783.

53. Abdel-Hadi, O.N; 'Flow of Heat and Water Around Underground Power Cables', Ph.D thesis, University of Berkeley, Oct 1978.

54. Anders, G.J; Radhakrishna, H.S; 'Computation of temperature field and moisture content in the vicinity of current carrying underground power cables'. Proceedings of IEE, 1988, **135**, Pt.C, (1), pp51-59.

55. Freitas, D.S; Prata, A.T; de Lima, Aloisio; 'Thermal performance of underground power cables with constant and cyclic currents in presence of moisture migration in the surrounding soil', IEEE Transactions on Power Delivery, 1996, **11**,3, pp1159-1170.

56. Preece, R.J; Hitchcock, J.A; 'Preliminary theoretical studies of the temperature and moisture distributions around a nornally buried e.h.v cable', 1966, CERL Report, RD/L/N 139/66.

57. Buonanno, G.; Carotenuto, A; Dell'Isola, M. and Villacci, D; 'Effect of radiative and convective heat transfer on thermal transients in power cables', 1995, IEE Proceedings on Generation, Transmission and Distribution, Vol 142, 4, pp436-444.

58. Kjellgren, J; 'A Combined Temperature and Water Content Model for Bare Soil', 1997, Geoscience and Remote Sensing, IGARSS '97. 'Remote Sensing - A Scientific Vision for Sustainable Development'., 1997 IEEE International , Volume: 4 , pp 1962-1965.

59. SoilVision Version 2.0 Manual. Detailed Operation. 1st Edition. SoilVision Systems Ltd. pgs. 93.

60. 'General Specification for Civil Engineering Work', Volume 1, Section 6, 1992 Edition, Corrigendum No2/2001 (September),Standards Unit, Civil Engineering Department, The Government of Hong Kong Special Administrative Region of the People's Republic of China.

61. Mochlinski, K; ' Field tests on thermal properties of soil and their effect on cable ratings', ERA Report, 1962, pp1-42.

62. Rider, N.E; A note on the physics of soil temperature', Wealth, 1957, **12**, (8), pp241-246.

63. Wiseman, R.J; Burell, R.W; ' Soil thermal characteristics in relation to underground power cables' , AIEE Committee Report, 1960,pp 792-815.

64. Preece, R.J; Hitchcock, J.A; 'Heat and moisture transfer around a heat source in porous media. Part 1: Physical model and basic theory' , CERL Report, RD/L/N 52/65,pp1-10.

65. 'Soil thermal resistivity and thermal stability measuring instrument. Volume 1: Determination of soil thermal stability and other soil thermal properties' , Ontario Hydro Research Laboratory,EPRI Report, 1981, pgs 1(1)-6(1).

66. FRITSCH Electromagnetic Laboratory Sieve Shaker *'Analysette-3'* Operation Manual, Fritsch GmbH, pp 2-6.

67. Brooks, R.H, Corey, A.T. 'Hydraulic properties of porous media. Hydrological Paper 3'. 1964. Colorado State University, Fort Collins.

68. Gardner, W;. 'Mathemathics of isothermal water conduction in unsaturated soils.', 1965, Highway research Board Special Report 40 International Symposium on Physico-Chemical Phenomenon in soils, Washington D.C, pp 78-87.

69. Van Genuchten, M.Thesis; 'A closed-form equation for predicting the hydraulic conductivity of unsaturated soils', 1980, Soil Science Society of America Journal, **44**, pp 892-898.

70. Fredlund, D.G, Xing, A; 'Equations for the soil-water characteristics curve.', Canadian Geotechnical Journal, **31**, No.3, 1994, pp 521-532.

71. Ewen, J; 'Heat and moisture transfer for buried cables', 1983, Msc Thesis, University of College Cardiff.

72. Radhakrishna, H.S; 'Heat flow and moisture migration in cable backfills.', 1968, Ontario Hydro Research Quarterly, 2nd Quarter.

73. Mayhew, Y.R, Rogers, G. F. C; 'Thermodynamics and transport properties of fluids.' 1976, 2nd Edition. Basil Backwell, Oxford Publishings.

74. Vukovic, M.,Alndjelko, S. ; 'Determination of hydraulic conductivity of porous media from grain-size composition. ', 1992, Water Resources Publications, Littleton, Colorado.

75. Kunze, R.J, Uehara, G., Graham, K.; 'Factors important in the calculation of hydraulic conductivity.' , 1968, Proceedings of Soil Science Society of America, **32**, pp 760-765.

76. Fredlund, D.G, Xing, A; 'Predicting the permeability function for unsaturated soil using the soil-water characteristic curve.', 1994, Canadian Geotechnical Journal, **31**, No.3. pp 533-546.

77. Campbell, J.D; 'Pore pressures and volume changes in unsaturated soils.',1973, Ph.D Thesis, University of Illinois at Urbana-Champaign, Urbana-Champaign III.

78. Mualem Yechezkel; 'A new model for predicting the hydraulic conductivity of unsaturated porous medium.', 1976, Water Resources Research, **12**, No. 3, pp 513-522.

79. Fredlund M.N; 'Design of a knowledge based system for unsaturated soil properties', 1996, M. Sc. Thesis, University of Saskatchewan, Saskatoon, Sasketchewan, Canada.

80. International Critical Tables. Vol. VI. McGrawHill Publishing.

81. Krischer, O. , Rohnalter, H; 'Warmeleitung und Dampdiffusion in feuchten Gutern.' , 1940, Verein Deut. Ing-Forschungsheft 402.

82. Gurr, C.G, Marshall, T.J, Hutton, J.T; 'Movemnet of water in soil due to a temperature gradient' , 1952, Soil Science, **79**, pp 257-265.

83. Rollins, R.L, Spangler, M.G, Kirkham, D; 'Movement of soil moisture under a thermal gradient.' , 1954, Highway Research Board of Proceedings. **33**, pp 492-508.

84. Preece, R.J; ' The measurement and calculation of physical properties of cable bedding sands.' , 1975 , Part2: Specific thermal capacity, thermal conductivity and temperature ratio across air filled pores. CEGB, Lab note no. RD/L/N 231/74.

85. Kimball, B.A, Jackson, R.D, Reginato, R.J, Nakayama, F.S, Idso, S.B, 'Comparison of field-measured and calculated soil heat fluxes.' , 1976, Soil Science of American Journal Vol. 40, pp 18-24.

86. Sepashkah, A.R , Boersma, L. ;'Thermal conductivity of soils as a function of temperature and water content.', 1979, Soil Science of American Journal. Vol. 43, pp 439-444.

87. DaPonte, P., DiPippo, R., Fowler, A.J, Meressi, T., Welch, J.R.; 'Deteremination of thermal conductivity and thermal diffusivity of soils.' , 1999, Geothermal Resources Council Transactions, Vol. 23, Oct 17-20. Pp 119-122.

88. Nicolas, J., Andre, Ph., Rivez, J.F, Debbaut, V., 1993. Rev. Science Instruments. American Institue of Physics. Vol. 64, Pt. 3, pp 774-780.

89. Boggs, S.A, Chu, F.Y, Radhakrishna, H.S, Steinmanis, J; 'Measurement of soil thermal properties – technique and instrumentation.' ,1980 , IEEE Transcations on Power Apparatus and System, Vol PAS-99, No.2. pp. 747- 752.

90. Manohar, K., Yarbrough, D., Booth, J.R, ; 'Measurement of apparent thermal conductivity by the thermal probe method.' 2000, Journal of testing and evaluation, American Society for Testing and Materials. Vol. 28, No. 5, pp 345-351.

91. Chaney, R.C, Ramanjaneya, G, Hencey, G, Kanchanastit, P, Fang, H.; 'Suggested test method for determination of thermal conductivity of soil by thermal needle method. ', 1983, Geotechnical Testing Journal, ASTM. Vol. 6. No.4, pp 220-225.

92. Johansen, O.1975. Thermal conductivity of soils. Ph.D Theses (CERREL Draft Translation 637, 1977), Trondheim, Norway.

93. Brandon, T.L, Mitchell, J.K; 'Factors influencing resistivity of sands.' , 1989, Journal of Geotechnical Engineering. Vol. 115, No.12, pp 1683-1698.

94. Touloukian Powel, V.R, 'Thermophysical properties of matter Vol. 2', TPRC Data Series. Thermal conditions non-metallic solids.

95. Tarnawski, V.R, Leong, W.H, Bristow, K.L, 2000. 'Developing a temperature-dependent Kersten function for soil thermal conductivity'. International Journal of Energy Research, Vol. 24. pp 1335-1350.

96. Tarnawski, V.R, Gori, F., Wagner, B., Buchan, G.D, 2000. 'Modelling approaches to predicting thermal conductivity of soils at high temperatures'. International Journal of Energy Research, Vol. 24. pp 403-423.

97. Campbell, G.S, Jungbauer, J.D, Bidlake, W.R, Hungerford, R.D, 1994. 'Predicting the effect of temperature on soil thermal conductivity'. Soil Science, Vol. 158, No.5, pp 307-313.

98. Farouki, O, 1981. Thermal properties of soils, CRREL Monograph 81-1, US Army Corps of Engineers, Hanover, New Hampshire, USA.

99. Fort, Karel ,2004. Type 160: Floor heating and hypocaust. A part report for TRNSYS simulations on climate engineering. TRANSSOLAR Klima Engineering.

100. Hatton, A. , Awbi, H. B., 1995. Convective heat transfer in rooms, Building Simulation '95, Fourth Int. Conf., Proceedings, Madison Wisconsin, USA, 1995.

101. Theed, J.E; 'Environmental Parameters for Cable Rating', Ph.D thesis, University of Southampton, March 1999.

102. FEMLAB Reference Manual - Reference Guide. Version 2.3. 'The Partial Differential Equations'. An Adobe Acrobat PDF File.

103. Thomas, H.R; Sansom, M.R; 'Fully coupled analysis of heat, moisture and air transfer in unsaturated soil', Journal of Engineering Mechanics, 1995, **121**, 3, pp393-405.

104. Thomas, H.R; Li, C.L.W; 'An assessment of a model of heat and moisture transfer in unsaturated soil', Geotechnique, 1997, **47**,1, pp113-131.

105. Fethi Azizi; 'Applied Analyses in Geotechnics', 2000, Spon Press.

106. Preece, R.J; Hitchcock, J.A; ' A comparison between the measured and predicted thermal performance of a typical sand backfill', 1976, CERL Report RD/L/N 24/76.

107. Handbook of Soil Mechanics. Vol I:Soil Physics. 'Soil Structure', pp84-86.